Artificial systems for in vitro gene expression

Aleksandra Bednarska

▶ **To cite this version:**

Aleksandra Bednarska. Artificial systems for in vitro gene expression. Agricultural sciences. Université Paris Saclay (COmUE), 2015. English. NNT : 2015SACLN016 . tel-01272067

HAL Id: tel-01272067

https://theses.hal.science/tel-01272067

Submitted on 10 Feb 2016

HAL is a multi-disciplinary open access archive for the deposit and dissemination of scientific research documents, whether they are published or not. The documents may come from teaching and research institutions in France or abroad, or from public or private research centers.

L'archive ouverte pluridisciplinaire **HAL**, est destinée au dépôt et à la diffusion de documents scientifiques de niveau recherche, publiés ou non, émanant des établissements d'enseignement et de recherche français ou étrangers, des laboratoires publics ou privés.

NNT: 2015SACLN016

THESE DE DOCTORAT
DE L'UNIVERSITE PARIS-SACLAY,
préparée à l'Ecole Normale Supérieure de Cachan

ÉCOLE DOCTORALE N° 577
Structure et dynamique des systèmes vivants

Spécialité de doctorat biophysique

Par

Mme Aleksandra BEDNARSKA DELPLANQUE

Artificial systems for *in vitro* gene expression

Composition du Jury:

M. Johannes GEISELMANN	Directeur de Recherche Université Joseph Fourier, Grenoble	Président du Jury Rapporteur
M. Rachid RAHMOUNI	Directeur de Recherche Université d'Orléans	Rapporteur
Mme Cécile SYKES	Directrice de Recherche Institut Curie, Paris	Examinatrice
M. Arnaud BUHOT	Ingénieur de Recherche CEA Grenoble	Examinateur
Mme Claude NOGUES	Chargée de Recherche ENS de Cachan	Co-encadrante de thèse
M. Malcolm BUCKLE	Directeur de Recherche ENS de Cachan	Directeur de thèse

TABLE OF CONTENT

ABBREVIATIONS

AFM	Atomic Force Microscopy
biot	biotin
bp	base pair(s)
dsDNA	double stranded DNA
EG	ethylene glycol
FT-IR	Fourier Transform InfraRed
kbp	10^3 base pair(s)
NiR-FP	Near InfraRed Fluorescent Protein
nt	nucleotide(s)
NTP	ribonucleoside triphosphate(s)
RNAP	DNA dependent RNA polymerase
SAM	self-assembled monolayer
SPRi	Surface Plasmon Resonance imaging
ssDNA	single stranded DNA
TIRF	Total Internal Reflection Fluorescence
wCA	water contact angle

Chapter I

INTRODUCTION

1. Introduction to biosensors

The large demand for precise and rapid detection of biomolecules and the need to define their mechanisms of interaction requires large improvements in biosensing techniques in term of sensitivity, specificity and rapidity of detection. A vast number of detection techniques is used in a wide range of existing biosensors to generate answers for many biological questions. The choice of a particular sensing method is closely related to a specific application, level of sensitivity or reproducibility.

In this Section, a brief introduction to biosensor techniques is presented with a strong emphasis on label-free optical biosensors, their applications and integration into a multi-array geometry and a microfluidic platform.

1.1. Concept of biosensors

The definition of a biosensor is a device that uses biological components to detect the presence or indicate the amount of biomaterial in a solution. Each biosensor is composed of a biorecognition element integrated with a transducer that the signal and generates transformed (comprehensible) data (Figure 1.1).

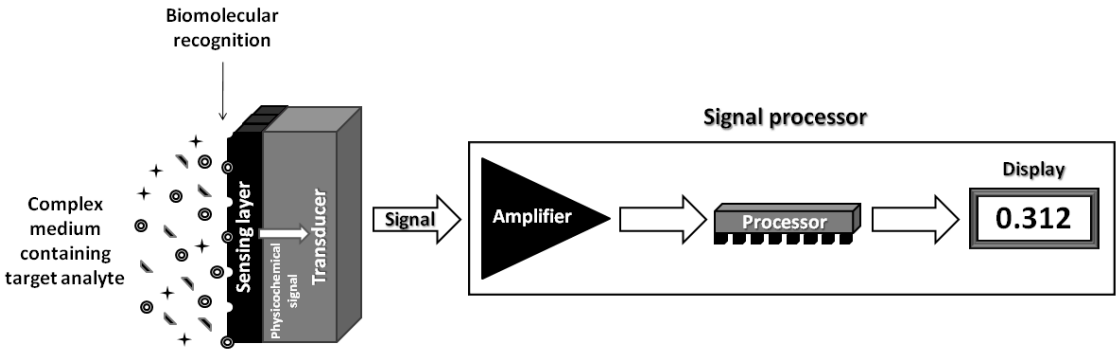

Figure 1.1. Schematic diagram of a biosensor consisting of a bioreceptor and a transducer that processes the signal and generates data. *Adapted from: (1)*

Biosensors can be applied to detection of various types of macromolecules, including: nucleic acids, proteins, antibodies and antigens, organelles, cells, microorganisms and drugs. Biosensors are now omnipresent in many different fields, such as medicine and biomedical research, pharmaceutics and drug discovery, environmental and food industries, security and defense.

The development of a biosensor requires a multidisciplinary approach. A crucial element in surface based biosensors involves ligand immobilization. Efficient immobilization is necessary for optimal analyte capturing and elimination of non-specific interactions. The design of a microfluidic system needs to take into account sample delivery (injection and use of homogenous laminar flow, increasing efficiency of analyte transport etc.), reduction of sample consumption and detection time. The signal-to-noise ratio can be optimized by either increasing the specific signal or by decreasing the background noise or ideally both. Finally, special attention must be paid to the detection format (e.g. direct binding, sandwich-type binding, competitive binding and so on) and data analysis, including extraction of information regarding analyte concentration or binding kinetics.

1.1.1. Label-free biosensors

Numerous biosensing methods require labelling of biomolecules. The most common labelling technique involves the use of fluorescent tags (2). Fluorescence intensity indicates the presence and the amount of a target molecule. Other widely used

labels are radioactive markers and nano objects such as quantum dots or nanoparticles. Although in many cases labelling improves sensing capabilities down to single molecule detection (3), using any kind of label may structurally and functionally interfere with an assay and decrease detection accuracy (4). Additionally, labelling requires supplementary steps in probe preparation that induces extra time and costs.

Therefore, label-free techniques are particularly attractive. Label-free detection can be performed in real time, giving quantitative and kinetic information about biomolecular interactions. Three of the most widely used label-free biosensing technologies are: optical biosensors, acoustic biosensors and microcalorimetry (5).

1.2. Main types of biosensors

The huge variety of accessible methods, devices and detected species makes the biosensor field very complex and elaborated. To facilitate discussion a division of biosensors may be drawn up based on different factors, such as the examined species or interactions, biosensor designs and detection methods. Here, surface based biosensors are listed and briefly described based on the detection principal, namely electrochemical, mechanical and optical biosensors (Figure 1.2).

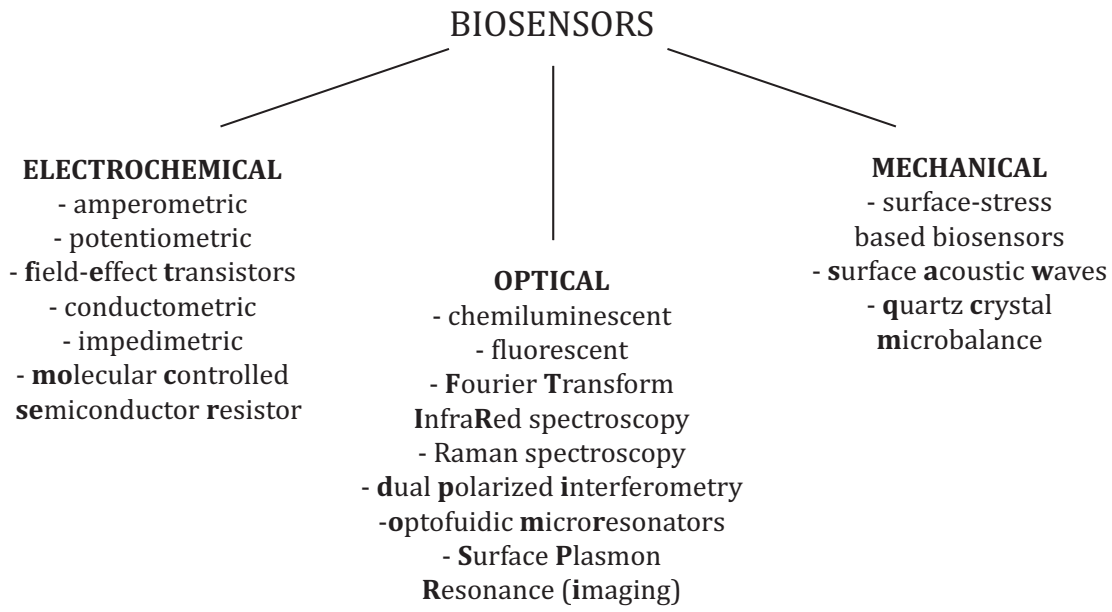

Figure 1.2. Division of surface based biosensors based on their detection principles.

1.2.1. Electrochemical biosensors

A common feature of electrochemical biosensors is a measurement of changes that occur during biochemical reactions when electrons are produced or consumed. A standard system is built of two electrodes: a working one and a reference one. It detects changes in ionic strength, pH, hydration or enzymatic redox reactions (6). Electrochemical biosensors are applied mainly to indicate the presence of molecules such as glucose, cholesterol and H_2O_2 and as DNA sensors. They are highly sensitive, stable and fast; therefore they are broadly applied in diagnostics. A variety of measured parameters and the ease of on-chip integration are the main advantages for large scale and cost-effective fabrication.

Broadly used electrochemical biosensors are based on amperometric, potentiometric, conductometric and impedimetric principles. Others use electric fields to control the conductivity of a channel between two electrodes in a semiconducting material. In field-effect transistor (FET) devices one can distinguish ion selective field effect transistor (ISFET), enzyme-sensitized field effect transistors (EnFET) or immuno-sensitized field effect transistors (ImmunoFED) (7). Molecular controlled semiconductor resistors (MOCSER) are electrochemical biosensors in which the organization of self-assembled monolayers on a semiconductor substrate induces charge transfer (8, 9). This charge transfer process affects the electronic properties of the substrate and may induce variations in conductivity. MOCSER biosensors serve as a gas-phase and liquid-phase biosensor and they have been successfully applied to detect amino acids and antibody - antigen interactions (10).

1.2.2. Mechanical biosensors

The principal of mechanical biosensors is to convert an applied force into a measurable displacement (11). The devices are often reduced in the physical scale to micro- and nano-objects. They are characterized by short time of response, high sensitivity and a low sample volume.

Surface-stress based biosensors are a significant group of bioMEMS (bio micro electro-mechanical systems) devices. They are usually piezoelectrical micro cantilevers or micro membranes that register variations of resistance in the piezoresistive layer as a

response to a change of mass when the analyte binds to the pre-functionalized surface (12). Other biosensors using piezoelectrical properties are acoustic wave based biosensors that generate and detect acoustic waves on the surface of a piezoelectric crystal. The wave is potentially very sensitive towards any changes on the surface, such as mass loading or viscosity (13). Also quartz crystal microbalance (QCM) biosensors measure a difference in deposited mass per unit area by recording the changes in frequency of a quartz crystal resonator. When the mass on a crystal surface increases related to analyte binding, the thickness increases and consequently the frequency of oscillation decreases.

1.2.3. Optical and optofluidic biosensors

Optical biosensors are found in a diverse group of sensing devices that use light in ultraviolet (UV), visible or near-infrared (NIR) regions (14). Since optic based biosensors differ significantly between each other, they also use distinctive properties of light and electromagnetic field to detect interactions with analyzed samples, for instance absorbance, fluorescence and luminescence, interferometry, Raman-scattering, light refraction, cavity resonance or surface plasmon resonance (15, 16). Optical biosensors are robust devices with high throughput and sensitivity that greatly depend on the distance to a sensor surface since the electromagnetic field responsible for sensing typically decays exponentially with the distance from the surface. These biosensors have many advantages, mainly in low detection limit, small volume of analyzed probes (17) and fast analysis process.

Optical biosensors coupled with microfluidic systems (optofluidic biosensors) are often integrated in multiplex geometry chips to create lab-on-chip devices. Microarrays are fabricated by immobilizing biologically relevant molecules (e.g. oligonucleotides, proteins, peptides, carbohydrates, antibodies etc.) on a sensor chip prior to contact with analyzed samples delivered, for example, in a continuous flow. Probe molecules are used to trap targets from the applied sample through specific interactions (i.e. nucleic acid hybridization, nucleoprotein complex formation, ligand–receptor interaction or immunodetection). Detection of specific contacts between immobilized ligands and analytes from the examined sample results in changes in the optical signal that can be translated into a qualitative or quantitative response. Direct detection of biomolecules

allows determination of sample concentration, monitoring molecular reactions in real time, and to determine affinity and kinetic constants (16). Screening several samples simultaneously provides a powerful analytical tool that significantly shortens the analysis time and reduces the amount of analytes and reagents. This kind of analysis is applied in fundamental research, medical diagnostics, food quality control, drug development or environmental monitoring (18). Therefore, to be efficient the system must be compact, miniaturized, easy to fabricate and cheap.

Three optical biosensors are described in detail below: micro ring resonators (Section 1.2.3.1), total internal reflection fluorescence (TIRF) microscopy (Section 1.2.3.2) and surface plasmon resonance imaging (Section 2).

1.2.3.1. Micro ring resonator based biosensor

Optical biosensors based on micro resonators in a photonic circuit are an emerging part of biosensing technology, providing a high efficiency in (bio) molecule detection. Micro ring cavities are used to measure very small concentrations of chemicals in a solution or to study interactions of analytes *via* surface adsorption. A micro ring resonator is composed from a planar waveguide and closed circles in which light is propagated with total internal reflection (19). Polarized light is transported from the optical input to the micro ring and from the micro ring to the output where the photodetector detects both TE and TM polarizations. The straight waveguide is in close contact with micro rings (Figure 1.3). Because of the very narrow gap between these two elements (usually around a hundred or so nanometers), propagating light can be coupled from the waveguide into the micro ring resulting in light resonance. The propagation of electromagnetic waves in the cavity is quasi-infinite without any bandwidth limitations. This makes a micro ring resonator a very sensitive device with a broad range of applications. It enables quantitative and real time measurements and identification of samples with extremely low limit of detection in terms of analyte concentration and volume (15, 16, 20).

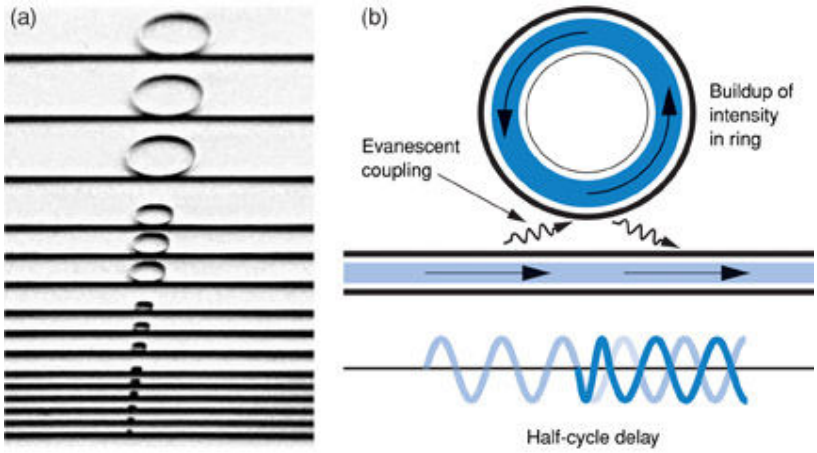

Figure 1.3. (a) Micro ring resonators with different cavity diameters (from 5 to 50 µm); **(b)** Scheme of a micro ring resonator.
Adapted from: www.str.llnl.gov/str/Oct06/Krishnan.html

The main aim is to follow and detect modulations of resonant wavelengths that occur when biomolecules bind to the surface of the micro ring resonator or bulk refractive index changes in the surrounding environment (18, 21). Variations are registered in real time with a very low limit of detection, reaching 10^{-8} RIU (relative intensity unit). These changes result in the shift of resonant wavelengths (Figure 1.4) that can be used to measure the binding affinity and to estimate kinetic constant rates of the reaction. Measured signals are compared to a reference that allows removal of systematic errors.

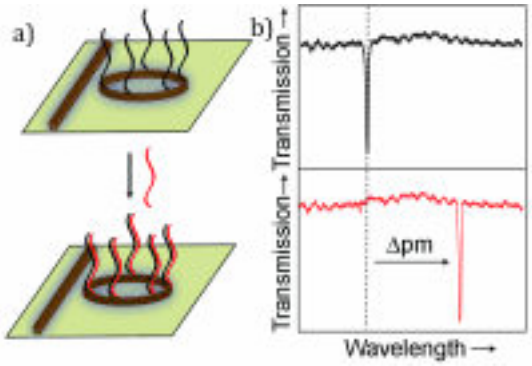

Figure 1.4. Principles of micro ring resonator biosensor **(a)** Detection of nucleic acid hybridization; **(b)** shift of the resonant peak wavelengths caused by binding of the analyte (here complementary RNA) to the micro ring surface. *Adapted from: (22).*

Micro ring resonators are fabricated using Silicon-On-Insulator (SOI) technology and photolithography process of polymers, such as negative photoresist SU-8. This gives the possibility to build compact devices with very good optical characteristics. Additionally, integration of microresonators with a microfluidic system significantly increases sensing capabilities allowing real time detection within lab-on-chip devices.

Micro ring resonator based biosensors may be applied to detect pathogens in the blood (23, 24), nucleic acids (22), low salt concentrations (25), biotin-streptavidin interactions etc. In particular, a collaboration between physicists from the LPQM laboratory and our group at the LBPA laboratory at ENS Cachan aimed at detecting two hundred molecules interacting with surface of a polymer (SU-8) based micro ring resonator for immunodetection applications (20).

1.2.3.2. Total Internal Reflection Fluorescence (TIRF) Microscopy

Total Internal Reflection Fluorescence (TIRF) is an optical phenomenon well suited to investigate molecular and cellular events occurring at solid - liquid interfaces (26) where the evanescent electromagnetic field is induced. TIRF microscopy is applied to study in real time specific biochemical and biophysical processes, for example cell binding process, blood coagulation, intramembranous transport, adherence and mobility of microorganisms (26). It is also used to characterize molecular processes at a single molecule scale (27-29).

TIRF effects occur when a light beam passing through a solid medium of a high reflective index (n_2; e.g. glass prism) is reflected at the interface with a lower refractive index medium or a sample (n_1) under an incident angle (θ_i) greater than the critical angle θ_c (Figure 1.5):

$$\theta_c = sin^{-1}\left(\frac{n_1}{n_2}\right)$$

where $n_1 > n_2$.

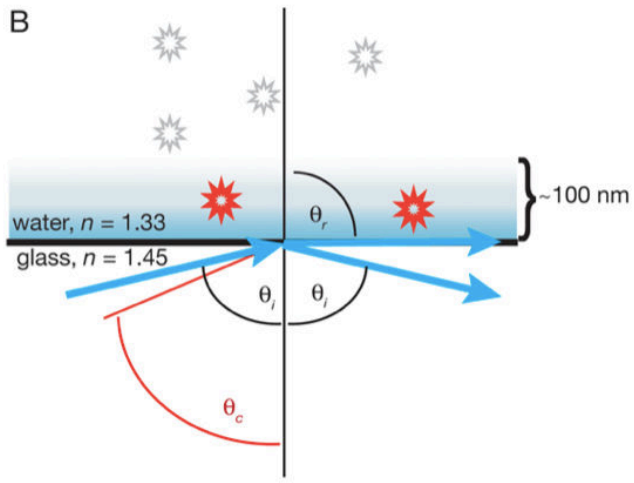

Figure 1.5. Principles of Total Internal Reflection Fluorescence (TIRF) microscopy. A light beam arriving at the critical angle θ_c produces an evanescent field that penetrates a few hundred nanometers into the medium and thus it excites only fluorophores within this distance. *Adapted from: (30).*

Although the incident light beam reflects internally at the interface, a fraction of energy of the incident light is transmitted to a standing evanescent wave that penetrates a liquid medium. The intensity (I) of the evanescent wave decays exponentially with a perpendicular distance (z) and it excites fluorescent molecules that are within 200 nm from the interface:

$$I(z) = I_0 e^{\frac{-z}{d}}$$

where

$$d = \frac{\lambda_0}{4\pi} [n_1^2 \, sin^2\theta - n_2^2]^{-\frac{1}{2}}$$

for angles of incidence $\theta > \theta_c$ and light wavelength in vacuum λ_0 (26).

There are two main types of TIRF microscope setups: prism-based TIRF (26) and objective-based TIRF (27). Additionally, TIRF system can be coupled with various fluorescent techniques that give access to additional information, for example: epifluorescent microscope (31), fluorescence recovery after photobleaching (FRAP) (32), fluorescence correlation spectroscopy (FCS) (33), fluorescence resonance energy transfer (FRET) (29) or atomic force microscopy (AFM) (34).

Currently, the LBPA possesses a TIRF microscope under development to enable study of biological interactions at a single molecule level. It is believed that properly functionalized surfaces would allow selective immobilization of molecules to monitor their behavior and interactions under the microscope.

2. Surface Plasmon Resonance

To date, the most commonly used optical label-free technique is Surface Plasmon Resonance (SPR). This technique is widely applied to examine various biomolecular interactions between immobilized ligands and analytes delivered in a microfluidic flow to the sensor surface. Mass variations occurring on a gold surface during the analyte binding are coupled with changes in refractive index near the gold layer and serve to determine specificity and affinity of those interactions.

SPR technique has been used to identify a large range of biomolecular interactions, including protein - protein interactions (35), nucleic acid hybridizations (36, 37), nucleoprotein interactions (38-40), protein - carbohydrates (41), protein - peptide (42-44) and protein - aptamer (45, 46) interactions and immunorecognition reactions (47-49) such as: antibody - bacteria (50, 51), antibody - cell (52). SPR sensors serve to screen complex samples, including serum, milk, plasma or cell extract for binding partners and determining binding affinity (53, 54). SPR is also used for drug discovery, biomarker identification, food industry, immunogenicity tests or biopharmaceutical development (55, 56).

SPR biosensors are successfully applied to define concentration of analytes in samples. To perform these measurements, the interaction level is compared with an injected analyte concentration. Also more complex reactions are examined with SPR systems, for instance to determine simultaneously interactions during the study of antibody specificity to map epitopes with monoclonal antibodies (57). SPR is also applied to perform chain reactions on the chip, such as monitoring production of proteins *in situ* (58).

In this Section, the principles of SPR and methods of how to analyze data obtained from measurements will be explained. Afterwards, main differences in SPR methods and coupling of SPR with other techniques will be discussed.

2.1. Principles of Surface Plasmon Resonance (SPR)

SPR is a sensing technique that detects changes at a surface by measuring changes in the angle of incident p-polarized light under its total internal reflection. The monochromatic light travels through a medium of a high refractive index (glass prism) till the interface between this medium and another of lower optical density (air or sample solution). Photons arriving at the interface between two dielectric media at an angle greater than the angle of total internal reflection produce an evanescent wave that propagates into the medium of lower refractive index. This evanescent wave, under certain conditions will enter into resonance with the amplitude vector of free electrons (plasmons) in the metallic thin layer. Binding of a ligand to an immobilized molecule on the metallic layer will induce a change in the local refractive index. This change is related to the change in mass at the surface by the Clausius-Mossotti relation:

$$\frac{n_1^2 - 1}{n_1^2 + 2} = \frac{N\alpha}{3\xi_0}$$

where α is the polarizability of the molecule, N is the number density which is equal to $\rho N_A/M$ and M is the molar mass. In a commercial instrument such as BIAcore, the unit of measurement are expressed as Resonance Units (RU) where a change of incident angle of 10^{-4}° is equivalent to a change of 1 RU. Empirically the actual responses in RU as a function of the change of surface molecules concentration (for example a globular protein) is that 1 RU is equivalent to a change in surface concentration of about 1 ng/mm^2 (59).

From three principal geometries used to obtain a plasmon excitation by light: grating (60), Otto and Kretschmann (61) configurations (schematically presented in Figure 1.6), the Kretschmann configuration is the most often applied in SPR (62). In this configuration a thin film is deposited directly on the top of a glass prism surface. The incident p-polarized light, after total internal reflection, generates an electromagnetic evanescent wave on the conducting metal (gold) surface at the interface of a high refractive index prism and a low refractive index liquid medium as explained above.

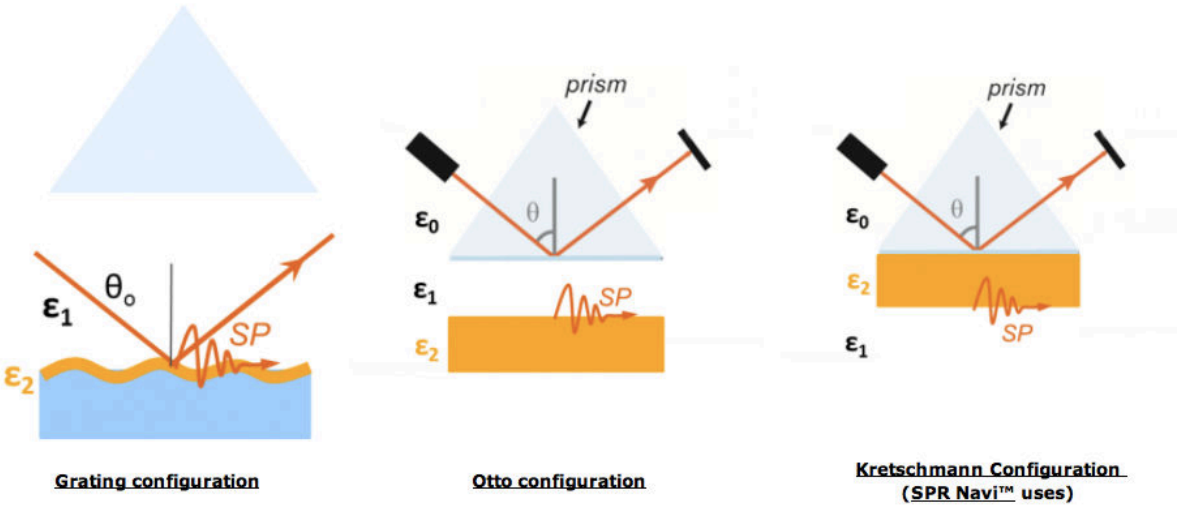

Figure 1.6. Schematic presentation of grating, Otto and Kretschmann prism configurations. *Adapted from: http://www.bionavis.com/technology/spr*

The concept of surface plasmon comes from the analysis of a metal - dielectric interface by Maxwell's theory where surface plasmons can be treated as propagating electron density waves (plasma) occurring at the interface between metal and dielectric. Surface plasmons (SP) can propagate along a metallic surface with the wave-vector (k_{SP}) dispersion relation:

$$k_{SP} = \sqrt{\frac{\varepsilon_1 \varepsilon_2}{\varepsilon_1 + \varepsilon_2}}$$

where ε_1 and ε_2 are respectively dielectric constants of the metal and the medium in contact with it.

The energy of the incident light is strongly coupled to photons onto the surface plasmon evanescent wave. The relationship between k_X wave vector incident light and the angle of incident light (θ) can be expressed as:

$$k_X = n \sin \theta$$

where n is a refractive index of a glass prism.

Resonance is achieved by matching the wave vector of the incident light in the direction of the interface and the wave vector of surface plasmon oscillations:

$$k_X = k_{SP}$$

There is a decrease in intensity of reflected light at the angle of resonance as presented in Figure 1.7a. Changes occurring at the interface (e.g. correlated with mass variations as a consequence of a ligand-analyte binding process) result in a shift of the resonance curve (Figure 1.7b). Changes observed in a measured parameter (resonance angle) over time serve to generate a kinetic curve, which historically has been referred as a sensorgram (Figure 1.7c).

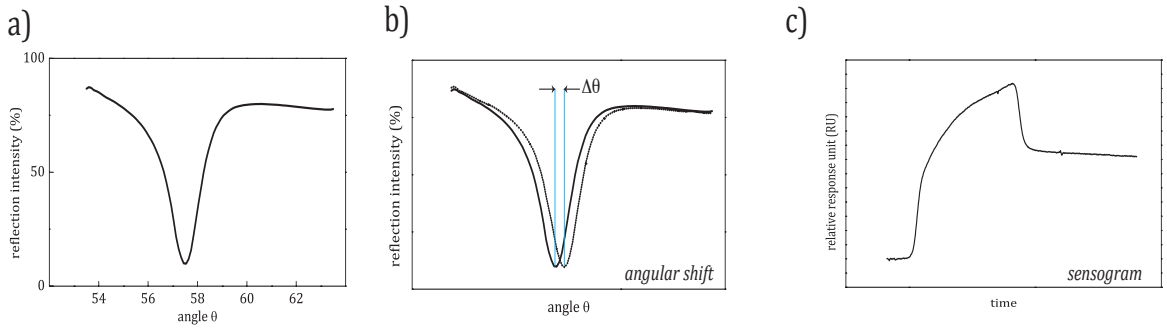

Figure 1.7. Examples of SPR results: **(a)** plasmon curve registered by SPR; **(b)** angular shift of a plasmon resonance; **(c)** sensorgram: variation of the angle θ as a function of time.

It is worth noticing that the signal at the interface decays exponentially with the distance from a gold layer. As a consequence, the SPR technique interrogates interactions only at or close to the metallic surface.

2.2. Information obtained by SPR and its analysis

Kinetic analysis provides information about the specificity of (bio) molecular interactions and aids in the determination of the mechanism of binding and dissociation in a quantitative manner. In the following Section, data analysis will concentrate uniquely on SPR, knowing that similar treatment is applicable to most biosensors that generate data concerning changes in a reaction over time.

The simplest model to describe adsorption of molecules to a surface is given by the Langmuir isotherm that describes a dependence of a perfect gas adsorbed to the surface at different pressures and at a fixed temperature (63, 64). Classically, the equilibrium between molecules of gas adsorbed to the surface and molecules of gas in a dynamic

state can be directly related to the equilibrium between molecules adsorbed to and desorbed from a surface.

In the present context, the interaction between analyte A binding to the immobilized ligand B can be expressed by the equation:

$$A + B \underset{kd}{\overset{ka}{\rightleftharpoons}} AB$$

where AB stands for the complex created on the sensor surface, k_a is the association rate and k_d – the dissociation rate. From the differential rate equation:

$$\frac{d[AB]}{dt} = k_a\,[A][B] - k_d\,[AB]$$

one can obtain the association equilibrium constant as a ratio of two rate constants, given by:

$$K_a = \frac{k_a}{k_d}$$

The unit for association constant (k_a) is $M^{-1}s^{-1}$ and has a value from 10^3 to 10^7 $M^{-1}s^{-1}$ in typical biological systems. The unit for the dissociation constant (k_d) is s^{-1} and it generally is between 10^{-1} and 10^{-6} s^{-1}. Classically in biochemistry the inverse of the equilibrium association constant is used; this equilibrium dissociation constant (K_d) is expressed in M^{-1} and depends on a number of factors. Under standard physiological conditions in biological systems (25°C and 1 atm pressure) K_d has always the same value for a given reaction, regardless of the analyte concentrations (65).

An alternative method to estimate the affinity of a reaction involves measuring steady state levels of saturation as a function of analyte concentration. Knowing the dependence between the total concentration of free analyte and the fractional saturation (Y) of sites on ligand B saturated with analyte A, one can estimate the K_d for this interaction, based on the plot presented in Figure 1.8.

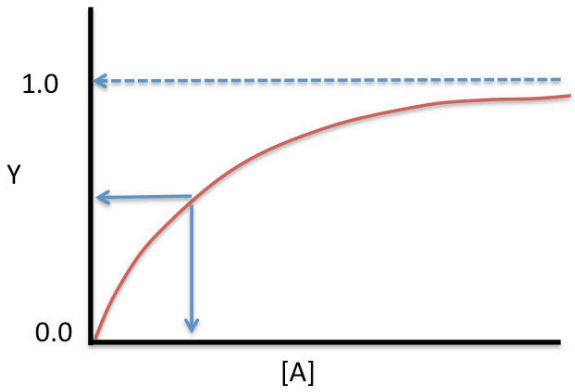

Figure 1.8. A simple saturation plot used to estimate K_d (affinity constant) value.

K_d can be obtained when a fractional saturation is a half value of the asymptote. This is presented as:

$$\frac{1}{2} = \frac{[A]}{K_d + [A]}$$

and thus:

$$K_d + [A] = 2\,[A]$$

giving therefore:

$$K_d = [A]$$

In the SPR technique, changes in refractive index caused by interacting molecules are monitored in real time (40, 66). A sensorgram can be extracted from most of biosensors that use surfaces to trap interacting molecules from a solution. Consequently, association and dissociation rate constants can be determined separately. This allows more detailed analysis of the binding mechanism and it is a significant step forward in comparison to a classical steady-state analysis of biomolecular interactions. When the analyte is injected over the biochip surface, changes in the detected signal are monitored and plotted in the form of a sensorgram (Figure 1.9). A typical sensorgram consists of the following phases: (i) baseline: a buffer solution is passed over the sensor; (ii) association phase: at the time t=0 the buffer solution containing an analyte passes over the sensor surface and binds to the immobilized ligands; (iii) steady state phase: the amount of analyte associating and dissociating to and from the ligand is equal (iv) dissociation phase: the flowing solution is switched back to the running buffer and

analyte dissociates from the ligand. Association (k_a) and dissociation (k_d) rate constants are determined from the sensorgram.

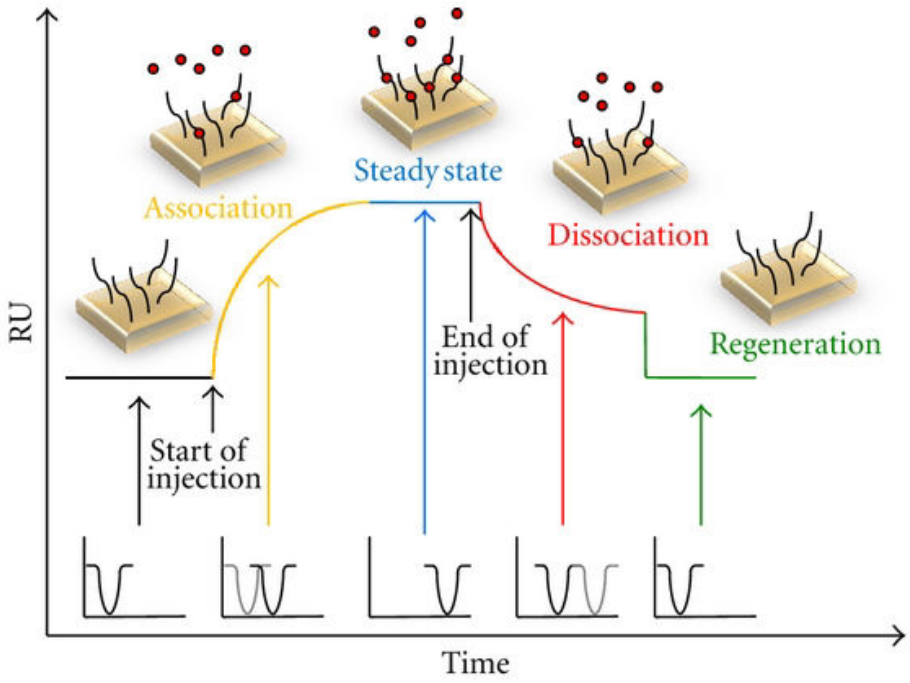

Figure 1.9. Sensorgram of SPR presenting different phases of a biomolecular intereaction. *Adapted from (67).*

In order to interpret the schema shown in Figure 1.9, a model for the interaction is required. In the majority of cases a simple Langmuir binding isotherm as described above is used. In this simple case, the dissociation phase is given by the expression:

$$R_t = R_0 \exp^{-k_d t}$$

where R_t is the response at time t and R_0 the response at the start of the dissociation phase. A fit of this part of the curve thus gives the apparent dissociation rate k_d. With this calculated rate constant and a known concentration C the association rate can be derived from the expression:

$$R_t = \left[\frac{k_a C R_{\max}}{k_a C + k_d}\right]\left\{(1 - \exp^{-(k_a C + k_d)t})\right\}$$

Interpretation of sensorgrams is limited by the kinetic model used to analyze the reaction and a number of parameters needs to be considered before attributing quantitative values to derived constants (68).

2.3. Classification of SPR: differences between SPR, SPRi and LSPR

The first commercially available SPR system (BIAcore) presented in 1980s used the Kretschmann configuration (69). Since then, several alternative configurations have appeared with improvements of sensitivity and resolution, the introduction of structural innovations, facilitating data processing and analysis and increasing throughput.

2.3.1. BIAcore technology

The most common SPR based instruments are from BIAcore technology (Uppsala, Sweden). BIAcore technology is based on the automated label-free optical detection of biological molecules and their interactions in real time. Essentially, it measures changes in resonance angle as a function of the concentration of material at the surface (Figure 1.10).

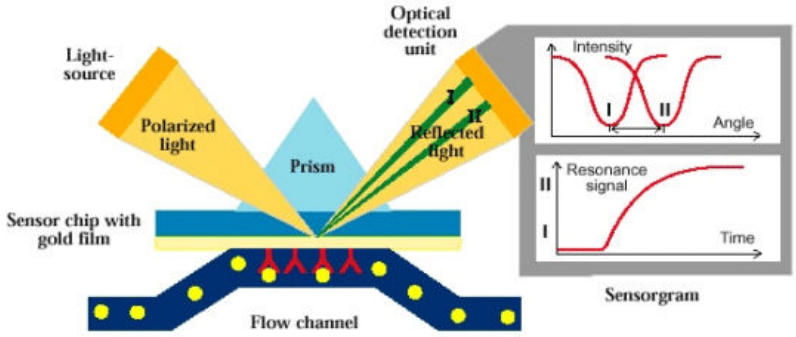

Figure 1.10. Basic SPR instrument configuration, included SPR Kretschmann geometry and sensorgrams obtained during the measurements. *Adapted from: www.biacore.com*

BIAcore instruments are used to detect a wide range of specific molecules and their interactions with immobilized ligands, to screen samples for finding a binding partner and to measure kinetic interactions and binding affinities. The systems can detect molecules as small as 180 Da. The measured concentrations, depending on the BIAcore model, are in a range of pM with a limit of detection reaching 0.01 RU.

2.3.2. Surface Plasmon Resonance imaging (SPRi)

Surface plasmon resonance imaging is an advanced version of a classical SPR and it has remarkable advantages over the traditional BIAcore technology, including a charge-coupled device (CCD) camera for signal detection that offers the possibility for simultaneous analysis of up to several hundreds of biological interactions. SPRi significantly shortens manipulation time and sample consumption since interactions between analyte and all immobilized ligands are monitored simultaneously during the same injection (Figure 1.11). The SPRi platform linked with a microfluidic system is thus ideal for the design of a whole on-chip reaction allowing the synthesis of proteins on-chip (58) or RNA aptamers (70).

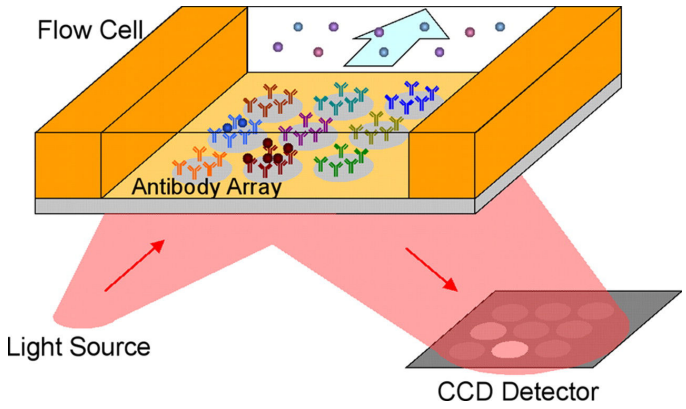

Figure 1.11. Principles of surface plasmon resonance imaging. As for the classical SPR approach light from a narrowband light source is collimated, and sent to a prism at the angle of total internal reflection. A CCD camera collects the reflected light, allowing visualization of the entire sensor surface in real time. *Adapted from (71).*

A CCD camera allows interrogation of the whole biosensor surface on which spots containing different ligands may be immobilized. Spots without any ligand serve as controls for non-specific interactions or with alternative ligands for positive and negative control. The size of each spot, defined by the presence of biomolecules varies from tens to hundreds μm^2. SPRi has been successfully applied to a wide range of complex measurements that requires high-density microarrays for high-throughput analysis of biomolecular interactions, such as: proteomic analysis, drug discovery, point-of-care diagnosis or biomarker screening (47, 72, 73).

The most widely commercially available SPRi instruments are currently SPRi-plex GenOptics Horiba (France), GWC Technologies (USA), IBIS Technologies B.V. (Netherlands) and GE Healthcare (Sweden).

2.3.3. Localized Surface Plasmon Resonance (LSPR)

Localized surface plasmon resonance (LSPR) is a technique that uses noble metal nanoparticles and surface plasmon phenomenon. The gold nanoparticles typically exhibit LSPR at visible and near-infrared frequencies caused by the collective oscillations of conductive electrons induced by light illumination (74). Because of their size, metallic nanoparticles are characterized by a sharp spectral absorption and scattering peaks, as well as a strong electromagnetic field near their surface. The localized electromagnetic field around the metal surfaces is very sensitive to environmental refractive index changes. Environmental changes, at the interface between media and metals, can be traced by monitoring the changes of metal LSPR characteristics as in SPR or SPRi. Moreover, LSPR is not sensitive to changes of temperature and requires only simple optical extinction measurement. LSPR based gold nanoparticle biosensors are also integrated in a microfluidic system and have been successfully used to detect DNA (75), proteins (76) or antibody – antigen interactions (77).

2.3.4. Further developments of SPR

Widespread accessibility and the broad possibility of SPR applications make this technique very popular amongst researchers and encourage further improvement and development. One of the directions of SPR sensor development is focused on a miniaturization of the system in order to create portable platforms suitable for point-of-care applications. In the concept of miniaturized SPR sensors all optoelectrical elements are integrated in a monolithic platform based on SPR spectroscopy (78).

Currently, many research groups develop SPR by integrating new methods of sensing and structural design to improve sensitivity and enhance performance of sensing measurements. Optimization of conditions includes constant flow injection, thermostatic control and improvement of components, such as light source, prism and

CCD camera quality and data processing methods (79). Also combining SPR with other techniques opens up new possibilities and promises a significant progress for the detection and investigation of biomolecular interactions. Several examples of those combined techniques are presented below, in the Section 2.4.

2.4. SPR coupled with other techniques

Coupling of SPR with other techniques gives additional information about examined sample and may significantly improve the understanding of a given biological event. There are many integrated systems supplied from commercial SPR producers that directly combine SPR with other detection methods. One of them is SPR coupled with Matrix-Assisted Laser Desorption/Ionization Mass Spectrometry (SPRi MALDI-MS) for the identification of protein components (44, 80) or antigens (81). Horiba Scientific has recently commercialized a technique to directly couple SPRi to MALDI-MS. It enables a multiplex quantification of samples bound to ligands immobilized to the biochip and molecular characterization by MS analysis of analytes directly on a biochip without further elution.

In addition to MALDI associated SPR other promising combinations exist (69). A promising approach determines the nature and structure of bound molecules using an SPRi coupled with Fourier Transform (FT-SPRi) (43). Molecular Imprinting Polymer (MIP) has been performed to selectively bind DNA to a surface (82), whereas coupling SPRi with Scanning ElectroChemical Microscopy (SECM) allowed direct visualization of localized electropolymerization (83). Digital electrowetting-on-dielectric (EWOD) coupled with SPR was found to be a remarkable alternative to the traditionally used microfluidic system (48, 84-86). A temperature scanning system finds new applications in SPRi monitoring, for example in DNA point mutation detection (87).

2.5. SPRi-plex GenOptics

The majority of SPR studies described in this manuscript were performed with a SPRi-plex GenOptics instrument (Horiba, Orsay, France). SPRi-plex GenOptics allows the characterization of biological interactions with a detection limit of 5 pg/mm^2 for samples of ≥ 200 Da. In this Section a brief description of the instrument will be

presented. The main elements of this platform are: (i) optical system, (ii) biochip, (iii) microfluidic system, (iv) software.

The optical system used in SPRi-plex GenOptics (Figure 1.12a) is constructed with a source of incident near infrared light (high stability LED, 810 nm), a mobile mirror, and a CCD camera with optical lateral resolution of 40 µm.

The sensor chip (Figure 1.12b) is a prism with a high refractive index (SF 10; n=1.707987 at λ=830 nm) coated with a thin gold layer (between 45 and 50 nm thick). The gold thin layer is functionalized using an appropriate surface chemistry protocol (see Section 3) prior to ligand spotting. Ligands can be deposited on a surface sensor using a spotter or manually using a micropipette. The working surface of the sensor is about 1 cm^2 thus allowing the deposit of up to several hundred spots. In order to prevent spots from drying, the biochip is maintained in a humid environment during the ligand incubation period.

The SPRi-plex GenOptics platform has an in-built microfluidic system (Figure 1.12a) composed of a continues flow pump with flow rate ranging from 2 to 2000 µl/min. Injection occurs through a loop thus injection volumes are limited merely by the size of the loop which in practice vary between 20 to 2000 µl and samples are then conducted across into a hexagonal sensor cell (11 µl volume). The system is equipped with a temperature controller based on a Peltier effect (88) allowing temperature control from 15 up to 40°C. The microfluidic system incorporates a degasser to avoid air bubbles.

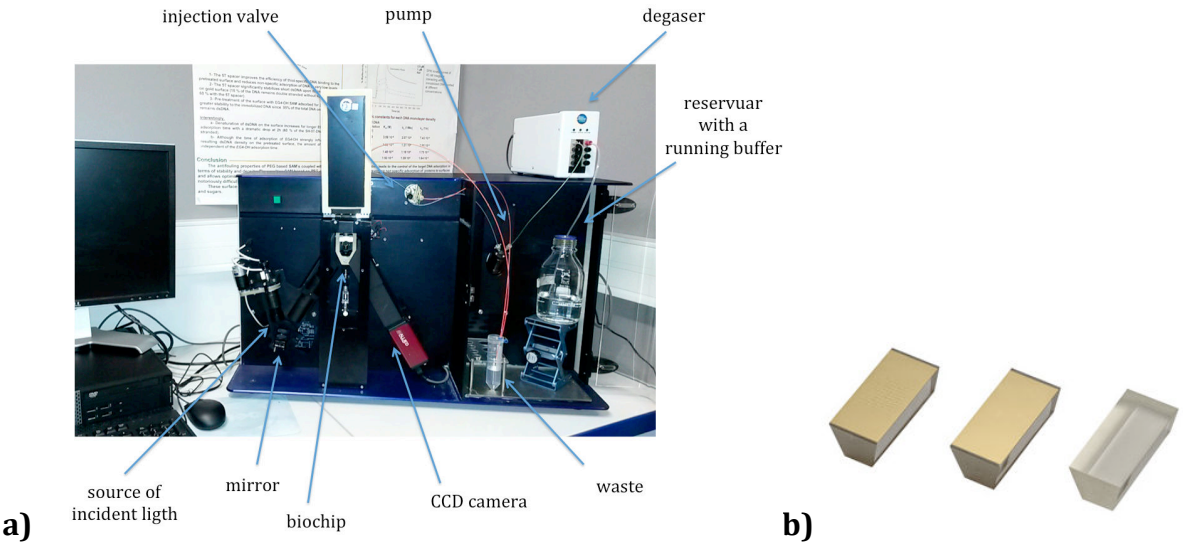

Figure 1.12. Instrumental characteristics: **(a)** SPRi-plex GenOptics, **(b)** From right to left, glass prism without and with an evaporated gold layer and with spots of biomolecules on the gold surface.

The SPRi-plex GenOptics instrument is equipped with dedicated software that programs and monitors the experiment. The software interface allows control of the mirror that selects the optimal angle for the plasmon shift changes and the microfluidic system, thus regulating running buffer and sample flow rates, and the injection volume. During the experiment changes in refractive index are directly recorded. Two kinds of cell images are obtained: the real time images that show the image of the cell and the differential images that register real time changes in the refractive index.

Typical results are shown in Figure 1.13 where an image of the surface is translated in real time into a sensorgram showing the evolution of the change in % of reflected light as a function of time at selected spots on the surface.

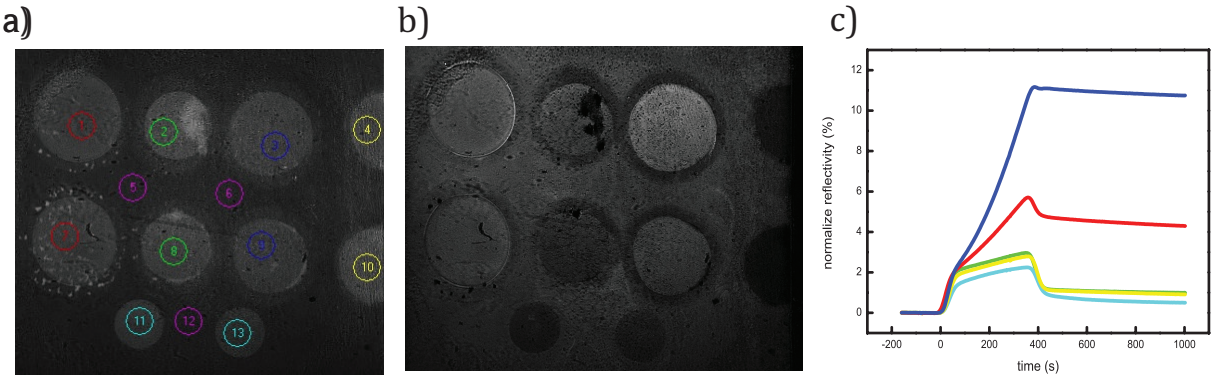

Figure 1.13. Data obtained from SPRi experiment: **a)** flow cell image with selected area on the surface; **b)** differential image showing variation of image contrast on a surface in real time; **c)** sensorgram showing the variation of the % reflected light intensity as a function of time at selected spots on the surface.

3. Surface chemistry in biosensors

Bioconjugation of surfaces is an integral part of the development of surface based biosensors (89). Surface ligand immobilization has a direct impact on the relevance and on the sensitivity of the biosensor. Parameters like ligand density and orientation, ligand structure and surface related non-specific interactions must be controlled in order to optimizing a biosensor (90). Due to the huge range of potential macromolecular interactions and the wide variety of surfaces used in biosensing applications, a universal protocol for surface functionalization does not exist. The (bio) conjugation strategy is strictly specific to a particular biological system and the surface chemistry should be optimized to expose the functional or recognition sites as a function of the ligand properties, size and shape (91). Additionally, for a robust biosensor, the surface chemistry and immobilized ligand should be stable over the time of the interaction and allow repeated characterization (92).

There are several techniques commonly available for efficient immobilization of biomolecules of interest to surfaces. These methods can be classified into two main categories based on the mechanism of attachment of the ligand to the surface: through covalent bond formation and non-covalent coupling (e.g. electrostatic, hydrophobic, hydrophilic and affinity interactions) (89).

3.1. Methods of surface functionalization

Immobilization of target molecules on surfaces for biosensing applications must be optimized to simultaneously prevent non-specific interaction of the analyte with the surface so that only specific interactions between the analyte and the immobilized target are detected, to prevent steric hindrance by adjusting the target surface density and to control the target orientation on the surface to allow the interaction to occur as it would if diluted in solution. In addition, the binding of biomolecules to surfaces should avoid denaturation not to affect their biological activity.

Immobilization of target molecules can either be performed directly if they have a functional group that interacts strongly with the surface or through a pre-functionalized surface with either a polymer or a self-assembled monolayer that contain a functional group to allow the controlled adsorption of the target molecule.

3.1.1. Self-Assembled Monolayer (SAM) on gold surfaces

Many surfaces can be functionalized with a self-assembled monolayer with organic molecules having a reactive functional group that specifically and spontaneously reacts with a specific surface to form a stable bound: thiol group on metallic surfaces (gold), carboxyl group on metallic surface and silane on oxidized surface (silicon, metal oxide, glass) for example.

There are two methods to adsorb a molecular monolayer on a solid substrate: (i): Langmuir–Blodgett (LB) where a pre-formed monolayer of amphiphilic molecules is first formed on water and then transferred to a solid surface which is either hydrophobic or hydrophilic; (ii) self-assembled monolayer (SAM) where bi-functionalized molecules are on one side attached with a strong bound to the surface and contain, generally at the other end, a functional head group that can be either directly the ligand or react/interact specifically with the target molecule.

Considerable attention has been given to the creation of SAMs on noble metal surfaces, and more specifically gold surfaces. Thiolated SAMs deposited on gold have been extensively characterized as they spontaneously form densely packed monolayer (93) and are of particular interest for sensing, electrochemical, and optical or piezoelectric applications.

Thiolated molecules (SH-R) react spontaneously with metallic surfaces to form a stable complex (45 kcal/mol (94), compared for example to ~83 kcal/mol for a C—C bond). According mainly to the incubation time and the thiol concentration SAMs on gold are densely packed with molecules standing proud from the surface (Figure 1.14).

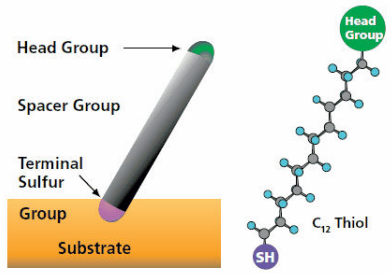

Figure 1.14. Structure of a thiolated molecule forming a SAM on metallic surfaces. *Adapted from (95).*

Voltametric studies confirmed deprotonation of thiol groups during adsorption on gold and the formation of bonds based on the formula (51):

$$R - SH + Au \rightleftarrows R - S - Au + e^- + H^+$$

An alkyl chain of minimum eight carbons (96), generally used as a spacer between the thiol group and the functional head group improves the self-assembly stability *via* Van der Waals interactions between neighboring molecules in the SAM. In addition, upon binding the molecules optimize their interactions with the neighboring molecules by orienting upward on the surface until saturation of the surface, as presented in Figure 1.15.

The simple immersion of a clean metallic substrate in a solution (ethanol, hexane, acetonitrile or water) containing thiolated molecules leads to their chemisorption and form a dense self-assembled monolayer with time (Figure 1.15). The saturation of the surface is reached at different adsorption times depending on the thiolated molecule concentration, solvent and temperature. In addition, the final structure of the SAM and molecular density strongly depend on the chemical nature and size of the functional head group of the thiolated molecule.

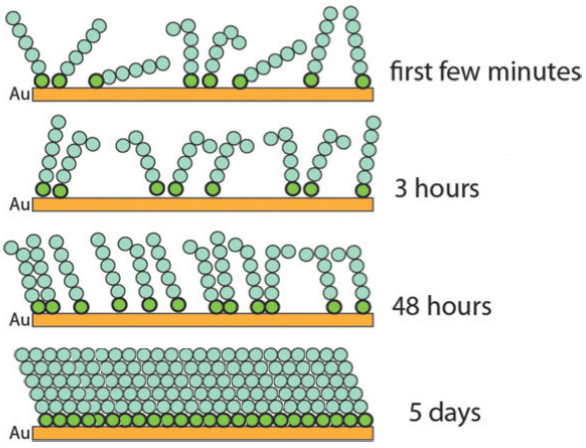

Figure 1.15. Formation of a dense self-assembled monolayer on gold as a function of the incubation time. *Adapted from (96).*

The pertinent choice of the functional head group of the molecules that composes the SAM allows tuning of the properties of the SAM. For example using decanethiol of long (typically 18) alkyl chains, the formation of a dense monolayer on a clean gold surface leads to a highly hydrophobic surface and to a hydrophilic surface when a terminal methyl group is replaced by a hydroxyl group. Whitesides *et al.* demonstrated in 1998 (93) that having an *n* ethylene glycol (with *n* ranging from 4 to 6) as a head group prevented non-specific interactions of biomolecules (essentially proteins and DNA) directly to the surface and lead to an efficient antifouling surface modification. In addition, it was shown that such gold surface modifications also efficiently prevented biomolecule denaturation upon immobilization (37, 47).

For biosensor applications, two approaches have been developed: either the target molecule contains an accessible thiol group (5' or 3' thiolated ssDNA or/and dsDNA, presence of a cysteine at a surface of a protein) so that it can be directly bound to a gold surface, or the SAM functional head group is chosen so it can react or interact with the target molecules (lysine, cysteine or terminal amine of proteins or peptides, 5' or 3' thiolated ssDNA or/and dsDNA, available primary amine of amino acid in a protein). In all cases, the target molecules are large (few kDa to few hundred kDa) so the surface coverage has to be optimized to avoid crowding and steric hindrance upon interaction with the analyte. In addition, the choice of the surface immobilization method often determines the orientation and stability of target molecules on the surface.

Mixed SAMs obtained by immersing gold surfaces into a diluted solution of the target molecule and inactive or inert molecules allows control of the surface density of the target (97), therefore controlling steric hindrance. Diluting different ratios of each molecule for identical adsorption time controls the target surface density, which therefore can be optimized for all target size. Additionally, the nature of the inactive molecules is primordial so as not to affect the sensing event while inhibiting non-specific interactions with the surface. Furthermore, in the SAM mixture, the spacer chain can be adjusted so that the target molecule is fully accessible to interact as it would be in solution as illustrated in Figure 1.16 (98).

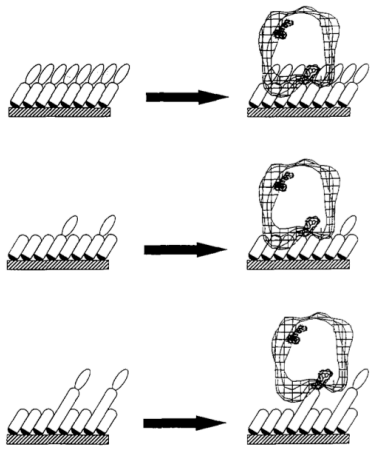

Figure 1.16. Immobilization of a biomolecule to full and mixed SAMs: **(top)** pure and 'short' alkenethiols where the binding of the ligand is sterically hindered; **(centre)** mix SAM of 'short' and 'medium' alkenethiols still showing steric hindrance upon binding of the ligand; **(bottom)** mixed SAM of 'short' and 'long' alkenethiols allowing binding of the ligand with no steric hindrance. *Adapted from (98).*

Thiolated SAMs on gold surfaces can be extensively characterized with respect to the molecular density and orientation using Contact Angle measurements (CA), Fourier Transform InfraRed (FT-IR), X-ray photoelectron spectroscopies (XPS), scanning electron microscopy (SEM), atomic force microscopy (AFM), Surface Plasmon Resonance (SPR) and Quartz Crystal Microbalance (QCM).

The flexibility in choosing different functional groups of the monolayer head makes SAM an excellent tool for surface functionalization and an intermediate to immobilize a wide range of bio molecules, such as nucleic acids, peptides, proteins for selective sensors.

3.1.2. Surface coating

Long polymer chains grafted to surfaces are an alternative to self-assembled monolayers for surface functionalization. Similarly to SAMs, they create an anti-fouling layer that minimizes nonspecific interactions of biomolecules directly to the surface and increases the stability of immobilized biological species. However, the density of functional head groups that allows immobilization of biomolecules is often difficult to control, therefore the density of ligands as well as their orientation on the surface is more difficult to optimize than in the case of SAMs.

Long macromolecular chains can be either covalently bound to the surface or immobilized *via* physical bound (e.g. electrostatic, hydrophobic). They eventually can also be deposited on surfaces by spin coating. In all cases, deposition of long polymeric chains on surfaces often leads to random orientation. Nevertheless, some control can be obtained by using side grafting, block side grafting or end-grafting, as presented in Figure 1.17a. According to the density of adsorbed polymer, the structure of the thin layer on the surface differs: mushroom-like regimes (when the tethered chains are isolated and their structures do not differ significantly from polymers in bulk), brush-like regimes (when the chains are strongly stretched and densely grafted onto the surface) or intermediate – overlapping mushroom-like regimes, as shown in Figure 1.17b (99, 100). Polymers can fully cover the surface even when their density does not reach the surface saturation as their long chains collapse and form mushroom-like or overlapping-mushroom-like states on the surface.

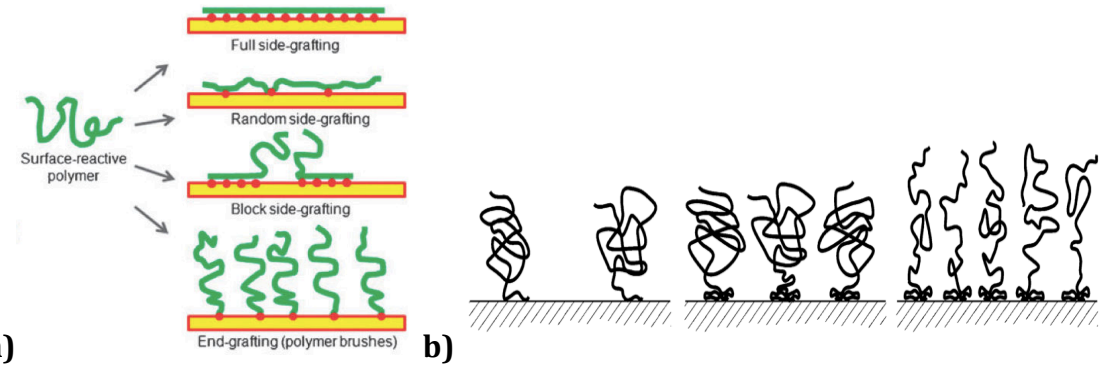

a) **b)**

Figure 1.17. Tethered polymer chains participating in a surface functionalization. **(a)** Different modes of binding to the surface. *Adapted from (101).* **(b)** Mushroom, overlapping mushroom and brush regimes. *Adapted from (100).*

Two of the most widely used polymers for surface functionalization are dextran and polyethylene glycol (PEG). They are efficient anti-fouling substances that significantly lower non-specific protein adsorption on surfaces and are cell-resistant. Both, PEG and dextran, can be bi-functional polymers: they may contain one functional group for their stable anchoring to the surface and one to conjugate specifically to a (bio) molecule. Dextran is a linear polysaccharide built from connected 1,6-glucose units. Each glucose monomer could be modified with one carboxyl group that can be activated to form an amide bond with a primary amine present in biomolecules. As a multivalent molecule, dextran is used for high-density surface immobilization of biologically active molecules. It extends the volume where molecules can anchor and interact with ligands, leading to an increase of sensitivity and specificity. On the other hand, PEG as a divalent macromolecule has a very strict and limited number of sites available for biomolecule coupling (usually one binding site per monomer, except so-called 'star-configuration' PEGs). Therefore, to obtain higher densities of immobilized bioactive molecules dextran-coated surfaces are preferred.

Long macromolecular chains tend to form coils rather than fully extended brushes since this state increases the configurational entropy (101). It is therefore difficult to determine the exact thickness of the formed thin layer, which is crucial for optical biosensors that use an evanescent wave, like in SPR experiments. The evanescent wave extends approximately up to 200 nm away from the surface (depending on the wavelength of incident angle) to sense biomolecules adsorbing on the surface. Because the evanescent wave intensity decreases exponentially away from the surface, the sensitivity of the detection is optimal within the few tens of nanometers from the surface. An additional drawback of the polymer biofunctionalization is the random orientation and distribution of the anchoring group that is therefore not always available to react with biomolecules (Figure 1.18).

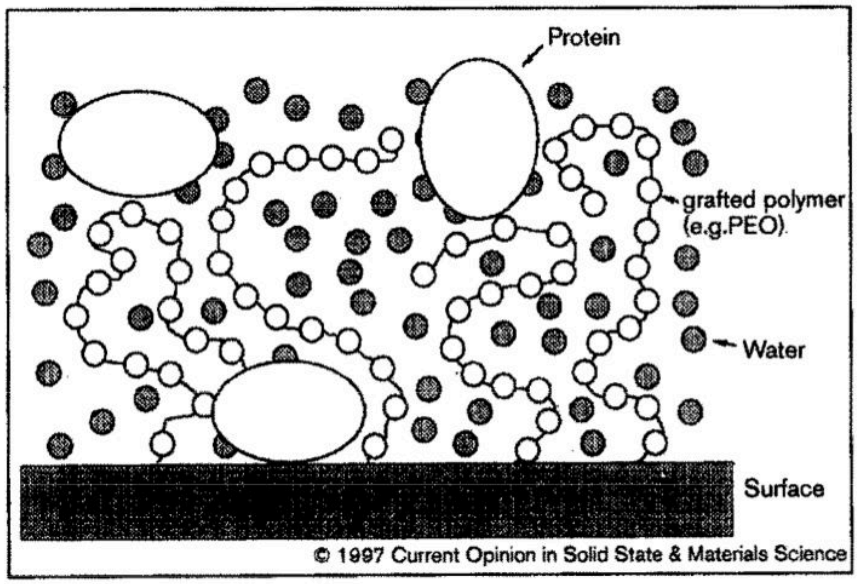

Figure 1.18. Schematic distribution of proteins in contact with tethered polymer layer. *Adapted from (99).*

3.2. Biomolecule conjugation and immobilization techniques

A well-controlled immobilization of ligands on the surface in terms of density, orientation and availability is essential for quantitative detection of analyte present in solution. Since antifouling SAMs on a surface allow adjusting the ligand surface density, the following part of this Section will concentrate on describing different immobilization methods on pre-treated surfaces using a functionalized SAM (89).

3.2.1. Covalent bond formation

Covalent bond formation at the interface between the ligand and a functionalized SAM allows an efficient immobilization. While the ligand is exposed toward the solution, it can interact as it is in the solution. The immobilization process is therefore multi-step. Since a wide range of linkers is available, it can be optimized to a specific system and thus the ligand orientation is also optimized. The SAM reactive site that has not reacted with the ligand has to be blocked before any further experiments. Thus the selectivity of the detection would not be affected and the non-specific binding of biomolecules directly to the surface would be reduced.

3.2.1.1. Amide bond formation and EDC/NHS coupling reaction

The conjugation of primary amine and carboxyl group leads to the formation of amide bonds – one of the most common covalent bonds in nature, present for example between amino acids in peptides and proteins. Primary amine groups are often exposed on the surface of proteins and antibodies or they can be added to 5'- or 3'-end of DNA and RNA molecules (90). Primary amines can be coupled to carboxyl, aldehydes, epoxides or anhydrides groups exposed on a head of a SAM adsorbed on the substrate surface.

To facilitate coupling of primary amines to carboxyl groups 1-ethyl-3-(3-dimethylaminopropyl)-carboiimide (EDC) is commonly used (102). It is a zero-length coupling agent that reacts with a carboxyl group by forming an amine-reactive O-acylisourea intermediate (90). Moreover, addition of (sulfo-) N-hydroxysuccinimide (NHS or sulfo-NHS) stabilizes the amine-reactive intermediate by converting it into an amine-reactive succinimide ester (Figure 1.19). The coupling reaction is very fast and efficient, however, a reactive ester can be rapidly hydrolyzed in aqueous solution. Therefore, to achieve the most efficient reaction, carefully stored or freshly prepared reagents should be used. In certain situations, the presence of both carboxylates and amines on one of the biomolecules to be conjugated with EDC may lead to uncontrolled self-polymerization and consequently to loss of effectiveness. To overcome this issue, excess of EDC should be removed before adding a biomolecule, for example through extensive surface rinsing.

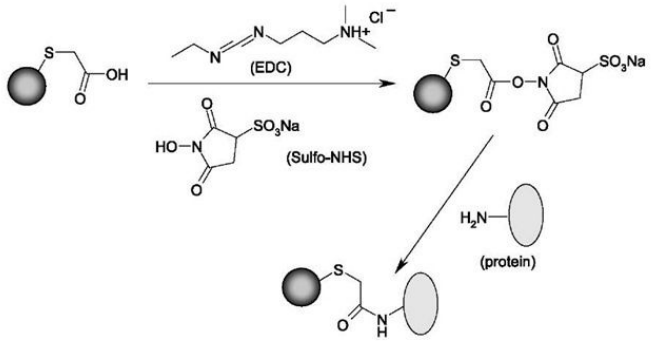

Figure 1.19. EDC/NHS conjugation reaction between carboxyl and amine groups leading to formation of amide bond.

3.2.1.2. Thiol-based conjugation and maleimide coupling

Maleimide groups react specifically with thiols. The reaction generates a stable 3-thiosuccinimidyl ether linkage. This approach is an alternative to amide bond formation when the only exposed group available for immobilization is thiol. It can be used to efficiently immobilize proteins *via* cysteine amino acid (103). Cysteine residue may be genetically introduced into a specific site of a target protein (preferably far from the active site) and thus allows for properly orientated immobilization (89).

On the other hand, thiolated molecule can be directly grafted to the gold surface. Thiol-modified single stranded DNA (ssDNA) immobilized on a gold surfaces can be hybridized with a complementary ssDNA conjugated with an antibody or a protein to direct their spatial assembly on the surface (104).

3.2.1.3. Click chemistry

Click chemistry refers to a group of reactions that are fast, simple and efficient. They are broadly applied to immobilize (bio) molecules, for instance on functionalized silane surfaces (92). The most widely used click reaction is copper (I) - catalyzed cycloaddition between alkyne and azide that gives a 1,2,3-triazole ring (105):

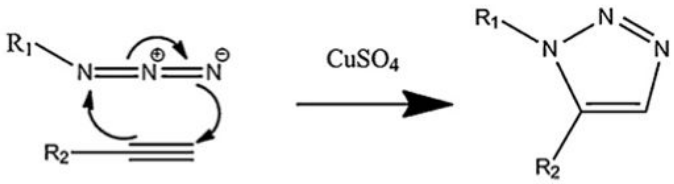

Azide and alkyne groups are highly inert towards biological molecules and they are easily introduced into organic compounds by nucleophilic and electrophilic processes (90). Azide-alkyne cycloaddition reaction is highly regioselective and promotes the spatial orientation of immobilized biomolecules. However, the disadvantage of this method is the fact that the immobilized (bio) molecule must be modified prior to their immobilization to a surface that might affect their affinity to the specific biomolecule.

3.2.2. Non-covalent coupling

Non-covalent conjugation between a molecule of interest and a biosensor surface includes electrostatic, hydrophobic/hydrophilic and affinity interactions. Non-covalent immobilization often results in a less stable immobilization. Affinity based interactions such as receptor – substrate recognition (e.g. biotin – avidin) or antibody – antigen detection are widely used since they are very robust and specific.

3.2.2.1. Ionic coupling

Ionic adsorption is a simple one-step method to immobilize molecules. Principally, charged biological species can be coupled to a surface with an opposite charge. Binding can be stronger when the amount of charges on the surface and the biomolecule is higher providing so-called multi-punctual binding (90). This method is directly related to the adsorption of negatively charged nucleic acids (e.g. DNA or RNA) to positively charged surfaces. Proteins such as antibodies can also be electrostatically adsorbed to the surface. This issue is directly related to their isoelectric point (pI) and the pH at which biological molecules are neutral (106). By varying the pH of a system, it is possible to couple a variety of proteins: cationic, anionic or neutral (105). However, this example also indicates the extreme sensitivity of ionic coupling technique and potential ease of biosensor degradation in variable conditions. This strategy is therefore rarely used for biosensing applications but it has to be taken into account as it often leads to non-specific interactions with a complex solution.

3.2.2.2. Hydrophobic coupling

Similar issues as ionic coupling concern also hydrophobic (and analogically – hydrophilic) interactions. Proteins and antibodies can be adsorbed to the hydrophobic surface directly or by previous modification with a functional hydrophobic group, for example cholate or cholesteryl (107). As in the case of ionic binding, hydrophobic conjugations also suffer from the need to modify native biomolecule that might affect its activity. Similarly, controlling the orientation and the amount of molecules is of paramount importance.

3.2.2.3. Affinity interactions

Immobilization *via* affinity interactions is based on the selective affinities of biological species that can be applied to surface functionalization. Herein three of the most often-used affinity-based conjugation strategies will be presented: biotin – avidin interaction, antibody – antigen interaction and immobilization *via* a histidine tag (35). Other techniques also used to conjugate biomolecules are: glutathione S-transferase (GST) tag and maltose binding protein (MBP) tag methods (108).

Biotin – avidin interactions. Biotinylation of surfaces or biological molecules is a common strategy as biotin can be easily introduced into oligonucleotides and proteins (109). The extremely high affinity of the avidin – biotin interaction ($K_d = 10^{-14}$ M) found broad applications in different biological domains, including the development of biosensors. The main method of bioconjugation using avidin–biotin chemistry comprises 'sandwich' reactions: functionalization of a surface with biotin, following by avidin immobilization and incubation with a biotinylated molecule (108) or direct functionalization of a surface with avidin, following incubation with a biotinylated molecule (Figure 1.20). Since avidin has a tetrameric structure and can bind up to 4 biotins, it is important to control the stoichiometry and characterize the density of immobilized molecules. It is worth to notice that avidin is a glycoprotein with a high isoelectric point ($pI_{avidin} \approx 10$) that in the following steps of biosensor development can promote nonspecific interactions. However, there are several analogues of avidin (streptavidin, extravidin or neutravidin) with lower pI that are not glycoproteins, for example streptavidin (90).

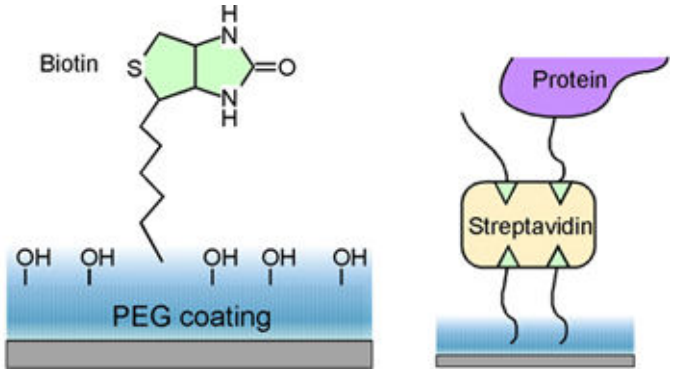

Figure 1.20. Immobilization of protein on the biotinylated surface. *Adapted from www.proteinslides.com*

Antibody – antigen interactions. The nature and specificity of antibodies can be used in biosensor applications in two different modes: directly as a sensing element to recognize and bind antigens or as a linker to immobilize (bio) molecules of interest. However, in both situations it is crucial to couple antibody to a surface to provide full accessibility to the antigen recognition site(s) (Figure 1.21).

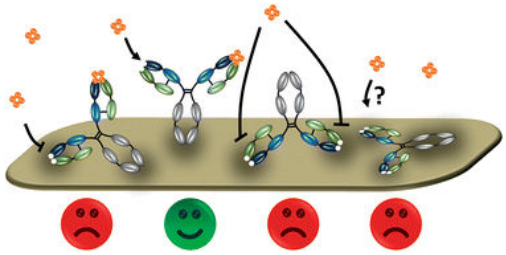

Figure 1.21. Random orientation of antibodies immobilized on the surface. *Adapted from (110).*

Histidine-tagged proteins. A widely-used non-covalent immobilization strategy comprises recombinant proteins (108). Genetic addition of six terminal histidine residues (6-His tag) in the C- or N-terminus of a protein acts as a chelating agent, which binds specifically to a metal cation immobilized on the surface. Recombinant polyhistidine proteins can be grafted to the surface through a nickel-chelated complex, e.g. Ni-nitriloacetic acid (NTA), as presented in Figure 1.22. The tetradentate ligand (NTA) forms a hexagonal complex with a metal cation (Ni^{2+}, Cu^{2+}, Zn^{2+}, Co^{2+}) leaving two binding positions for coupling of the 6-His sequence (89).

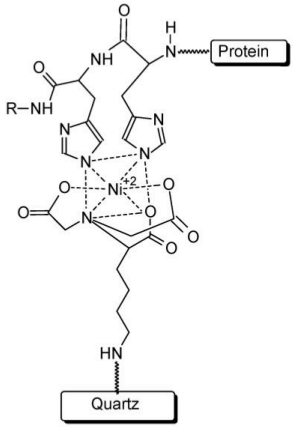

Figure 1.22. Binding of His_6-tagged protein to a functionalized surface. *Adapted from (89).*

4. Challenges for biosensor development

The development of surface based biosensors requires solving complex problems. A number of divers factors can play an important role in controlling the optimization of a device. Some of these aspects will be discussed below.

4.1. Complexity

An attractive possibility offered by biosensor technology is to mimic some extent conditions that are prevalent in a cell. However, it is difficult to precisely imitate *in vivo* conditions, thus a proper approximation is desired. Nevertheless, control of parameters, such as density, orientation, flexibility and surface rugosity coupled with changes in the local environment on the surface (pH, temperature, viscosity) offers unique possibilities to approach *in vivo* conditions. Furthermore, the enzymatic activity of biological molecules at or close to a surface may also be affected thus opening up novel functional interpretations.

Finally, an important point concerns the relationship between the actual copy number of biological species in a single cell and the situation on the biochip. The number of biomolecule copies in a cell is generally relatively low. For example, within a cell population a typical single cell contains from one (haploid) to two (diploid) copies of genetic material. In *E. coli* population, protein copy numbers range in average from 10^{-1} to 10^{4} per cell, while mRNA copy numbers from 10^{-3} to 10^{1} per cell. In *Saccharomyces cerevisiae*, cells were estimated to contain 10^{1} to 10^{5} copies of protein and only 10^{-1} to 10^{2} copies of mRNA. Similarly, in mouse fibroblasts, the copy numbers of protein and mRNA were calculated to be 10^{2} to 10^{8} and 1 to 10^{4}, respectively (111). On the other hand, the amount of (bio) molecules immobilized on a sensor surface or delivered to a chip is often a few orders of magnitude higher. Therefore, results obtained *in vitro* are averaged with the assumption that similar effects occur in crowded but heterogeneous cellular conditions.

4.2. Nonspecific interactions

Reducing or even eliminating nonspecific interactions in surface based biosensors is of paramount importance. Nonspecific adsorption in a biosensor can occur at two levels: during surface functionalization when a (bio) molecule is immobilized on the sensor surface or during the recognition event when an analyte is presented to the target at the surface.

Nonspecific interactions, especially in a quantification context can completely falsify the results. Firstly, because they introduce competing reactions to that which one is trying to fit to a specific model. Secondly, they can severely reduce the active concentration of analyte available for the specific interaction. Thirdly, nonspecific interactions between the surface and immobilized molecules can cause conformational changes that affect the active site and successively decrease the level of possible interactions. Finally, inefficient coupling of ligands to a surface can affect the function of the immobilized ligand and in many cases induces aberrant binding behavior.

As outlined above, surface chemistry and knowledge of the physical chemistry of the surface-liquid interface have a large extent attempted to solve these problems. In addition, other parameters must be optimized; one of the most important of these concerns microfluidics.

4.3.Microfluidic systems in the surface dependent biosensors

In resent years microfluidic systems have attracted significant attention in applications to many important fields, such as clinical diagnostics, chemical analysis, environmental monitoring, drug discovery or biosensing (112, 113). The main concept of microfluidic biosensors is to integrate the analytical functions necessary for biochemical analysis onto a chip, including sample preparation, surface pretreatment, detection of interactions and eventually separation or sorting of analytes. Microfluidics add numerous advantages in biosensing applications, including: reduced consumption of samples and reagents, laminar flow, improved kinetic analysis, sample recovery and homogenous distribution. The high surface to volume ratio enhances analyte mass transport, resulting in shorter assay processing time and increased detection limit (74). Additionally, biochemical reactions are more efficient due to the reduction of dilution

and diffusion effect. Microfluidic systems are easily automatized. Experiments may be sequenced and controlled for better efficiency and precision. However, it is important to note that analytes in microfluidic systems are exposed to extraordinary physical conditions, such as high surface tension or high interface-to-volume ratio. Therefore analytical information might significantly differ from that predicted or obtained by conventional bulky methods (114).

4.3.1. Plasmofluidic systems – microfluidics into SPR devices

The combination of microfluidics and plasmonics in sensing applications is well established and has been successfully applied into surface plasmon resonance (SPR) based biosensors (115). SPR technologies integrated with microfluidics are broadly commercialized, e.g. in BIAcore, Horiba or GWC systems. Customized SPR with modified fluidic systems have also been adapted to specific applications.

The combination of a multiplex array with microfluidics allows effective parallelization of numerous experiments on a single chip, e.g. in SPR imaging device or multi-microchannel SPR. Using a microarray with tens to thousands of samples examined at the same time notably reduces the procedure costs and analysis time.

An important advantage of microfluidic systems is the autonomy. Analyte flow rate, pressure and the injected volume can be modified. Multiple valve injectors allow complex experiments to be programmed where several samples are subsequently injected without introducing undesired dead volumes or any disturbance in the flow.

A microfluidic flow cell by definition is small, in the range of tens of microliters, thus it can be filled quickly with a reduced dilution effect. Although in principle a refractive index sensor is almost insensitive to volume changes of the sensing cell, the efficiency of a biosensor may be lowered by the rate at which analyte is transported to a transducer (116). Therefore, precision in cell design and an optimized flow rate are important to perform an efficient analysis.

The constant development of microfluidic based biosensors is of interest in many research groups. Fusion of microfluidics and plasmonics has been already successfully applied in SPR biosensors, ‘lab-on-a-chip’ and ‘point-of-care’ devices. Further progress in this field will be focused on both: improvement of sensing and finding new applications, including real sample detection and analysis.

4.4. Mass transport and analyte recapturing

Data obtained from SPR experiments generally cover the whole recognition process, including association and dissociation constants. Diffusion, mass transport and analyte rebinding are effects that may significantly disrupt the interpretation of kinetic data and the estimated rate constants obtained from SPR experiments. When the binding process is diffusion limited, the sensor detection limit and response time are altered by the analyte mass transport. The mass transport is dependent on numerous factors, including diffusion coefficient, analyte flow rate and flow cell dimensions (117).

The concentration of analyte passing from the bulk solution to the surface is not constant over time. Under certain conditions analyte concentration in the immediate vicinity of the sensing surface could be severely depleted. In this case (generally explained by a rapid association rate between the immobilized ligand and the analyte) the rate-limiting step becomes diffusion of the analyte from the bulk to the surface. As a result, the estimated association rate value actually reflects this rate rather than the chemical reaction (118). Additionally, after dissociation of the analyte from the ligand, the analyte can be eventually recaptured to an adjacent ligand thus reducing the apparent dissociation rate.

To identify and overcome this artifact, it is necessary to inject the analyte at different flow rates and/or decrease the density of immobilized ligands. High flow rate will prevent dilution of sample, reduce the height of the unstirred solvent layer and increase the transport rate of analyte to and from the surface (117). Low density of immobilized ligand will minimize crowding effects on the sensor surface and prevent analyte from being recaptured before complete dissociation. Another possibility is to include a mass transport effect as an additional step in the binding reaction:

$$A_0 \rightleftarrows A + B \rightleftarrows AB$$

The step $A_0 \rightleftarrows A$ stands for the transport of the analyte in the bulk solution to the sensor surface with a transport coefficient k_m, while $A + B \rightleftarrows AB$ stands for the binding of the analyte to the immobilized ligand on the sensor surface. This assumption allows better calculation of kinetic rates (96).

5. RNA metabolism and gene expression processes

The first step in gene expression involves production of RNA transcribed from a DNA template. The flow of genetic information is often presented by the so-called central dogma of biology (Figure 1.23). Information contained in a sequence of DNA is both replicated in order to duplicate the entire genetic material before cell division and transcribed selectively into RNA. Subsequent to transcription, information from the RNA sequence is decoded into a sequence of amino acids that build proteins during the translation process. RNA has three main roles in protein synthesis. First, messenger RNA (mRNA) carries information about the correct order of amino acids present in a synthesized protein that exists in a form of three successive nucleotides (this triplet is called a codon). Second, transfer RNA (tRNA) transports a specific amino acid and acts as a transducer interprets the information stored in mRNA with the help of a third type of RNA, ribosomal RNA (rRNA) to produce a linear sequence of amino acids.

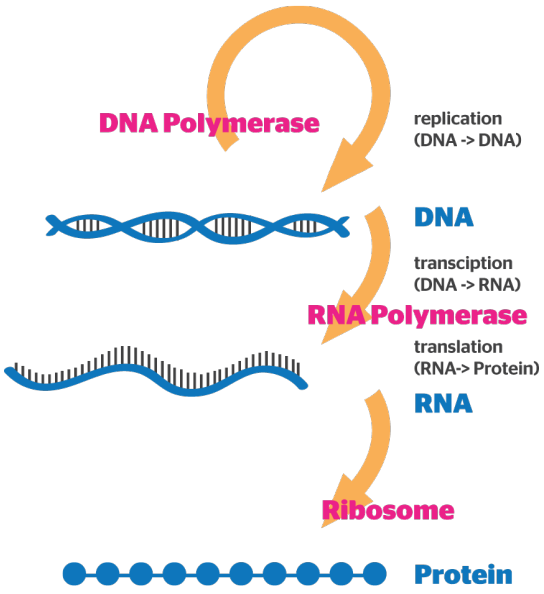

Figure 1.23. Central dogma of biology. *(Adapted from: www.primal-living.com.au)*

5.1. Gene expression in *Prokaryotes*

Gene expression is the entire process where the information encoded in DNA is transferred and decoded to produce proteins. This process differs significantly in its

details and complexity between *Archeae, Prokaryotes* and *Eukaryotes* and in this dissertation only that which concerns *Prokaryotes* will be described and discussed.

5.1.1. DNA-dependent synthesis of RNA

Unlike DNA polymerase, transcription of RNA by an RNA polymerase (RNAP) does not require a primer. Synthesis of RNA using DNA-dependent RNA polymerase (RNAP) is composed of three main phases: initiation, elongation and termination. Regulation of transcription occurs at each of these levels, however, the main focus of regulation of transcription occurs during polymerase binding and the initiation of transcription.

RNAP elongates an RNA strand by adding ribonucleotide units to the 3'-hydroxyl end, thus synthesizing RNA molecules in the direction 5' → 3'. The 5'-triphosphate group of the first residue in an RNA molecule is not cleaved to release a pyrophosphate (PP_i). 3'-oxygen in a growing RNA participates in a nucleophilic attack on the α-phosphate of a following ribonucleoside triphosphate (NTP) precursor, resulting in the formation of a phosphodiester bond and the release of a PP_i. The schematic reaction is as follows:

$$(NMP)_n + NTP \rightarrow (NMP)_{n+1} + PP_i$$

RNAP copies only one strand of the dsDNA to carry out RNA synthesis. During transcription two strands of DNA separate locally to create an open region that is transformed into a transcriptional bubble that in the case of *E. coli* RNAP is approximately 14 – 17 bp long (Figure 1.24). The template strand is copied in the 3' → 5' direction that is antiparallel to a newly synthesized RNA strand. The non-template (also called 'coding') strand has the same sequence as the nascent RNA transcript. Ribonucleotides are added to the sequence by Watson-Crick base-pairing selection and interactions with the template DNA strand. During the elongation phase of transcription, the growing RNA oligomer temporarily forms a short hybrid with a DNA template (~8 nt long) that is dehybridized followed by rewinding of two DNA strands (119). The elongation rate of a transcript by *E. coli* RNAP proceeds at 50 to 90 nt/s (120).

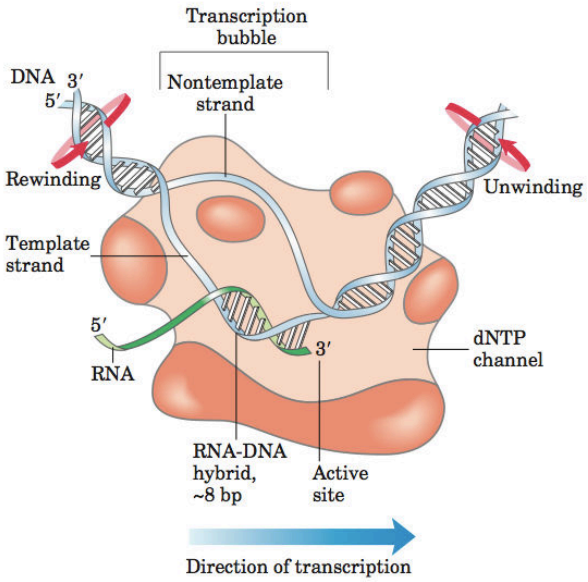

Figure 1.24. Transcription by *Escherichia coli* RNA polymerase. *Adapted from (121).*

E. coli RNAP does not have a separate proofreading 3' → 5' exonuclease active site (122, 123), thus the error rate for transcription is relatively high in comparison to DNA replication and corresponds to 1 in 10^4 or 1 in 10^5 mismatched ribonucleotides incorporated per nascent RNA (124). Since RNA does not store genetic information and is relatively quickly degraded and replaced, errors occurring in the RNA sequence are less important than in the case of genetic DNA replication. However, RNAPs pause while a mispaired base is added during transcription and mismatched nucleotides from the 3' end of RNA transcript are removed by direct reversal of the polymerase reaction (121).

5.1.2. Promoter site recognition

RNAP interacts with a specific sequence of DNA – promoter – recognized as the DNA region to which the enzyme binds and where transcription starts. Promoters control the transcription of all genes. In the most common class of bacterial promoters two or more functionally important sequences upstream of the transcription start site are recognized by RNAP. In *E. coli*, these are located at positions -10 ('Pribnow box') and -35 (125). These regions of DNA interact specifically with the σ subunit family of bacterial RNAP and undergo conformational changes during formation of a transcriptionally competent initiation complex. Although such sequences are not the

same for all classes of bacterial promoters, certain nucleotides are commonly present and generally AT-rich consensus sequences are present, namely: TATAAT for the -10 region and TTGACG for the -35 region (126) (Figure 1.25). Another characteristic region is the GCGC discriminator responsible for stringent and growth regulation (127). The majority of mutations occurring in the consensus sequences have a significant influence on the efficiency of RNAP binding and transcription initiation.

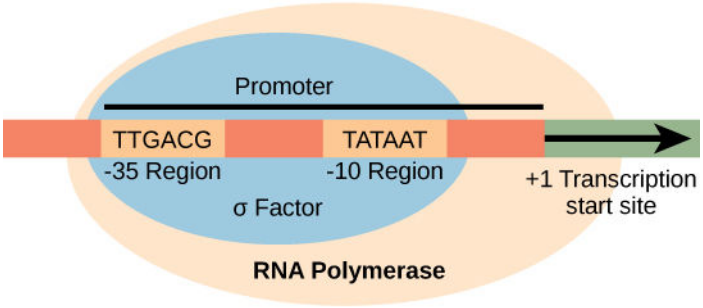

Figure 1.25. DNA promoter sequence interacting with the σ subunit of *E. coli* RNAP. *Adapted from www.boundless.com*

5.1.3. Transcription initiation phase

Transcription initiation, which is one of the main steps in RNA synthesis, is composed of two major parts: recognition and binding of RNAP to the DNA specific site, and transcription initiation.

Promoter search by RNAP on the DNA sequence involves a combination of 2-D and 3-D diffusion processes implying sliding, hopping and intersegment transfer (128, 129) as is presented in Figure 1.26.

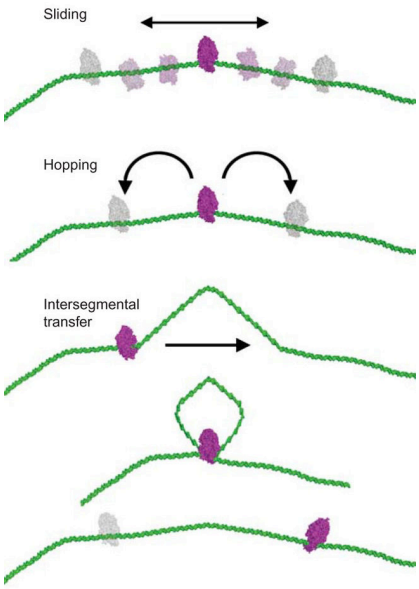

Figure 1.26. Protein movement along a DNA template in order to localize a binding site. From top to bottom: sliding, hopping and intersegmental transfer of a protein. *Adapted from (129).*

The transcription initiation process is complex and consists of several intermediate states (130):

$$R + P \rightleftarrows RP_C \rightleftarrows RP_O \rightleftarrows RP_{init} \rightleftarrows TC$$

In this scheme, R stands for RNAP, P – promoter, RP – transcribing complexes, RP_{init} – the initiating transcription complex and TC – the elongation complex. After recognition of the promoter sequence, RNAP interacts with a promoter DNA forming a thermodynamically unstable closed complex (RP_c) which further isomerizes into a thermodynamically stable locally melted open complex (RP_o) (131-133). Conformational changes accompany the transition from the initiation to the elongation phase of transcription. This transition causes the movement of the transcription complex away from the promoter site (this process is also called promoter clearance).

However, before the complex leaves the promoter definitively, abortive and repetitive initiation occurs and results in the synthesis and release of numerous short transcripts. After formation of the first RNA phosphodiester bond, RNAP may be trapped in an abortive mode (134, 135). The enzyme can initiate transcription and elongate a

few nucleotides (from 2 to 16 nt) without dissociating from the promoter. If the promoter clearance step is slow, short oligomers are released and re-initiation can occur many times before a runoff transcript is produced (136). The distribution and amount of the abortive initiation products vary significantly depending on the DNA template and RNAP.

5.1.4. Transcription elongation phase

In *Prokaryotes*, the movement of the transcription complex away from the promoter site and start of the elongation phase are tightly associated with the rearrangement of the RNAP structure. The spatial orientation of the transcription complex components changes significantly during the transition from the initiation to the elongation phase that takes place when 9 – 12 nt of nascent RNA are synthesized (137). This transition is associated with σ^{70} subunit translocation. The σ^{70} subunit is either stochastically released from the transcription complex (138, 139) or remains associated, however its affinity for the complex decreases (140, 141). The associated σ^{70} factor continues scanning DNA for the promoter-like sequences that may induce transcriptional promoter-proximal pausing (142, 143).

Afterwards, the RNAP proceeds along the template DNA, melting the downstream dsDNA without the necessity of a separate helicase protein, and hybridizing the strands behind.

The rate of RNA elongation is non-uniform: pausing, arresting and termination during RNA synthesis occurs regularly (144). Pausing is a temporary delay in RNA synthesis that is modulated by various supporting proteins or other types of signals (145, 146), such as interactions between a nascent RNA hairpin and an RNAP (147). Pausing is considered to be an important element of the control of gene expression through the regulation of the rate of transcription elongation.

5.1.5. Transcription termination phase

Control of specific termination of RNA synthesis is essential in order to not release pre-mature RNA transcript that would enable the synthesis of a protein. Therefore *Prokaryotes* have developed two main transcription termination processes: factor ρ-

dependent and ρ-independent (Figure 1.27).

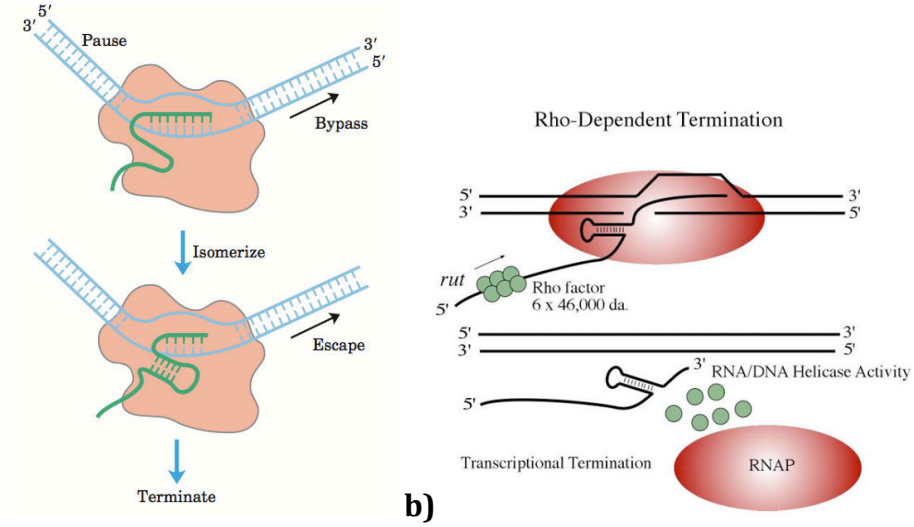

Figure 1.27. Model of **a)** ρ-independent termination of transcription; **b)** ρ-dependent termination of transcription. *Adapted from (121) and www.bio.miami.edu.*

In ρ-independent transcription (also 'intrinsic') termination, synthesized RNA transcript has a self-complementary sequence that forms a GC-rich hairpin structure of length of 15 to 20 nt (Figure 1.27a). This structure causes conformational changes leading to structural isomerization, followed by transcription termination and nascent RNA dissociation (148, 149).

In the case of the ρ-dependent terminators (Figure 1.27b), ρ factor (an RNA – dependent ATPase (150)) interacts with a nascent RNA and migrates until it reaches a transcription complex in the termination site where it participates in releasing of an RNA oligomer (151-153). However, the overall mechanism of ρ mediated termination is still largely unknown.

5.1.6. Regulation of RNA transcription and gene expression in *E. coli*

Transcription is the first step in the complex and energy-requiring pathway of gene expression and protein synthesis. In order to economize energy, this process must be strictly controlled and regulated, especially in the early initial stages.

The *E. coli* genome encodes for more than 250 additional regulatory proteins that participate in the control of RNA transcription and gene expression *in vivo.* They are generally called transcription factors and usually are grouped as activators and repressors (154). One of the major activator proteins in *E. coli* is the cAMP receptor protein that increases the transcription of genes coding for enzymes that participate in the metabolism of sugars other than glucose in the absence of glucose in the cell (155). Similarly, the lac repressor is one of the best-characterized repressors that blocks transcription of certain genes for lactose metabolism during the absence of lactose (156).

5.2. *Escherichia coli* RNA polymerase

Escherichia coli is a model organism used in numerous studies concerning biochemical and biophysical processes that occur in *Prokaryotes*. Nowadays, RNA transcription and the structure of *E. coli* RNAP are relatively well characterized and described in the literature.

5.2.1. Construction of *E. coli* RNA polymerase

The DNA-dependent RNA polymerase (RNAP) of *E. coli* is a multisubunit protein consisting of four subunits ($\alpha_2\beta\beta'\omega$) of a molar mass 390 kDa in the core enzyme and a fifth variable subunit – σ in the holoenzyme. This holoenzyme (Figure 1.28) integrates several functions into a single molecular machine: recognition and binding to the specific sequence on the promoter, separation of dsDNA during the initiation of transcription and progressive synthesis during elongation.

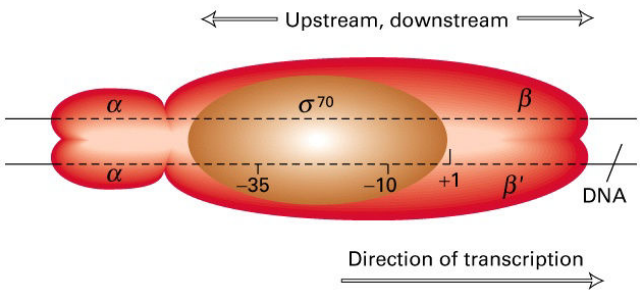

Figure 1.28. Schematic presentation of *Escherichia coli* RNA polymerase. *(Adapted from www.namrata.co)*

5.2.1.1. Sigma subunit

The σ subunit interacts transiently with the core enzyme and promotes specific binding to the DNA promoter site. It is responsible for the initiation of transcription by formation of an open complex and entry of RNAP into a transcription start point on the DNA (157). When the σ subunit is released, it leaves a core RNAP engaged in a growing, nascent RNA chain. This leads to the start of the 'sigma cycle' (158).

The σ subunit in *E. coli* RNAP exists in several forms, however the most common is a 'housekeeping sigma' σ^{70}, so named because of its molar mass of 70 kDa. *E. coli* RNAP holoenzyme can be constructed also with other σ factors, such as σ^{32} (32 kDa) that interacts with heat-shock genes and is specific to heat-shock promoters (159) or σ^{54} that occurs during a nitrogen starvation and recognizes promoters for genes encoding enzymes needed for recycling of organic nitrogen compounds (160). Using different σ subunits coordinates the expression of various genes in a cell, depending on the cell's physiology and various stress conditions. A host of different σ factors exist in a range of prokaryotic organisms (161).

5.2.1.2. Other subunits

The subunits that constitute the *E. coli* RNAP core enzyme have a well documented role in enzyme structure and function (162). Available crystallographic data of the core and holo enzymes have produced high resolution models of the 3D structure of RNAP and provided information on the role of individual subunits (163). For instance, the α subunit recognizes an AT-rich recognition element within DNA promoters located in the region between -40 and -60 (with respect to start site for RNA production) of certain highly expressed genes and the large subunits β and β' form the catalytic active center of the enzyme. The ω subunit is not essential for transcription, however it stabilizes the enzyme by assisting in subunit assembly.

5.2.2. *Lac*UV$_5$ promoter

Extensive studies of the fine positioning of RNAP on the *lac*UV$_5$ promoter have allowed a detailed characterization of transcription in *E. coli*. *Lac*UV$_5$ is a relatively strong promoter that has been well described in terms of the recognition process and the formation of a kinetically competent transcription complex (164). It contains mutations that allow efficient transcription in the absence of cAMP (165). Kinetic stages of interaction between the *lac*UV$_5$ promoter and *E. coli* RNAP at 37°C are schematically presented as:

$$\mathrm{R} + \mathrm{P} \underset{k_{-1}}{\overset{k_1}{\rightleftarrows}} \mathrm{RP_c} \underset{k_{-2}}{\overset{k_2}{\rightleftarrows}} \mathrm{RP_i} \underset{k_{-3}}{\overset{k_3}{\rightleftarrows}} \mathrm{RP_o}$$
$$K_{\mathrm{I}} \qquad K_{\mathrm{II}} \qquad K_{\mathrm{III}}$$

where the major species at equilibrium is an open complex of RNAP and promoter (RP$_o$) and the major transient species is a closed complex (RP$_c$) (166). The rate-limiting step in this reaction is an isomerization corresponding to the k_2 step and open complex formation (k_3) is not limited by the rate at which DNA is locally melted. The overall kinetic binding constant (K_B) at 37°C for RNAP on *lac*UV$_5$ promoter in solution was established to be 160 μM (164). The regions of DNA template reacting directly with RNAP include the -10 and -35 sequences (132), however the whole footprint for RNAP in an open complex extends to more than 50 nt in length (165, 167).

5.3. T7 RNA polymerase

T7 RNAP encoded by the bacteriophage T7 is a single subunit enzyme of molar mass 98.8 kDa. Thanks to its relative simplicity, it is commonly used as a model system for biochemical and biophysical studies of a transcription process and the structure of DNA-dependent RNAP. The enzyme is very active *in vivo* and *in vitro*, using both linearized and supercoiled DNA templates. T7 RNAP is highly selective for its promoters and it is capable of transcribing any DNA template linked to its promoters without any additional proteins (168).

The highly conserved 23-nucleotide sequence (TAATACGACTCACTATAGGGAAA) recognized as a T7 promoter is situated from -17 to +6 on the template DNA with respect to the start site of transcription (169). Although the consensus promoter

sequence ends at -17, footprinting experiments suggested protein-DNA contacts as far back as -21 (170).

Simplified initiation kinetic studies suggest a two-step DNA binding mechanism:

$$R + P \underset{k-1}{\overset{k1}{\rightleftharpoons}} RPc \underset{k-2}{\overset{k2}{\rightleftharpoons}} RPo \xrightarrow{NTPs} RNA$$

where RNAP (R) binds to the DNA promoter (P) and forms a closed complex (RP_c) that isomerizes fast to an open complex (RP_o) followed by the synthesis of RNA in the presence of four ribonucleotides (NTPs: ATP, UPT, GTP and CTP) (169, 171).

T7 RNAP also enters into an abortive cycling phase of transcription and synthesizes a large amount of small oligoribonucleotides of lengths from 2 to 12 nt (172). T7 RNAP has an elongation rate *in vitro* of ~230 nt/s (173) that is about six times faster than that from *E. coli* RNAP.

5.4. Kinetic characterization methods

Initial studies on the kinetics and physical properties of *E. coli* RNAP were carried out by McClure in the 1980s (136, 174). They were performed by measuring steady state kinetics (164, 174). Since that time, numerous techniques have been used to characterize interactions occurring during the transcription process, including: abortive initiation assays, kinetic burst experiments, filter binding assays, footprinting and chemical modification of DNA, quantitative transcription, template competition assays or stopped flow kinetics (175). However, the majority of these techniques have limitations, such as studies in a bulk or homogenous solution that are not compatible with *in vivo* conditions that are known to be extremely crowded and in a heterogeneous and variable environment. Therefore, surface plasmon resonance (SPR) techniques have recently attracted significant attention as a robust alternative for the analysis of nucleoprotein interactions in real time in very confined conditions (40, 175) that may artificially simulate a crowed environment. SPR is used to measure small changes in refractive index linked to the mass variations occurring on the sensor surface. This technique serves for measuring interactions between DNA immobilized on the surface and proteins in solution and can be used to monitor binding of RNAP to DNA templates, forming the active initiation or elongation complex (40, 66).

A precise kinetic analysis provides additional information about transcription complex formation during the RNA synthesis. It allows monitoring of changes in the gain or loss of mass that is associated with events occurring during transcription, such as release of a sigma subunit (in *E. coli* RNAP), synthesis of RNA transcript and release of RNAP and nascent RNA during the termination.

OBJECTIVES AND MOTIVATIONS

Gene expression is a crucial process occurring in each living cell and leads to the synthesis of a functional gene product based on the information stored in the genetic material and transferred during multiple steps, involving transcription, translation and protein maturation. The process is highly regulated at each level but a major part of the control is associated with the initial phase of transcription where DNA is copied to RNA transcripts by the DNA-dependent RNA polymerase (RNAP). Although the transcription process is relatively well characterized especially in *Prokaryotes*, many elements concerning RNAP and its interactions with the DNA template remain poorly understood, especially with respect to the dynamics of promoter recognition, escape and elongation in a cell like context where molecular density, concentrations and nearest neighbour effects are prevalent.

The goal of this thesis was to develop a robust method that would allow real time monitoring of RNAP activity *in vitro* in thoroughly controlled conditions. Special attention has been focused on surface-based biosensors that could be used to characterize the main steps of the transcription reaction: recognition and binding of RNAP to a specific promoter sequence of DNA, subsequent isomerization and formation of a transcription complex, transcription and synthesis of an RNA strand and finally termination.

Optofluidic surface-based biosensors are known from their high sensitivity and the possibility of real time process monitoring, factors that are extremely useful for affinity determination and kinetic analysis. For example, in Surface Plasmon Resonance (SPR), the principles of detection are based on the real time monitoring of differences in the reflectivity of p-polarized light at a fixed angle due to changes in mass at the interface between the sensor surface and its surrounding solution. These changes necessarily occur between a ligand (e.g. DNA template) immobilized on a sensor surface and an

analyte (e.g. RNAP enzyme) passed over the surface in a microfluidic system. In addition, under *in vitro* conditions in an SPR apparatus, parameters such as temperature, flow rate and composition of the system may be strictly controlled, and indeed the density and orientation of ligands immobilized on the surface could be arranged to approach as much as possible the crowded environment of a living cell.

However, in order to control conditions during the transcription process in surface-based biosensors special attention has to be paid to the specific immobilization procedure of ligands on a biochip surface. Consequently, to obtain information about the density, specificity and accessibility of immobilized ligands, a detailed characterization of the functionalized surfaces was carried out. Two distinct surfaces - polymer coated glass and thin gold layers were biofunctionalized and characterized prior to immobilization of DNA strands in a controlled manner, using a self-assembled monolayer (SAM). Several strategies were tested in order to determine the most reliable functionalization method and to obtain a wide range of surface densities – depending on the desired application.

Functionalized surfaces were used to monitor in real time, the kinetics of transcription with two proteins: a monomeric T7 RNAP and a multisubunit *E. coli* RNAP. Kinetic analysis was performed to compare the rates of nucleoprotein complex formation and transcription process carried out by these polymerases. Studies were performed using immobilized DNA oligomers with a specific promoter site as a template. Various conditions were tested to obtain relevant kinetic information, for instance the length of the immobilized DNA, the position of the specific promoter sequence with respect to the point of immobilization and the direction of subsequent transcription, i.e. either towards or away from the surface. To confirm that RNA transcription on immobilized DNA fibres took place in the SPRi apparatus, relevant products were collected, detected and characterized.

The future development of this project would involve continuous improvement of biosensors dedicated to *in vitro* gene expression. Special attention will be focused on the adaptation of the methods and strategies put in place here to other optofluidic systems (e.g. micro ring based resonator or total internal fluorescent reflection microscopy) that would give additional information about the interactions. The final goal is controlled RNA synthesis that would be an intermediate step to investigate real time *in vitro* protein production.

Chapter II

MATERIALS AND METHODS

1. Surface fabrication and characterization

All surfaces presented and discussed in this manuscript were fabricated in a clean room from the Institut d'Alembert at the Ecole Normale Supérieure of Cachan. The clean room has a cleanliness class of 100 000, 50% rate of hygrometry and a constant temperature at 21°C.

1.1. SU-8 surface fabrication

SU-8 photoresist polymer surfaces were fabricated on 2-inch silicon wafers (ACM-PVD, France) and microscope glass slides as described in (176). Briefly, before the deposition procedure, silicon wafers were cleaned for 10 min in the UVO-Cleaner (model 42-220, Jeligth, USA) and glass slides were cleaned with ethanol and acetone followed by cleaning in UVO-Cleaner for 10 min. 2 – 3 µm thick SU-8 films were obtained by spin-coating of SU-8 2002 solution (Micro-Chem, USA) with the following program: 7 s at 500 rpm with acceleration 100 rpm/s, followed by 30 s at 3000 rpm with acceleration 300 rpm/s using Spin-Coater RC8, Suss MicroTech. In order to evaporate a remaining solvent, films deposited on Si wafers were softbaked on a hotplate for 1 min at 65°C, followed by 2 min at 95°C and films deposited on glass slides were softbaked on a hotplate for 6 min at 65°C. Samples were flood-exposed in UV light for 15 to 30 s, using

the UV-Aligner MJB4, Suss MicroTech. Post-exposure baking on a hotplate was performed for 1 min at 65°C, followed by 3 min at 95°C for a silicon wafer and 6 min at 95°C for a glass slide. Samples were hardbaked in the oven under three different conditions: at 90°C for 5 h, at 120°C for 3 h or at 180°C for 2 h. The thickness of prepared surfaces was controlled with a contact profilometer (see Section 2.1.3). Surfaces were stored under nitrogen or used directly in experiments.

1.2. Gold surface fabrication

Glass slides with evaporated gold thin layers were used to characterize biomolecule immobilization methods. Glass prisms with a high refractive index (SF 10; n=1.707987 at λ=830 nm) were used as a substrate in experiments with a Surface Plasmon Resonance imaging (SPRi). Prisms and microscope glass slides were cleaned by sonication in isopropanol, followed by cleaning with acetone, drying in a nitrogen flow and a 5-minute treatment in UVO-Cleaner. The surface of the microscope glass slide was activated by Reactive Ion Etching (RIE) at 30 mT for 10 min followed by thermal evaporation of few nanometers chromium and 50 nm gold layer at the pressure $6.5 \cdot 10^{-6}$ mbar. The clean prism surfaces were activated by Reactive Ion Etching (RIE) prior to thermal evaporation of a 50-nm gold layer. Prepared surfaces were stored under nitrogen.

1.3. Surface characterization

The thickness of freshly prepared SU-8 or gold layers was controlled by a height profile measurement with a Dektak 150 Surface Profiler, Veeco. Thin scratches through the coating gold or SU-8 layer to the surface of a glass slide, prism or silicon substrate were made using a semi-sharp tool. The samples were placed in the stage and the position of the stylus was adjusted and placed close to the scratched area. The surface was scanned by the stylus with a width of 500 – 1000 μm using the profile 'Hills and Valleys'. The differences in height between a plain surface and a scratched area were calculated with applied software.

Additionally, the surface topography and the rugosity before and after activation pre-treatment of the SU-8 thin film (description in the following Sections) were

controlled by an atomic force microscopy (AFM) Veeco nanoscope V equipped with microcantilever tips OMCL-AC240TS-R3 (Olympus, Japan). Measurements were performed in tapping mode with a scan rate of 1 Hz and scan sizes of 1 and 5 µm. Images were taken at a minimum of three randomly selected areas. The software Nanoscope was used for the post-measurement analysis: option 'Section' was selected to calculate a root mean surface roughness (spectral RMS amplitude).

Water contact angle measurements were performed to characterize the hydrophobicity of the SU-8 surfaces. Measurements were carried out with a Digidrop MCAT Analyser (GBX, France). All measurements were taken at room temperature. 0.5 µl of deionized water droplets were dispensed from a needle and the water contact angle was calculated on captured images 500 ms after the drop deposition on the SU-8 surface. Each given value was the average of five consecutive water contact angle measurements.

2. Surface functionalization and strategies of biomolecule immobilization

SU-8 thin films and gold thin layers surfaces were functionalized in order to immobilize biomolecules in a stable and controlled manner.

2.1. Amide bond formation

Amide bonds are covalent bonds that are formed when the hydroxyl group from a carboxylic acid is replaced by amine or ammonia. Here, amide bonds were formed between the carboxylic group present on a surface and the amine group ($-NH_2$) present on the (bio) molecules: tetramethylrhodamine cadaverine (tamra-cadaverine; Invitrogen – Molecular Probes) or DNA-NH_2 (oligonucleotide modified with an amine group at 5' end).

Functionalization of SU-8 surface. 2-µm-thick SU-8 film was exposed to UV/ozone treatment using UVO-Cleaner (low pressure mercury vapor grid lamp: 28,000 µW/cm^2 at 254 nm). Exposure of the sample lasted from 15 s to 20 min. Pretreated surfaces were

immersed in a diluted solution of EDC/NHS (ratio 1:1; EDC: 0.4M N-[3-Dimethyl-aminopropyl]-N-ethylcarbodiimide hydrochloride; NHS: 0.1M N-Hydroxysuccinimide; both purchased from Sigma-Aldrich) for 30 – 60 min. After rinsing with double distilled water, two protocols were applied: (i) samples were incubated for 1 to 2 hours either directly with 10 µM tamra-cadaverine in 10 mM sodium acetate buffer (NaOAc) pH 5.2 or with 1 to 10 µM oligoDNA-NH_2 in PBS (phosphate buffer saline) buffer or (ii) samples were incubated for 1 to 2 hours with 0.1 mM $CA(EG)_8$ or $CA(EG)_{24}$ (carboxy-amine n-ethylene glycol solutions, Thermo Scientific) diluted in water. PEGylated SU-8 surfaces were then immersed in the EDC/NHS solution for 1 h and rinsed with a buffer solution or sonicated in a buffer solution twice for 2 min before incubation with tamra-cadaverine or DNA-NH_2 as described previously. Unreacted activated carboxyl groups on the surface were blocked by incubating the surface with 1 M ethanolamine pH 8.5 for 10 min.

Functionalization of gold surfaces. Glass slides or glass prisms with a 50-nm gold layer were immersed in a solution of 0.1 mM 1-undecanethiol substituted with a hydroxyl-terminated tetra(ethylene glycol) (11-mercaptoundecyl tetra(ethylene glycol), *EG-OH*; Sigma-Aldrich) diluted in ethanol for exactly 30 s and rinsed thoroughly with ethanol for 30 min. The gold surfaces were then immersed in a solution of 1 mM $S(CH_2)_{11}(OCH_2CH_2)_6$-COOH (*EG-COOH*, Prochimia, Poland) for 5 – 120 min and rinsed thoroughly with ethanol for 30 min. Carboxylated pre-functionalized gold surfaces were activated with EDC/NHS as described above for the SU-8 surfaces. 10 µM tamra-cadaverine in 10 mM NaOAc buffer pH 5.2 or oligoDNA-NH_2 of different concentrations diluted in 0.4 M phosphate buffer pH 7.0 were incubated on the surface for 0.5 to 2 h in a humid chamber in order to avoid spot drying. Unreacted activated carboxyl groups on the surface were blocked by incubation with 1 M ethanolamine pH 8.5 for 10 minutes.

2.2. Hydrophobic coupling with cholesteryl and cholate moieties

SU-8 thin film and pre-functionalized gold surface were used as a support for immobilization of cholesteryl- and cholate-modified (bio) molecules based on hydrophobic interactions.

Synthesis of cholate- and cholesteryl-modified (bio) molecules. (i) DNA oligomers modified with a tetraethylene glycol cholesteryl (TEG-chol) group in 5' end were purchased from Eurogentec. (ii) Tamra-cholate (tamra-chol) was synthesized by mixing 100 µM tamra-cadaverine and 100 µM Na-deoxycholate in different ratios and their coupling with 0.4 M EDC and 0.1 M NHS for 2 hours. Analytical thin layer chromatography was performed on aluminum-percolated plates of Silica Gel 60F-254 in order to verify the efficiency of synthesis tamra-chol molecule. A mixture of acetone/dichloromethane/methanol (3:1:1) was used as eluent.

Pre-functionalization of gold surface. Glass slides or glass prisms with a 50-nm gold layer were immersed in the solution of 4.5 mM 1-undecanethiol (Sigma-Aldrich) diluted in ethanol for 16 h to create a dense and highly hydrophobic self-assembled monolayer. Samples were then rinsed with ethanol for 30 min.

(Bio) molecule immobilization. Different concentrations of DNA-chol and tamra-chol in water, PBS or phosphate buffer were incubated with SU-8 thin film or pre-functionalized gold surface from 1 min to 2 hours and rinsed with an appropriate solution (water, PBS or phosphate buffer, respectively).

2.3. Gold – thiol bond formation

Immobilization of DNA oligomers modified with a thiol group in 5' end (DNA-SH) was performed with a protocol adapted from (37). Briefly, a 50-nm gold layer was immersed in a solution containing 0.1 mM of 11-mercaptoundecyl tetra(ethylene glycol) (*EG4-OH*) diluted in ethanol for exactly 30 s. Afterwards, the gold surfaces were thoroughly rinsed with pure ethanol for 30 min. The DNA solution in water or 0.4 M phosphate buffer pH 7.0 was spotted on the pre-treated surface at different concentrations and incubated overnight in a 100% humid chamber to prevent the DNA solution from drying.

2.4. ExtrAvidin – biotin bond formation

Glass slides or glass prisms with a 50-nm gold layer were immersed in a solution containing 0.1 mM of 11-mercaptoundecyl tetra(ethylene glycol) (*EG4-OH*) diluted in

ethanol for exactly 30 s and rinsed thoroughly with ethanol for 30 min. The gold surfaces were then immersed in a solution of 1 mM $^{-}S(CH_2)_{11}(OCH_2CH_2)_6$-biotin (*EG-biot*, Prochimia, Poland) for 5 – 120 min and rinsed with ethanol for 30 min. Surfaces were incubated for 1 hour with 1 to 100 nM extrAvidin (Sigma-Aldrich) diluted in PBS and rinsed gently with PBS buffer. Biotinylated oligonuceotides (DNA-biot) were incubated on the surface for 0.5 to 2 h in a humid chamber in order to avoid spot from drying.

3. Immunodetection of biomolecules immobilized on a surface

The interaction between an antigen immobilized on the surface and an antibody delivered to the surface with a microfluidic flow was tested to confirm the specificity of molecule grafting on the surface and their accessibility for interacting. Modified tetramethylrhodamine (tamra) molecule and its specific monoclonal antibody – anti-tetramethylorhodamine rabbit IgG fraction (anti-tamra, Invitrogen Molecular Probes) were used to model the antigen – antibody reaction.

3.1. Detection on SU-8 surface by fluorescence intensity variation

SU-8 thin films pre-treated as described in Section 2.2.1 were used to immobilize 10 µM tamra-cadaverine (in 10 mM NaOAc buffer pH 5.2) with 1% *v/v* glycerol. Spots of tamra-cadaverine of diameter ~300 µl were deposited using a Vikalex Spotter (Vikalex Technologies, France). 10 µg/ml of anti-tamra diluted in PBS buffer was incubated on the tamra-cadaverine functionalized SU-8 film before the surface was rinsed with 10 mM glycine–HCl pH 2.0 to remove retained antibodies. All reactions were performed under liquid on the protected SU-8 surface; microfluidic flowcells were prepared on the glass slides using Sticky Slides VI$^{0.4}$ (Ibidi, Germany). Three cycles were carried out for the reaction between immobilized tamra-cadaverine molecules and anti-tamra in the microfluidic flowcell, followed by surface regeneration with a glycine solution. Fluorescence images were recorded using an inverted epifluorescence microscope (Leica MicroSystems) equipped with a 4× objective and fluorescence filters suitable for tamra (excitation bandpass 510 – 560 nm, emission bandpass 590 – 680 nm). The average fluorescence intensity was calculated using ImageJ Software (NIH) after

subtracting a background for each spot.

3.2. Detection on a gold surface by SPRi

0.2 to 1 µl spots of 10 µM tamra-cadaverine were deposited and incubated for 0.5 to 2 hours on the 50 nm gold layer pre-treated as described in Section 2.2.1. 0.2 to 1 µl spots of 10 µM tamra-chol were incubated for 0.5 to 2 hours on the 50 nm gold layer pre-treated as described in Section 2.2.2. Glass prisms were introduced into the Surface Plasmon Resonance imaging apparatus (SPRi-plex, GenOptics – Horiba; detailed description of SPRi-plex specification can be found in Chapter I, Section 1.1.3.1) and incubated for 2 hours with PBS as the running buffer. Different concentrations of anti-tamra diluted in PBS buffer were injected to the microfluidic flow with a flowrate of 25 µl/min and flowed across the immobilized tamra molecules for 6 min. Variations in mass detected on the gold surface – liquid interface were recorded as the difference in relative reflectivity signal. Obtained data were analyzed with BIAevaluation and OriginLab softwares; curves were fitted to a simple Langmuir binding model to obtain kinetic constants.

4. Oligonucleotides and molecular biology methods

Oligonucleotides listed below were used to characterize the biofunctionalized surfaces, to amplify desired DNA fragments and for molecular cloning. The sequence of initially used plasmid (pIVEX 2.3d) can be found in Appendix 1.

4.1. Oligonucleotides for characterization of surface biofunctionalization strategies

Modified and non-modified oligonucleotides were used to verify the density and specificity of dsDNA adsorbed to the surface depending on the DNA length (50, 500 and 1000 bp) and analyzed surface chemistry. Short (50 bp) oligonucleotides and primers were purchased from Eurofins and Eurogentec. Oligonucleotides were modified on the 5’ end with amine (-NH_2), thiol (-SH), biotin (-biot) or tetra-ethylen glycol cholesteryl (-

chol) groups and non-modified (-OH). Additionally, a pentathymine spacer (-*5T*-) was introduced between the functional 5‘ end group and the DNA sequence.

The shortest oligonucleotides (50 bp) were hybridized by heating the two complementary strands in a molar ratio of 1.1:1 of modified to non-modified strand respectively, for 10 min at 95°C in a PBS or 0.4 M phosphate buffer (pH 7.0) and slowly cooled down to the room temperature. Longer DNA fragments (500 and 1000 bp) were obtained by amplification in 30-cycle standard PCR reactions using one modified (‘primer rev’) and one non-modified primer (‘primer for’). Plasmids ‘pIVEX-UV5’ and ‘pIVEX-NiRFP’ were used as matrices to amplify fragments of 500 and 1000 bp, respectively.

Table 2.1. Sequences of oligonucleotides and primers used to amplify DNA fragments that were applied for characterization of gold surface (bio) functionalization methods. Sequences ‘50bp DNA’ and ‘Primer rev SH’ were separated from a functional group by the presence of a pentathymine spacer (-*5T*-).

Name	Modification	Exact length (bp)	Sequence (5’ → 3’)
50bp DNA	OH/NH_2/SH/biot/ chol	55	-*5T*- TCC ATC AGT CAC TCG CCG GAT CCA TCT TGA GAC TCT GTC ACA CGT AGT CG
50bp DNA-comp	OH	50	CGA CTA CGT GTG ACA GAG TCT CAA GAT GGA TCC GGC GAG TGA CTG ATG GA
500bp DNA	OH/NH_2/SH/biot	495	*Sequence can be found in Appendix 1.1.*
1 kbp DNA	OH/NH_2/SH/biot	1037	*Sequence can be found in Appendix 1.1.*
Primer for	OH	19	TCC GGC GTA GAG GAT CGA G
Primer rev	OH/NH_2/biot	23	GGA TAT CCG GAT ATA GTT CCT CC
Primer rev	SH	23	-*5T*- GGA TAT CCG GAT ATA GTT CCT CC

4.2. Strategies of plasmid constructions and oligonucleotides for plasmid constructions

All constructed plasmids were generated from a commercially available plasmid pIVEX2.3d (Roche) dedicated to high level expression His_6-tagged proteins in a cell-free Rapid Translation System (RTS) *E. coli* system. Restriction endonuclease and T4 DNA ligase (New England Biolabs) were used according to the standard protocols.

Plasmid pIVEX 2.3d-NiRFP was generated by a double digestion of pIVEX 2.3d plasmid with XhoI and NdeI endonucleases and ligation of NiR-FP gene amplified by PCR from a plasmid pNirFP-N, kindly obtained from Dr. Feifei Liang and Dr. Michael Tovey in the LBPA.

Plasmid pIVEX 2.3d-UV5 was generated by PCR amplification of a sequence of pIVEX 2.3d plasmid, excluding the T7 promoter sequence. Ligation of a 203 bp $lacUV_5$ promoter into the amplified fragment was performed with In-fusion enzyme (Clontech Laboratories) according to a standard protocol.

Plasmid pIVEX 2.3d-UV5-NiRFP was generated from pIVEX 2.3d-UV5 plasmid by a double digestion of pIVEX 2.3d-UV5 plasmid with XhoI and NdeI endonucleases, followed by ligation of NiR-FP gene amplified by PCR from a plasmid pNirFP-N.

All plasmids were transformed into XL10 gold or BL21 (DE3)pLysS competent *E. coli* strains according to the standard protocol and plate into LB agar plate containing 100 µg/ml ampicillin. Separate clones were inoculated in 3 ml of LB media containing 100 µg/ml ampicillin. Plasmids were purified from 3 ml overnight *E. coli* cultures in LB media using MiniPrep Purification kit (Qiagen). Cloned sequences and mutations were verified by DNA sequencing (Eurofins MWG Operon).

4.3. Labeling and modifications of DNA oligomers

Oligonucleotides and primers were purchased from Eurofins and Eurogentec. They were modified at the 5' end with amine (-NH_2), thiol (-SH), biotin (-biot) or tetra-ethylene glycol cholesteryl (-chol) groups and non-modified (-OH). Additionally, the functional group was separated from the relevant sequence by a pentathymine spacer (-*5T*-).

^{32}P-α ATP nucleotide was used to label DNA oligomers at the 5' end. 25 µl DNA at a high concentration (usually 100 µM) was incubated with 4 µl ^{32}P-α ATP and 2 µl polynucleotide kinase (PNK, New England Biolabs) in 50 µl reaction mix at 37°C for 30 min and afterwards purified using Bio-Spin 6 size exclusion microcolumn (BioRad).

^{32}P-γ ATP nucleotide was used to label DNA oligomers at the 3' end. 25 µl DNA at a high concentration (usually 100 µM) was incubated with 4 µl ^{32}P-γ ATP, 2 µl transferase terminal (New England Biolabs) and 5 µl $CoCl_2$ in 50 µl reaction mix at 37°C for 30 min and afterwards purified using Bio-Spin 6 size exclusion microcolumn (BioRad).

5. RNA synthesis and kinetic analysis of formation DNA – RNA polymerase complexes

RNA synthesis reactions were performed with special attention to keep RNase-free conditions. RNA synthesis was carried out with two DNA-dependent RNA polymerases (RNAP): (i) bacteriophage T7 RNA polymerase (T7 RNAP, Thermoscientific) and (ii) *Escherichia coli* RNA polymerase holoenzyme (*E. coli* RNAP, Tebu-bio). Circular plasmids or DNA oligomers as listed in Appendix 1.3 were used as a matrice to synthesize RNA strands.

5.1. *In vitro* RNA synthesis and characterization

a) With bacteriophage T7 RNAP. Double stranded DNA (100 ng – 1 µg) was incubated at 37°C for 1 – 24 hours with T7 RNAP (50 nM – 2 µM; Thermoscientific), 1 U/µl nonspecific RNase inhibitor (Ribolock, Thermoscientific), 0.5 – 2 mM of three ribonucleotides (ATP/GTP/CTP), 0.495 – 1.99 mM UTP and 0.005 – 0.02 mM fluorescein-12-UTP (Roche) in a buffer containing 40 mM Tris-HCl (pH 8 at 25°C), 6 mM $MgCl_2$, 10 mM NaCl and 2 mM spermidine. The reaction mix was then incubated with 2 U of DNase I (Thermoscientific) at 37°C for 30 min in order to remove DNA template. The reaction was stopped by adding one volume of deionized formamide and heating at 95°C for 5 min.

b) With *E. coli* RNAP. Double stranded DNA (100 ng – 1 µg) was incubated at 37°C for 1 – 24 hours with *E. coli* RNAP (1 – 5 nM, tebu-bio), 1 U/µl nonspecific RNase inhibitor, 0.5 – 2 mM of four ribonucleotides (ATP/GTP/CTP/UTP) with or without

0.125 – 0.5 mM ApA (iba Lifescience) in a buffer containing 20 mM HEPES (pH 8.4 at 25°C), 10 mM $MgCl_2$, 100 mM KCl. The reaction was then incubated with 2 U of DNase I at 37°C for 30 min in order to remove DNA template. The reaction was stopped by adding one volume of deionized formamide and heating at 95°C for 5 min.

c) RNA characterization. Electrophoresis in agarose gel was performed to characterize the product of RNA synthesis. The reaction mixed with one volume of deionized formamide as described above was heated at 95°C for 5 min, rapidly cooled down on ice and directly loaded on a 1.5% agarose gel in 1x TAE buffer (40 mM Tris pH 7.6, 20 mM glacial acetic acid, 1 mM EDTA) that was pre-run for 15 min at 50 V in 1x TAE buffer. Samples were mixed with a loading buffer (1 mg/ml ethidium bromide, 60% glycerol, 1 mM EDTA pH 8.0). Gels were scanned in Typhoon Imager with two filter settings: (i) excitation at 532 nm and emission at 526 nm to visualize a signal from fluorescein and (ii) excitation at 532 nm and emission at 610 nm to visualize a signal from ethidium bromide.

5.2 Characterization of interactions DNA – RNAPs using SPRi

Monitoring the interactions between DNA and RNA polymerases using the SPRi-plex GenOptics apparatus was performed in order to characterize the kinetics constants of transcription reactions and analyze products of those reactions obtained while DNA was immobilized on the surface.

Plasmids containing a RNAP promoter sequence (see Appendix 1.3) were amplified by standard PCR reactions with one non-modified and one modified primer in order to obtain two orientations of oligomers immobilized on a surface as schematically presented in Figure 2.1. 1 µM of amplified DNA was immobilized in a gold prism using one of the surface chemistry approach described in Sections 2.2.1, 2.2.3 and 2.2.4.

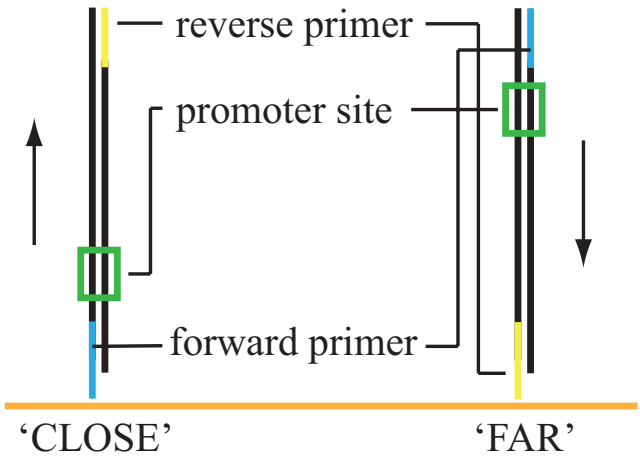

Figure 2.1. Orientations of DNA oligomers immobilized on the surface through the primer modified on 5' end using one of the strategies for biomolecule immobilization (see Section 2). Blue – forward primer, yellow – reverse primer, green box – promoter sequence. Arrows show the direction of RNAP movement; 'close' and 'far' stand for the position of the promoter site with respect to the surface.

Prisms placed in the SPRi apparatus were incubated at 37°C in an appropriate running buffer to equilibrate the system. Reaction mixtures were composed as described in Section 2.5.1a and b with the absence of DNA. They were injected to the microfluidic flow with a flowrate of 25 µl/min and flowed across the gold surface with immobilized DNA oligomers for 6 min. Variations in mass detected on the gold surface – liquid interface were recorded as the difference in relative reflectivity signal. Data were analyzed with BIAevaluation and OriginLab softwares; to obtain kinetic constants curves were fitted to a suitable binding model.

5.1. Synthesis of RNA using SPRi

All materials (pre-functionalized prism, buffer compositions and reaction mix) were prepared as described in the previous Sections. 1 µM of DNA oligomers were deposited and incubated on the prism. The reaction mixture was injected into the microfluidic system with a flowrate of 25 µl/min, flowed across the gold surface with immobilized DNA oligomers during 6 min or the flow was stopped for about 15 hours. Afterwards, the flow was re-started and the through-flow was collected at 0.5 or 1 min intervals. The

collected fractions were mixed with one volume of deionized formamide and analyzed by agarose gel electrophoresis as described in Section 2.5.1 c.

Chapter III

SURFACE BIOFUNCTIONALIZATION CHARACTERIZATION STUDIES

1. Introduction

Surface-dependent biosensors belong to the largest and most diversified group of biosensing devices. This group comprises mechanical, electrochemical and optical biosensors. Typically, one or several ligands are immobilized specifically on a biochip surface and their interactions with analytes delivered to the system in solution are analyzed and translated into a digital response. It is therefore imperative that special attention is paid to the properties of the biosensor surface (the biochip).

In the design of biosensor surfaces many characteristics need to be taken into consideration including hydrophilicity/hydrophobicity, roughness, and the amount of accessible functional groups. In general developments, functionalization can be universally applied to both, 2- and 3-dimensional objects (e.g. flat surfaces, micro- and nanoparticles). However, each method must be optimized for the particular case due to the complexity of the biosensor field. As a general principle, functionalized supports must be biologically inert, limiting non-specific interactions to a minimal level and optimizing parameters such as the density and accessibility of immobilized molecules.

In the present studies two substrates were functionalized, characterized and applied to biosensing: negative photoresist polymer SU-8 films and thin gold layers. SU-

8 polymer has been employed in a micro ring based resonator technique where it was used to detect interactions between immobilized antigen and antibodies in solution (20). Thanks to its unusual optical properties, especially concerning low levels of auto fluorescence (177), functionalized SU-8 thin films have also been applied as supports in total internal reflection fluorescence (TIRF) microscopy to monitor interactions between (bio) molecules at a single molecule level (Chapter I, Section 1.2.3.2). On the other hand, functionalized thin gold layers are commonly used in SPR technology for detection and monitoring of biomolecular interactions. Functionalization of both types of surfaces has been developed in parallel in order to apply them to the subject of this thesis, namely to attempt to follow *in vitro* gene expression. The main goal of this thesis was carry out real time monitoring and attempt kinetic analysis of various steps in protein production, especially RNA transcription. Following Sections in this Chapter will describe the characterization of various methods applied to functionalization of SU-8 and gold surfaces. Special attention was been paid to determine the density and accessibility of immobilized molecules as well as the level of non-specific interactions and the optimization of the approach was designed with this in mind.

2. SU-8 surface biofunctionalization by UV/ozone (UVO) activation

Thin films of SU-8 negative photoresist polymer were functionalized by exposure to UV/ozone (UVO) radiation. The hypothesis was that this pre-treatment method was effective in breaking surface-exposed epoxy groups and, by creation of hydroxyl and carboxyl groups, increased the hydrophilicity and enhanced functionality of the polymer film. Analysis of the SU-8 thin film after UVO pre-treatment was performed in order to characterize the properties of activated SU-8 surface and establish optimal conditions to control covalently bound molecules.

Covalent immobilization of two distinct molecules *via* amide bond formation was characterized. Firstly, a small fluorescent molecule – tamra-cadaverine was adsorbed on the pre-treated surface in order to obtain data about the density and accessibility of immobilized ligands. Secondly, DNA oligomers modified with amine groups were immobilized to determine if the functionalization method was universal and could be

transferred to other applications in biosensing, different than those already described micro ring based resonator (20).

These studies have been published (176). A copy of this peer-reviewed article can be found in Appendix II.

2.1. Characteristics of SU-8 negative photoresist polymer

SU-8 (Figure 3.1) is a negative photosensitive polymer with a low Young's modulus and excellent chemical and thermal stability, widely used in the manufacture of extremely robust microstructures, essentially microfluidic systems and bioMEMS (178, 179). Moreover, the optical properties of SU-8, i.e. its thermal resistance and transparency in the near UV and visible light, coupled with its relatively low refractive index compared to silicon-on-insulator (SOI) technologies, make it an ideal material for optical waveguides and the development of label-free biosensors (20, 180).

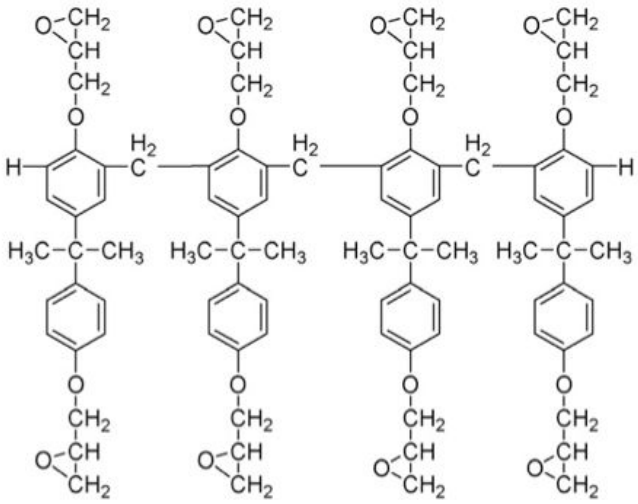

Figure 3.1. Chemical structure of the SU-8 polymer.

However, the surface of SU-8 is highly hydrophobic, thus incompatible with many applications in biotechnology due to nonspecific interactions of (bio) molecules (181-183). Therefore, SU-8 surface modifications have been developed to enhance its wettability and to allow controlled immobilization of (bio) molecules of interest (184-187). Modifications consist essentially of activating SU-8 surfaces using wet or dry pre-

treatment methods for subsequent control of (bio) molecular adsorption. Wet pre-treatment methods involve a cross-linker that reacts directly with free epoxy groups present on the SU-8 surface (185, 187) (Figure 3.1) or with hydroxyl and/or carboxyl groups generated by acid and/or alkali treatment (183-185). Dry pre-treatment methods use oxygen or ammonia plasma treatment (188) or pyrolytic dissociation of ammonia in a hot wire chemical vapor deposition (HWCVD) setup (186). Nevertheless, both wet chemical and dry surface techniques increase the surface roughness significantly. This is detrimental for liquid distribution in a static fluid micro device and it results in an unsteady secondary flow in a flowing micro channel (189, 190). In addition, surface roughness induces optical loss in waveguides due to scattering on sidewalls (191), and promotes non-specific adsorption of (bio) molecules to the surface (177).

Biofunctionalization of the thin (~2 μm) SU-8 film that was developed during these studies was carried out using two distinct methods: covalent (bio) molecule grafting to the surface pre-treated with UV/ozone (UVO) exposure, followed by amide bond formation, and non-covalent immobilization of cholesteryl- and cholate-modified molecules based on hydrophobic coupling to the SU-8 surface. SU-8 surfaces, functionalized with these methods have found applications as a support to immobilize ligands in optofluidic biosensors, such as micro ring resonator (20). Additionally, results from the hydrophobic coupling method could be applied directly to the functionalization of the 50-nm thin gold layer used in Surface Plasmon Resonance imaging (SPRi).

2.1.1. UV/ozone (UVO) surface pre-treatment

UV/ozone (UVO) treatment is an inexpensive, fast and convenient method applied to modify the surfaces of various polymers (192-194). Although, short UVO treatment has relatively weak oxidizing power, exposure to UV radiation increases the polymer surface energy by breaking molecular bonds on the surface (e.g. in epoxy groups) and ozone aeration which adds polar oxygen atoms to create carboxyl and hydroxyl groups (194). It increases the hydrophilicity and improves wettability properties. UVO exposure is applied as a robust pre-treated method to activate the surface, followed by molecule adsorption or immobilization.

2.2. Characterization of SU-8 surface after UV/ozone treatment

SU-8 polymer thin film was exposed to UVO in order to improve its reactivity and to optimize its use in biology related applications, such as surface-based biosensors.

To prepare a thin SU-8 layer, the solution of monomeric SU-8 2002 was spin-coated on a glass or silicon substrate, followed by hard-baking in three different conditions: 90°C for 5 h, 120°C for 3 h and 180°C for 2 h in order to access a range of cross-linking densities on the SU-8 polymer surface (195, 196). The degree of SU-8 reticulation, and thus the amount of reactive epoxy groups present on the surface, was largely dependent on the hard-baking step (195-197). Such-hard-baked surfaces were exposed to UVO for 15 s up to 20 min. The influence of UVO exposure time on SU-8 surface properties was tested by measuring surface thickness with a profilometer, determining wettability by water contact angle (wCA) measurements, defining its roughness with atomic force microscopy (AFM) and identifying surface-exposed functional groups with Fourier Transform Infra-Red (FT-IR) spectroscopy.

All methods and materials were used as described in Chapter II, Section 1. The thickness of freshly spin-coated and hard-baked SU-8 films was systematically measured prior to experiments. The preparation protocol of an SU-8 layer led to an SU-8 film thickness of 2 µm ± 15% that was taken as a standard value used in all further works.

Water contact angle (wCA) technique measures wettability of smooth surfaces: the more hydrophobic the surface, the lower the value of wCA. wCA allowed characterization of the evolution of the SU-8 surface energy for each UVO exposure time. As shown in Figure 3.2a, starting from a wCA of 83.5° ± 1.5°, independently from the hard-baking conditions and in agreement with published data (183, 185, 197), the wCA decreased below 30° after 10 min of UVO exposure and reached a plateau around 22° after 20 min of UVO treatment.

The increase of surface energy of the SU-8 surface after UVO treatment might be explained by the creation of polar groups at the SU-8 surface upon oxidation (197). The use of a surface-profiling stylus demonstrated that the thickness of the SU-8 layer was not affected even after 20 min of UVO exposure (data not shown). In addition, it has been demonstrated that the optical properties of an SU-8 waveguide (a crucial factor in the development of micro ring resonator biosensors) were not altered by such UVO treatment (20). The wCA measurements were extremely reproducible and no significant

difference between the left and the right wCA (±0.3°) could be measured (Figure 3.2b), indicating that the UVO treatment did not affect the SU-8 surface roughness.

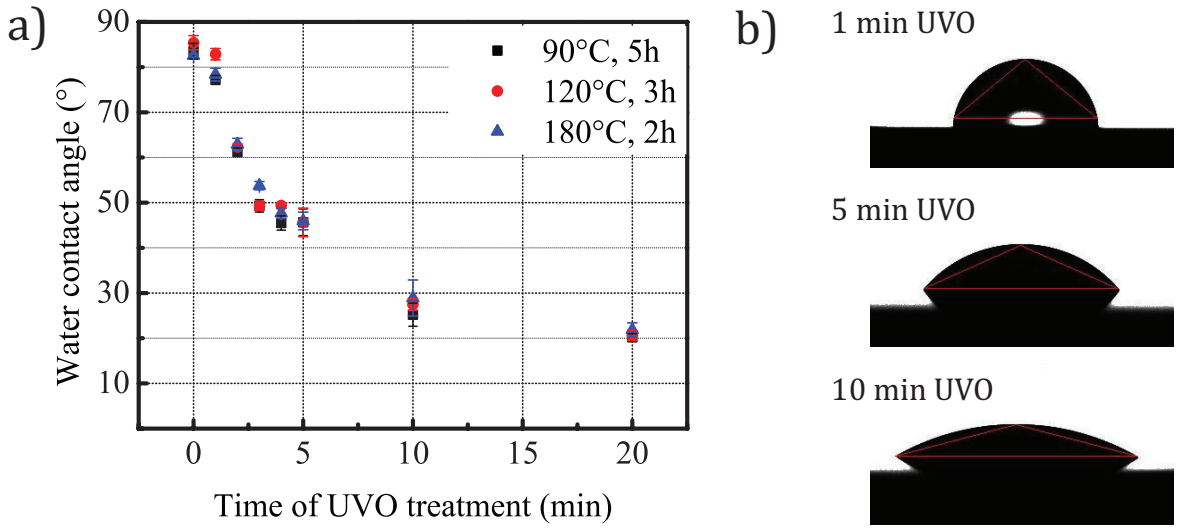

Figure 3.2. (a) Variation of the wCA with increasing UVO exposure time of SU-8 thin film prepared with three different hard-baking conditions. Each data point corresponds to the average of five wCA measurements. **(b)** Examples of water droplet geometries deposited on the SU-8 surfaces hard-baked at 120°C for 3 h and exposed to UVO for 1, 5 and 10 min (from top to down, respectively). The images were taken 500 ms after placing the drop on the surface.

Roughness is an important factor for the characterization of surfaces for biosensing applications. It can increase significantly the surface area, thus the molecular density and accessibility of immobilized ligands would be different than in the case of a 2-dimensional atomically flat surface. However, if the surface roughness is smaller than the size of molecules, one can assume a two-dimensional geometry of the area that is desired for the determination of the number of (bio) molecules bound to the surface. Surface roughness values may be obtained directly from surface-profile or AFM measurements (198). AFM provides images of surface topography by mechanically moving a probe tip across the sample to detect the morphology of the surface. Data can then be analyzed in a dedicated software program to identify various parameters, such as root-mean-square (RMS) roughness and peak-to-valley roughness.

Here, to characterize the roughness surface of the SU-8 thin layer, both peak-to-valley and RMS roughness were measured by AFM on three SU-8 samples before and after UVO treatment. Figure 3.3 shows AFM images and the corresponding height profiles with the RMS roughness analysis of SU-8 thin film hard-baked at 120°C for 3 h before and after 5 min of UVO treatment. The SU-8 surface before UVO was homogeneous, with a peak-to-valley roughness of 1.7 nm and a RMS roughness of 0.121 nm (Figure 3.3a). After 5 min under UVO, the surface remained homogeneous with a peak-to-valley roughness of 1.9 nm and a RMS roughness of 0.144 nm (Figure 3.3b). In addition, post-exposure hard-baking conditions had no significant influence on the SU-8 surface roughness before and after UVO treatment time (Figure 3.3c).

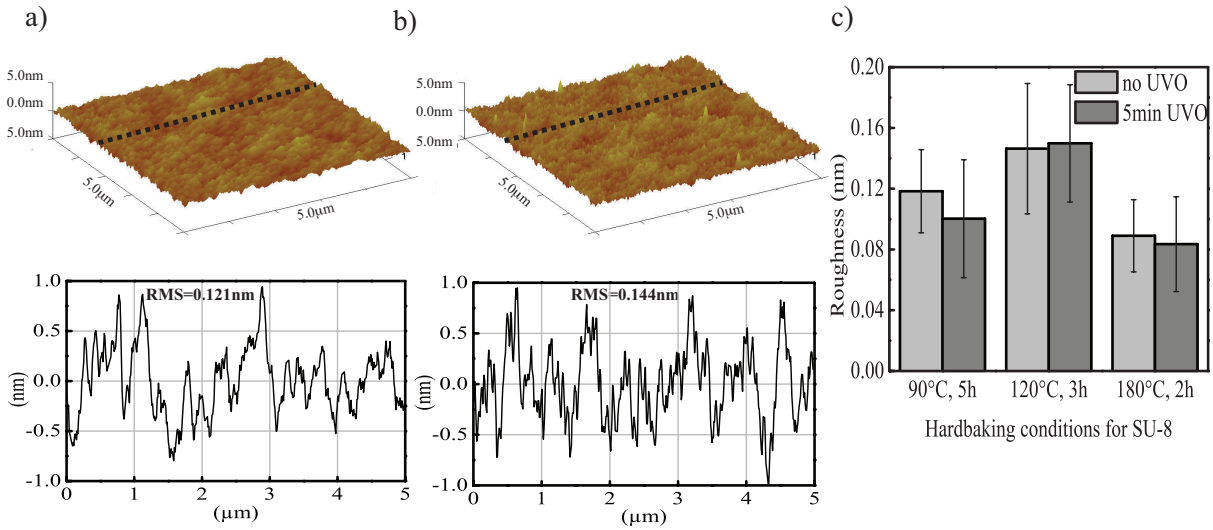

Figure 3.3. AFM topography images and height profiles of SU-8 surfaces hard-baked at 120°C for 3 h: **(a)** before UVO treatment and **(b)** after 5 min of UVO treatment. Dotted lines indicate where the height profiles were taken. **(c)** Comparison of the root-mean-square (RMS) roughness for SU-8 films hard-baked with different conditions. Standard deviations were calculated based on three randomly selected areas; four height profiles per area were taken.

Fourier Transform Infra-Red (FTIR) spectroscopy is a method commonly used to identify functional groups in samples. The absorption peaks correspond to the frequencies of relevant bond vibrations present in the molecules constituting the

material. In the case of SU-8 polymer films, the most relevant signals are listed in Table 3.1.

Table 3.1. Vibration frequencies of typical groups found in SU-8 polymer, analyzed by FT-IR spectroscopy.

Vibration frequencies [cm^{-1}]	**Corresponding functional group**	**References**
862 – 913	Epoxy ring	(199)
1030 – 1295	C–O and C–O–C	(195)
1502 – 1608	Phenyl group	(186, 199)
~ 1700	C=O (from carbonyl group)	(197)

FT-IR spectra performed before and after 30 s and 5 min UVO exposure (Figure 3.4) demonstrated significant changes in the intensity of several peaks. While the intensity of peaks corresponding to the long molecular chains of SU-8 polymer was not affected by UVO treatment, significant variations were observed for peaks corresponding to epoxy groups and to carboxyl groups (197). As the UVO treatment time increased, the intensity of the signal from the epoxy groups decreased concomitantly with an increase in peak intensity corresponding to carboxyl groups.

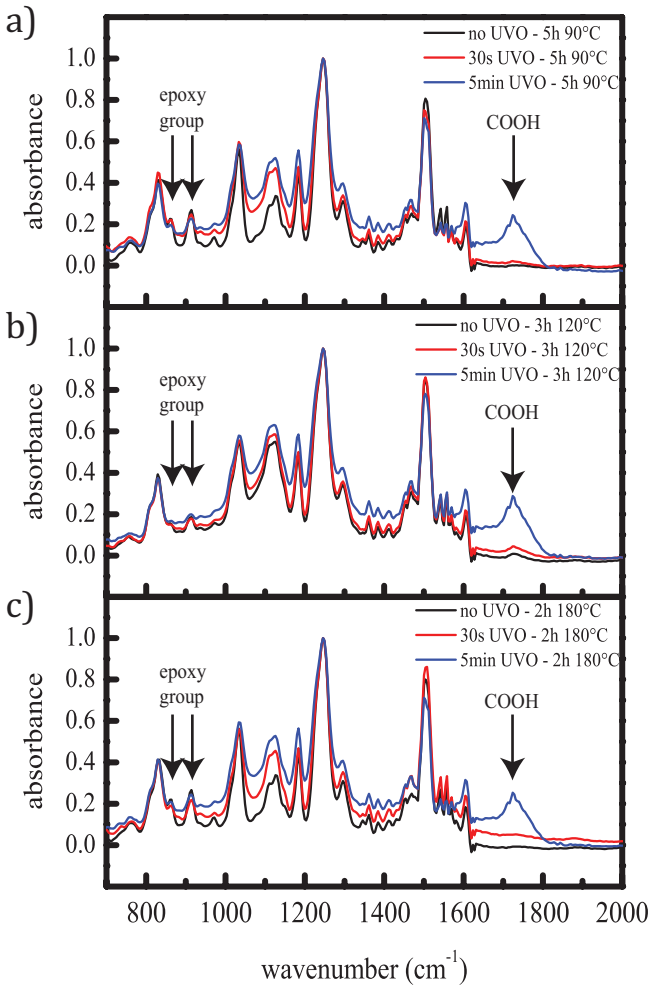

Figure 3.4. FT-IR spectra of SU-8 film prepared with three hard-baking conditions: **(a)** 5 h at 90°C, **(b)** 3 h at 120°C, **(c)** 2 h at 180°C; before and after 30 s and 5 min of UVO treatment. Peaks of epoxy (862 and 913 cm^{-1}) and carboxyl groups (wide peak around 1700 cm^{-1}) are indicated with arrows. All spectra were normalized to the peak at 1246 cm^{-1}.

Most of the epoxy groups within the thin SU-8 layer were cross-linked during the post-exposure baking step (197), thus it was deduced that the small peak intensities of the epoxy groups corresponded to epoxy groups present on the surface of the SU-8 film. In addition, the increase in carboxyl group peak intensity after 5 min of UVO treatment was larger than the decrease in the intensity of the epoxy groups peaks, indicating that oxidation of SU-8 was reaching the bulk of the SU-8 layer after relatively long UVO exposure times (5 min). Therefore, activation of the SU-8 surface with 30 s UVO exposure time should allow efficient (bio) molecule immobilization.

Of particular interest was that, although there was the presence of carboxyl groups and lower peak intensities corresponding to epoxy groups on the SU-8 film hard-baked at 120°C for 3 h before UVO treatment, yet no carboxyl groups were detected on the SU-8 film prepared under the other two hard-baking conditions. The presence of carboxyl groups on the SU-8 surface could be due to oxidation of epoxy groups at the surface and/or to the presence of some residual solvent from the thin SU-8 film (195). This observation was, in both hypotheses, coupled with a lower peak intensity of the epoxy group on the surface of SU-8 hard-baked at 120°C for 3 h than with the other hard baking conditions.

FT-IR revealed that changes in the oxidation state of the SU-8 layer occurred both at the surface and in the bulk of the SU-8 film for long UVO exposure times (up to 5 min). While the amount of reactive epoxy groups on the SU-8 surface was defined by the degree of reticulation of the polymer upon the post exposure hard-baking, the surface density of carboxyl groups could be potentially controlled by short UVO exposure time (30 s). Consequently, the exposure time of SU-8 microstructure to UVO should allow modulation of the surface density of subsequent (bio) molecules following chemisorption.

2.3. Covalent binding of tamra-cadaverine to the surface

The potential of binding (bio) molecules on UVO activated SU-8 thin films was tested with the chemisorption of tamra-cadaverine. Tetramethylrhodamine 5-carboxamide (tamra) cadaverine contains a diamine cadaverine that has one free amine group and one attached to a fluorescent rhodamine moiety (Figure 3.5). Tamra-cadaverine molecule has two distinctive features that were used here. Firstly, free amines can react with an activated carboxyl group (e.g. *via* EDC/NHS-mediated reactions) to form an amide bond, therefore demonstrating the ability of binding biological molecules that possess free amine groups (DNA, proteins, antibodies, peptides). Secondly, the fluorescent property of tamra-cadaverine (absorption wavelength 545 nm and emission wavelength 580 nm) allows quantification of the number of immobilized molecules. Additionally, the tamra residue has a dedicated antibody (‘anti-tamra’) used in quenching-based assays (200) that allowed recognition of specific antibody – antigen interactions.

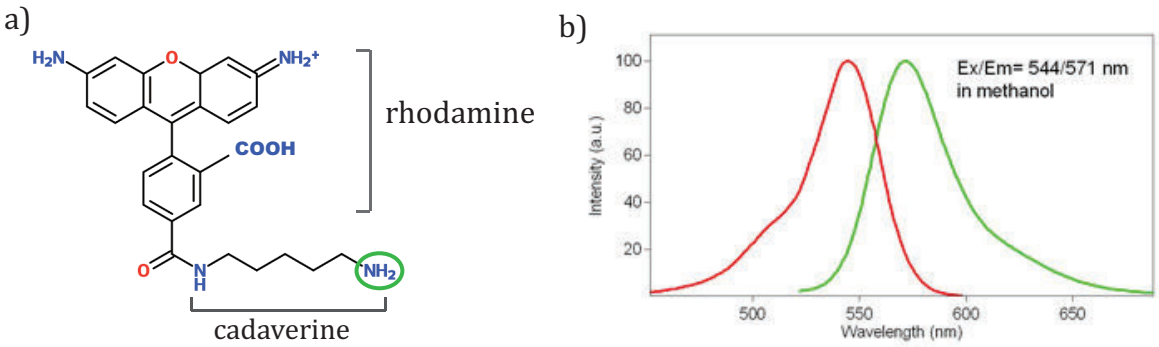

Figure 3.5. (a) Tetramethylrhodamine 5-carboxamide (tamra) cadaverine molecule with pointed rhodamine and cadaverine groups. An amine group used to couple carboxyl group on the SU-8 surface is marked with a green circle. **(b)** Spectra of tamra-cadaverine excitation and emission. Peak maxima occur at 544 and 571 nm for excitation and emission, respectively.

Tamra-cadaverine was bound to activated SU-8 surfaces through specific reactions with carboxyl groups *via* an EDC/NHS-mediated coupling. Amide bonds formed at the interface provided a useful model to quantify the amount of molecules immobilized on the surface by measuring the intensity of tamra fluorescence when excited at 580 nm. All procedures were performed as described in Chapter II Sections 1 – 3, including: SU-8 substrate preparation, surface exposition to UVO for time from 0 to 5 min, and chemisorption reaction: incubation of the SU-8 surfaces with a solution of EDC/NHS for 60 min, thoroughly rinsing with distilled water and incubation with 10 µM solution of tamra-cadaverine for 60 min. Samples were then dipped in a buffer solution (10 mM sodium acetate buffer, pH 5.2) and either agitated for 20 min twice or sonicated twice for 2 min in the same buffer. The density of tamra-cadaverine grafted on SU-8 surface was calculated based on a calibration curve (Figure 3.6): the fluorescence signal of 1 µl of tamra-cadaverine solution in increasing molarities was measured to obtain a linear calibration curve. The used concentration range was chosen according to the intensity of fluorescent signals from analyzing samples (using a Typhoon scanner). Therefore the calibration curves and the number of moles per unit area for each sample were within the same intensity range that allowed calculation of the number of molecules per unit area with relatively good approximation.

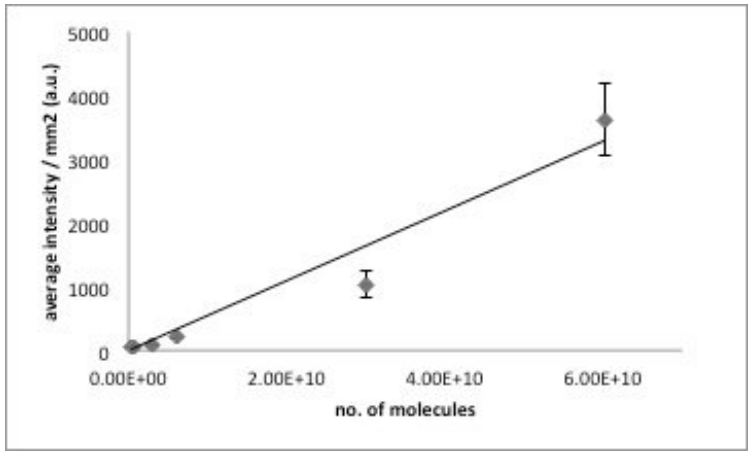

Figure 3.6. Example of a calibration curve of tamra-cadaverine concentration range used to deduce the density of immobilized tamra-cadaverine molecules.

The influence of UVO treatment time on the density of tamra-cadaverine molecules immobilized on the SU-8 sample hard-baked at 120°C for 3 h is shown in Figure 3.7a. For the SU-8 not exposed to UVO treatment, the density of surface retained tamra-cadaverine was not negligible. In addition, the surface molecular density after sonication was significantly lower than for samples rinsed thoroughly and agitated in a large volume of buffer, indicating that the retained molecules were covalently attached to the SU-8 surface. It followed that the presence of residual reactive epoxy and carboxyl groups at the interface, highlighted by FT-IR (Section 2.1 and Figure 3.4), was in itself sufficient to allow some specific binding. Secondly, the molecular density on the surface increased for UVO treatment shorter than 1 min and decreased significantly with longer exposure. In all cases, removing most non-covalently bound molecules *via* sonication of samples strengthened the observation that the UVO exposure of SU-8 surfaces between 30 s and 1 min created the highest density of reactive carboxyl groups at the interface. Longer UVO activation time most likely oxidized SU-8 surfaces forming unreactive chemical groups, leading to lower densities of bound molecules. To conclude, the highest density of immobilized molecules ($1.9 \cdot 10^{10}$ molecules/mm^2) was obtained when SU-8 thin films were exposed to UVO radiation for 30 s or 1 min.

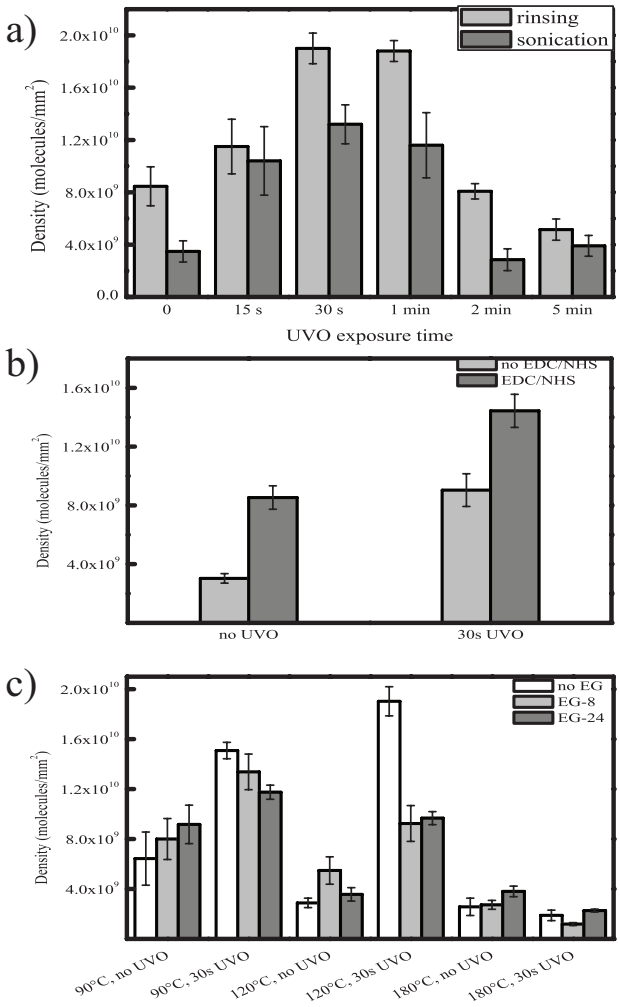

Figure 3.7. Density of tamra-cadaverine molecules per mm² immobilized on the SU-8 surfaces: **(a)** depending on UVO exposure time and rinsing method; SU-8 thin film hardbaked at 120°C for 3 h, activated with EDS/NHS and rinsed twice with 10 mM sodium acetate buffer pH 5.2 or sonicated twice for 2 min; **(b)** depending on the EDC/NHS pre-incubation step; **(c)** depending on the surface pegylation method. SU-8 films were hardbaked in three different conditions, activated with EDS/NHS, activated or not by 30-s UVO treatment. Standard deviations were calculated based on six independent measurements.

To demonstrate the specific adsorption of tamra-cadaverine on the UVO activated surface, the molecular density on the SU-8 surface was calculated in conditions lacking the EDC/NHS pre-incubation step (Figure 3.7b). The density of tamra-cadaverine increased significantly when EDC/NHS was applied on SU-8 thin layer both with and

without UVO surface treatment, confirming the specific adsorption of tamra-cadaverine on the SU-8 surface. The tamra-cadaverine density on the surface without UVO was three times higher after pre-incubation with EDC/NHS than without EDC/NHS pre-treatment, confirming the presence of COOH groups on the surface hardbaked at 120°C for 3 h and the low level of non-specific interactions (corresponding to 1/3 of the specifically bound tamra-cadaverine). After 30-s UVO exposure the level of non-specific binding of tamra-cadaverine increased three fold (when no EDC/NHS was applied to the surface) relative to the SU-8 surface without UVO treatment. Finally the surface density was $1.4 \cdot 10^{10}$ molecules/mm^2 while the non-specific interaction was $9.0 \cdot 10^9$ molecules/mm^2 when both UVO and EDC/NHS were applied to the SU-8 surface prior to the tamra-cadaverine deposition. It is important to note that the amount of non-specific interactions of tamra-cadaverine with the SU-8 surface after UVO treatment and with EDC/NHS pre-treatment was expected to be significantly lower than the non-specific interactions when no EDC/NHS was employed. Indeed, EDC/NHS pre-treatment activated COOH groups therefore the specific interaction (formation of an amide bond) was largely favored over the non-specific interactions, as demonstrated on the sample with no UVO treatment.

Although rinsing SU-8 surfaces by sonication was shown to remove non-covalently bound molecules efficiently, it may pose a problem for biological applications through denaturation of biomolecules, such as proteins or dsDNA. Thus, to decrease non specific interactions of tamra-cadaverine and subsequent anti-tamra adsorption with the SU-8 surface, the effect of pre-functionalization with carboxyl-amine *n*-ethylene glycol ($CA(EG)_8$ and $CA(EG)_{24}$) was studied (37, 47, 201).

The influence of the EG chain-length and short UVO treatment on the density of tamra-cadaverine for each SU-8 hard-baking condition is presented in Figure 3.7c. Short-time UVO treatment was shown to significantly increase tamra-cadaverine density on the bare surface for the three hard-baking conditions (Figure 3.7c, no EG). Furthermore, it was clearly demonstrated that hard-baking conditions influenced molecular density. Thus, in agreement with data presented above and for samples with no UVO treatment and no EG, the tamra-cadaverine surface density was the highest after hardbaking at 120°C for 3 h. Although pre-immobilization of $CA(EG)_8$ or $CA(EG)_{24}$ did not significantly influence tamra-cadaverine surface density for SU-8 film hard-baked at 90°C for 5 h and 180°C for 2 h, a lower tamra-cadaverine surface density for samples

pre-functionalized with $CA(EG)_8$ or $CA(EG)_{24}$ and hard-baked at 120°C for 3 h was observed. Comparing with the tamra-cadaverine surface density after sonication (Figure 3.7a), the amplitude of the drop in molecular density was similar, indicating that pre-treatment of the surface with $CA(EG)_8$ or $CA(EG)_{24}$ produced an efficient anti-fouling layer. Tamra-cadaverine surface density was lower following immobilization on pre-functionalized SU-8 surfaces than on the untreated SU-8 film rinsed with sonication ($9.5 \cdot 10^9$ and $1.3 \cdot 10^{10}$ molecules/mm^2, respectively) indicating that the final amount of reactive carboxyl groups was lower. Moreover, the EG chain-length had no influence on the tamra-cadaverine surface density.

SU-8 thin film hard-baked at 120°C for 3 h then activated by 30 s UVO treatment was adopted as a standard protocol for preparing SU-8 surfaces, since it resulted in homogeneous samples with fewer disparities in the density of immobilized molecules (Figure 3.7c). To demonstrate the relevance of the surface modification method for biosensing applications, a quenching assay between immobilized tamra-cadaverine molecules and interacting anti-tamra was performed.

Spots of a diameter of ~300 µm were immobilized on the pre-treated SU-8 surface. Fluorescent microscope images at different times following injection of anti-tamra across the surface are shown in Figure 3.8a. Injection of anti-tamra caused a decrease in the fluorescence intensity, while surface regeneration with 10 mM glycine-HCl (pH 2.0) was effective in the signal enhancement. The relatively small variations in fluorescence intensity observed during the three cycles of interaction/regeneration may be explained by the low quenching efficiency after complex formation. Indeed, as characterized in the literature, quenching efficiency was not expected to exceed ~57% of the initial intensity of the free tamra fluorophore diluted in a buffer solution (200). In addition, since the average distance between tamra-cadaverine immobilized on the SU-8 surface was approximately 7 nm (deduced from Figure 3.7c), not all immobilized tamra-cadaverine molecules could be involved in a complex with anti-tamra because of possible steric hindrance.

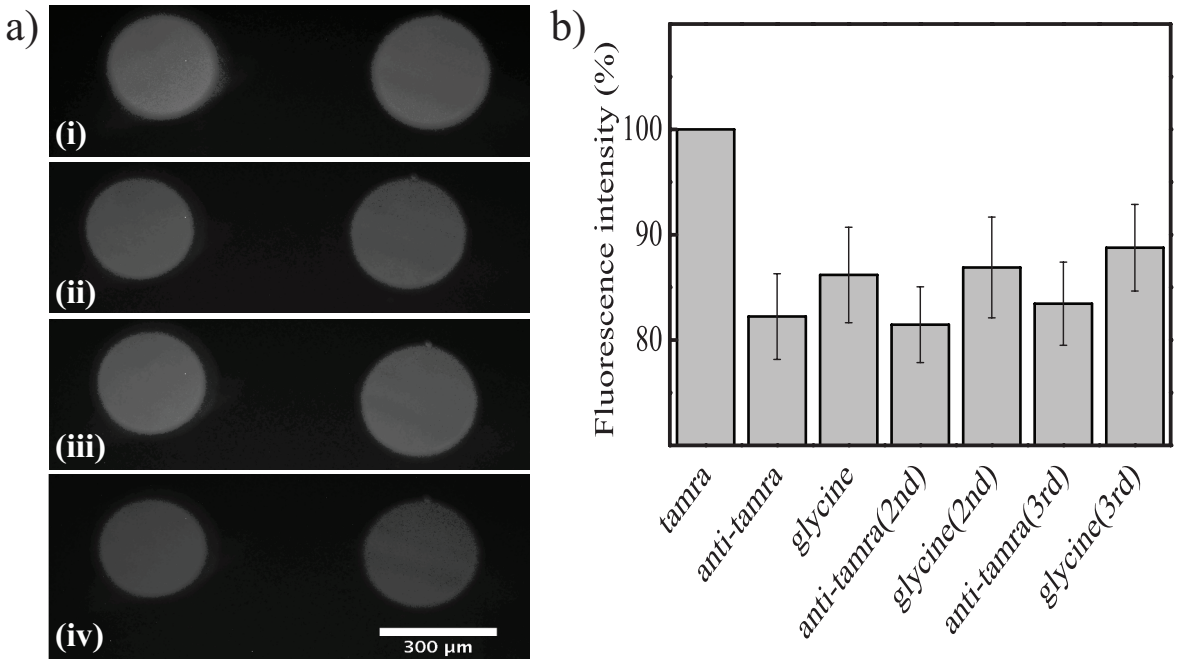

Figure 3.8. (a) Fluorescent microscope images of tamra-cadaverine and anti-tamra interaction cycle. (i) Image of spots of immobilized 10 µM tamra-cadaverine, (ii) image taken after injection of 10 µg/ml anti-tamra and rinsing with PBS buffer, (iii) image taken after regeneration of the surface with a solution of 10 mM glycine–HCl pH 2.0 (202) and (iv) image taken after an additional injection of anti-tamra and rinsing with PBS buffer. **(b)** Changes in fluorescence intensity during three reaction cycles. Standard deviations were calculated based on four independent measurements.

Quantification of the fluorescence intensity on each tamra-cadaverine spot and in each step of the association/regeneration cycle summarized the variation of fluorescence intensity during three cycles of injection and regeneration (Figure 3.8b). Considering the initial fluorescence intensity of the immobilized tamra-cadaverine spots to be 100%, a drop in the intensity of fluorescence to approximately 82% was observed after first anti-tamra/tamra-cadaverine complex formation on the SU-8 surface. The fluorescence signal was recovered up to 86% after regeneration with 10 mM glycine solution. The loss of the signal from the immobilized tamra-cadaverine after regeneration might be due to desorption of tamra-cadaverine non-covalently bound to the surface but initially involved in complex formation and from an undissociated complex that remained irreversibly on the surface. A second injection of anti-tamra again decreased the detected fluorescent signal to 81% and a second regeneration of the

surface allowed total recovery of the signal intensity. A third cycle of association/regeneration showed similar variation of the fluorescence intensity demonstrating the specificity of the interaction on the pre-treated SU-8 surface.

2.4. Covalent binding of DNA strands to the surface

UVO-activated SU-8 surfaces were tested to covalently immobilize DNA oligomers. SU-8 thin films were prepared with a standard protocol described in Chapter II, including three surface hard-baking (at 180°C for 5 h, at 120°C for 3 h and at 90°C for 5 h) and its activation with 30-s UVO exposition. 50 base pairs DNA (sequences of DNA listed in Appendix I) were immobilized on the pre-treated surface. One of the DNA strands was modified with an amine group at the 5' end (DNA-NH2) that served to couple carboxyl groups created on the SU-8 film surface followed by UVO exposure and activation with EDC/NHS solution. To quantify the density of immobilized molecules and determine the stability of dsDNA immobilized on a surface, a second DNA strand was fluorescently labeled using a cyanine dye Cy5 or labeled on the alpha phosphate group with a ^{32}P isotope of a modified adenosine monophosphate. The specificity of DNA immobilization was controlled using a sample, which had the same DNA oligomer without the functional amine group ('DNA-OH').

It was demonstrated that the level of nonspecific interactions was high, indicating that the surface was not optimally protected from the non-specific adsorption of DNA molecules, even when $CA(EG)_8$ was applied. A lack of reproducibility and a significant error bar characterized the majority of the results. It is worth noticing that radioactive labeling followed by quantitative analysis is a very sensitive method, allowing the detection of small amounts of material, up to 10 fg of DNA (203). Nevertheless, for the same reason this method demonstrated a very significant dispersion in results. To reduce the amount of these nonspecific interactions, surfaces with deposited DNA were rinsed with 0.1 – 1 % sodium dodecyl sulphate (SDS) solutions, since SDS is an anionic surfactant regularly used to lower surface tension and to disrupt non-covalent interactions. The level of nonspecific interactions decreased, however this method was not reproducible in all experiments and thus was not applied further.

Overall, the method presented here was not sufficiently optimized to be used regularly for the specific covalent binding of DNA oligomers to a SU-8 surface. To

improve the use of UVO activated SU-8 surface several steps in the protocol need to be adjusted, including protection of the surface from non-specifically bound molecules and optimization of the accessibility of immobilized dsDNA for further reactions, e.g. interactions with sequence-specific proteins.

2.5. Conclusions

SU-8 photoresist polymer is widely used in the fabrication of micro devices for biosensing applications. UV/ozone (UVO) surface pre-treatment was presented here as an effective straightforward method to increase the hydrophilicity of SU-8 films and improve specific covalent binding of molecules in a controlled manner. UVO lead to a milder surface oxidation than argon or oxygen plasma treatment therefore the SU-8 surface roughness was not affected by UVO exposition (193) as demonstrated by water contact angle (wCA), FT-IR spectroscopy and AFM. The fluorescent properties of tamra-cadaverine allowed optimization of experimental conditions to favor specific chemisorption of molecules on the UVO activated SU-8 surface. Optimal conditions to obtain covalent immobilization of tamra-cadaverine with high density were established as SU-8 thin film hard-baked at 120°C for 3 h and UVO treatment for 30 s. Quantitative analysis of immobilized tamra-cadaverine demonstrated that a two-step surface modification where the surface was first protected with an ethylene glycol monolayer lead to an increase in binding specificity. To prove the controlled binding and accessibility of immobilized molecules, three cycles of reversible interactions between anti-tamra antibody and tamra-cadaverine immobilized on the surface of SU-8 were presented. Finally, the UVO functionalization method was applied to immobilize DNA oligomers modified with amine groups. Further studies demonstrated that covalent immobilization of DNA oligomers on UVO pre-treated surfaces was difficult to reproduce and the level of non-specifically adsorbed DNA was high.

According to the results presented above, UVO surface treatment can be used as an efficient method to develop SU-8 based biosensors. This method could be applied to immobilize small molecules possessing an exposed primary amine group, such as tamra-cadaverine. By varying UVO radiation times, one could tune the desired properties of the surface, such as hydrophilicity and density of bound molecules. Relatively hydrophobic surfaces and the highest density of exposed carboxyl groups was obtained for short UVO

exposure time (30 s to 1 min) while longer UVO exposure times increased the hydrophilicity of the surface but decreased the amount of accessible carboxyl groups, reaching extreme hydrophobicity after 15 min of UVO exposure. A two-step reaction where the surface was first protected with an ethylene glycol monolayer minimized nonspecific adsorption to the hydrophobic surface.

The example of immunodetection with molecules immobilized to the UVO-activated surface illustrated a reliable biosensing application of SU-8 thin film biofunctionalization. It was demonstrated not only that the surface modification allowed immobilization of biomolecules in a controlled manner but also that it did not impact on the functional integrity of the surface, proving that UVO surface treatment was a very promising method having a significant potential to be developed in biosensor techniques, such as micro ring resonators (20) or TIRF microscopy.

However, the present method was not transferable for immobilization of other (bio) molecules. The example with immobilized DNA oligomers, that are relatively big molecules possessing numerous charged groups, demonstrated that the surface protection must be optimized. The present protocol, including using short ethylene glycol molecules ($CA(EG)_8$) was not sufficient to specifically immobilize charged molecules, such as DNA oligomers and proteins.

Since the surface functionalization strategy presented above was multistep and not transferable to immobilization of another molecules, an alternative functionalization method based on non-covalent hydrophobic interactions, was developed and the findings are presented below in Section 3.

3. Hydrophobic surface biofunctionalization by coupling of cholesteryl-modified molecules

3.1. Cholesteryl-based hydrophobic coupling

Cholesterol is an amphiphilic steroid widely distributed in biology, mainly as a compound of membrane phospholipid bilayers. In addition, cholesterol has found various applications in science and technology, e.g. in artificial liposomes and micelles to biosensing applications and to stabilize drug delivery processes (107). Cholesterol and cholesterol-modified polymers are also broadly used in self-assembled monolayers and Langmuir-Blodgett films (204). In order to avoid a high energetic cost incurred for exposing hydrophobic moieties to the aqueous interface, hydrophobic parts of molecules approach each other and continue to self-assemble and, in critical situations, form structures such as micelles (205). Attractive forces between hydrophobic parts of the molecules lower the surface energy by promoting aggregation and clustering (206) or by adsorption to hydrophobic supports.

It has been demonstrated that DNA oligomers modified with a cholesteryl group were specifically immobilized on the hard-baked SU-8 films (207, 208). These findings demonstrated a robust, fast and efficient one-step process for immobilizing (bio) molecules and thus inspired the research described here to apply hydrophobic coupling to functionalize sensor surfaces. Clear advantages of non-covalent chemisorption include fast functionalization and regeneration of surfaces. This provides high reproducibility and the possibility of re-using exactly the same surface to monitor subsequent interactions, for example in SPRi technology.

Amphiphilic molecules with a planar sterol ring present in cholesteryl- and cholate-modified molecules were used to (bio) functionalize 2-dimensional surfaces based on hydrophobic coupling with surfaces such as SU-8 thin films or hydrophobically pre-functionalized gold layers. The hypothesis was that hydrophobic coupling of these molecules could be a universal functionalization method, dependent only on the surface properties (e.g. level of hydrophobicity and roughness) and conditions of incubation. To confirm this statement, studies were carried out on two distinct hydrophobic surfaces: SU-8 thin film and gold surfaces modified with a hydrophobic monolayer that showed

analogous properties to SU-8. Optimal conditions for the controlled non-covalent immobilization of fluorescent tamra molecules modified with a cholate moiety and DNA oligomers modified with a cholesteryl moiety were established. Additionally, the accessibility of immobilized molecules and their potential use in further biosensing reactions was tested and confirmed.

3.2. Biomolecule synthesis

Cholesterol is composed of a highly hydrophobic sterol skeleton and an aliphatic hydrocarbon tail (Figure 3.9a and b). It can be easily conjugated with (bio) molecules of interest, i.e. by coupling reactions with carboxyl groups present in the aliphatic tail or esterification of the polar hydroxyl group present in the cholesterol ring that leads to cholesteryl ester formation. In this work, both cholesteryl ester and the salt of cholic acid were used. Sodium deoxycholate (Figure 3.9c) is an ionic nontoxic detergent widely used to disrupt and dissociate protein interactions. Similarly to cholesteryl, Na-deoxycholate is composed of a sterol skeleton and an aliphatic hydrocarbon tail. The molecule terminates with a sodium carboxylate moiety that can be conjugated with a primary amine *via* EDC/NHS chemistry.

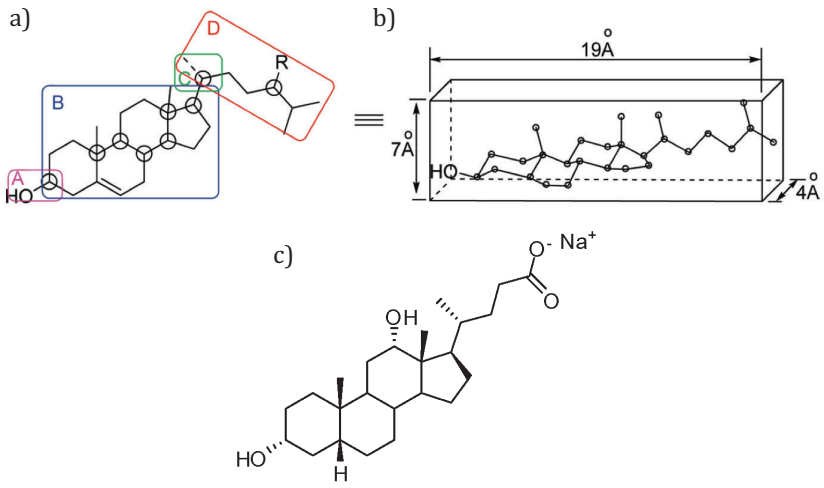

Figure 3.9. (a) Four domains in the cholesterol molecule: A – hydroxyl group, B – sterol ring, C – carbon C20 determining the confirmation of a side tail, D – aliphatic tail; **(b)** Spatial composition and dimensions of a cholesterol molecule; **(c)** Sodium deoxycholate molecule. *Figure 3.9 a and b adapted from (209).*

3.2.1. Tamra-cholate

The fluorescent molecules conjugated with cholesteryl or cholate groups used here were not commercially available. They were synthesized in the laboratory, taking advantage of the presence and accessibility of sodium carboxylate group placed at the extremity of the hydrocarbon tail (Figure 3.9c). Na-deoxycholate was activated with EDC/NHS and conjugated with tetramethylrhodamine (tamra) cadaverine according to the protocol described in Chapter II Section 2.2.

The efficiency of synthesis was controlled using analytical thin layer chromatography. Solutions of conjugated tamra-deoxycholate in ratios 1.1:1, 1:1, 1:2 and 1:4, and control solutions of tamra-cadaverine (T), Na-deoxycholate (ch), tamra-cadaverine and Na-deoxycholate (T+ch) were spotted on the bottom of a thin aluminium percolated silica plate and eluted with the mixture of acetone/dichloromethane/methanol (3:1:1) as presented in Figure 3.10. Taking advantage of the pink color of rhodamine in visible light, plates could be analyzed directly. Analysis of the control samples demonstrated that the majority of tamra cadaverine itself was not able to migrate in the chosen solvent and thus a well-defined spot was present at the bottom of the plate, where the solution was applied and only a small amount of the solution migrated (Figure 3.10, line 1). Na-deoxycholate solution did not show any visible movement (Figure 3.10, line 2). Moreover, the presence of non-conjugated Na-deoxycholate in the solution did not have any influence on the behaviour of tamra cadaverine, as shown in Figure 3.10, line 3.

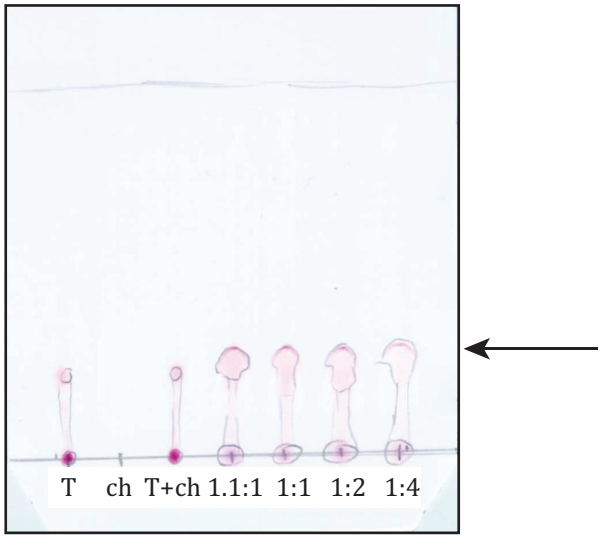

Figure 3.10. Analytical thin layer chromatography with spotted samples (from left to right): tamra cadaverine ('T'), Na-deoxycholate ('ch'), tamra cadaverine and Na-deoxycholate ('T+ch'), conjugated tamra cadaverine with Na-deoxycholate with molar ratios 1.1:1, 1:1, 1:2 and 1:4 ('1.1:1', '1:1', '1:2' and '1:4', respectively). Black arrow represents the end of migration of conjugated tamra cadaverine with Na-deoxycholate. The upper line represents a solvent front during sample migration.

In order to enforce conjugation of all tamra cadaverine molecules with a Na-deoxycholate, first synthesis was performed with a slight excess of tamra (molar ratio 1.1:1). However, further analysis demonstrated that regardless of the molar ratio (1.1:1, 1:1, 1:2 and 1:4) a comparable amount of tamra-cadaverine molecules was invariably conjugated with Na-deoxycholate, as shown in the developed plate (Figure 3.10, lines 4 – 7). Traces visible in the bottom part of the plate most probably came from tamra cadaverine not conjugated with Na-deoxycholate.

Tamra cadaverine deoxycholate ('tamra-chol') molecules used in further experiments were conjugated at the molar ratio 1.1:1 of tamra cadaverine and Na deoxycholate, respectively. It is worth noticing that in the described synthesis the purification step was intentionally omitted. The presence of EDC/NHS would not have had any effect on subsequent experiments, since surfaces were thoroughly rinsed before tamra-chol deposition and prior to any quantitative analysis or other measurement. Additionally, sample purification in a chromatography column after synthesis required a significant amount of material or resulted in extensive dilution and thus was avoided.

3.2.2. DNA-cholesteryl

DNA oligomers with deoxyribose-cholesteryl modifications are commercially available (Eurogentec company). In this case, the cholesteryl moiety is linked to deoxyribose *via* a tetraethylene glycol (TEG) spacer (Figure 3.11). Oligomers possessing this modification at the 5' end were immobilized on SU-8 films and thin hydrophobic gold layers, as described in the following Sections.

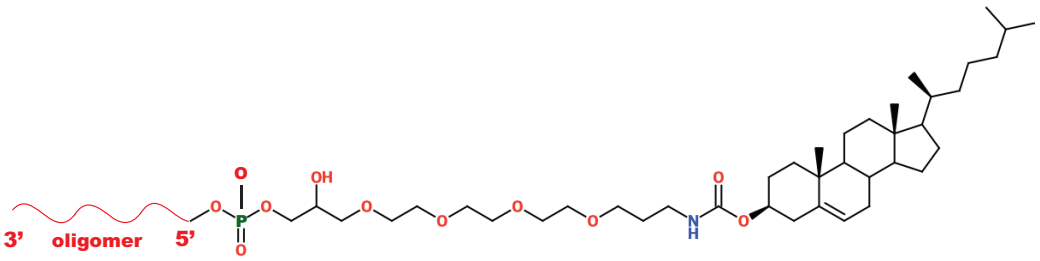

Figure 3.11. Deoxyribose cholesteryl tetraethylene glycol (TEG-chol) modification of DNA oligomer at 5' end.

3.3. Coupling of tamra-chol to the hydrophobic surface

The fluorescent properties of tamra molecules modified with cholate moiety (tamra-chol) were used to optimize conditions for the immobilization of amphiphilic molecules on hydrophobic surfaces. Experiments were performed with SU-8 thin film fabricated as described in Chapter II, Section 2 and hard-baked at 180°C for 2 h, since previous measurements of water contact angle and surface roughness (Chapter III, Section 2.2) confirmed similar values obtained independently from the thin film hard-baking conditions (180°C for 2 h, 120°C for 3 h and 90°C for 5 h). The standard thickness of prepared films was 2 µm ± 15%. Surfaces were used directly to immobilize cholate-modified molecules without any modification and/or activation step.

3.3.1. Influence of the concentration and incubation time

Firstly, the density of immobilized tamra-chol molecules was defined with respect to incubation time and the spotted solution concentration. Density was measured in the same way as described in Section 2.3 for immobilized tamra-cadaverine. Briefly, calculations were performed based on a calibration curve; the fluorescence signal of 1 µl of tamra-chol solution of increasing molarity was measured to obtain a linear calibration curve. The concentration range used was chosen according to the intensity of fluorescent signals from analyzing samples (using a Typhoon scanner) and therefore allowed calculation of the number of molecules per unit area with relatively good approximation.

SU-8 surfaces were immersed in tamra-chol solutions of concentrations ranging from 1 to 20 μM for times from 1 to 20 min. As could be deduced from Figure 3.12, the density of immobilized molecules strongly depended on the incubation time when the tamra cadaverine concentration was 1 μM. For higher concentrations, the number of immobilized molecules was only influenced by the concentration of the tamra solution and not by the incubation time. From 2 to 4 μM the density of immobilized tamra-chol molecules increased to reach a plateau from 5 μM tamra-chol solution at a molecular density estimated between $2.5 \cdot 10^{10}$ and $3 \cdot 10^{10}$ molecules/mm^2. These values corresponded to results obtained previously by other research groups where immobilization of 20-base DNA-chol oligomers provided a DNA density of 10^{10} – 10^{11} molecules/mm^2 (207). Additionally, based on the data presented here, the adsorbed tamra-chol molecules were taken as having formed a monolayer, since a plateau in the number of molecules immobilized on the surface was reached, independent of the applied conditions, including incubation time and concentration of solution used.

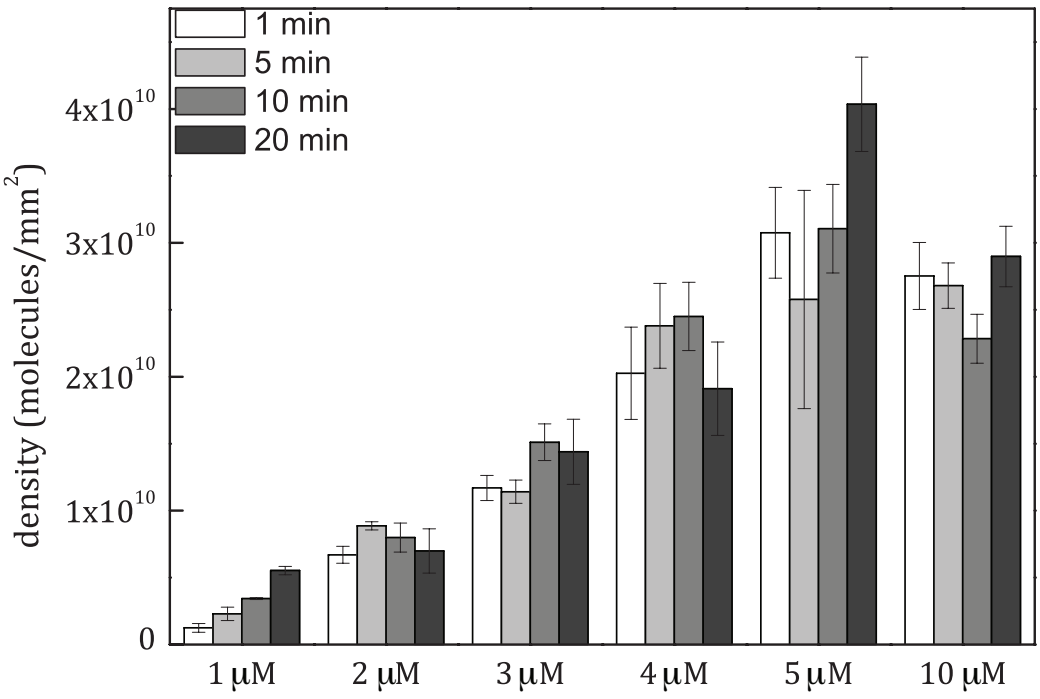

Figure 3.12. Density of tamra-chol molecules immobilized on the SU-8 surfaces depending on a concentration of the spotted solution (1 – 10 μM) and incubation time (1 – 20 min). Standard deviations were calculated based on six independent measurements.

The relatively planar construction of a sterol ring might promote interactions with a hydrophobic support. Here it was assumed that cholate- or cholesteryl-modified molecules interacted with a hydrophobic surface *via* the sterol ring. Based on data presented in Figure 3.9b and in reference (209), the surface area occupied by a single sterol ring was estimated to be $6.4 \cdot 10^{-13}$ mm^2 and by a sterol ring with an attached hydrocarbon chain – $7.6 \cdot 10^{-13}$ mm^2. To estimate the surface occupied by an adsorbed single molecule possessing a sterol ring, both situations were considered, since the position of the hydrocarbon chain may cause steric hindrance and thus the area dedicated to a single molecule would increase. Taking into account these two values, the theoretical maximal density of immobilized cholate- or cholesteryl-modified molecules was calculated to be between $1.3 \cdot 10^{12}$ – $1.5 \cdot 10^{12}$ molecules/mm^2. These values were clearly above values obtained experimentally ($\sim 3 \cdot 10^{10}$ molecules/mm^2). However, it was hypothesized that the presence of tamra-cadaverine moiety covalently bound to the hydrocarbon chain caused supplemental steric hindrance that might increase the area occupied by a single molecule. In addition, nonspecific interactions between immobilized molecules and a hydrophobic surface could occur. In order to characterize the specificity, accessibility and potential application of immobilized tamra-chol, the studies concerning immunosensing applications were carried out and results are presented below, in Section 3.2.3.

3.3.2. Removal of adsorbed molecules and surface reusability

Immobilization of tamra-chol on the SU-8 surface based on noncovalent hydrophobic coupling is a reversible interaction. In certain situations (e.g. when regeneration of a surface is compromised by the stability of the studied interaction or when it is important to recover material without damaging it) non-covalent binding is of interest as it allows removal of the monolayer and re-immobilization in an identical manner in terms of density and orientation. To establish the most efficient method for surface renewal, the conditions of controlled molecule removal were characterized by studying the influence of the solvent composition, pH, sonication and rinsing time. The list of examined solvents included: water, acidic solution of 1 M sodium acetate (pH 5.2), basic solution of 1 M tris (pH 9.0), organic solution of cyclohexane, acetone and absolute ethanol. SU-8 surfaces with a monolayer of the maximal density ($3 \cdot 10^{10}$

molecules/mm^2) formed by immobilized tamra-chol were immersed in the solvents for 1 and 10 min. The amount of molecules remaining on the SU-8 surface was quantified by comparing the densities as illustrated in Figure 3.13. Ethanol and acetone were the most efficient solvents for tamra-chol removal. Neither basic, nor acidic solutions were sufficient to totally remove adsorbed molecules. Also rinsing with water and further 10-min sonication of the immersed surfaces did not release all tamra-chol from the surface. Likewise, cyclohexane did not remove the immobilized molecules and therefore it was considered as an ineffective method. In all the above cases increased incubation time (from 1 to 10 min) did not improve the desorption efficiency.

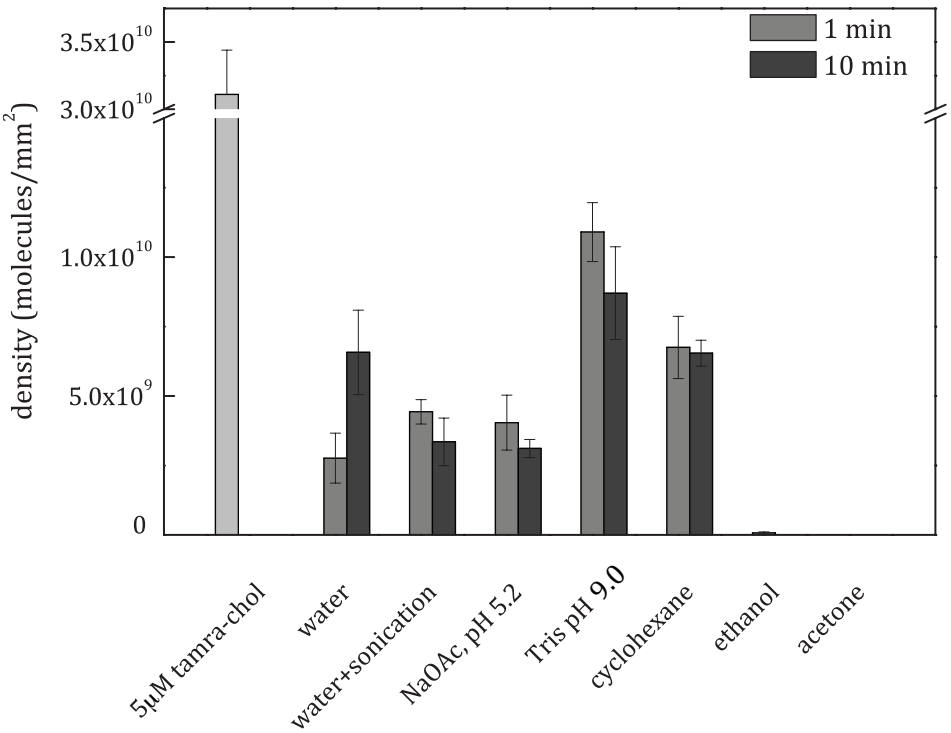

Figure 3.13. Influence of various solvents for efficient desorption of tamra-chol immobilized on the SU-8 surface, based on the density of remaining molecules. Samples were rinsed with various solutions for 1 and 10 min. Standard deviations were calculated based on five independent measurements.

Results in Figure 3.13 demonstrated that ethanol and acetone were considered to be optimal solvents for hydrophobic surface regeneration. To prove that the chosen solvents did not affect the hydrophobic properties of the surface and that the surface could be used multiple times, a 10 μM solution of tamra-chol was incubated on the SU-8

film followed by surface immersion in acetone and ethanol, and subsequent immobilization of 10 μM tamra-chol. As shown in Figure 3.14, regeneration of the hydrophobic surface after almost complete removal of the adsorbed tamra-chol monolayer was feasible. Considering that the initial amount of immobilized tamra-chol gave 100% of a fluorescent signal, immersion of the functionalized surface for 10 min in acetone or absolute ethanol decreased this signal to 20% and 11%, respectively. Subsequent immobilization of tamra-chol on these surfaces allowed recovery of 72% of the fluorescence signal in the case of acetone (Figure 3.14a) and 100% in the case of ethanol (Figure 3.14b).

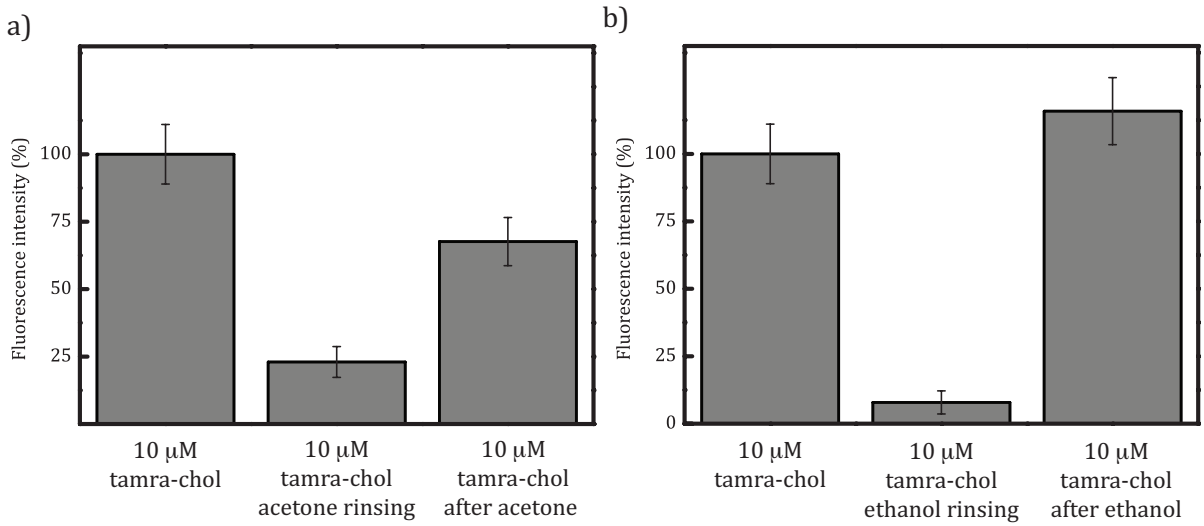

Figure 3.14. Fluorescence intensity immobilized tamra-chol throughout a cycle of regeneration: desorption and immobilization of 10 μM tamra-chol during surface regeneration with **(a)** acetone and **(b)** absolute ethanol.

Based on these results, absolute ethanol was shown to be more efficient than acetone and other solutions tested to remove a fluorescent monolayer of tamra-chol adsorbed *via* hydrophobic coupling. Absolute ethanol removed up to 90% of adsorbed molecules. It was previously found that the long-range attractive forces in hydrophobic surfaces decreased with increasing ethanol concentration, since molecules of ethanol interacted with the hydrophobic surface *via* hydrogen bonds (210, 211). In other words, the presence of ethanol was sufficient to create a less hydrophobic environment at the interface (212). Therefore, the wetting properties of the SU-8 surface significantly

increased and thus hydrophobic interactions between the SU-8 film and sterol rings got weaker leading to tamra-chol desorption.

Additionally, it was demonstrated that the use of ethanol did not have any influence on the surface properties; hence subsequent immobilization of molecules at the same concentration was proved to lead to reproducible molecular surface density.

As stated above, functionalization of hydrophobic surfaces based on amphiphilic molecule coupling is postulated to be a universally applicable technique. To prove it, studies of tamra-chol immobilization on a hydrophobic gold layer were performed. Solutions of 1-undecathiol in ethanol were used to form a highly hydrophobic self-assembled monolayer on the 50-nm gold layer evaporated on a glass prism. Functionalized prisms were used in SPRi experiments to confirm the general applicability of this technique. An additional advantage of this technique would be the high reproducibility of the surface monolayer throughout regeneration cycles. This could be applied in SPRi experiments where kinetic data can be extracted.

The influence of concentration and efficiency of surface regeneration were examined. Solutions of 5 µM tamra-chol were injected in the SPRi apparatus and passed for 4 min at a flow rate of 25 µl/min over a hydrophobic monolayer adsorbed on a gold layer. After rinsing with running buffer for several minutes, the surface was regenerated by subsequent injection of 10 µl of absolute ethanol at a flow rate of 25 µl/min. Variations of the refractive index over time are shown in the sensorgram in Figure 3.15a. The characteristic phases that can be distinguished on the sensorgram were as follows: before 0 s – a stable signal from a running buffer solution passing over the surface, representing the experimental baseline; upon injection of the sample solution (5 µM tamra-chol in a running buffer) the signal increased indicating the adsorption of the molecule to the sensor surface; 240 s (marked with the arrow in Figure 3.15a) – sample injection was stopped and the injected solution was replaced by the running buffer with a distinct refractive index that caused subsequent decrease of the signal. It is important to notice that the curve during the subsequent dissociation phase did not reach previous level, indicating that injected molecules altered the signal through adsorption *via* hydrophobic coupling to the surface. In the following part of the sensorgram (from t = 620 s), the signal increased following injection of ethanol. After injection was stopped the signal returned to the baseline level, suggesting that tamra-chol molecules that were adsorbed on the surface before the injection of ethanol were totally desorbed following

ethanol injection. Subsequently, the solution of 10 µM tamra-chol was passed over the same surface for 4 min, followed by surface regeneration with ethanol and injection of 20 µM tamra-chol solution for 6 min. Superimposed sensorgrams from these experiments are shown in Figure 3.15b. Differences in the maximum signal intensity were due to three injections of tamra-chol solutions at increasing concentrations (5, 10 and 20 µM, respectively) and thus having different refractive indexes. All curves, regardless of the injected concentration of tamra-chol, reached similar values at the end of the dissociation phase (about 2 % difference of relative reflectivity) that were clearly above the baseline. It was assumed that these values corresponded to a monolayer formed of tamra-chol immobilized on the hydrophobic surface. The same trend was observed for functionalization of SU-8 surfaces (Section 3.3.1) thus indicating that the adsorption stopped at a monolayer or a sub monolayer.

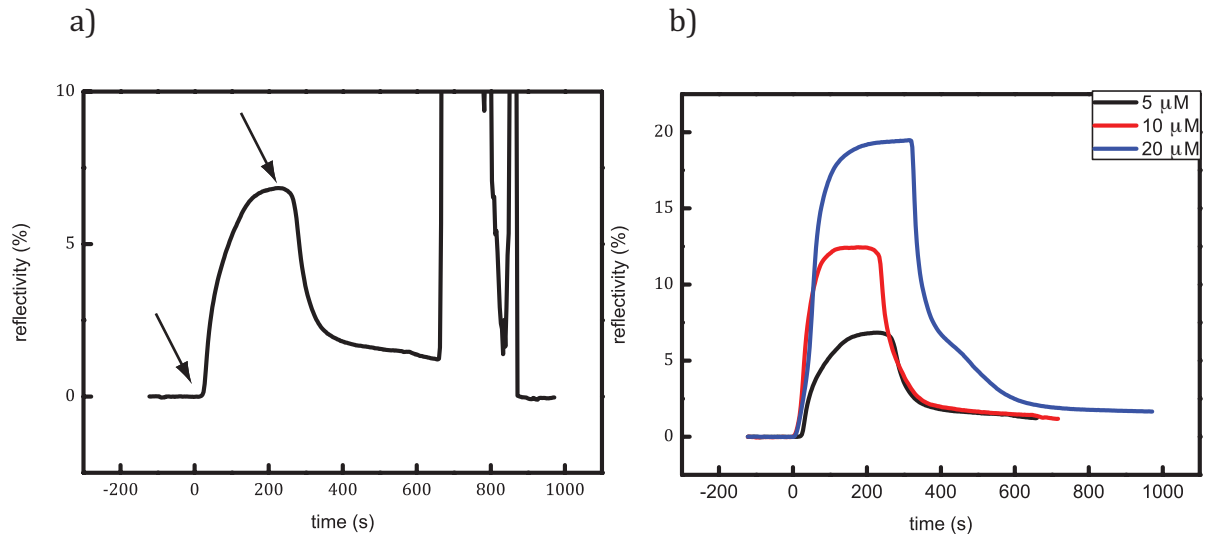

Figure 3.15. a) SPRi sensorgram of immobilization of 5 µM tamra-chol on the hydrophobic gold surface and its subsequent removal with absolute ethanol; the beginning and end of tamra-chol injection is marked with arrows; **b)** Superimposed SPRi sensorgram of immobilization of 5, 10 and 20 µM tamra-chol on the hydrophobic gold surface after regeneration with ethanol on the same surface.

From these results, it was concluded that functionalization of a hydrophobic surface with cholate-modified molecules was a simple and fast one-step method leading to the formation of a monolayer contained immobilized amphiphilic molecules at a

moderate density that depended on the solution concentration and/or incubation time. As demonstrated, for low concentrations (≤ 1 μM tamra-chol) the incubation time influenced the density but for higher concentrations, the saturation of the surface was very fast and independent of the incubation time. Undoubtedly, the possibility of complete renewal and re-use of the same surface with a simple immersion in ethanol was a remarkable advantage that allowed work on a fresh monolayer and in addition reduced surface fabrication costs and shortened the manipulation time.

3.3.3. Immunosensing applications

The functionalized hydrophobic gold surfaces with immobilized tamra-chol molecules were used to study the accessibility of immobilized molecules and to demonstrate the relevance of the surface modification method for potential use in biosensing applications. An immunosensing assay between immobilized tamra-chol molecules and anti-tamra antibodies was performed. The test was carried out in an SPRi apparatus, using tamra-chol molecules immobilized on the hydrophobic gold sensor, as described in the previous Section. Non-covalent binding *via* the hydrophobic interaction was compared to the conventional method of immobilization of (bio) molecules on SPR biochips *via* covalent amide bond formation between an activated EDC/NHS carboxyl group and a primary amine of tamra cadaverine molecules. In the control system, tamra cadaverine was coupled to the gold surface functionalized with a self-assembled monolayer of short thiolated alkyne chains. Thiolated *n*-ethylene glycol molecules modified with carboxyl groups (EG-COOH) were coupled with the amine moiety of tamra cadaverine molecules after the activation with an EDC/NHS solution. The detailed protocol can be found in the Chapter II Section 2.1.

Solutions of anti-tamra were injected into the SPRi apparatus and passed over two separate surfaces functionalized with tamra-chol or tamra cadaverine (the control experiment) for 4 min. Examples of sensorgrams are shown in Figure 3.16. Three different concentrations of anti-tamra antibody: 13.5, 20 and 27 nM were injected and passed over the surfaces. Comparisons of antigen – antibody interactions registered for tamra-chol immobilized on the hydrophobic surface (Figure 3.16 a, c, e) and tamra cadaverine covalently bound to the surface (Figure 3.16 b, d, f) showed similarities in sensorgram curves. All sensorgrams had similar amplitudes and overall shapes.

Additionally, the signal for the dissociation phase in all cases confirmed that interactions between antibody and antigen were extremely stable; a characteristic feature of a typical antibody – antigen interaction measured in SPR (47, 213).

Figure 3.16. Kinetic analysis of antibody – antigen interactions carried out in SPRi for **(a)** 10 μM tamra-chol immobilized on the hydrophobic surface and interacted with 13.5 nM anti-tamra antibody, **(b)** 10 μM tamra cadaverine immobilized covalently on the surface *via* amide bond and interacted with 13.5 nM anti-tamra antibody, **(c)** 10 μM tamra-chol immobilized on the hydrophobic surface and interacted with 20 nM anti-tamra antibody, **(d)** 10 μM tamra cadaverine immobilized covalently on the surface *via* amide bond and interacted with 20 nM anti-tamra antibody, **(e)** 10 μM tamra-chol immobilized on the hydrophobic surface and interacted with 27 nM anti-tamra antibody, **(f)** 10 μM tamra cadaverine immobilized covalently on the surface *via* amide bond and interacted with 27 nM anti-tamra antibody. Antibody was injected in PBS buffer. Red curves represent curve fitting. Kinetic data: dissociation rate k_d, association rate k_a and binding affinity K_D were calculated from 4 different experiments (n=4) for tamra-chol and 3 different experiments (n=3) for tamra cadaverine independent measurements.

tamra-chol - antitamra (n=4)

a)

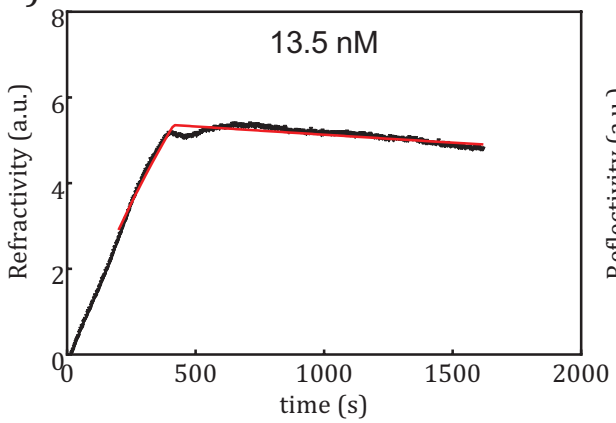

k_a (1/Ms)	k_d (1/s)	K_D (M)
$4.8 \cdot 10^4 \pm 2.5 \cdot 10^3$	$1.2 \cdot 10^{-4} \pm 1.2 \cdot 10^{-5}$	$2.4 \cdot 10^{-9} \pm 1.5 \cdot 10^{-10}$

c)

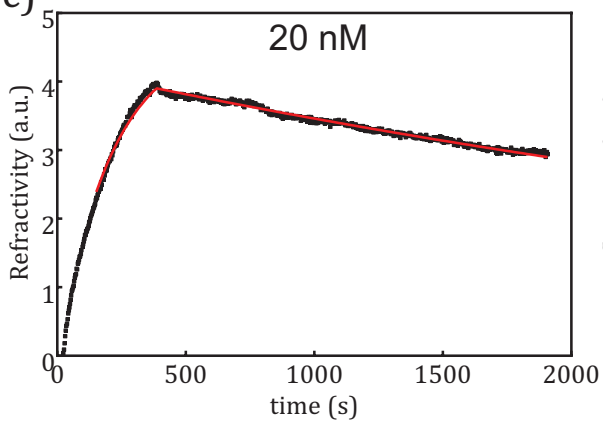

k_a (1/Ms)	k_d (1/s)	K_D (M)
$2.2 \cdot 10^5 \pm 1.9 \cdot 10^4$	$1.5 \cdot 10^{-4} \pm 3.8 \cdot 10^{-5}$	$6.7 \cdot 10^{-10} \pm 1.5 \cdot 10^{-10}$

e)

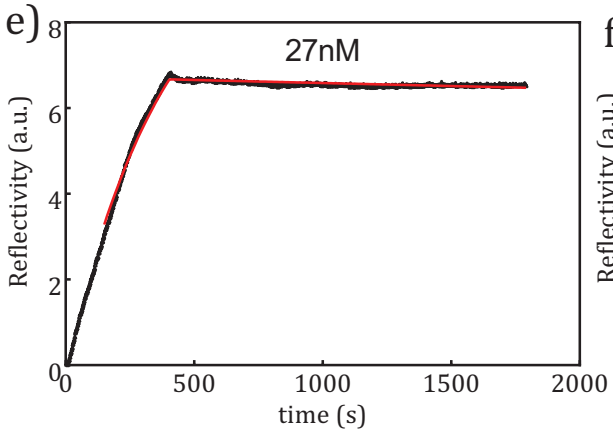

k_a (1/Ms)	k_d (1/s)	K_D (M)
$9.7 \cdot 10^4 \pm 1.3 \cdot 10^4$	$3.3 \cdot 10^{-5} \pm 1.2 \cdot 10^{-5}$	$3.3 \cdot 10^{-10} \pm 9.1 \cdot 10^{-11}$

tamra-cadaverine - antitamra (n=3)

b)

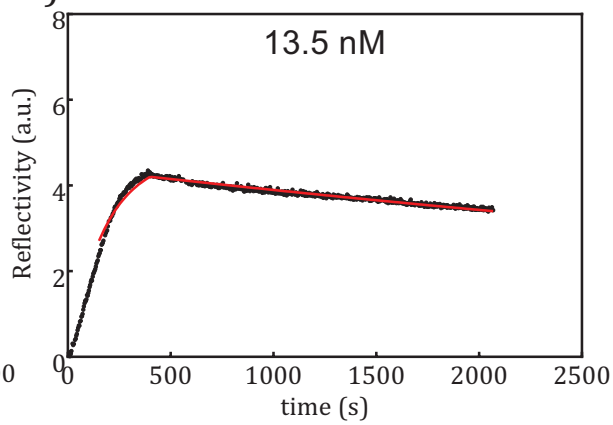

k_a (1/Ms)	k_d (1/s)	K_D (M)
$2.7 \cdot 10^5 \pm 2.0 \cdot 10^5$	$6.1 \cdot 10^{-5} \pm 4.6 \cdot 10^{-5}$	$2.4 \cdot 10^{-10} \pm 4.0 \cdot 10^{-11}$

d)

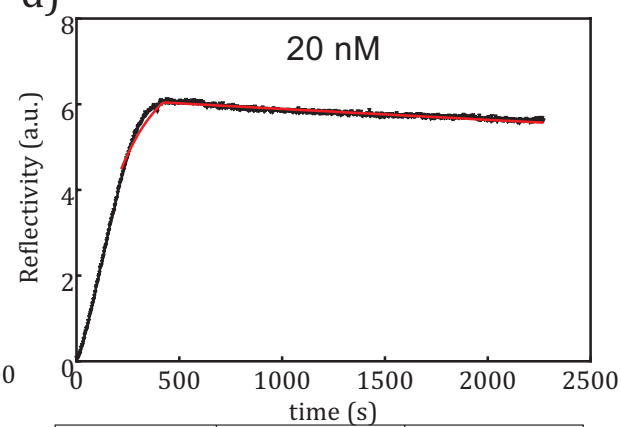

k_a (1/Ms)	k_d (1/s)	K_D (M)
$3.0 \cdot 10^5 \pm 1.4 \cdot 10^5$	$3.3 \cdot 10^{-5} \pm 6.7 \cdot 10^{-6}$	$1.4 \cdot 10^{-10} \pm 8.6 \cdot 10^{-11}$

f)

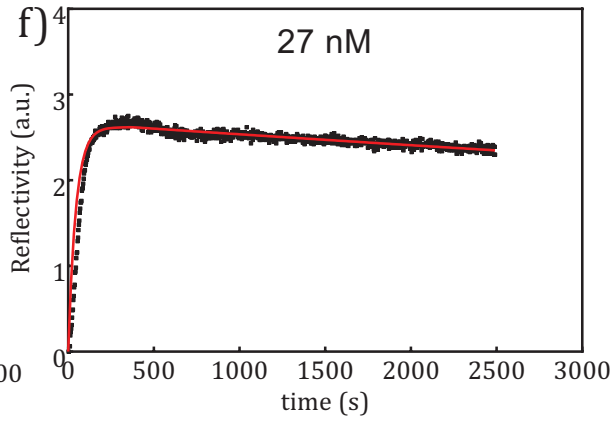

k_a (1/Ms)	k_d (1/s)	K_D (M)
$5.0 \cdot 10^5 \pm 3.4 \cdot 10^5$	$3.0 \cdot 10^{-5} \pm 2.1 \cdot 10^{-5}$	$1.4 \cdot 10^{-10} \pm 6.8 \cdot 10^{-11}$

After relatively long dissociation times (~20 min), the surface was regenerated in order to remove bound antibodies. Principally, surfaces were regenerated with 10 and 100 mM glycine solution (pH 2.0). However, this method was inefficient and even after numerous regeneration trials, antibody remained bound to the surfaces functionalized in both manners (data not shown). However, in the case of a hydrophobic surface, the injection of ethanol enabled complete removal of antigen from the surface and the surface would be re-used. Therefore, solutions of increasing anti-tamra concentrations (13.5, 20 and 27 nM) were injected after regeneration of the surface with absolute ethanol followed by tamra-chol immobilization (Figure 3.16 a, c, e).

These results were correlated with data obtained from various immunosensing experiments between anti-tamra and tamra-cadaverine bound covalently to the biochip surface. BIAevaluation software was used to fit all curves based on a simple Langmuir asymptote model 1:1. Kinetic rates (dissociation rate k_d, association rate k_a and binding affinity K_D) were calculated for n=4 independent measurements for tamra-chol and n=3 independent measurements for tamra cadaverine. Kinetic data for tamra molecules immobilized covalently and non-covalently did not differ significantly from each other and were comparable with previously obtained results describing well-characterized antibody – antigen interactions (214).

3.4. Immobilization of DNA oligomers on a hydrophobic surface

The functionalization of a hydrophobic surface *via* coupling with cholate-modified tamra (tamra-chol) molecules has thus been characterized and the method has been shown to be universally applicable and independent of the nature of the surface, SU-8 thin film or hydrophobic gold layer. In order to examine the efficiency of the method for the immobilization of other (bio) molecules, immobilization of cholesteryl-modified DNA oligomers (DNA-chol) on the hydrophobic surface was characterized. Firstly, a quantitative analysis of immobilized oligomers was performed, depending on the stock solution concentration and incubation time. Afterwards, the established method was applied to examine accessibility of DNA-chol on a hydrophobic gold surface by demonstrating the enzymatic digestion of oligomers.

3.4.1. Quantitative analysis of immobilized DNA

50 bp DNA oligomers modified with cholesteryl tetraethylene glycol moieties ('DNA-chol') were coupled to the hydrophobic surfaces in order to characterize the density of immobilized DNA-chol as a function of the stock solution concentration and immobilization time.

The influence of DNA-chol concentration on the number of immobilized molecules during short incubation times was examined. During the characterization of tamra-chol densities, whole surfaces were immersed in the fluorescent solution. Since the available amount of DNA was much lower than in the case of fluorescent tamra-chol, a method of 'sliding DNA' was developed. Based on the hydrophobic properties of the surface and its low affinity for hydrophilic liquids, the surface was placed at an appropriate slope that enabled sliding of a deposited drop as schematically shown in Figure 3.17b. This system was used to deposit 50-base single stranded DNA-chol. DNA labelling with ^{32}P isotope was performed to study immobilized DNA at low concentrations, since a radioactive labelling is more sensitive than a fluorescent one. Concentrations of applied DNA-chol varied from 2 to 7 μM and the contact of a solution with the SU-8 surface lasted several seconds. The effect of this short-time incubation is presented in Figure 3.17a as a digital image of an exposed storage phosphor screen with a captured latent image produced by ^{32}P radiation. Upon laser-induced stimulation in a Typhoon scanner, light was emitted from the storage phosphor screen in proportions of the amount of radioactivity in the sample that resulted in the presented image. One can observe the traces of molecules left after a DNA-chol droplet passing. Two intensive points visible at the beginning and in the end of a sliding droplet path represented the places where the droplet was deposited and then, where it was stopped and dried. With the exception of these areas, the paths were homogenously covered with the DNA solutions. Increased trace intensity was strongly related to the applied concentration of DNA-chol, from 2 to 7 μM. This clearly demonstrated that for the short incubation time, solution concentration had a significant influence on the number of immobilized molecules, as it was proved with tamra-chol deposition on SU-8 surface (Section 3.2.1 and Figure 3.12). Calculations based on the signal intensity measured within traces demonstrated that the ssDNA surface density varied from $1 \cdot 10^4$ molecules/mm^2 to $1 \cdot 10^5$ molecules/mm^2, depending on the stock solution concentration (Figure 3.17c).

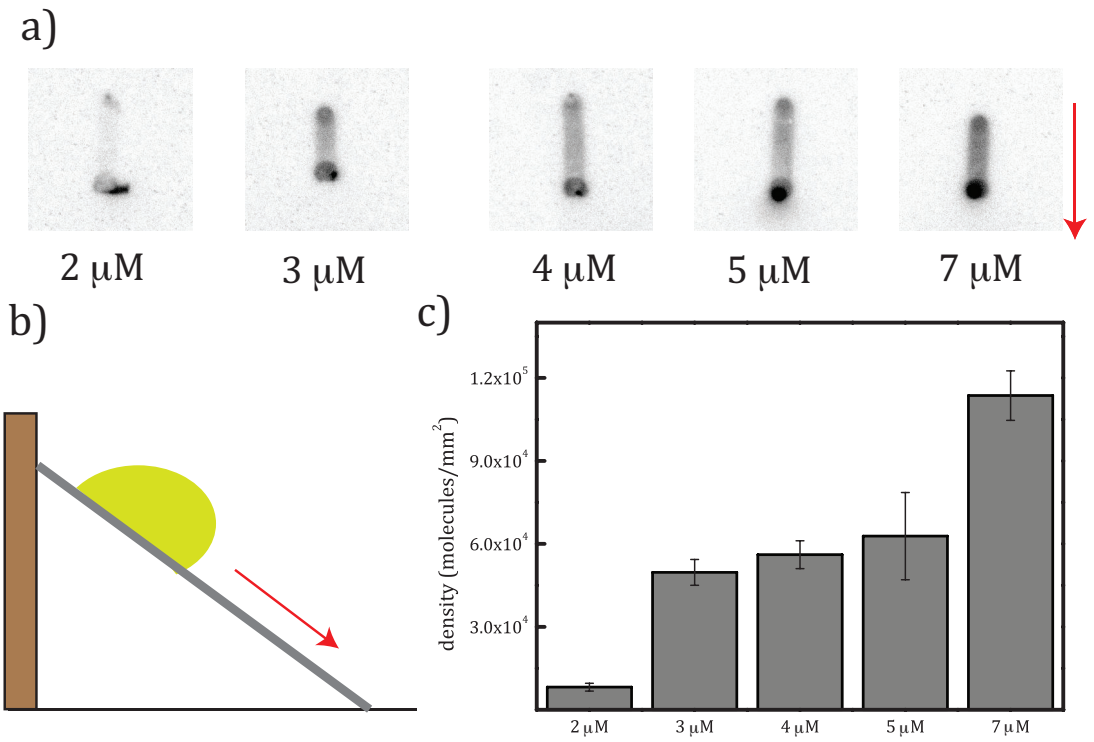

Figure 3.17. Immobilization of DNA-chol on a SU-8 surface **(a)** Traces left after radioactive ssDNA-chol droplet sliding on the SU-8 surface; **(b)** Illustration of sliding of ssDNA-chol droplet on the hydrophobic SU-8 surface placed under a specific slope. Red arrows indicated the direction of the droplet movement. **(c)** Density of immobilized ssDNA-chol on the SU-8 surface, deposited *via* a 'sliding method', measured within sliding traces. Calculations were based on a calibration curve of known increasing molarities of radioactive molecules.

To obtain a denser monolayer of immobilized DNA-chol, the incubation time was extended. Preliminary tests were performed with the lower concentrated ssDNA (2 – 7 µM) labeled with ^{32}P. However, the following studies were carried out with the fluorescently marked DNA, since this was easier to manipulate and was quicker to prepare (no need for post-synthesis enzymatic modifications to add the fluorescent label). Solutions of single stranded DNA-chol hybridized with a complementary strand labeled with a Cy5 fluorophore at the 5' extremity (1, 5 and 10 µM) were spotted on SU-8 surfaces and incubated for 30 min followed by extensive rinsing with PBS buffer. The densities of immobilized double stranded DNA-chol were compared with the same dsDNA not modified with a cholesteryl group based on the intensity of the fluorescent

signal (Figure 3.18). Two distinct conclusions may be drawn from the data. Firstly, the average density of immobilized dsDNA-chol was about $6 \cdot 10^{10}$ molecules/mm^2, independent of the stock solution concentration. Secondly, the density of non-specifically bound molecules was significantly lower than in the case of DNA-chol. This supported the hypothesis that the presence of cholesteryl moieties promoted interactions with the hydrophobic surface, thus one could assume that immobilization of DNA was specific and mediated *via* the cholesteryl group.

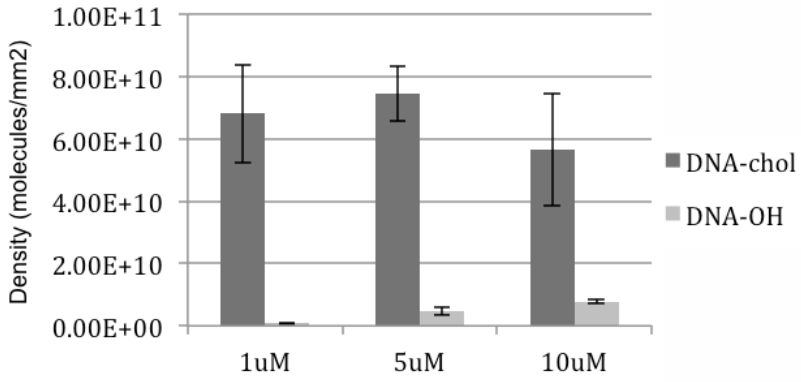

Figure 3.18. Density (in molecules/mm^2) of dsDNA with and without cholesteryl modification immobilized on the SU-8 surface. Standard deviations were calculated based on five independent measurements.

3.4.2. Enzymatic digestion of immobilized DNA-chol

As already defined above, the characterized functionalization method was universal and efficient for both cholesteryl- and cholate-modified molecules immobilized on a hydrophobic SU-8 surface and a hydrophobic gold surface. However, to prove the specificity of binding and accessibility of immobilized DNA-chol molecules for further reactions, enzymatic digestion of dsDNA modified with cholesteryl moiety and immobilized on the hydrophobic gold surface was demonstrated.

Previously hybridized dsDNA-chol containing a sequence recognized by BamHI endonuclease (sequences of oligonucleotides listed in Appendix I) was immobilized on the hydrophobic gold surface. Over-night immersion of the 50-nm gold layer evaporated on a glass prism in a solution of 1-undecanethiol in ethanol (procedure described in Chapter II, Section 2.3) caused formation of a hydrophobic self-assembled monolayer on

the gold surface that was used for direct coupling of dsDNA-chol. The surface was inserted in the SPRi apparatus followed by extensive rinsing with a running buffer specific for the BamHI restriction enzyme (100 mM NaCl, 50 mM Tris-HCl, 10 mM $MgCl_2$, 100 µg/ml BSA; pH 7.9). Stabilization of the signal implied that only specifically bound molecules remained on the surface. The effect of two sequential injections of BamHI enzyme on the immobilized dsDNA at room temperature is shown in Figure 3.19 in a form of a superimposed SPRi sensorgram, the curves for the two injections differed considerably. During the first injection (Figure 3.19, black curve), and following the customary increase due to bulk refractive index changes, material was retained on the surface and slowly dissociated after injection. The second injection of enzyme however resulted not only in reduced binding but also in a substantial loss of material from the surface subsequent to injection of the enzyme. These experiments were carried out at room temperature and not 37°C the optimal for BamHI. However it is clear that the enzyme is binding and digesting the bound DNA on the surface.

Control experiments on DNA without the restriction sites did not exhibit this behavior thus testifying to the specificity of the reaction.

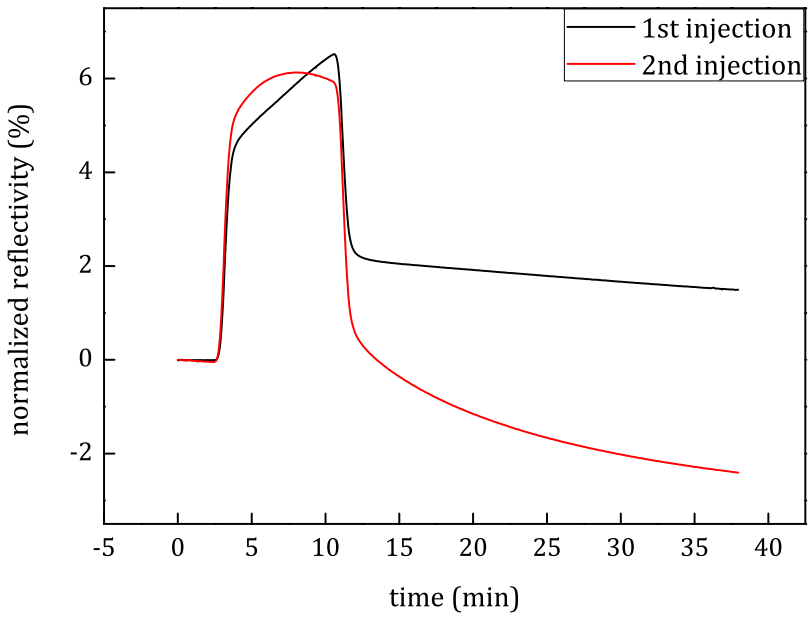

Figure 3.19. Superimposed SPRi sensorgram of two successive digestions of immobilized dsDNA-chol with BamHI endonuclease.

3.5. Conclusions and perspectives

This Section described the creation and functionalization of a hydrophobic surface based on coupling with cholate- and cholesteryl-modified molecules. The presence of a hydrophobic sterol ring attached to a (bio) molecule promoted interactions with a hydrophobic surface. The influence of incubation time and solution concentration on the density of immobilization of two different molecules (small fluorophore tamra and 50-base DNA oligomer) on the hydrophobic surface was examined. A rapid method of surface regeneration with a simple immersion in ethanol was developed and described. Moreover, it was shown that (bio) molecules of interest immobilized on the functionalized surfaces were accessible and used in biosensing applications, i.e. immunosensing assay and DNA digestion with a specific restriction enzyme.

Whilst most immobilization techniques involve numerous time-consuming steps, such as surface pre-treatment or modification, incubation times lasting several hours and multiply rinsing (215, 216), the method presented here was straightforward for SU-8 surfaces and did not require any long and complex preparation. In the case of gold surfaces, pre-treatment involved only an overnight incubation in reactive solution (undecanethiol in ethanol) followed by surface rinsing. Non-covalent adsorption of modified (bio) molecules of interest was the simplest and fastest method to automate since steps involving substrate activation and/or modification were not needed. (Bio) molecules modified with the moiety containing a sterol ring (e.g. cholate, cholesterol or cholesteryl) could be deposited directly on the hydrophobic surface.

Several seconds of incubation and 10 minutes rinsing were sufficient to form a stable monolayer of immobilized molecules. However, the density of the immobilized molecules depended on the initial concentration of the solution and/or incubation time. For the low-concentration solutions (≤1 μM) and short incubation times (≤1 min) the density of immobilized molecules was strongly controlled by two parameters, as demonstrated in Sections 3.3.1 and 3.4.1 for the examples of tamra-chol and DNA-chol immobilization, respectively. In addition, it was demonstrated that the density of immobilized molecules reached a plateau, indicating that surface saturation was reached. Considering the theoretical maximum surface density (calculated according to the footprint of the molecules as discussed already in Section 3.3.1) one can conclude

that saturation was reached at a sub monolayer density of around $1.3 \cdot 10^{12}$ – $1.5 \cdot 10^{12}$ molecules/mm^2.

The amphiphilic structure of DNA molecules possessing a cholesteryl moiety allowed their adsorption to a hydrophobic surface. This opens the possibility of fabricating Langmuir-Blodgett films with DNA-chol molecules immobilized on SU-8 films. It has already been shown that DNA-based surfactants behave like detergents and were surface-active at fluid surfaces, such as air-water and oil-water interfaces (217). Additionally, various Langmuir and Langmuir-Blodgett films were made with amphiphilic molecules modified with cholesterol or/and DNA (204, 218). Developing this method would allow fabrication of controlled monolayers with a higher surface density than those obtained with DNA-chol. This could be used in different applications where dense DNA monolayers are required.

It is worth remarking that these studies and data published in the literature (207, 208) treated with only short DNA oligomers (20 – 50 bases) and the effects of longer lengths are relatively poorly studied. It is not trivial to synthesize oligomers in excess of 50 bp. To obtain longer fragments of DNA and overcome issues with synthesis, cholesteryl-modified primers were used in standard PCR amplifications. However, amplified DNA fragments could not be purified with standard PCR purification methods, since size-exclusion columns did not allow the efficient DNA-chol elution. Finally, after several attempts concerning the purification step of DNA-chol, it was decided to perform all DNA-related studies with 50-base oligomers. In order to overcome this problem, an alternative way of getting long cholesteryl-modified oligomers must be found. One possibility could include PCR product purification by HPLC or by post-synthesis labelling of DNA-NH_2 oligomers with Na-cholate after EDC/NHS activation, using the same protocol as described in Section 3.2.1.

Surfaces functionalized with noncovalently bound (bio) molecules based on hydrophobic coupling can be used repeatedly since efficient regeneration was demonstrated. As shown in Section 3.2.2, immersion of samples in absolute ethanol efficiently and rapidly removed immobilized (bio) molecules. Furthermore, re-use of these surfaces was demonstrated for the example of immunodetection presented in Section 3.3.3. This feature opens up broad possibilities for potential applications. For instance, the application of hydrophobic surfaces functionalized with cholate- or cholesterol-modified ligands to SPRi-based experiments would allow rapid reproducible

regeneration of surfaces obviating errors initiated by denaturation of target molecules caused by harsh regeneration conditions.

Going further, one could create a system where high affinity complexes could be formed and analyzed with SPR. These complexes could be released from the surface *via* ethanol rinsing and, further analysis applied for example in a mass analyzer. The development of a robust protocol could thus improve assays based on the identification of proteins captured on DNA during complex sample screening (44). First of all, one could obtain a substantial amount of a specific nucleoprotein complex, if a significant amount of DNA were to be immobilized on the SPR sensor surface. In addition, extensive rinsing would remove all non-specifically bound molecules and only specific complexes would remain bound to the surface. Additionally, native proteins are not required in MALDI experiments, thus the potential denaturation of proteins during ethanol release would not affect the analysis.

Data presented in this Section demonstrate that functionalization based on cholate- and cholesteryl-modified (bio) molecule binding to the hydrophobic surface could be applied to immunosensing assays (Section 3.3.3) and specific digestion of immobilized oligomers *via* restriction enzymes (Section 3.4.2). However, it was hypothesized that this method was more universal and could be used to analyze other interactions, such as nucleoprotein and protein-protein complex formation, sample screening assays, *in situ* DNA hybridization, and identification of DNA mutations. The simplicity of sample preparation and the possibility of chip re-utilization even in the case of very stable complex formation increase the potential of this method in biosensing applications. Nevertheless, in the case of interactions concerning the use of proteins special attention needs to be made for their stability on hydrophobic surfaces.

4. Comparative study of biomolecule immobilization methods on gold surface

The majority of studies using gold in biosensing involve gold nanoparticles, Quartz Crystal Microbalance (QCM) or surface plasmon resonance (SPR). Gold nanoparticles have rather unusual physicochemical features useful for biological applications (219). They possess excellent optical and optoelectronic properties, i.e. plasmon resonance absorption, conductivity, redox attributes etc. Gold nanoparticles are easily synthesized and variations in their size and shape significantly change certain properties. QCM technology takes advantage of piezoelectric mass sensing during biological recognition. Piezoelectric transducers allow very sensitive label-free detection of molecules. They are not only mass sensors but they can also detect interfacial phenomena, viscoelastic properties of the adhered biomaterial, surface charges of adsorbed molecules, and surface roughness (220). A thin layer of gold in SPR serves to generate surface plasmon as a response to light excitation which are then used in various applications, for example detection of biological interactions. In addition, thin gold layer provides high chemical and biological stability and high sensitivity resolution.

Physicochemical characteristic of gold offers the possibility of variable functionalization with a wide range of organic or biological ligands for the selective binding and detection of small molecules and biological targets. Gold can be functionalized in many ways, however the most common technique is based on gold – thiol interactions. These are extremely strong, easily-formed and robust covalent bonds. In addition, sulphur is broadly available and therefore thiol-gold interactions can be used to immobilize numerous molecules, such as polymers to cover the gold surface (e.g. dextran and polyethylene glycol), short chain based molecules to form a self-assembled monolayers (SAM) (e.g. *n*-ethylene glycol and 11-mercaptoundecaonic acid) or to directly immobilize (bio) molecules of interest (e.g. thiolated DNA oligomers or proteins *via* accessible cysteine moieties (47)). A wide range of modifications in thiolated molecules immobilized to gold allows the construction of systems where immobilized polymers or head groups of SAM are coupled with (bio) molecules of interest. These features provide universality for biosensing applications of gold-based systems.

Surface functionalization and controlled immobilization of ligands on a sensor chip are crucial elements in the fabrication of any surface-based biosensor. During biochip

preparation several requirements should be fulfilled. First of all, immobilized ligands must remain in their native form and their interacting site (e.g. antigen binding site in antibodies or active site in enzymes) should be as fully accessible for interaction with the analyte as it would be in solution. Even though immobilization often involves ligand modification, such as adding a linker or a functional group, this process should take place as far as possible from the region of interest. For example, it is recommended to modify and immobilize antibodies *via* the constant region of the heavy chain (Chapter I, Figure 1.3.8) that is thus far from the binding site and unlikely to affect the recognition event.

The next crucial issue concerning (bio) molecule immobilization on a sensor surface is verification of ligand density. Depending on the biosensor application different densities are required ranging from, single-molecule studies in total internal reflection fluorescent (TIRF) microscopy to densely packed monolayer structures. It is crucial to estimate the amount of immobilized (bio) molecules on the surface area and to choose the most appropriate functionalization strategy for a given application. Too high amount of immobilized (bio) molecules may result in steric hindrance and thus limit access to the recognition site in the immobilized ligand. Also recapture of analytes after dissociation a neighbor ligand may lead to severely underestimated dissociation rates.

Another important point to note during surface (bio) functionalization is the influence of the surface. Usually, each biosensing technique requires a dedicated surface that is optimized for a specific application. For instance, in SPR, a presence of a thin metal layer at the interface is fundamental to create a plasmon by electron excitation. In general the field intensity decays exponentially to about 200 nm from the surface. The immobilized ligand must therefore be placed within this region in order to obtain reliable results. On the other hand, too close proximity to the surface can cause undesirable interactions, for example non-specific adsorption of (bio) molecules to hydrophobic surfaces. Therefore, to overcome this obstacle, surfaces are generally protected with an antifouling layer composed of oligomers or polymers, such as *n*-ethylene glycol (37) or dextran (221), as discussed in Chapter I.

The goal of the studies described in this Section was to compare various gold functionalization strategies in order to obtain information about the effects of the density of immobilized DNA oligomers, their stability on functionalized gold surfaces and the degree of nonspecific interactions.

4.1. Quantitative analysis of immobilized linear DNA on a functionalized gold surface

Several strategies for the immobilization DNA oligomers on a gold thin layer pre-functionalized with *n*-ethylene glycol molecules have been compared in this Section. Self-assembled monolayers (SAM) composed of thiolated *n*-ethylene glycol (*n*-EG) at a moderate density constitute a robust antifouling agent that protects immobilized (bio) molecules from the surface (37, 47, 176). Modification of *n*-EG molecules allows surface functionalization with various groups, including amine, carboxyl, thiol, biotin etc. In these studies, modified oligomers were grafted to functionalized gold surfaces *via* gold – thiol bond formation, amide bond formation and non-covalent interactions between biotin and extrAvidin, and additionally compared with functionalization by hydrophobic coupling of cholesteryl-modified DNA. The analysis of results was focused on the density of bound DNA as a function of the oligomer length and concentration and specificity. All studies were performed with DNA oligomers labeled with ^{32}P at the 3' or 5' end immobilized on a 50-nm gold layer evaporated on a glass slide.

To examine the density of immobilized oligomers as a function of oligomer length, 1 μM dsDNA of three different lengths: 50, 500 and 1000 bp with a specific modification were incubated on pre-functionalized surfaces. After given incubation times, surfaces were extensively rinsed with an appropriate buffer, followed by sample incubation in a developing cassette as described above and in Chapter II, Section 2.

Studies concerning the stability of immobilized DNA on the pre-functionalized surface were performed on short DNA (50 nt). Oligomers at 10 μM concentration were labeled with modified adenosine triphosphate (ATP), having a ^{32}P isotope on the alpha or gamma phosphate group. Samples (as presented schematically in Figure 3.20) were tested in order to determine the molecular stability of immobilized DNA as a function of density. Single stranded DNA (marked as 'ssDNA') was modified at the 5' extremity with an appropriate functional group and at the 3' extremity with alpha ^{32}P-ATP. These oligomers were also hybridized with a complementary strand without any modification (marked as 'dsDNA-X*' where X stand for the strand modification: thiolated, biotinylated or aminated). Other oligomers consisted of hybridized dsDNA where one strand was modified with a functional group and the other with a ^{32}P-ATP isotope (marked as 'dsDNA*'). All oligomers were compared to determine the density of immobilized

oligomers depending on their nature: ssDNA and dsDNA. The comparison between dsDNA-X* and dsDNA* determined the stability of the hybridized oligomer and indicated the amount of dehybridization when dsDNA was bound to the pre-functionalized surface. The dependence of the density of immobilized dsDNA-X* on the concentration of the incubated solution: 1 and 10 μM was also examined. In addition, the density of all samples was compared with a 50-bp control DNA (marked as 'dsDNA-OH') that did not possess a functional modification.

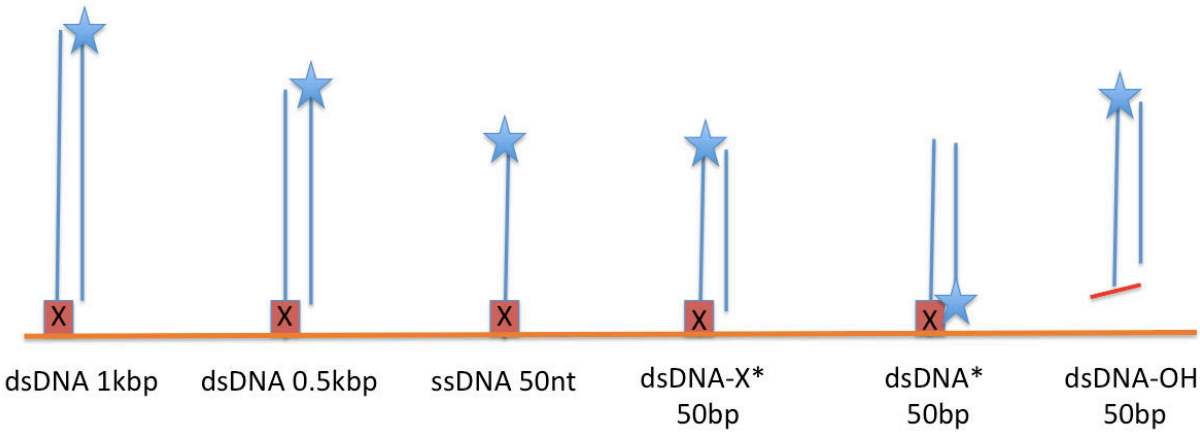

Figure 3.20. Schematic representation of DNA samples immobilized on a pre-functionalized gold surface. From left to right: 'dsDNA 1 kbp' – 1037 bp dsDNA; 'ds 0.5kbp' – 495 bp dsDNA; 'ssDNA 50 nt' – 50 base ssDNA; 'dsDNA-X* 50bp' – 50 bp dsDNA labeled with a functional group ('X') and a radioactive isotope on the same strand; 'dsDNA* 50bp' – 50 bp dsDNA labeled with a functional group ('X') and a radioactive isotope on two different strands; 'dsDNA-OH 50bp' – control 50 bp dsDNA without a functional group. Star stands for a radioactive labeling. Red square with X is for a functional group, depending on the functionalization strategy: thiol (-SH), amine (-NH2) or biotin (-biot).

4.1.1. Gold – thiol bond formation

The strength of covalent interactions between gold atoms and thiol sulphur is commonly used to obtain robust self-assembled monolayers (SAM) for biosensor applications (36). Both, formation and properties of SAMs based on thiol-gold interactions are extensively described in the literature (222). In this Section, characterization studies of the density of thiol-modified DNA oligomers immobilized on

a gold thin layer are presented in order to obtain comparative data and to indicate similarities and differences between various surface functionalization strategies. Characterization of thiol – gold functionalization strategy is discussed first, since it is the most commonly used.

50-nm gold layers evaporated onto a glass slide were pre-functionalized by immersion in a solution of thiolated ethylene glycol (EG-OH) diluted in absolute ethanol for 30 s prior to over-night incubation with ^{32}P radioactive labeled thiolated DNA (DNA-SH), as described in Chapter II. After extensive rinsing with phosphate buffer and incubation in a developing cassette, the signal from immobilized radioactive DNA-SH was quantified. Results presented in Figure 3.21a show the density of immobilized short (50 bases) DNA-SH. Thiolated ssDNA was bound to a higher density than dsDNA, giving respectively $5.8 \cdot 10^{13}$ and $2.7 \cdot 10^{13}$ molecules/cm^2. These values correlate well with data previously published in the literature (36, 37). It was deduced that this functionalization strategy did not have any influence on the double helix and immobilized 50 bp remained hybridized on the gold surface. The densities of double stranded DNA labeled radioactively on one of two strands ('dsDNA*' for labeling on the immobilized strand and 'dsDNA-SH*' for the hybridized strand) were respectively $2.7 \cdot 10^{13}$ and $3.3 \cdot 10^{13}$ molecules/cm^2. This showed that the pre-functionalized gold surface did not decrease the stability of immobilized dsDNA that remained in its double-stranded form.

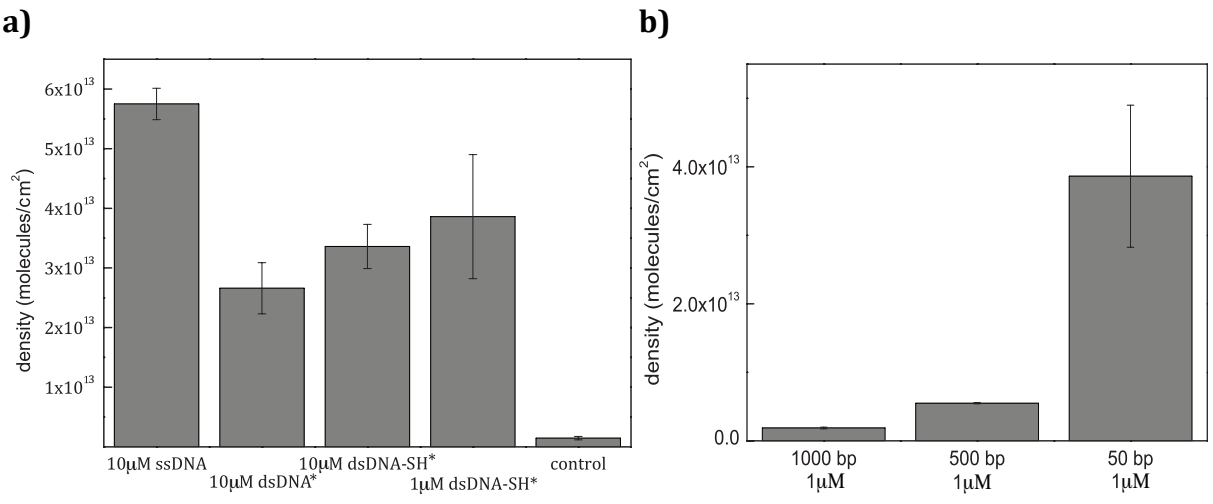

Figure 3.21. (a) Density of immobilized 50-base DNA-SH on pre-functionalized gold surfaces; **(b)** Density of immobilized dsDNA-SH on pre-functionalized gold surfaces. Standard deviations were calculated based on three independent measurements.

The concentration (1 or 10 μM) solutions of dsDNA-SH spotted on the surfaces had no impact on the density of the immobilized molecules. Spotting of dsDNA-SH at both concentrations and overnight incubation gave comparable densities of immobilized molecules (around $3 \cdot 10^{13}$ molecules/cm^2) within the error bars of the experiment. This indicated that after overnight (~16 hours) incubation of dsDNA-SH solution on the gold surface the number of immobilized molecules was independent of the initial concentration of the solution in the range of 1 to 10 μM. Measured densities for all the short (50 nt) oligomers suggested a high specificity of immobilization *via* thiol-gold bond formation. Measured densities were compared with a control sample that did not possess a thiolated modification. The density of immobilized DNA-SH was in a range 2.7 – $5.7 \cdot 10^{13}$ molecules/cm^2, while for the control sample it was $1.4 \cdot 10^{12}$ molecules/cm^2 - a difference of more than one order of magnitude.

Comparison of the densities of immobilized DNA-SH as a function of oligomer lengths depicted in Figure 3.21b clearly showed that the density decreased with increasing DNA length. Namely, measured values were: $4 \cdot 10^{13}$ molecules/cm^2 for 50 bp DNA-SH, $5 \cdot 10^{12}$ molecules/cm^2 for 500 bp DNA-SH and $2 \cdot 10^{12}$ molecules/cm^2 for 1000 bp DNA-SH. These results showed that longer molecules, possessing only one reactive group led to less dense monolayers immobilized on the functionalized surface.

In summary, gold surface functionalization for immobilizing DNA *via* thiol – gold bond formation is a well known and commonly used method effective to produce high density and controlled immobilization (36). The data presented here demonstrated that ssDNA was immobilized to a greater degree than its double stranded analogue. Additionally, long incubation times (~16 hours) were effective in producing constant densities of immobilized DNA, regardless of the initial solution concentrations. The dependence of density on the length of the immobilized oligomers showed that shorter oligomers formed denser monolayers than longer oligomers prepared under the same conditions. A low level of nonspecific interactions showed that the 30-second immersion in EG-OH solution produced a reliable anti-fouling layer giving protection both from nonspecific adsorption and denaturation of the double helix as previously described (37).

4.1.2. Amide bond formation

Amide bonds formed between carboxyl group and primary amines are very common in nature; they are formed between functional groups in amino acids in order to create peptides and proteins. In laboratory conditions this coupling reaction can be mediated using a zero-length cross-linking agent 1-ethyl-3-(3-dimethylaminopropyl)-carbodiimide (EDC) that forms a reactive ester. The stability of the ester increases in the presence of N-hydroxysuccinimide (NHS) or N-hydroxysulfosuccinimide (sulfo-NHS). These coupling substances are water-soluble and can be easily removed by filtration, dialysis or, as in the present case, by rinsing.

In our studies a gold surface was first incubated for 30 s with 11-mercaptoundecyl tetra(ethylene glycol) (EG-OH) diluted in ethanol to form a SAM with a low molecular density. Secondly, the surface was immersed in a solution of 1 mM $^{-}S(CH_2)_{11}(OCH_2CH_2)_6$-COOH (EG-COOH) for times ranging from 5 to 120 min that allowed SAM formation of increasing carboxyl densities. Carboxylated surfaces were then activated with a solution of EDC/NHS as described in Chapter II followed by deposition of ^{32}P radioactive labeled DNA modified with an amine group at its 5' extremity ('DNA-NH_2'). DNA was diluted in a 0.4 M phosphate buffer (pH 7.0) to concentrations of 1 and 10 μM. After 2 hours of incubation time, samples were extensively rinsed with a phosphate buffer and incubated in a developing cassette prior to quantitative analysis.

The analysis of short (50 bases) DNA densities spotted at a concentration of 10 μM demonstrated that immobilization of single stranded DNA (ssDNA) provided a higher density than double stranded DNA (dsDNA). Based on data presented in Figure 3.22a, the density of immobilized ssDNA was $1.5 \cdot 10^{11}$ molecules/cm^2 when the immersion time in EG-COOH was from 5 min to 60 min and $8 \cdot 10^{11}$ molecules/cm^2 for an immersion time in EG-COOH of 120 min. The surface density of dsDNA was around $2 \cdot 10^{10}$ molecules/cm^2 for immersion times in EG-COOH 5 min and $3 \cdot 10^{11}$ molecules/cm^2 for 120 min of EG-COOH immersion time. These differences could be explained by that the fact that a double helix of 50 bp is stiffer than its single stranded counterpart and requires more space and time for its terminal amine to react with the surface than the more flexible ssDNA under the same conditions.

In addition, a similar number, ~$2.5 \cdot 10^{11}$ molecules/cm^2, of immobilized dsDNA molecules ('dsDNA-NH_2*' for DNA labeled with ^{32}P on the strand having an amine

modification and 'dsDNA*' for DNA labeled with ^{32}P on the complementary, previously hybridized strand) indicated that the close presence of the gold surface did not have a negative impact on the stability of hybridized 50 bp DNA (47) and that dsDNA did not dehybridize in these conditions.

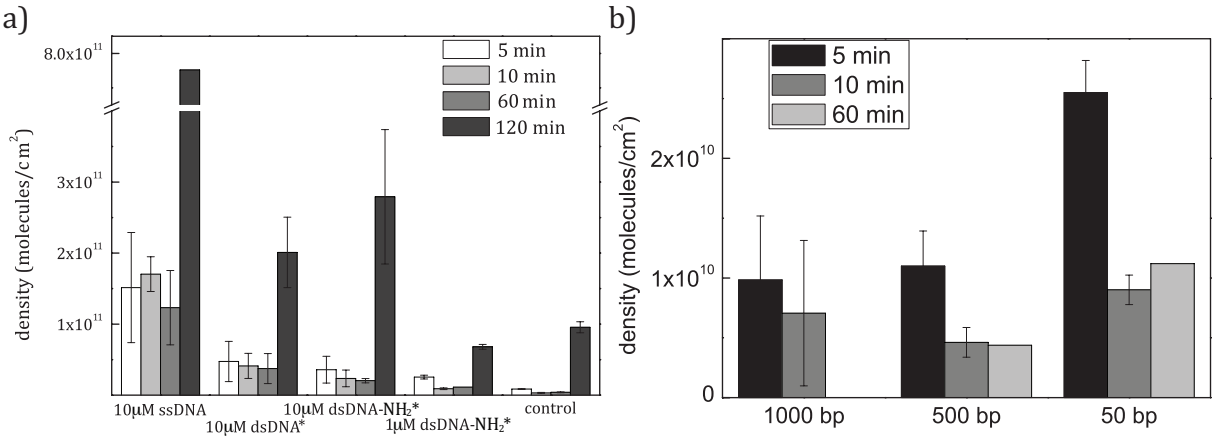

Figure 3.22. Density of immobilized aminated DNA on the pre-functionalized gold surface: **a)** 50-base DNA-NH_2; **b)** dsDNA-NH_2 of different lengths. 5, 10, 60 and 120 min indicate surface immersion time in 1 mM EG-COOH solution. Standard deviations were calculated based on three independent measurements.

The next conclusion concerned the composition of the formed antifouling SAMs. The density of immobilized EG-OH on the surface was constant for all samples; only the density of EG-COOH was varied according to the incubation time for each SAM formation. Since the density of SAM was strongly related to the incubation time, it was assumed that the longer the immersion in the EG-COOH solution, then the denser the SAM that would be obtained and therefore more carboxyl groups present on the surface could be coupled with amines.

Indeed, analysis of the data presented in Figure 3.22a confirmed that 120-min immersion in EG-COOH solution lead to the higher number of immobilized molecules, independently from the nature of DNA (single and double stranded). However, taking into account the 10 μM control dsDNA sample that did not possess amine modifications, one could draw the conclusion that 120-min incubation of EG-COOH on a gold surface caused also an increase in the number of non-specifically bound DNA molecules of around 2.5 fold. Because under these conditions a higher number of polar carboxyl

groups were exposed on the surface, this could also cause an increase in the hydrophilicity of the system and thus nonspecific adsorption of molecules.

In the next step, the number of immobilized DNA molecules was analyzed as a function of the concentration of the deposited DNA solutions. 50 bp dsDNA at concentrations of 1 and 10 μM were spotted and incubated following the standard protocol described in Chapter II. A quantitative analysis demonstrated that spotting of less concentrated solutions resulted in a lower density of immobilized DNA (Figure 3.22a): samples with 10 μM dsDNA produced a density of $2 \cdot 10^{10}$ - $3 \cdot 10^{11}$ molecules/cm^2 and with 1 μM dsDNA between $1 \cdot 10^{10}$ and $8 \cdot 10^{10}$ molecules/cm^2. This could be explained by the fact that binding was at higher concentration of spotted biomolecules increased the probability of a coupling event.

In the last comparative analysis, the influence of DNA length on the density was examined. 1 μM DNA of three lengths: 50, 500 and 1000 bp was immobilized on the surface based on a standard procedure (Figure 3.22b; sequences of DNA listed in Appendix I). The number of immobilized DNA molecules was higher for short 50 bp DNA ($1 \cdot 10^{10}$ – $3 \cdot 10^{10}$ molecules/cm^2) in comparison to longer molecules 500 and 1000 bp where the calculated density was between $4 \cdot 10^9$ and $1 \cdot 10^{10}$ molecules/cm^2. Evidently the lower density of immobilized long DNA strands could be explained by the fact that these long molecules (170 and 340 nm for 500 and 1000 bp DNA, respectively, based on the assumption that 1 bp ≈ 0.34 nm) possessed only one reactive group that was hardly accessible to be coupled with an activated carboxyl group.

Taking into account all the results one could conclude that the density of immobilized DNA-NH_2 molecules depended on several factors, such as the density of carboxyl groups in a functionalized antifouling monolayer, the nature of DNA (single and double stranded DNA), the concentration of the deposited solution and the DNA length. These results also confirmed that the proximity to a gold surface did not have any influence on the stability of short (50 bp) dsDNA.

4.1.3. ExtrAvidin – biotin bond formation

Bonds formed between biotin and avidin or its analogues (e.g. neutravidin, extrAvidin or streptavidin) are known to be amongst the strongest non-covalent interactions in nature, with extremely high affinity constants $K_D \approx 10^{-15}$ M. The ease,

speed and robustness of these interactions has ensured that avidin – biotin complexes are commonly used in numerous and varied biological applications, i.e. to immobilize modified (bio) molecules on biochip surfaces (223).

In our studies, biotin and extrAvidin were used to immobilize biotinylated DNA oligomers (DNA-biot) on pre-functionalized gold surfaces *via* a sandwich reaction. Surfaces pre-functionalized with a SAM of EG-OH and EG-biot ($^{-}S(CH_2)_{11}(OCH_2CH_2)_6$-biotin) were entirely covered with a solution of extrAvidin in PBS buffer prior to immobilization of DNA-biot. In order to obtain the optimal amount of immobilized molecules, various concentrations of immobilized extrAvidin were tested. Principally, three solutions of 1, 50 and 100 nM extrAvidin in PBS were spotted on the pre-functionalized 50-nm gold layer evaporated on a glass prism. The prism was inserted into the SPRi apparatus and 1 μM solution of 50 bp dsDNA-biot was injected and passed over the chip for 6 min. The SPRi sensorgram (Figure 3.23) illustrated changes in the refractive index at the interface as a response to the interaction with a biotinylated analyte. The injected biotin reacted with extrAvidin immobilized on the surface proportionally to the concentration of the spotted extrAvidin. However, extrAvidin in the concentration range 1 and 50 nM was not sufficient to bind significant amounts of biotinylated analyte, as the intensity of the signal in the dissociation phase corresponded to the background (black curve). On the other hand, the signal from spots with 100 nM extrAvidin (blue curve) remained constant after binding DNA-biot and upon rinsing with PBS indicating a stable and specific interaction. The noise present during all monitoring process occurred because the overall changes in the refractive index were registered close to the detection limit. Based on the these data, it was concluded that 100 nM extrAvidin immobilized on the gold surface pre-treated with EG-OH and EG-biot was appropriate to bind biotinylated molecules and this concentration of extrAvidin was used in all the following studies.

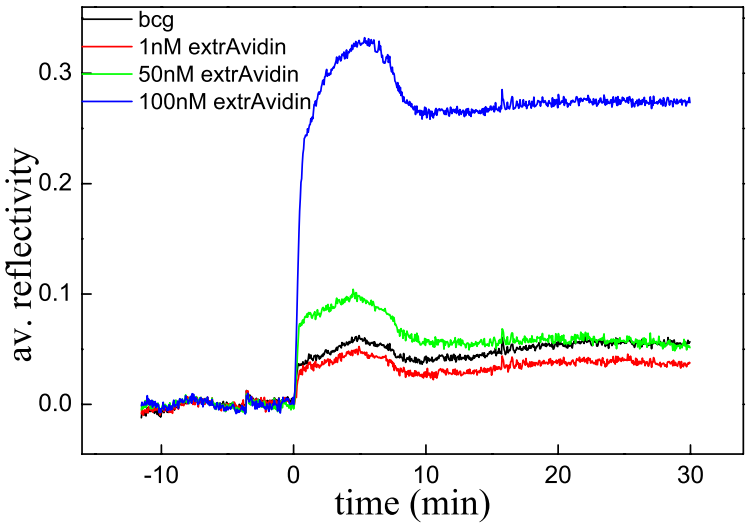

Figure 3.23. SPRi sensorgram of interactions between injected 1 µM dsDNA-biot (50 bp) with extrAvidin immobilized on pre-functionalized gold surface. The analyte was injected for 6 min.

In order to obtain different amounts of accessible biotin molecules immobilized on the biochip surface, gold surfaces were immersed for 30 s in EG-OH solution, followed by incubation with 1 mM EG-biot for times ranging from 5 to 120 min, based on the procedure described in Chapter II. Pre-treated surfaces were incubated with 100 nM solution of extrAvidin in PBS buffer for 1 hour, followed by rinsing with PBS buffer and 2-hour incubation with spotted DNA solutions. Analogous quantitative analysis of immobilized ^{32}P-labeled DNA-biot densities as in the case of amine-modified DNA (Chapter III, Section 4.1.2) was performed. Results are summarized in Figure 3.24.

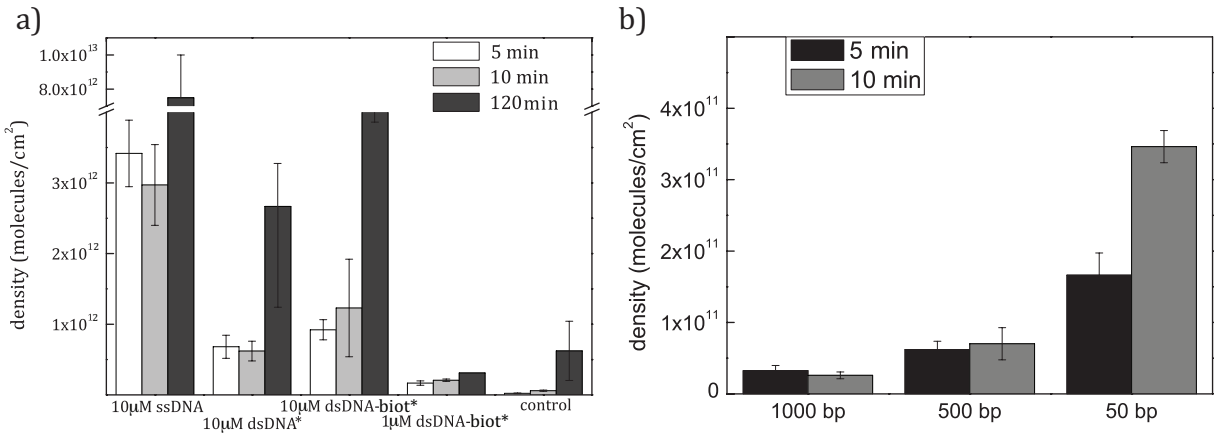

Figure 3.24. Density of biotinylated DNA immobilized on the pre-functionalized gold surface *via* biotin – extrAvidin sandwich reaction: **(a)** 50-base DNA-biot **(b)** dsDNA-biot of different lengths. 5, 10, and 120 min indicate surface immersion time in 1 mM EG-biot solution. Standard deviations were calculated based on three independent measurements.

The density of immobilized short (50 bases) DNA in concentration 10 μM was compared as a function of the EG-biot incubation time and DNA structure (single and double stranded). Values obtained for ssDNA varied from $3 \cdot 10^{12}$ molecules/cm^2 for 5 min immersion in EG-biot solution to $8 \cdot 10^{12}$ molecules/cm^2 for 120-min immersion. For dsDNA the number of immobilized molecules ranged from $7 \cdot 10^{11}$ molecules/cm^2 for 5 min immersion in EG-biot solution to $4 \cdot 10^{12}$ molecules/cm^2 for 120-min immersion. The amount of immobilized ssDNA was higher than dsDNA. Based on these data, it was concluded that longer immersion times in EG-biot solution were effective in creating higher densities of immobilized EG-biot molecules and therefore in higher densities of immobilized DNA on the surface pre-functionalized with 100 nM extrAvidin.

The densities of immobilized 10 μM 50 bp dsDNA radioactively labeled on one of the strands ('dsDNA*' for labeling on the complementary strand and 'dsDNA-biot*' for radioactive labeling on the biotinylated strand) were compared; measured values showed no significant difference. Densities were from ~$8 \cdot 10^{11}$ molecules/cm^2 for 5 min immersion in EG-biot solution to ~$4 \cdot 10^{12}$ molecules/cm^2 for 120-min immersion. This indicated that immobilized dsDNA was stable. The proximity of the gold surface and/or the presence of biotin – extrAvidin complex did not have a negative influence on the double-helix structure and did not cause dehybridization of the strands.

Similarly as in the case of immobilization of amine-modified DNA, for DNA-biot a significant difference in density was observed depending on the concentration of the deposited solution. When 1 μM dsDNA-biot was incubated on the surface, the density was about $2 \cdot 10^{11}$ molecules/cm^2, whereas the incubation of 10 μM dsDNA-biot in the same conditions created a density of $1 \cdot 10^{12}$ – $4 \cdot 10^{12}$ molecules/cm^2 (Figure 3.24a). This density difference of nearly one order of magnitude may be explained by the fact that higher concentrations of deposited oligonucleotides might promote binding since the possibility of a coupling event was higher.

These data showed that most of the DNA oligomers were immobilized specifically *via* biotin–extrAvidin interaction, since the density of the control DNA (not biotinylated) was nearly two orders of magnitude lower. In addition, the data showed that this functionalization strategy was effective for more specific immobilization than in the case of immobilization of amine-modified DNA, since the ratio of specific to non-specific interactions was higher for biotinylated samples than for aminated: 1:0.04 and 1:0.18, respectively.

The density of immobilized DNA-biot as a function of DNA length (Figure 3.24b) confirmed the statement made in Sections 4.1.1 and 4.1.2 that the longer the DNA, then the less dense the DNA monolayer formed. Spotting and immobilization of 1 μM dsDNA-biot in lengths of 50, 500 and 1000 bp gave the following densities of immobilized oligomers: $2 \cdot 10^{11}$, $7 \cdot 10^{10}$ and $3 \cdot 10^{10}$ molecules/cm^2, respectively.

In summary these results suggest similar conclusions as those for immobilized amine-modified DNA on pre-functionalized gold surfaces (Section 4.1.2). The density of immobilized DNA-biot molecules depended on several factors, such as the amount of functional biotin groups in a pre-functionalized antifouling monolayer and the number of accessible extrAvidin molecules, the nature of the DNA (single or double stranded DNA), the concentration of the deposited solution and the DNA length. These results confirmed that the presence of a proximal gold surface had no influence on the stability of short 50 bp dsDNA.

4.2. Conclusions and remarks

In these Sections various strategies for DNA oligomer immobilization on the pre-functionalized gold surfaces were described. The gold surfaces were incubated with a mixed SAM of thiolated *n*-ethylene glycol. Thanks to head group modifications in *n*-ethylene glycol molecules, several functionalization strategies were available and allowed immobilization of modified DNA molecules in different ways, including covalent bond formation (amide and Au – thiol) and non-covalent interactions (biotin – extrAvidin affinity interactions and hydrophobic coupling).

The presence of SAM in these systems had several functions. First of all immobilized *n*-ethylene glycol molecules provided functional groups for immobilization of modified DNA oligomers. SAM functionalized with carboxyl groups followed by activation with an EDC/NHS solution was coupled with amine-modified molecules. Accessible biotin on the top of a formed SAM was used to capture extrAvidin. ExtrAvidin possesses four binding sites and at least one of them was coupled to EG-biot, remaining binding sites were used to capture biotinylated molecules (here DNA-biot) and thus to create a sandwich-like immobilization system. Additionally, a dense SAM formed from 1-undecanthiol provided a hydrophobic surface that was applied to graft cholesteryl modified DNA as discussed in Section 3 of this Chapter.

The other important role of SAM was to protect immobilized (bio) molecules from nonspecific interactions by controlling the distance from the gold surface. The density of deposited DNA oligomers without functional groups (DNA-OH) was about 1 – 2 orders of magnitude lower than in the case of immobilized specifically modified DNA. It turned out that even a loose monolayer of *n*-ethylene glycol had antifouling properties and significantly reduced adsorption of (bio) molecules (37).

The following conclusions could be drawn from data concerning gold surfaces functionalized with differently modified DNA molecules. Immobilization of short (50 bases) DNA oligomers gave higher density binding for ssDNA than dsDNA. As mentioned above, the structure of ssDNA is more flexible than ds DNA and thus it was hypothesized that a functional group placed at the extremity of a molecule could reach the pre-functionalized surface faster. In the case of dsDNA structure, the rigidity of the double helix therefore resulted in fewer adsorbed molecules. This appeared to be independent of the DNA incubation time since thiolated oligomers deposited on the surface for ~16

hours also showed a higher density for single stranded molecules than their double stranded analogues (Figure 3.20a).

It was demonstrated that short (> 25 bp) dsDNA immobilized on surfaces did not remain double stranded and they dehybridized easily, even though dsDNA of the same length remained hybridized in solution (224). In order to characterize the stability of 50 bp DNA immobilized on gold surfaces, a test with double-labeled DNA was performed. Two identical samples of previously hybridized dsDNA were incubated on the pre-functionalized gold surface. In both of them one strand had one radioactively labeled ^{32}P adenosine triphosphate: either the strand possessing the functional group (-NH_2, -biot and –SH) or the complementary one. Quantitative analysis showed that in each functionalization method the number of immobilized molecules was similar in both samples indicating that the vicinity of the surface did not have any influence on immobilized 50 bp dsDNA. Since longer dsDNA oligomers possessed more hydrophobic bonds that kept oligomers in their double helix structure, it was assumed that immobilized 500- and 1000-bp dsDNA remained fully hybridized.

The characterization of DNA density as a function of oligomer lengths suggested that the length of bound DNA was directly related to the density of the monolayer formed. This could be explained by the difficulty of access of a functional group placed at the extremity of a DNA molecule to the head group present on the top of SAMs. Long dsDNA molecules (170 and 340 nm for 500 and 1000 bp DNA, respectively, based on the assumption that 1 bp ≈ 0.34 nm) are longer than the persistent length and thus are flexible and thus the active group present in the end of the strand could be hidden within a structure, therefore less accessible for coupling reactions. In this situation even long incubation times (16 hours for DNA-SH) led to a significantly lower density of immobilized long DNA.

It was demonstrated that longer immersion of a gold surface in functional *n*-ethylene glycol (EG-NH_2 and EG-biot) produced higher densities of accessible functional groups on the top of formed SAMs. This resulted in a higher amount of immobilized modified DNA. This tendency was observable for all the functionalization methods. In addition, 120-min immersion in modified *n*-EG significantly increased the number of immobilized molecules. Two possibilities could explain this phenomenon. First, long immersion of a gold surface in *n*-EG solution formed a dense SAM that possessed a high number of functional groups accessible for coupling to modified DNA. Second, a dense

SAM reduced nonspecific adsorption to gold atoms and promoted interactions between head groups of SAM and DNA. However, for the 120-min incubation with *n*-ethylene glycol the number of bound molecules increased in all samples, including the control ones. One could assume that this was related to increased hydrophilicity and thus to increased amounts of non-specific interactions between the head groups of SAM and DNA.

The effects of the immobilization strategy on the density of immobilized DNA molecules indicated that immobilization *via* gold – thiol bond formation produced the highest number of immobilized molecules, reaching 10^{13} molecules/cm^2. This is also the best known and characterized gold functionalization method (36, 37). Two strategies of DNA immobilization, *via* biotin – extrAvidin interaction and amide bond formation, produced densities of immobilized DNA between 10^9 and 10^{12} molecules/cm^2 depending on applied conditions, such as the nature of the DNA (ssDNA or dsDNA), the concentration of deposited solution and DNA length. These effects are summarized in Table 3.2.

Density of DNA immobilized based on hydrophobic coupling with cholesteryl moieties was not examined as other techniques reported in this Section. Certain obstacles were met during the amplification and purification of long (500 and 1000 bp) oligomers. Size-excluded columns used to purification of PRC reaction product did not allow a sufficient DNA-chol elution after PCR amplification with a cholesteryl-modified primer, probably because of the cholesterol moiety presence. One of the possibilities to overcome this problem would be using of HPLC technology to the PCR product purification. However, in the discussed situation, data concerning dsDNA-chol density presented in Section 3 were used for comparison. Density of short (50 nt) fluorescently-labelled DNA-chol immobilized on the hydrophobic SU-8 and gold surface was studied. Non-covalent adsorption of cholesteryl-modified DNA to hydrophobic gold surface was effective in diverse surface densities that were in a range of 10^{10} molecules/mm^2 and were strongly dependent on the applied conditions, such as DNA concentration and/or incubation time. It was demonstrated that few-second immobilization time allowed decreasing the molecular density to the range of 10^4 molecules/mm^2 (see Section 3.4.1).

Table 3.2. Density of modified DNA immobilized on pre-functionalized gold surfaces (in molecules/cm^2).

Modification / DNA nature	SH	NH_2	biot
50 nt ssDNA	Up to $6 \cdot 10^{13}$	Up to $8 \cdot 10^{11}$	Up to $8 \cdot 10^{12}$
50 bp dsDNA	Up to $5 \cdot 10^{13}$	Up to $4 \cdot 10^{11}$	Up to $5 \cdot 10^{12}$
500 bp dsDNA	Up to $5 \cdot 10^{12}$	Up to $1 \cdot 10^{11}$	Up to $1 \cdot 10^{11}$
1000 bp dsDNA	Up to $2 \cdot 10^{12}$	Up to $1 \cdot 10^{11}$	Up to $3 \cdot 10^{10}$

Taking into account the characteristics discussed above for the different immobilization strategies, their similarities in specificity and differences in the amount of bound DNA, one can now choose an immobilization strategy that is optimized for a specific application. For instance, for a dense monolayer of immobilized DNA for *in vitro* protein production, the most preferable would be immobilization *via* thiol – gold bond formation. A more moderate density of immobilized DNA, for example to examine nucleoprotein complex formation, could be provided by DNA immobilization *via* amide bond formation or biotin–extrAvidin interactions. On the other hand, functionalization by hydrophobic interactions would be optimal to obtain low density of immobilized DNA or to examine stable complexes with extremely low dissociation rate constants. In this case, the surface could be easily regenerated *via* ethanol rinsing that removed all remaining complexes, as has been already discussed in Chapter III, Section 3.4.

Taking into account all data presented here, it can be concluded that different functionalization strategies to immobilize DNA on a gold surface effectively produce different surface densities. The density of immobilized oligomers can be easily tuned by changing certain parameters in a functionalization protocol, for instance immersion time in a modified *n*-EG solution and concentration and/or incubation time of deposited DNA. In addition, independent of the applied functionalization strategy, a SAM formed from *n*-ethylene glycol molecules demonstrated its antifouling properties by reducing nonspecific adsorption to treated gold surfaces.

Chapter IV

SURFACE PLASMON RESONANCE IMAGING TO FOLLOW RNA POLYMERASE ACTIVITY IN REAL TIME

1. Introduction

Gene expression is a crucial event in the cell cycle. The process is controlled at several key points, and logically, during the initiation of RNA transcription. Numerous studies performed over several decades have attempted to describe the mechanism, the kinetics, and the link between structure and function for the role of DNA dependent RNA polymerases (RNAP) and template DNA in transcription (132, 141, 166). The approach described here attempts to address certain aspects of transcription kinetics, taking advantage of the ability to organize DNA on a surface and control parameters such as orientation and density. Two models *in vitro* of transcription systems involving *E. coli* and T7 RNAP were studied using Surface Plasmon Resonance imaging (SPRi) technology. DNA templates were immobilized as monolayers on pre-functionalized 50-nm thick gold sensor surfaces and proteins were introduced to the surfaces using a microfluidic continuous flow set up at constant temperature (37°C). Experiments were carried out under a number of controlled conditions in order to access the effects of

immobilized DNA density, length and the position of the specific promoter sequence on the DNA with respect to the surface. RNA products obtained during the transcription reactions were collected and characterized and correlated with the changes in the biosensor signal during the various processes.

1.1. Application of SPRi to real time *in vitro* monitoring

Surface Plasmon Resonance imaging (SPRi) has already been described (see Chapter I, Section 2). The advantages of its use in this particular study include:

1. Multiplex biochip surfaces
2. Efficient anti-fouling surfaces, therefore high signal to noise ratios;
3. Controlled monolayer DNA surfaces in which the DNA brush is well organized and readily accessible to analytes;
4. Access to apparent kinetic rate constants and relative affinities;
5. A signal that changes over time as mass accumulates at a surface thus ideal for following polymerization events;
6. Efficient microfluidics allowing coordinated injection of material such as nucleotide triphosphate substrates to initiate RNA transcription.

1.2. Examined cases

Based on the results presented in the previous Chapter, the immobilization of DNA oligomers on the gold surface *via* thiol – gold bond formation was chosen as the most appropriate biofunctionalization strategy. This method of gold surface functionalization allowed the formation of well-structured DNA monolayers of known density (~10^{13} molecules/cm^2). In addition, a short *n*-ethylene glycol linker between the DNA and the surface created an ordered monolayer with strong antifouling properties, thus obviating DNA denaturation upon immobilization and reducing nonspecific interactions between analytes and the surface (37).

Experiments with T7 RNAP were carried out with DNA containing a 17-mer T7 promoter sequence (TAATACGACTCACTATA (169)) and for experiments with *E. coli* RNAP DNA templates had a 203 bp sequence of *lac*UV_5 promoter (132). For the T7 promoter sequences an additional sequence of an intrinsic T7 terminator

(AACCCCTTGGGGCCTCTAAACGGGTCTTGAGGGGTTTT) located 32 bp before the end of the oligomer was included. Two different lengths of DNA were used for both RNAPs: short ones: 371 bp for T7 RNAP and 495 bp for *E. coli* RNAP, and long ones: 1037 bp for T7 RNAP and 1161 bp for *E. coli* RNAP. The long DNA fragments contained a sequence coding for NiR-FP (Near InfraRed Fluorescent Protein (225)). The sequences of the fragments are listed in Appendix I.

In order to study the influence of the direction of transcription by the RNAP, DNA fragments were immobilized at the SPRi surfaces in such a way that the specific promoter sequence was placed close to or far from the point of immobilization (Figure 4.1). Thus essentially two directions of subsequent transcription could be followed, either towards ('far') or away ('close') from the surface.

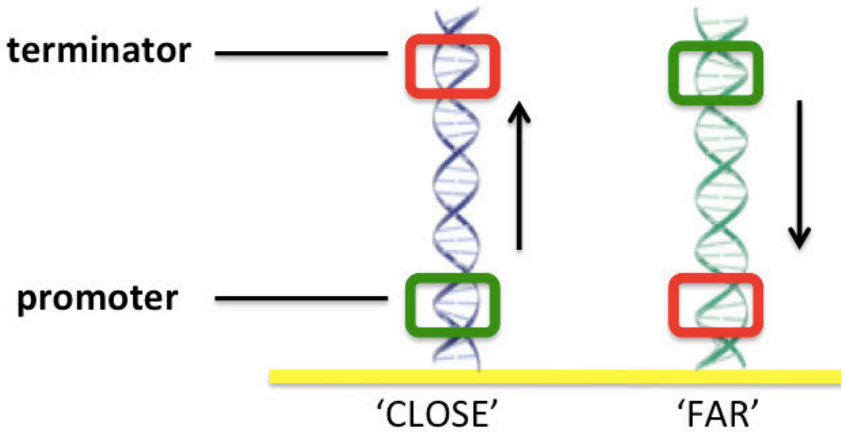

Figure 4.1. Strategies of DNA template immobilization on the sensor surface with the localization of the specific promoter site (green squares) and terminator site (red square): 'close' to and 'far' from the sensor surface. Arrows indicate the direction of the RNAP movement during the subsequent transcription downstream of the promoter site.

2. DNA – T7 RNAP interactions measured by SPRi

The T7 RNAP system involving the monomeric (98.8 kDa) RNA polymerase has been extensively studied from the point of view of transcription (169, 171). The multisubunit RNA polymerases whether *E. coli* RNAP (40, 133, 166) or eukaryotic RNAP (226-228) are necessarily more complex but share certain common features with the T7

system. A major difference at least between the T7 and *E. coli* enzymes concerns the fact that the latter has an associated sigma factor that at some point after escape into elongation dissociates from the holo enzyme (see Chapter I, Section 5.1.4), whereas the T7 protein remains intact from promoter recognition (initiation) through to nascent RNA release and dissociation (termination). In both cases major conformational changes are associated with the enzymes during the transition from initiation to the elongation complexes.

The T7 RNAP carries out a high productivity of transcription without the presence of additional transcription factors (229). It is a relatively stable enzyme in different environmental conditions, and successful transcription can be observed even at room temperature (58, 230).

In the following studies, SPRi technology was used to characterize *in vitro* transcription with T7 RNAP and DNA templates (listed in Table 4.1) immobilized on the sensor biochip in order to determine apparent rates for the various processes and to characterize transcription products.

Table 4.1. Nomenclature of oligomers used in the studies concerning RNA transcription with T7 RNAP. An additional description of oligomers can be found in Section 1.2.

Name	Feature of oligomers
'371 close'	371 bp dsDNA with the T7 promoter site located close to the immobilization point
'371 far'	371 bp dsDNA with the T7 promoter site located far from the immobilization point
'1kb close'	1037 bp dsDNA with the T7 promoter site located close to the immobilization point
'1kb far'	1037 bp dsDNA with the T7 promoter site located far from the immobilization point
'cont'	control, 495 bp dsDNA without the T7 promoter site

Four DNA samples containing a specific T7 promoter sequence and a control sample without this sequence (Table 4.1) were immobilized on an SPRi surface at the concentration of ~1 μM in 0.4 M phosphate buffer (pH 7.0) and incubated over night in a humid chamber to avoid drying of the spots. After insertion into the SPRi apparatus, the

biochip was extensively rinsed with running buffer (40 mM Tris-HCl pH 8.0, 6 mM $MgCl_2$, 10 mM NaCl and 2 mM spermidine) until a stable sensorgram (baseline) signal was obtained indicating that all the DNA remaining on the surface was covalently bound (*via* SH – Au bonds).

2.1. Kinetics of DNA – T7 RNAP complex formation

The relative stability of complexes formed between the immobilized DNA samples and injected RNAP could be assessed by measuring the apparent affinity constants (K_D). Kinetic binding data were obtained using titration series. This method involves sequential injections of analyte in different concentrations without any regeneration steps (231, 232). In the type of experiment shown in Figure 4.2, T7 RNAP at increasing concentrations (from 0.05 μM to 5 μM) was flowed across the DNA containing surfaces for 6 min at a flow rate of 25 μl/min. At the end of each injection period running buffer was continuously passed across the surface. The biochip surface was not regenerated between following injections. Changes in the refractive index correlated with mass changes as described earlier produced the type of sensorgram shown in Figure 4.2a.

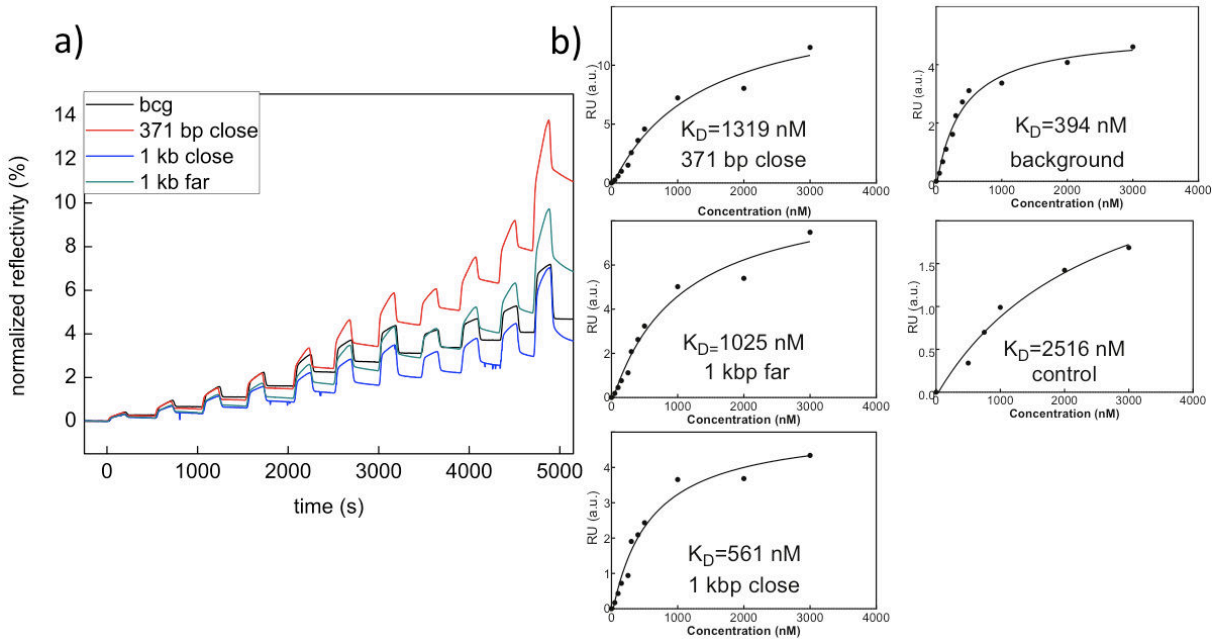

Figure 4.2. Kinetic titration series of T7 RNAP and DNA immobilized on a gold surface measured by SPRi: **(a)** sensorgram of interactions between immobilized DNA oligomers and T7 RNAP injected in increased concentrations: 0.05 μM, 0.1 μM, 0.15 μM, 0.25 μM, 0.3 μM, 0.4 μM, 0.5 μM, 0.75 μM, 1 μM, 2 μM and 5 μM; **(b)** apparent affinity constants plotted based on the sensorgram; from top to down and left to right: plots and K_D values obtained for samples: 371 bp close, 1 kbp far, 1 kbp close, background and control, respectively.

Analysis of the titration curve for background (Figure 4.2a, black curve) showed that T7 RNAP adsorbed irreversibly to the surface. The antifouling monolayer protected the immobilized DNA from denaturation and undoubtedly reduced the level of nonspecific interactions, however it was not sufficient to eliminate strong adsorption of injected protein. On the other hand, much lower affinity constants were obtained for samples where DNA was present (Figure 4.2). This demonstrated that the presence of DNA immobilized on the surface protected nonspecific binding of RNAP to the surface.

Increased concentrations of injected RNAP demonstrated that the injected enzyme continuously bound and confirmed nonspecific binding, not only to the promoter site but also to other sequences on the DNA. Nonspecific interactions between any protein and DNA are of necessity always present and they may strongly influence the measured kinetic parameters (175). In order to minimize the level of nonspecific adsorption of T7

RNAP to background and nonspecific sequences of DNA, the following experiments were performed with the low-concentrated enzyme (50 – 200 nM). The signals from background and control were minimalized by the use of low concentrations of polymerase.

2.2. Kinetics of transcription elongation

The following studies were performed to determine the influence of the concentration of injected T7 RNAP and the position of the binding site on the transcription reaction in the presence of nucleotide triphosphates (UTP, GTP, CTP and ATP collectively referred to as NTP). It was assumed that the addition of NTP to the immobilized DNA templates pre-incubated with the T7 RNAP bound specifically to the promoter region would initiate RNA synthesis. However, in crowded systems the accessibility of the specific binding site for a protein is strictly connected with the spatial geometry and the local environment (233, 234), and may impact on escape into elongation.

371-bp dsDNA oligomers with the T7 promoter located close to and far from the immobilization point (Figure 4.1, Table 4.1) were spotted on the SPRi surface as described above. The surface was inserted into the SPRi apparatus and rinsed thoroughly with running buffer at 37°C at a continuous flow rate of 25 µl/min. T7 RNAP in running buffer at two concentrations (100 nM and 500 nM) was injected for 6 min, followed by continuous washing with running buffer. After 10 min of dissociation, the NTP mixture at a concentration of 2 mM (in the case of 100 nM T7 RNAP) or 0.5 mM (for 500 nM T7 RNAP) of each nucleotide triphosphate was injected over the surface for 6 min. A second injection of four NTP under the same conditions (respectively, concentrations 2 mM or 0.5 mM of each NTP and 6 min injection) was performed after a further 5 min of dissociation following the previous injection. Typical sensorgrams are presented in Figure 4.3.

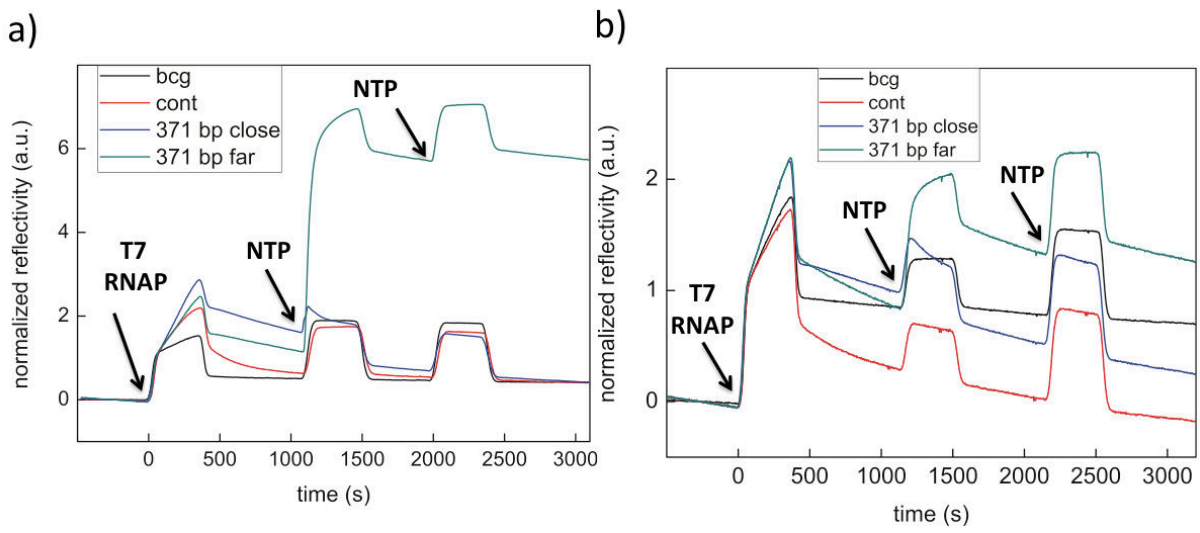

Figure 4.3. SPRi sensorgrams of three injections across immobilized DNA fragments: T7 RNAP and twice NTP (each event indicated by arrow) passed over a gold surface with immobilized DNA. Concentrations of injected solutions: **(a)** 100 nM T7 RNAP, 4 x 2 mM NTP; **(b)** 500 nM T7 RNAP, 4 x 0.5 mM NTP. 'Cont' – DNA without a T7 promoter site (red curve); '371 close' – 371 bp DNA with a T7 promoter binding site located close to the surface (blue curve); '371 far' – 371 bp DNA with a T7 promoter binding site located far from the surface (green curve). Black curve ('bcg') is a signal from areas of the pre-functionalized biochip surface.

The black curves ('bcg') correspond to signals from the pre-functionalized biochip surface with no DNA, indicated as background; the red curves ('cont') correspond to the signals from the control samples containing immobilized DNA without the specific promoter site; blue and green curves correspond to signals from specific samples: immobilized 371 bp DNA having the T7 promoter site either close (blue curve, '371 close') or far (green curve, '371 far') from the surface.

Comparison of sensorgrams presented in Figures 4.3 a and b confirmed the hypothesis that lower concentrations of injected proteins favored specific interactions of RNAP with the promoter sequence and minimized signal from the control and background (Section 2.1). Therefore, to facilitate the analysis only data obtained for injection of 100 nM T7 RNAP were examined in detail (Figure 4.3a). However, it is important to bear in mind that similar conclusions were drawn in cases where various concentrations of T7 RNAP and NTP were flowed across the DNA surfaces.

Injection of 100 nM T7 RNAP (Figure 4.3a, marked with the arrow "T7 RNAP") gave increases in signals showing that RNAP interacted with all the surfaces. From differences in amplitudes of the signals it was deduced that more material bound to the region with immobilized DNA than to the bare surface (black curve). In addition, comparison of the dissociation curves allowed differentiation of specific and nonspecific interactions. As expected, more RNAP remained bound to promoter containing sequences as seen by the higher amplitude at the end of the injection phase (2.5 - 3 a.u. for specific samples and 2 a.u. for the control).

The injection of the mixture of NTP produced significant changes depending on the sample (Figure 4.3a, indicated with the arrows "NTP"). Sensorgrams of the background (black curve) and the control DNA (red curve) did not show any significant changes, except a rapid increase and decrease of the signal related to changes in refractive index of the bulk solutions. On the other hand, differences between the two geometries of specific interactions with the promoter bearing DNA fragments were distinct and very clear.

The signal registered for the DNA template having the promoter site close to the surface (Figure 4.3a, blue curve) rapidly increased just after first injection of NTP (changes in amplitude from 2 to 2.5 a.u.) and then decreased regularly during the whole injection period. The end of the NTP injection resulted in a rapid drop of the signal (differences in amplitude of 1 a.u.). However, the baselines of two dissociation curves registered for this sample (dissociation after T7 RNAP injection and after first injection of NTP) were not the same. The rapid increase of the signal after injection of NTP could be interpreted as due to a combination of two events: a change in the refractive index caused by NTP solution injection and initiation of RNA transcription. In this case RNAP bound close to the surface initiated transcription and moved away from the surface. It was assumed that upon reaching the termination sequence on the DNA strand or the end of the DNA fragment, RNAP and nascent RNA would be released into the continuous flow solution. This hypothesis was supported by the decrease of the amplitude in signal at the end of the NTP injections (dissociation after RNAP injection: 2 a.u., dissociation after first NTP injection 1 a.u.).

A very different conclusion may be drawn from the analysis of the signal registered for the DNA template having the promoter site far from the surface (Figure 4.3a, green curve). As for the previous case, the injection of NTP resulted in a rapid increase of the

signal. However, the registered amplitude was much higher (changes in amplitude from 1 to 7 a.u.) than seen for the fragments with the promoter close to the surface and continued to increase steadily until the end of injection where it reached a final value of 7 a.u. In the following dissociation phase, the signal was stable, however the amplitude remained very high (5 a.u.). These changes could be explained by the synthesis of the transcript RNA but in contradiction with what was seen for the close promoter sequences there was a significant accumulation of mass. At least two hypotheses might explain this situation. First, the nascent RNA or/and RNAP after transcription of a DNA fragment were nonspecifically retained at or close to the surface and were not released to the solution. Second, the RNAP after proceeding to the end was released from the DNA template but then recaptured by a promoter site located on an adjacent promoter site. The relatively high density of immobilized DNA and the fact that a binding site was located at the extremity of a DNA strand could favor rapid re-binding to a DNA strand immobilized in the neighborhood and initiation of transcription to generate new RNA.

The second injection of NTP at a concentration of 2 mM each (Figure 4.3a, marked with the arrow "NTP") had a different effect than the first one. Similarly as during the first injection of NTP, sensorgrams of the background (black curve) and the control DNA (red curve) did not show any significant changes, except a rapid increase and decrease of the signal related to changes in refractive index of the bulk solutions. For the promoter located close to the surface no change in signal due presumably to transcription occurred, in other words one assumed that no active RNAP remained. On the promoter locater far from the surface again an increase was observed though to a much lesser extent that seen for the first injection of NTP's. A possibility was that perhaps most of the active RNAP had in fact translocated but molecules either rebound or stalled on the DNA could reinitiate transcription upon addition of the second batch of NTP.

Apparent dissociation constants were calculated for the complexes formed between injected 100 nM T7 RNAP and immobilized DNA: 371 bp oligomers in two geometries (T7 promoter located close and far from the surface) and the control DNA without the promoter sequence (Figure 4.4). Comparison of the dissociation rates demonstrated that dissociation from the control sample was faster than from the samples having the promoter sequences. This confirmed the higher affinity of T7 RNAP to the promoter than to a random DNA sequence.

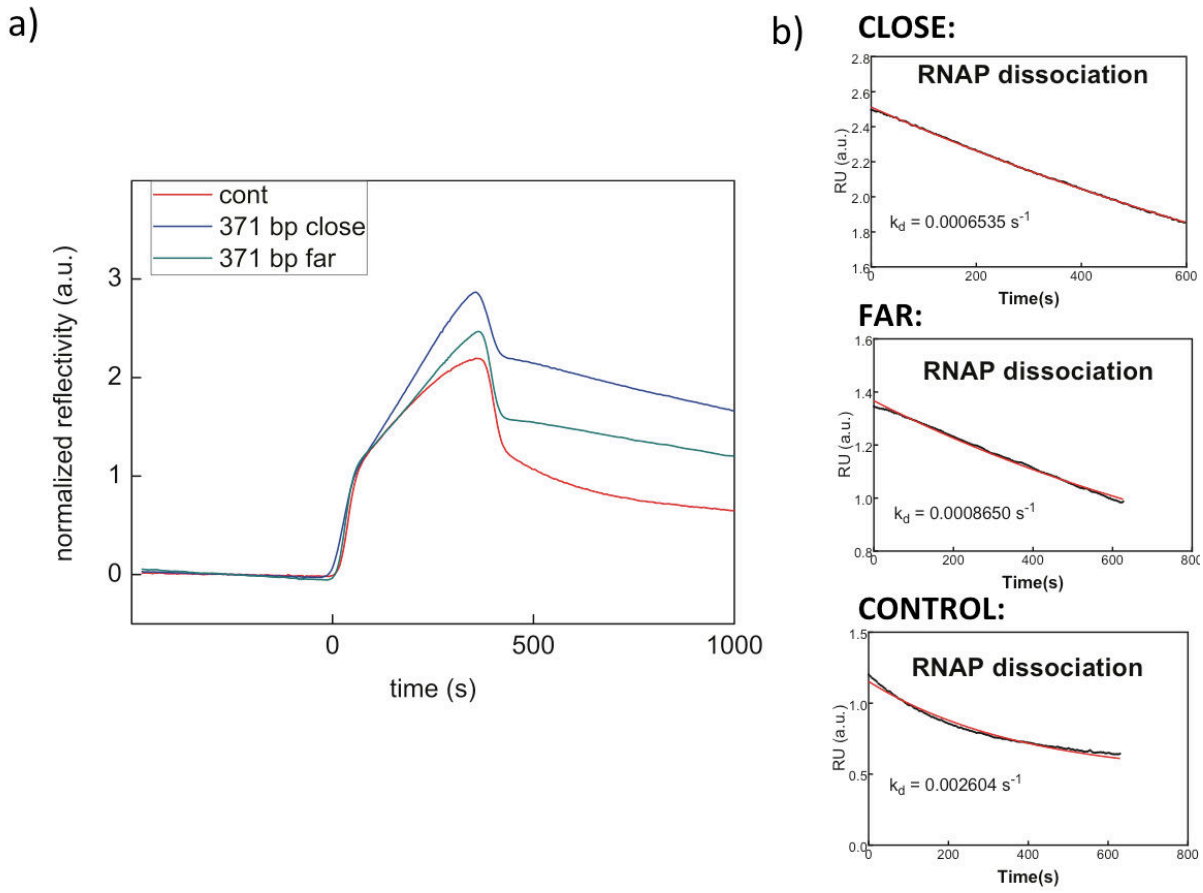

Figure 4.4. (a) Sensorgram and **(b)** calculated dissociation rates for the systems of immobilized dsDNA with a T7 promoter binding site and injection of 100 nM T7 RNAP. The dissociation parts were fit to a simple exponential decay given by $R_{(t)} = R_{(max)}e^{-k_d t}$ where $R_{(t)}$ was the signal at time t, $R_{(max)}$ was the maximal signal corresponding to the amount of complex before dissociation and k_d was the apparent dissociation rate constant.

It is important to notice that even when the same amount of DNA was immobilized in the "close" and "far" samples, the signals registered during injection of T7 RNAP differed. This could be explained by the different position of the promoter sequence. The flow close to the surface of the biochip is practically zero. When RNAP was bound to the promoter located close to the surface, dissociation from this region was diffusion limited. Therefore the local concentration would tend to increase and more RNAP would be retained pushing the association to form an initiating complex (Figure 4.4a).

Dissociation rates for the systems of immobilized dsDNA with a T7 promoter binding site after injection of 100 nM T7 RNAP and following injections of 4x2 mM NTP

were calculated for the two geometries of immobilized 371 bp DNA oligomers possessing T7 promoter sequence close or far from the surface (Figure 4.5).

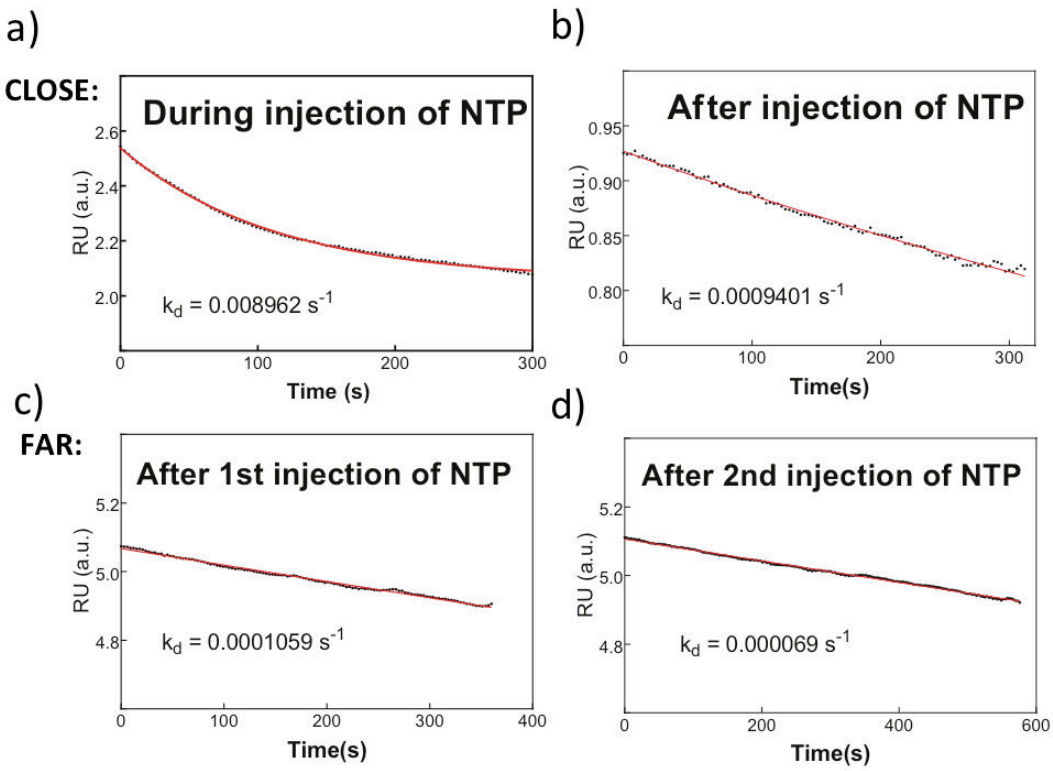

Figure 4.5. Sensorgrams and calculated dissociation rates for the systems of immobilized dsDNA with a T7 promoter binding site after injection of 100 nM T7 RNAP: **(a)** during the first injection of 4x2 mM NTP across 371 bp DNA with the T7 promoter located close to the surface; **(b)** after the first injection of 4x2 mM NTP across 371 bp DNA with the T7 promoter located close to the surface; **(c)** after the first injection of 4x2 mM NTP across 371 bp DNA with the T7 promoter located far from the surface; **(d)** after the first injection of 4x2 mM NTP across 371 bp DNA with the T7 promoter located far from the surface. The dissociation parts were fit to a simple exponential decay given by $R_{(t)} = R_{(max)}e^{-k_d t}$ where $R_{(t)}$ was the signal at time t, $R_{(max)}$ was the maximal signal corresponding to the amount of complex before dissociation and k_d was the apparent dissociation rate constant.

In the case of the "close" geometry, during the injection of the first NTPs the signal decreased rapidly, reflecting the transcription and then removal of both RNAP and RNA from the surface in the buffer flow (Figure 4.5a). The half-life of this complex was

calculated to be around 78 s. Since the injection of NTP lasted 6 minutes, likely almost all of the active RNAP would leave the surface. Indeed, values of k_d after injection of the first NTPs was low, similar to that of RNAP bound non specifically to the DNA (Figure 4.5b). This supported the idea that no more active RNAP was present.

In the case of the "far" geometry, complexes formed after injection of first and second NTPs were very stable (Figure 4.5 c and d). The exact composition of these complexes was unknown. One might assume that after the first injection of NTPs (Figure 4.5c) they contained mostly newly synthesized RNA retained on the surface and small amounts of stalled complexes composed of T7 RNAP and partially synthesized RNA. Complexes formed after the second injection of NTP were even more stable (Figure 4.5d) and they probably contained only RNA retained on the surface.

2.3. Characterization of RNA product synthesized on immobilized DNA templates

After characterization of transcription in SPRi, the next issue concerned the analysis of synthesized RNA. The key question was about the possibility of collecting and analyzing transcription products obtained in the SPRi apparatus. To answer these questions, the following studies were carried out.

2.3.1. Synthesis and characterization of a short transcript

Biochips with immobilized DNA were inserted into the SPRi apparatus and rinsed extensively until the SPRi signal stabilized at 37°C. The transcription mixture (2 µM T7 RNAP, 4 x 2 mM NTPs, including 1% *v/v* of UTP modified with fluorescein and 1 U/µl ribolock – a nonspecific inhibitor of RNase) diluted in the running buffer was injected across the surface and the flow was stopped for ~13 h during the injection period. Fractions of flow-through were then collected in intervals of 0.5 min from time t = 0 s to t = 7 min, where 0 was concomitant with re-starting the flow.

In order to assure that the flow-through contained synthesized RNA, samples were incubated with DNase and RNase and compared with control reactions of a plasmid DNA incubated with DNase and RNase. An *in vitro* experiment, analogous to this in SPRi, but

with the DNA template in solution was carried out (a detailed protocol can be found Chapter II, Section 5.1).

After denaturation, samples and controls (addition of 1 volume of deionized formamide, heating at 95°C for 5 min and rapid cooling down on ice and adding ethidium bromide) were loaded on 1.5% agarose gels and electrophoresis at 50 V for 3 hours was performed. Gels were scanned in a Typhoon scanner at two wavelengths: $\lambda_{ex}/\lambda_{em}$ = 532/610 nm for ethidium bromide and $\lambda_{ex}/\lambda_{em}$ = 532/526 nm for fluorescein. Figure 4.6 shows results obtained from an overnight incubation of RNAP mixture with the DNA templates immobilized on the pre-functionalized biochip in the SPRi apparatus and controlled reactions.

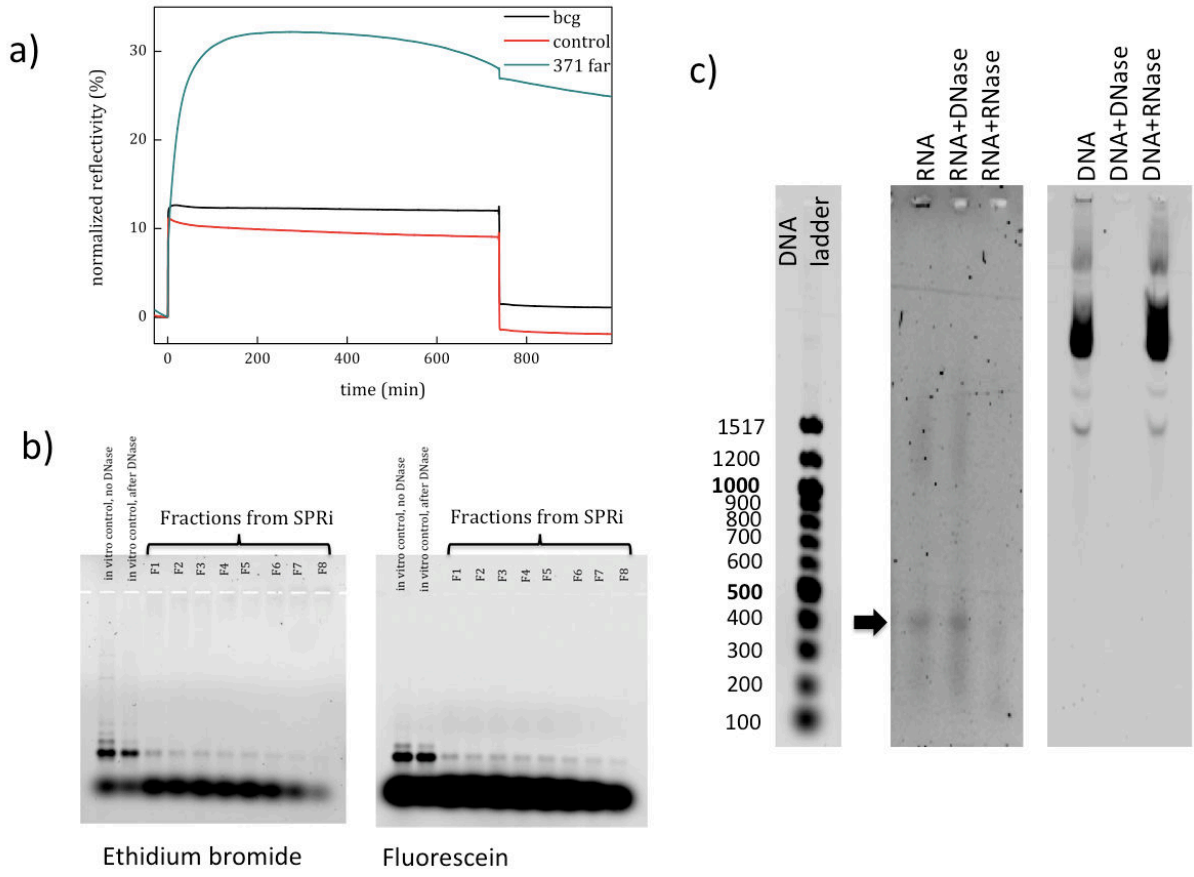

Figure 4.6. *In vitro* RNA synthesis. **(a)** Sensorgram of a ~13 h synthesis of RNA by T7 RNAP with immobilized DNA templates '371 far'. **(b)** 1.5 % agarose gel after electrophoresis, scanned at the wavelengths for ethidium bromide: $\lambda_{ex}/\lambda_{em}$ = 532/610 nm (in left) and fluorescein: $\lambda_{ex}/\lambda_{em}$ = 532/526 nm (in right). Lane 1: control in a solution, lane 2: control in a solution after incubation with DNase, following lanes: flow-through fractions collected from the SPRi apparatus after overnight reaction. **(c)** 1.5 %

agarose gel after electrophoresis, scanned at the wavelengths for ethidium bromide: $\lambda_{ex}/\lambda_{em}$ = 532/610 nm. Following lanes contained: 100 bp DNA ladder; flow-through fraction collected from the SPRi apparatus after overnight reaction ('RNA', indicated with a black arrow); the same fractions incubated with DNase ('RNA + DNase') and RNase ('RNA + RNase'); plasmid DNA ('DNA'); plasmid DNA incubated with DNase ('DNA + DNase') and RNase ('DNA + RNase'). Black arrow indicates RNA products.

Analysis of the data shown in Figure 4.6 after ~13 h reaction confirmed that RNA was synthesized from short DNA immobilized on the pre-functionalized gold sensor surface. Signals registered as SPRi sensorgrams (Figure 4.6a) increased rapidly and remained stable during the whole reaction time. Material then dissociated from the surface. Significant differences in signals amplitude from the control DNA (without a T7 promoter sequence, 'control' – red curve), the specific DNA (green curve) and the sensor surface ('bcg' – black curve) confirmed the specific changes in signal during the transcription reaction.

One band corresponding to the synthesized RNA could be distinguished in each fraction of the flow-through in the agarose gel scanned at the wavelengths for ethidium bromide and fluorescein (Figure 4.6b). Their lengths corresponded to those seen for the control reaction in solution (Figure 4.6b, lanes '*in vitro* control'). Also a comparison of two scans of the agarose gels one from fluorescein and one from ethidium bromide confirmed that the clear bands from the collected fractions were RNA oligomers. In addition, no smear was observed, confirming that the RNA transcripts were not degraded.

Additional tests were conducted to prove that the detected band on the agarose gel was RNA (Figure 4.6c). The sample was incubated with DNase or RNase. The band corresponding to the transcription product disappeared exclusively after incubation with RNase, therefore confirming that RNA was produced from DNA adsorbed on the surface of the biochip. The length of the RNA product was compared with a DNA ladder presented in the first lane. The length of expected transcripts was 285 nt. The length of the products was estimated to be about 400 nt. This discrepancy was probably due to differences in migration of single stranded RNA oligomers and double stranded DNA ladder or/and due to the presence of secondary structures in RNA (hairpins). Moreover, the agarose gels were also scanned with the fluorescein filters and the bands were

localized in exactly the same places thus confirming that the signal came from fluorescein molecules (Figure 4.6b). No smear was apparent, proving that the RNA transcripts were not degraded.

2.3.2. Synthesis and analysis of various transcription products

Two lengths of DNA oligomers of a chosen geometry (separately 'close' and 'far') were immobilized in equal amounts on the pre-functionalized sensor surface as described previously. After extensive rinsing and SPRi signal stabilization at 37°C, the transcription mixture (2 μM T7 RNAP, 4 x 0.5 mM NTP, including 1% *v/v* of UTP modified with fluorescein and 1 U/μl ribolock – a nonspecific inhibitor of RNase) in running buffer was injected across the surface and the flow was stopped overnight during the injection period. Fractions of flow-through were then collected in intervals of 1 min from time t = 0 s to t = 6 min, where 0 was identical with the moment of re-starting the flow and t = 6 min corresponded to the moment when injected RNAP mixture was released from SPRi tubing system. After denaturation (addition of 1 volume of deionized formamide, heating at 95°C for 5 min and rapid cooling down on ice) samples with added ethidium bromide were loaded on a 1.5% agarose gel and after electrophoresis at 50 V for 2 hours was performed. Gels were scanned in a Typhoon scanner at two wavelengths: $\lambda_{ex}/\lambda_{em}$ = 532/610 nm for ethidium bromide and $\lambda_{ex}/\lambda_{em}$ = 532/526 nm for fluorescein.

Figure 4.7 shows results obtained from the overnight incubation of RNAP mixture with the DNA templates immobilized on the pre-functionalized biochip in the SPRi apparatus.

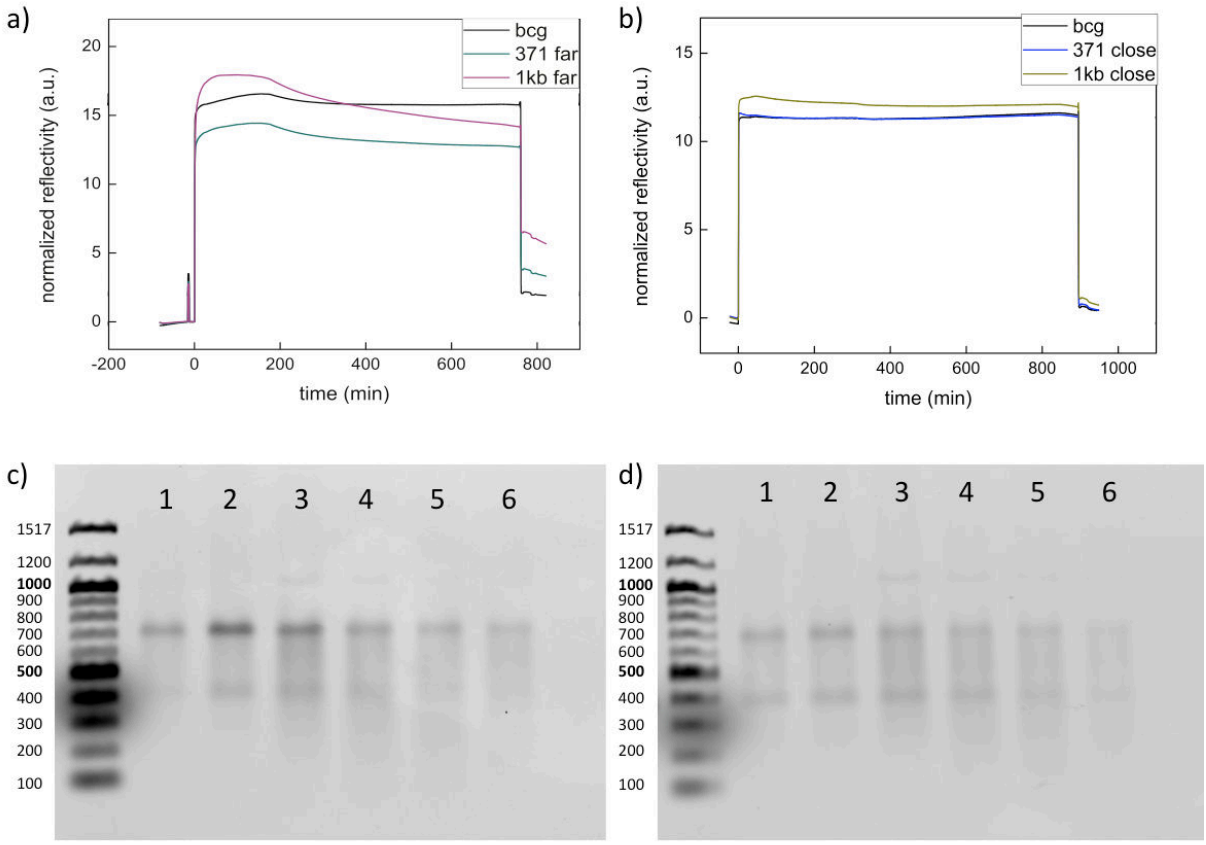

Figure 4.7. *In vitro* RNA synthesis on the SPRi biochip. Sensorgrams of the overnight synthesis of RNA by T7 RNAP with immobilized DNA templates: **(a)** '371 far' and '1 kb far'; **(b)** '371 close' and '1 kb close'. 1.5 % agarose gel after electrophoresis of flow-through fractions collected after overnight: **(c)** '371 far' and '1 kb far'; **(d)** '371 close' and '1 kb close'. In the gels the first lanes contained 100 bp DNA ladder, lanes 1 to 6 contained fractions collected at 1-minute intervals. Gels were scanned at the wavelengths for ethidium bromide: $\lambda_{ex}/\lambda_{em}$ = 532/610 nm.

Analysis of the data obtained from Figure 4.7 confirmed that RNA was synthesized from DNA immobilized on the pre-functionalized gold sensor surface. Signals registered as SPRi sensorgrams (Figure 4.7 a and c) increased fast and remained stable during the whole reaction time. Material then dissociated from the surface.

Two visible bands corresponded to the synthesized RNA could be distinguished in agarose gels (Figure 4.7 c and d). Their lengths compared with the DNA ladder presented in the first lane were estimated to be ~400 nt and ~750 nt. The theoretical lengths of full RNA transcript should be 285 and 951 nt as discussed in the previous

Section. These discrepancies could be again explained by the differences in migration of single stranded RNA oligomers and double stranded DNA ladder and the presence of secondary structures in RNA oligomers. However, the agarose gels were also scanned with the fluorescein filters and the bands were localized in exactly the same places thus confirming that the signal came from fluorescein molecules (data not shown). Only two clear bands were seen in the agarose gels shown in Figure 4.7. No smear was apparent, confirming that the RNA transcripts were not degraded.

The intensities of the bands (Figure 4.7 c) were compared with the analogous band in the other gel (Figure 4.7 d). Quantitative analysis carried out using dedicated software (Image quant) showed that the upper and lower band intensities were respectively about 5.2% and 3.8% stronger in the case of the 'far' geometry than for the 'close' configuration. These data demonstrated that RNA transcription by T7 RNAP on the immobilized DNA template with the promoter binding site placed far from the surface produced more transcripts than in the case of the opposite geometry.

A 6-minute interaction between the DNA template and RNAP was too short a time to synthesize an amount of RNA that could be visualized in agarose gels (data not shown). The product could be still analyzed by reaction with reverse transcriptase followed by a standard PCR amplification, for example with fluorescently labeled primers. Initial experiments were performed to analyze the transcription product in this manner, however, there was insufficient time to resolve some technical issues with the approach and more development is required.

The data presented above clearly demonstrated that RNA transcription occurred in the system where the DNA template was immobilized on an SPRi biochip and T7 RNAP was passed over the surface. The amount of transcripts produced depended strongly on the direction of transcription: RNAP moving towards the surface appeared to produce more RNA than in the opposite direction. This might be explained by the hypothesis suggested above, in which RNAP released near to the surface was recaptured by an adjacent promoter. In order to verify this statement, additional measurements need be carried out. It would be expected for example that by varying the density of immobilized DNA templates one should be able to control or even eradicate recapture. Clearly, overnight non-flow situations would exacerbate recapturing (this is the reason why overnight reactions were performed) so analysis would have to be restricted to sensorgrams and not to RNA products on gels.

2.4. Proposed reaction model

These experiments showed that T7 RNAP could interact more specifically with immobilized DNA fragments containing promoter sequences than with non-promoter containing DNA fragments. Complexes formed between RNAP and DNA with the T7 promoter sequence dissociated slower than those without the specific sequence.

In the transcription experiments the change in the SPRi signal was dependent on the anticipated direction of RNAP movement. When polymerase bound far and moved towards the surface, the signal significantly increased. When polymerase bound close to the surface and moved away, the signal first increased and rapidly decreased even during the injection phase. The SPRi signal intensity is a response to changes in the refractive index that are proportional to a mass variation registered at or close to the surface. It can be thus postulated that the observed changes were directly related to the synthesis of RNA and release or rebinding of RNAP.

We suggest that RNAP bound to the promoter site close to the surface and transcribing the sequence in the direction away from the surface was released with the flow. The same regularity in the signals has been reported for transcription observed by QCM (235). On the other hand, in the case when RNAP moved towards the surface, it was concluded that after transcription termination, the enzyme was rebound to a promoter site where it reinitiated transcription. The spatial geometry of the system and relatively high density of immobilized DNA templates support this hypothesis.

Finally, the through-flow from the reaction carried out in SPRi was collected in order to characterize potentially synthesized products. Short reaction times produced insufficient amounts of material to be detectable by available methods. The increase of the incubation time (from 6 minutes to overnight) was sufficient to accumulate the product for separation and visualization by agarose gel electrophoresis. Transcription with two geometries of immobilized DNA (promoter far from and close to the surface) was effective in obtaining nascent RNA with lengths related to the template lengths. However, when the T7 RNAP moved towards the surface, more transcripts were obtained. This difference might be explained by the higher productivity of transcription due to protein recapture.

In conclusion, based on the mass and refractive index changes registered by SPRi, certain kinetic parameters of transcription with T7 RNAP could be estimated. In the

examples shown here, RNA transcripts were successfully synthesized and characterized. Data obtained for the same DNA templates differed depending on the spatial orientation of immobilized DNA oligomers.

3. DNA – *Escherichia coli* RNAP interactions measured by SPRi

After characterizing the transcription process in the SPRi apparatus with T7 RNAP and proving that synthesis of a nascent RNA was possible under certain conditions, similar studies were carried out for *Escherichia coli* RNAP. Transcription was performed on two DNA templates of different lengths: 495 and 1161 bp. Both fragments possessed a 203 bp *lac*UV_5 promoter region (132, 166) placed close to the extremity of the DNA strand. Thiol modification on 5' end of one DNA strand allowed specific immobilization of templates on a pre-functionalized gold surface *via* thiol - gold bond formation. Two geometries were applied (Figure 4.1): in one the promoter sequence was located close to the surface (geometry "close"). In the second situation, the promoter was located far from the surface (geometry "far"). Subsequent movement of RNAP during transcription elongation would be either away from the surface (in the case of DNA in "close" geometry) or towards the surface (for DNA with "far" geometry). A brief descriptive of the DNA templates is presented in Table 4.2 and all the sequences used can be found in Appendix I.

Table 4.2. Nomenclature of oligomers used in the studies concerning RNA transcription with *E. coli* RNAP. Additional descriptions of oligomers can be found in Section 1.2.

Name	Feature of oligomers
'0.5 kb close'	495 bp dsDNA with the *lac*UV_5 promoter site located close to the immobilization point
'0.5 kb far'	495 bp dsDNA with the *lac*UV_5 promoter site located far from the immobilization point
'1 kb close'	1161 bp dsDNA with the *lac*UV_5 promoter site located close to the immobilization point
'1 kb far'	1161 bp dsDNA with the *lac*UV_5 promoter site located far from the immobilization point

3.1. Kinetics of DNA – *E. coli* RNAP complex formation

Similar procedures as described in Section 2.3 were applied to carry out transcription with *E. coli* RNAP from DNA templates immobilized on the SPRi chip. Two DNA fragments of different lengths (0.5 and 1 kbp) and the same spatial geometry ("close" or "far") containing a specific *lac*UV$_5$ promoter sequence (Table 4.2) were deposited on the pre-functionalized gold surface at a concentration of ~1 μM in 0.4 M phosphate buffer (pH 7.0). Samples were incubated overnight in a humid chamber to avoid spots' drying. After insertion into the SPRi apparatus, the biochip with immobilized DNA was extensively rinsed with running buffer (20 mM HEPES pH 8.0, 100 mM KCl, 10 mM NaCl and 0.005% *v/v* Tween surfactant) until a stable signal was reached. A typical experiment is shown in Figure 4.8.

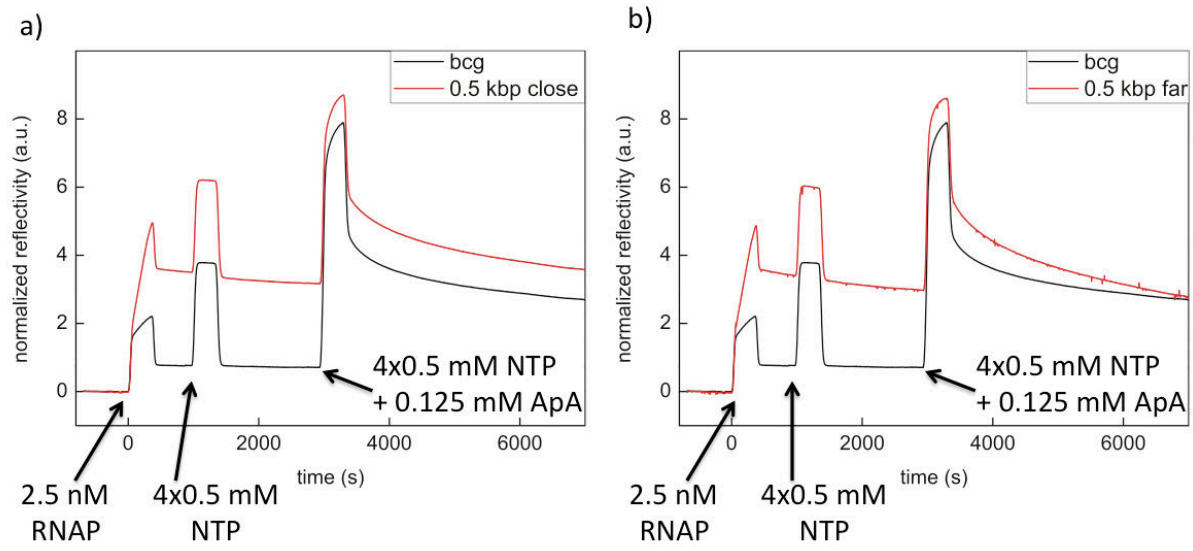

Figure 4.8. Sensorgrams of *E. coli* RNAP binding to the immobilized 0.5 kbp DNA immobilized on the gold surface in two geometries: **(a)** "close" – *lac*UV$_5$ promoter located close to the surface and **(b)** "far" – *lac*UV$_5$ promoter located far from the surface. Arrows indicate subsequent injections: (i) 2.5 nM *E. coli* RNAP; (ii) mix of four nucleotide triphosphates (NTP) at a concentration 0.5 mM each; (iii) mix of four nucleotide triphosphates (NTP) at a concentration 0.5 mM each and 0.125 mM dinucleotide ApA.

As seen in Figure 4.8, RNAP was first injected across the surface containing the DNA. In both the "close" and "far" configurations, RNA polymerase bound and formed a stable complex. Addition of NTP alone had little effect but addition of NTP in the presence of the initiating dinucleotide ApA caused a significant increase in signal in both cases. The effect of ApA on initiation *in vitro* is well documented as the presence of the initial dinucleotide obviates the restrictive K_m for initial dinucleotide formation (165). At the end of the injection period an increase in material was observed at the surface that then dissociated.

Comparison of the sensorgrams from the sample containing DNA with the *lac*UV_5 promoter sequence and the background (signal measured on the biochip surface protected with an antifouling monolayer of *n*-ethylene glycol) indicated a significant increase in the signal intensity in all samples after injection of ApA, including background. To characterize the ApA used in these studies in order to understand this nonspecific adsorption, additional experiments were performed. First, the absorption of ApA solution was measured in UV-spectrophotometer at the wavelength 260 nm, typical for nucleic acids. The spectra were identical with those from control samples of DNA (data not shown). This proved that the ApA solution was relatively pure and not contaminated with proteins. Secondly, 0.125 mM ApA was flown across an SPRi biochip with nonspecifically immobilized 2.5 nM *E. coli* RNAP. A sensorgram presented in Figure 4.9 confirmed a very strong adsorption for both, immobilized RNAP and the background.

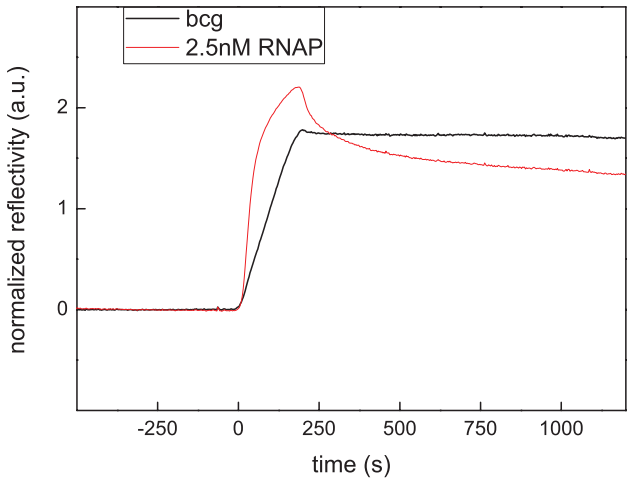

Figure 4.9. SPRi sensorgram registered for interactions between nonspecifically immobilized *E. coli* RNAP and 0.125 mM ApA.

Analysis presented above proved that ApA solution was pure and theoretically it should not have a negative impact for the transcription reaction. However, the strong adsorption registered in sensorgrams did not allow the analysis and interpretation of kinetic data of real time transcription. Additional studies are required to determine the influence of ApA.

3.2. Characterization of RNA products synthesized on immobilized DNA templates

The following experiments were carried out to determine if transcripts were however made in these conditions. After SPRi signal stabilization at 37°C, 150 µl of a transcription mixture (20 nM holoenzyme *E. coli* RNAP saturated with σ^{70} factor, 4 x 0.5 mM NTP, 0.5 mM ApA – first dinucleotide (165) and 1 U/µl ribolock – a nonspecific inhibitor of RNase) in running buffer was injected. The mixture was passed over the surface for 6 min with a flow rate of 25 µl/min or the flow was stopped overnight from the moment when the mixture was in contact with the biochip surface. Fractions of flow-through were collected at intervals of 1 min from time t = 0 s to t = 6 min, where 0 was identical with the moment of re-starting the flow and t = 6 min corresponded to the moment when the injected RNAP mixture was released from the SPRi tubing system. After denaturation (addition of 1 volume of deionized formamide, heating at 95°C for 5 min and rapid cooling down on ice) samples with added ethidium bromide were loaded onto 1.5% agarose gels and electrophoresis at 50 V was performed for 2 – 3 hours. Gels were scanned in a Typhoon scanner at the wavelengths of ethidium bromide: $\lambda_{ex}/\lambda_{em}$ = 532/610 nm.

A 6-minute reaction between immobilized DNA templates and free *E. coli* RNAP was too short to obtain detectable amounts of products (data not shown). On the other hand, the overnight reaction was effective in producing bands in the gel, probably arising from nascent RNA. Figure 4.10 shows results obtained from an overnight incubation of RNAP mixture with the DNA templates immobilized on the pre-functionalized biochip in the SPRi apparatus and compared with *in vitro* controls.

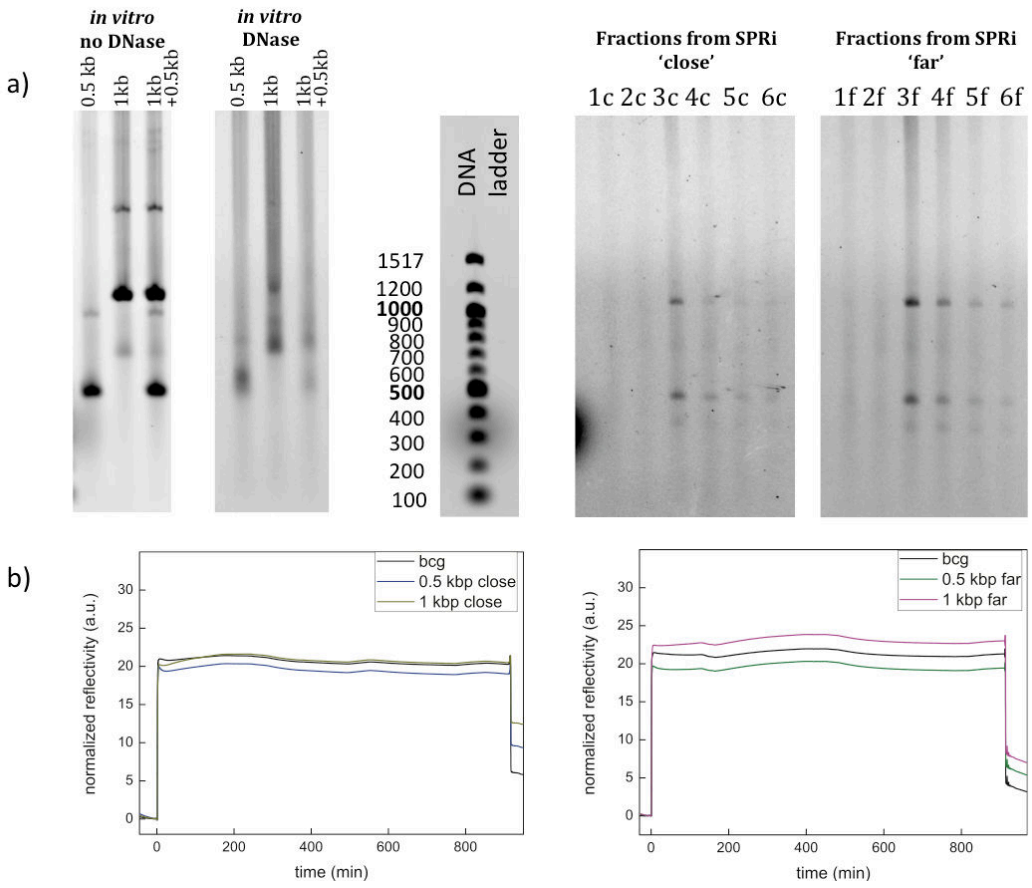

Figure 4.10. *In vitro* RNA synthesis on the SPRi biochip. **(a)** 1.5 % agarose gel after electrophoresis of through-flow fractions collected after overnight synthesis of RNA by *E. coli* RNAP with immobilized two DNA templates and *in vitro* controls. Following lanes (from left to right): three *in vitro* controls before and after DNase treatment, 100 bp DNA ladder, collected fractions from SPRi: 1c – 6c from "0.5 kb close" and "1 kb close" DNA templates; 1f – 6f from "0.5 kb far" and "1 kb far" DNA templates. Gel was scanned for the wavelengths for ethidium bromide: $\lambda_{ex}/\lambda_{em}$ = 532/610 nm. **(b)** Sensorgrams from overnight synthesis of RNA by *E. coli* RNAP with immobilized two DNA templates: "0.5 kb close" and "1 kb close" (in left); "0.5 kb far" and "1 kb far" (in right).

Analysis of the data presented in Figure 4.10 after ~15-hour reaction confirmed that RNA was synthesized under these conditions. The flow-through was collected after two separate 15-hour reactions (one for each spatial geometry of DNA template) and run in an agarose gel (Figure 4.10a) proving that RNA was produced. The comparison with the *in vitro* controls run in the same agarose gel allowed identification of the same bands for both reactions: in SPRi and *in vitro*. In samples represented in Figure 4.10a by

lanes 1c – 6c for DNA templates in geometry "close" and lanes 1f – 6f for DNA templates in geometry "far" two clear bands were visible. Additional bands and observed smear were probably due to a partial degradation of the product. The DNA ladder was used to estimate lengths of obtained two main products. They were calculated to be 486 and 1180 nt, while their predicted lengths supposed to be 299 and 965 nt. These differences were due to different migration of dsDNA ladder and single stranded RNA products that additionally could possess secondary structures.

Comparison of the intensity of the bands represented by two geometries of immobilized DNA templates (promoter sequence placed close or far from the surface) showed differences in the reaction efficiency. Similarly as for the example presented in Section 2.3 for transcription with T7 RNAP, also for transcription with *E. coli* RNAP transcription, the protein that was bound far and moved towards the surface produced more synthesized transcript. Since the scheme of the reaction was the same as for T7 RNAP, one could assume that an analogical reaction model could be applied for other RNAPs working in this kind of system. Briefly, it was hypothesized that RNAP after termination of transcription was released from the DNA template. When the protein was bound close to the surface and moved away, it was released from the crowded neighborhood to the solution. In contrary, when the protein proceeded towards the surface, after termination transcription and leaving the complex, it was rebound to the promoter site of a DNA strand immobilized nearby. This was effective in a higher productivity of RNA transcription in case of "close" geometry of a template. Calculations of the bands' intensity performed with Image Quant software allowed estimating that the signal intensity in the case of "far" geometry of immobilized DNA template was about 7% stronger than in the "close" geometry. Transcription efficiency was about 7% higher in the case of the "far" geometry. However, if the sigma factor is being released then how to explain rebinding? Two possibilities present themselves; either the sigma factor was in fact not released and released holo enzyme could rebind adjacent promoters, or released sigma factor could rebind to the core enzyme which in turn could be re-recruited to adjacent promoters, either case however did not represent a large proportion of events.

Signals registered as SPRi sensorgrams (Figure 4.10b) did not give a clear answer about the reaction progress. In both sensorgrams the signals rose dramatically after injection of the transcription mixture due to a different refraction index from the

running buffer. In addition, curves registered for both lengths of DNA template were nearly the same for both geometries. The only noticeable difference occurred for the samples "bcg" that represented a pre-functionalized gold surface without any immobilized DNA.

In conclusion, transcription between free *E. coli* RNAP and immobilized DNA templates possessing a specific promoter site was confirmed in the crowded confined conditions occurring in the SPRi apparatus. The efficiency of the reaction was related to the direction of RNAP movement: the direction towards the surface was effective in higher amount of synthesized RNA. The difference in a transcript amount was about 7% and it was remarkable in the agarose gel. RNA produced on SPRi chip was not degraded, however shorter products were identified and they were supposedly premature or aberrant transcripts.

4. Conclusions

Studies presented in this Chapter concerned the synthesis of RNA transcripts in the confined conditions associated with SPRi technology. Real time monitoring of interactions between immobilized DNA templates and free T7 RNA polymerase was used to determine apparent dissociation affinity of RNAP from template DNA (Section 2.1) and dissociation constants (Section 2.2). However, other kinetic rates of different transcription steps could be calculated, as has been carried out using other surface based techniques (235).

Studies performed with two polymerases: T7 RNAP and *E. coli* RNAP confirmed that transcription was possible in conditions where DNA with a specific promoter sequence was immobilized on the pre-functionalized SPRi biochip under specific controlled conditions

Short-time (6 min) incubation was not sufficient to obtain detectable amount of product, nevertheless future developments might give access to this. In the conditions used here the amount of template was very low compared to solution conditions. One could increase the number of accessible templates. In the examples used here the area occupied by DNA was estimated to be a few μm^2. However, it would be possible to cover the entire biochip surface with DNA and thus increase the occupied surface to several

cm^2. Another possibility used here would be to increase the incubation time. Also characterization of small amounts of product would be possible by for example using radioactively modified ribonucleotides or performing a reverse transcriptase reaction. This latter possibility was tested during these studies. The collected flow-through was incubated with a reverse transcriptase and a primer in order to obtain cDNA fragments. Afterwards, cDNA was amplified with a standard PCR reaction. However, technical problems arose that require some attention before this approach can be said to work.

Characterization of transcripts obtained during SPR based transcription studies has been previously reported (40), however because of the configuration of the SPR device used in these studies (BIAcore, carboxymethylated surface), questions such as those dealt with here could not be addressed, for example the effect of direction of transcription. The reaction model discussed in Sections 2.4 and 3.2 explained differences in the transcription efficiency depending on the direction of RNAP movement, either towards the surface or away from it. Nevertheless, to confirm the hypothesis that RNAP moving along DNA in the surface direction could be recaptured and could reinitialize transcription, additional studies are still required. These should involve monitoring transcription in SPRi as a function of the density of immobilized DNA in both geometries.

It is demonstrated here that SPRi could be used to follow *in vitro* transcription of long DNA templates (up to thousands of base pairs). This possibility could extend the real time monitoring not only to follow transcription from DNA to RNA but also to examine next steps in gene expression, such as translation of a nascent RNA into peptide chains, protein synthesis and maturation. It has been already demonstrated that protein synthesis in SPRi is reliable (58), however, as far as we are aware, the kinetics of these processes have not yet been followed. The end game would be to use SPRi to follow and characterize distinct steps in gene expression under very controlled *in vitro* conditions leading to the synthesis of proteins without the need for purification.

Chapter V

CONCLUSIONS AND PERSPECTIVES

The main goal of studies presented in this manuscript was to develop a robust biosensor that could be used to monitor in real time the process of gene expression. Optofluidic surface based biosensors were chosen as the most relevant techniques, since they allow changes occurring in a given system to be followed with an extremely low detection limit and in very confined but controlled circumstances. The thesis project was divided into two parts. The first part dealt with the characterization of surface biofunctionalization. The aim was to develop and improve protocols allowing immobilization of desired (bio) molecules onto a surface in a controlled manner. The second part was focused on studying the initial steps of gene expression, namely interactions between linear DNA immobilized on a gold surface and DNA dependent RNA polymerases (RNAP). These studies were performed with a Surface Plasmon Resonance imaging (SPRi) technique and focused on two enzymes: T7 bacteriophage RNAP and bacterial *Escherichia coli* RNAP. Products obtained during the *in vitro* transcription reactions were characterized.

Surface characterization studies were carried out with two distinct substances: a polymer film – SU-8 and a thin (~50 nm) gold layer. These studies explored various covalent and non-covalent methods of (bio) molecule immobilization.

SU-8 is a photoresist polymer extensively used in optical techniques (178, 179). Two notable biosensing applications for SU-8 may be found in micro ring based resonators (20) and as a support for total internal reflection fluorescent (TIRF)

microscopy. Thin gold sensor surface on the other hand, have mainly been used in SPR and quartz crystal microbalance techniques (QCM, (235)).

Functionalization of SU-8 films by covalent grafting of molecules was performed on surfaces pre-treated with UV/ozone radiation and activated with EDC/NHS coupling agent (see Chapter III, Section 2). It was used to form amide bonds between carboxyl groups on an SU-8 surface and primary amines in the target (bio) molecule. This functionalization method was successfully applied for a specific antigen-antibody test (176), but its general applicability to other biomolecules whilst *a priori* potentially straightforward was not systematically investigated here.

A second functionalization strategy based on non-covalent hydrophobic coupling with cholesteryl- and cholate-modified molecules was used to functionalize both SU-8 films and hydrophobically pre-functionalized thin gold layers (see Chapter III, Section 3). The general applicability of this method was confirmed by verification of several factors. (i) Different molecules possessing a sterol ring were immobilized: the data showed that a small fluorescent tetramethylrhodamine molecule modified with a cholate moiety and 50 bp DNA strand having a cholesteryl group could be specifically grafted on the surface. (ii) Depending on the conditions (bio) molecules were immobilized over a wide range of surface densities of between 10^4 and 10^{10} molecules/mm^2 for DNA oligomers. (iii) Surface regeneration and re-use were easily achieved by simple rinsing with ethanol solutions. All these factors demonstrated the huge potential of using non-covalent immobilization of modified (bio) molecules on hydrophobic sensors in surface based biosensors.

Several methods of gold surface biofunctionalization with DNA oligomers were compared (see Chapter III, Section 4). The strategies examined were: gold – thiol bond formation, amide bond formation and extrAvidin–biotin bond formation. The results obtained underlined the need to bear in mind the dependence of surface immobilization density on factors such as the overall binding strategy, immobilization conditions and DNA lengths.

Further development and application of surface biofunctionalization strategies will need to consider their extension to other supports and biological molecules. For instance, specific immobilization of proteins could serve to examine protein-protein or nucleoprotein interactions and, in the case of antibodies, to a specific immunodetection of antigens. Immobilization of proteins could be performed without any additional

modifications, if the spatial orientation of a certain protein allowed specific moieties to be used directly for example primary amines or some amino acids (lysine or cysteine) that could be used for direct grafting on the sensor surface.

In the second part of this manuscript, the most robust surface functionalization strategy was used to immobilize DNA oligomers and monitor interactions with RNAPs in real time, using SPRi technique. We attempted to follow the movement of RNAP polymerase as it transcribed an immobilized DNA template and were particularly interested in the effects of the orientation of the DNA with respect to the surface on this process. Studies were performed with two RNA polymerases (T7 and *E. coli*) in appropriate buffers at 37°C. Thiolated DNA with a specific promoter site (respectively, T7 RNAP or *E. coli* RNAP) of two lengths (few hundreds bp and ~1 kbp) were immobilized on gold surfaces pre-functionalized with short thiolated ethylene glycol molecules.

Interactions between DNA templates and T7 RNAP and/or T7 RNAP in the presence and absence of ribonucleotides (NTPs) were examined in order to determine certain apparent kinetic rate constants. Data from SPRi experiments allowed estimate several kinetic constants. In the final part of studies concerning T7 RNAP interacting with immobilized DNA templates, the transcription reaction in the SPRi apparatus was carried out for about 15 hours and the RNA content of collected through-flow was characterized. Biochemical analysis (gel electrophoresis and enzymatic reactions with DNase and RNase) confirmed that the obtained product was nascent RNA that corresponded with the expected transcript

The whole analysis of interactions between T7 RNAP and DNA having a T7 promoter sequence demonstrated a strong dependence on the DNA template orientation. Transcription was more productive where the promoter sequence was placed far from the surface and movement of RNAP during transcription elongation was towards the surface. The opposite geometry (where the promoter sequence was placed close to the surface and the movement of RNAP during transcription elongation was away from the surface) was also effective in the transcript but fewer transcripts were formed. A reaction model was proposed based on these observations (see Chapter IV, Section 2.4). Briefly, RNAP bound to the promoter site close to the surface and moving away during the transcription was released from surface and moved off into solution. However in the opposite geometry, after terminating transcription RNAP was diffusing

back through the monolayer and was recaptured by adjacent DNA strands containing the promoter sequence and available for another round of transcription thus explaining why more transcripts were being formed.

Similar studies were performed with *E. coli* RNAP and conclusions concerning the dependence between DNA template geometry and the reaction efficiency were similar (see Chapter IV, Section 3).

These studies concerning *in vitro* gene expression monitoring can now be extended in a number of directions, to address factors such as surface chemistry, biosensing techniques, characterization of transcription kinetic, controlled protein production, the presence of transcription factors and DNA architectural proteins and so forth.

As has already been mentioned, the development of the surface chemistry and biofunctionalization strategies would involve improving the methods and protocols developed here. The main goal would be to immobilize various (bio) molecules in a controlled manner over a wide range of surface densities. Optimized immobilization should provide uninhibited access to a target molecule's active site. It should also significantly limit the interactions between the surface and analytes. It is clear that the majority of available biofunctionalization strategies are not universal, therefore separate techniques should be proposed depending on the substrate and immobilized ligand nature.

The biofunctionalization techniques described in this manuscript centered upon two substrates: thin gold layer surfaces and SU-8 polymer film. Different methods of functionalization of thin gold layer allowed successful application to SPRi based studies (37, 39, 47, 72). To date, SU-8 thin films have been used in the micro ring based resonator applied to immunosensing with a very low level of detection (20). It is believed that optimization of SU-8 biofunctionalization to specifically and controlled adsorb a range of biomolecules (e.g. DNA, peptides) would extend the types of biosensors that could be designed simply because one could then access the optical properties of the SU-8 photoresist. This would greatly assist studies on the kinetics of biomolecular interactions simply by enlarging the dynamic range of how many molecules may be studied simultaneously, as it stands, at a surface, this extends from several hundreds to up to 10^{12}. Another optical technique that could take advantage of

the SU-8 surface biofunctionalization would be total internal fluorescent (TIRF) microscopy. The low auto fluorescence level of SU-8 thin films makes them a perfect support to immobilize (bio) molecules and to monitor changes in fluorescent signals as a function of biomolecular interactions.

To continue the real time analysis of *in vitro* gene expression, many more additional experiments are required to characterize kinetic rates related to key steps in the transcription process, including enzyme binding to and from the promoter, the transition from the initial complex to the forward stall position, the polymerization rate of RNA along DNA, and the release rate from the end of the template DNA. Also studies in SPRi performed with various densities of immobilized DNA templates could confirm or negate the proposed reaction model (see Chapter IV, Section 2.4). Similar studies could be extended for various polymerases in order to determine their similarities and differences in kinetic real time analysis.

The ultimate goal of this project is to develop a whole on-chip reaction leading to protein synthesis from a DNA template immobilized on a gold biochip in the SPRi apparatus (58). This would allow real time monitoring of the whole process of gene expression in confined but well characterized *in vitro* conditions. To perform these studies, the immobilized DNA template should contain specific sequences, including RNAP promoter binding sequences, ribosome binding sites, codon starts, desired gene sequences and codon stops. Injection of RNAP, amino acids and other components of transcription and translation (e.g. ribosomes) would be effective, firstly, in transcription of mRNA and, secondly, in its translation into a peptide sequence followed by protein maturation. This reaction is very complex and it may be challenging to obtain a native protein under these conditions. There would be several methods to determine the final product of translation reaction. The produced protein could be detected directly on the biochip after capture in a dedicated detection spot. For example, immobilization of specific antibodies would allow immunodetection of native proteins. In the case of poorly folded proteins, one could also carry out detection *via* His-tag and nickel-chelated complex formation (see Chapter I, Section 3.2.2.3). Both strategies have advantages and disadvantages concerning further protein detection *via* immobilization. Placing of the His-tag in N-terminal end could be effective in the protein (or peptide) capturing regardless of the terminal synthesis. It also means that all intermediate products (oligopeptides) would possess a His-tag and therefore would be captured *via* nickel-

chelated complexes. On the other hand, placing a His-tag on the C-terminal end would be effective in capturing only fully translated sequences which could significantly decrease a reaction yield. In both situations one has to take into account the situation where a 3-dimensional structure of a nascent peptide or protein would decrease a His-tag accessibility for further immobilization. Another characterization strategy would involve simple product collection. In this situation it would be possible to stop the flow in order to increase synthesis time (as was done in the case of transcription reactions described in Chapter IV, Sections 2.3 and 3.1). If the gene coded for a fluorescent protein collected fractions should give a fluorescent response that additionally might be quantified. In other situations, following analytical characterization using standard biochemical techniques (e.g. SDS PAGE electrophoresis or chromatography) or even mass spectrometry should provide all the required information about the expected product.

The thesis project proposed in this work required a multi-disciplinary approach and involved the use of a wide range of techniques and methodologies including surface science (surface fabrication in a clean room environment, surface biofunctionalization and characterization), optofluidics (use of SPRi technique), molecular biology (immunosensing reactions, preparation of DNA including cloning and PCR amplification, *in vitro* reactions with RNA polymerases, transcription product characterization *etc.*) and mathematical data analysis. Initial steps regarding characterization of surface biofunctionalization strategies and *in vitro* transcription studies have provided extremely promising results. Preliminary experiments on transcription in a biosensor have successfully showed that the process may be followed and controlled, that it allows many conditions unavailable in solution to be examined and that the next steps in the project, in which the synthesis of proteins in confined *in vitro* conditions can now be undertaken with a very high probability of success.

BIBLIOGRAPHY

1. Andrade C. OM, Faulin T., Hering V. and Parra Abdalla DS. (2011) *Biosensors for Health, Environment and Biosecurity*.
2. Bally M, Halter M, Voeroes J, & Grandin HM (2006) Optical microarray biosensing techniques. *Surface and Interface Analysis* 38(11):1442-1458.
3. Moerner WE (2007) Single-molecule chemistry and biology special feature: New directions in single-molecule imaging and analysis (vol 104, pg 12596, 2007). *Proceedings of the National Academy of Sciences of the United States of America* 104(39):15584-15584.
4. Haab BB (2003) Methods and applications of antibody microarrays in cancer research. *Proteomics* 3:2116–2122.
5. Cooper MA (2003) Label-free screening of bio-molecular interactions. *Analytical and Bioanalytical Chemistry* 377(5):834-842.
6. Kimmel DW, LeBlanc G, Meschievitz ME, & Cliffel DE (2012) Electrochemical Sensors and Biosensors. *Analytical Chemistry* 84(2):685-707.
7. Poghossian A & Schoning MJ (2014) Label-Free Sensing of Biomolecules with Field-Effect Devices for Clinical Applications. *Electroanalysis* 26(6):1197-1213.
8. Bavli D*, et al.* (2012) Detection and Quantification through a Lipid Membrane Using the Molecularly Controlled Semiconductor Resistor. *Langmuir* 28(1):1020-1028.
9. Capua E, Kumar TA, Tkachev M, & Naaman R (2014) The Molecular Controlled Semiconductor Resistor: A Universal Sensory Technology. *Israel Journal of Chemistry* 54(5-6):586-594.
10. Buell AK*, et al.* (2010) Surface Attachment of Protein Fibrils via Covalent Modification Strategies. *Journal of Physical Chemistry B* 114(34):10925-10938.
11. Arlett JL, Myers EB, & Roukes ML (2011) Comparative advantages of mechanical biosensors. *Nat. Nanotechnol.* 6(4):203-215.
12. Tamayo J, Kosaka PM, Ruz JJ, San Paulo A, & Calleja M (2013) Biosensors based on nanomechanical systems. *Chemical Society Reviews* 42(3):1287-1311.
13. Voiculescu I & Nordin AN (2012) Acoustic wave based MEMS devices for biosensing applications. *Biosensors & Bioelectronics* 33(1):1-9.
14. Borisov SM & Wolfbeis OS (2008) Optical biosensors. *Chemical Reviews* 108(2):423-461.
15. Monat C, Domachuk P, & Eggleton BJ (2007) Integrated optofluidics: A new river of light. *Nature Photonics* 1(2):106-114.
16. Ince R & Narayanaswamy R (2006) Analysis of the performance of interferometry, surface plasmon resonance and luminescence as biosensors and chemosensors. *Analytica Chimica Acta* 569(1-2):1-20.
17. Yin D, Deamer DW, Schmidt H, Barber JP, & Hawkins AR (2006) Single-molecule detection sensitivity using planar integrated optics on a chip. *Optics Letters* 31(14):2136-2138.
18. Claes T*, et al.* (2009) Label-Free Biosensing With a Slot-Waveguide-Based Ring Resonator in Silicon on Insulator. *Ieee Photonics Journal* 1(3):197-204.
19. Fan X*, et al.* (2008) Sensitive optical biosensors for unlabeled targets: A review. *Analytica Chimica Acta* 620(1-2):8-26.

20. Delezoide C*, et al.* (2012) Vertically Coupled Polymer Microracetrack Resonators for Label-Free Biochemical Sensors. *Ieee Photonics Technology Letters* 24(4):270-272.
21. Chao CY & Guo LJ (2003) Biochemical sensors based on polymer microrings with sharp asymmetrical resonance. *Applied Physics Letters* 83(8):1527-1529.
22. Qavi AJ & Bailey RC (2010) Multiplexed Detection and Label-Free Quantitation of MicroRNAs Using Arrays of Silicon Photonic Microring Resonators. *Angewandte Chemie-International Edition* 49(27):4608-4611.
23. Poshtiban S, Singh A, Fitzpatrick G, & Eyoy S (2013) Bacteriophage tail-spike protein derivitized microresonator arrays for specific detection of pathogenic bacteria. *Sensors and Actuators B-Chemical* 181:410-416.
24. Bahadoran M*, et al.* (2014) Modeling and Analysis of a Microresonating Biosensor for Detection of Salmonella Bacteria in Human Blood. *Sensors* 14(7):12885-12899.
25. Jian-Jun He LJ, and Mingyu Li (The 'Lord of the Rings' of optical biosensors. SPIE.
26. Axelrod D, Burghardt TP, & Thompson NL (1984) Total Internal-Reflection Fluorescence. *Annual Review of Biophysics and Bioengineering* 13:247-268.
27. Martin-Fernandez ML, Tynan CJ, & Webb SED (2013) A 'pocket guide' to total internal reflection fluorescence. *Journal of Microscopy* 252(1):16-22.
28. Hern JA*, et al.* (2010) Formation and dissociation of M-1 muscarinic receptor dimers seen by total internal reflection fluorescence imaging of single molecules. *Proceedings of the National Academy of Sciences of the United States of America* 107(6):2693-2698.
29. Zhao R & Rueda D (2009) RNA folding dynamics by single-molecule fluorescence resonance energy transfer. *Methods* 49(2):112-117.
30. Reck-Peterson SL, Derr ND, & Stuurman N (2010) Imaging single molecules using total internal reflection fluorescence microscopy (TIRFM). *Cold Spring Harbor protocols* 2010(3):pdb.top73-pdb.top73.
31. Manneville JB (2006) Use of TIRF microscopy to visualize actin and microtubules in migrating cells. *Methods in Enzymology, Vol 406, Regulators and Effectors of Small Gtpases: Rho Family,* Methods in Enzymology), Vol 406, pp 520-532.
32. Thompson NL, Burghardt TP, & Axelrod D (1981) Measuring Surface Dynamics of Biomolecules by Total Internal-Reflection Fluorescence with Photobleaching Recovery or Correlation Spectroscopy. *Biophysical Journal* 33(3):435-454.
33. Lieto AM, Cush RC, & Thompson NL (2003) Ligand-receptor kinetics measured by total internal reflection with fluorescence correlation spectroscopy. *Biophysical Journal* 85(5):3294-3302.
34. Brown AEX, Hategan A, Safer D, Goldman YE, & Discher DE (2009) Cross-Correlated TIRF/AFM Reveals Asymmetric Distribution of Force-Generating Heads along Self-Assembled, "Synthetic" Myosin Filaments. *Biophysical Journal* 96(5):1952-1960.
35. Wegner GJ, Lee NJ, Marriott G, & Corn RM (2003) Fabrication of histidine-tagged fusion protein arrays for surface plasmon resonance imaging studies of protein-protein and protein-DNA interactions. *Analytical Chemistry* 75(18):4740-4746.
36. Nelson BP, Grimsrud TE, Liles MR, Goodman RM, & Corn RM (2001) Surface plasmon resonance imaging measurements of DNA and RNA hybridization adsorption onto DNA microarrays. *Analytical Chemistry* 73(1):1-7.

37. Nogues C, Leh H, Lautru J, Delelis O, & Buckle M (2012) Efficient Antifouling Surface for Quantitative Surface Plasmon Resonance Based Biosensor Analysis. *PLoS One* 7(9).
38. Garcia BH & Goodman RM (2008) Use of surface plasmon resonance imaging to study viral RNA : protein interactions. *Journal of Virological Methods* 147(1):18-25.
39. Prorok P*, et al.* (2012) Highly Mutagenic Exocyclic DNA Adducts Are Substrates for the Human Nucleotide Incision Repair Pathway. *PLoS One* 7(12).
40. Pemberton IK & Buckle M (1999) Real time in vitro analysis of transcription by RNA polymerase on immobilized DNA fibres. *Journal of Molecular Recognition* 12(5):322-327.
41. Kanda V, Kitov P, Bundle DR, & McDermott MT (2005) Surface plasmon resonance imaging measurements of the inhibition of Shiga-like toxin by synthetic multivalent inhibitors. *Analytical Chemistry* 77(23):7497-7504.
42. Villiers MB*, et al.* (2010) Peptide-protein microarrays and surface plasmon resonance detection: Biosensors for versatile biomolecular interaction analysis. *Biosensors & Bioelectronics* 26(4):1554-1559.
43. Grasso G*, et al.* (2005) Activity of anchored human matrix metalloproteinase-1 catalytic domain on Au(111) surfaces monitored by ESI-MS. *Journal of Mass Spectrometry* 40(12):1565-1571.
44. Bouffartigues E, Leh H, Anger-Leroy M, Rimsky S, & Buckle M (2007) Rapid coupling of Surface Plasmon Resonance (SPR and SPRi) and ProteinChip (TM) based mass spectrometry for the identification of proteins in nucleoprotein interactions. *Nucleic Acids Research* 35(6):E39-E39.
45. Daniel C, Melaine F, Roupioz Y, Livache T, & Buhot A (2013) Real time monitoring of thrombin interactions with its aptamers: Insights into the sandwich complex formation. *Biosensors & Bioelectronics* 40(1):186-192.
46. Li Y, Lee HJ, & Corn RM (2006) Fabrication and characterization of RNA aptamer microarrays for the study of protein-aptamer interactions with SPR imaging. *Nucleic Acids Research* 34(22):6416-6424.
47. Nogues C*, et al.* (2010) Characterisation of Peptide Microarrays for Studying Antibody-Antigen Binding Using Surface Plasmon Resonance Imagery. *PLoS One* 5(8).
48. Wegner GJ, Lee HJ, & Corn RM (2002) Characterization and optimization of peptide arrays for the study of epitope-antibody interactions using surface plasmon resonance imaging. *Analytical Chemistry* 74(20):5161-5168.
49. Kanda V, Kariuki JK, Harrison DJ, & McDermott MT (2004) Label-free reading of microarray-based immunoassays with surface plasmon resonance imaging. *Analytical Chemistry* 76(24):7257-7262.
50. Bouguelia S*, et al.* (2013) On-chip microbial culture for the specific detection of very low levels of bacteria. *Lab on a Chip* 13(20):4024-4032.
51. Subramanian A, Irudayaraj J, & Ryan T (2006) Mono and dithiol surfaces on surface plasmon resonance biosensors for detection of Staphylococcus aureus. *Sensors and Actuators B-Chemical* 114(1):192-198.
52. Milgram S, Bombera R, Livache T, & Roupioz Y (2012) Antibody microarrays for label-free cell-based applications. *Methods* 56(2):326-333.
53. Villiers M-B*, et al.* (2009) Polypyrrole-peptide microarray for biomolecular interaction analysis by SPR imaging. *Methods in molecular biology (Clifton, N.J.)* 570:317-328.

54. Bartoli J, Roget A, & Livache T (2012) Polypyrrole-oligosaccharide microarray for the measurement of biomolecular interactions by surface plasmon resonance imaging. *Methods in molecular biology (Clifton, N.J.)* 808:69-86.
55. Maillart E*, et al.* (2004) Versatile analysis of multiple macromolecular interactions by SPR imaging: application to p53 and DNA interaction. *Oncogene* 23(32):5543-5550.
56. Malic L, Sandros MG, & Tabrizian M (2011) Designed Biointerface Using Near-Infrared Quantum Dots for Ultrasensitive Surface Plasmon Resonance Imaging Biosensors. *Anal. Chem.* 83(13):5222-5229.
57. Johne B, Gadnell M, & Hansen K (1993) Epitope Mapping and Binding-Kinetics of Monoclonal-Antibodies Studied by Real-Time Biospecific Interaction Analysis Using Surface-Plasmon Resonance. *Journal of Immunological Methods* 160(2):191-198.
58. Seefeld TH, Halpern AR, & Corn RM (2012) On-Chip Synthesis of Protein Microarrays from DNA Microarrays via Coupled In Vitro Transcription and Translation for Surface Plasmon Resonance Imaging Biosensor Applications. *Journal of the American Chemical Society* 134(30):12358-12361.
59. Stenberg E, Persson B, Roos H, & Urbaniczky C (1991) Quantitative-Determination of Surface Concentration of Protein with Surface-Plasmon Resonance Using Radiolabeled Proteins. *Journal of Colloid and Interface Science* 143(2):513-526.
60. Wassaf D*, et al.* (2006) High-throughput affinity ranking of antibodies using surface plasmon resonance microarrays. *Analytical Biochemistry* 351(2):241-253.
61. Kretschmann E (1971) Determination of Optical Constants of Metals by Excitation of Surface Plasmons. *Zeitschrift Fur Physik* 241(4):313-&.
62. Gwon HR & Lee SH (2010) Spectral and Angular Responses of Surface Plasmon Resonance Based on the Kretschmann Prism Configuration. *Materials Transactions* 51(6):1150-1155.
63. Langmuir I (1916) The constitution and fundamental properties of solids and liquids Part I Solids. *Journal of the American Chemical Society* 38:2221-2295.
64. Langmuir I (1918) The Adsorption of Gases on Plane Surfaces of Glass, Mica and Platinum. *Journal of the American Chemical Society* 40:1361-1403.
65. Lodish H BA, Zipursky SL, et al. (2000) *Molecular Cell Biology. 4th edition.* (New York).
66. Greive SJ*, et al.* (2008) Monitoring RNA transcription in real time by using surface plasmon resonance. *Proceedings of the National Academy of Sciences of the United States of America* 105(9):3315-3320.
67. Ritzefeld M & Sewald N (2012) Real-Time Analysis of Specific Protein-DNA Interactions with Surface Plasmon Resonance. *Journal of amino acids* 2012:816032-816032.
68. Myszka DG & Morton TA (1998) CLAMP (c): A biosensor kinetic data analysis program. *Trends in Biochemical Sciences* 23(4):149-150.
69. Homola J (2008) Surface plasmon resonance sensors for detection of chemical and biological species. *Chemical Reviews* 108(2):462-493.
70. Chen Y, Nakamoto K, Niwa O, & Corn RM (2012) On-Chip Synthesis of RNA Aptamer Microarrays for Multiplexed Protein Biosensing with SPR Imaging Measurements. *Langmuir* 28(22):8281-8285.
71. Lausted C, Hu Z, & Hood L (2008) Quantitative Serum Proteomics from Surface Plasmon Resonance Imaging. *Molecular & Cellular Proteomics* 7(12):2464-2474.

72. Beleoken E*, et al.* (2013) SPRi-Based Strategy to Identify Specific Biomarkers in Systemic Lupus Erythematosus, Rheumatoid Arthritis and Autoimmune Hepatitis. *PLoS One* 8(12).
73. Fenalti G*, et al.* (2007) GABA production by glutamic acid decarboxylase is regulated by a dynamic catalytic loop. *Nature Structural & Molecular Biology* 14(4):280-286.
74. Huang C*, et al.* (2009) Localized surface plasmon resonance biosensor integrated with microfluidic chip. *Biomedical Microdevices* 11(4):893-901.
75. Hutter E & Pileni MP (2003) Detection of DNA hybridization by gold nanoparticle enhanced transmission surface plasmon resonance spectroscopy. *Journal of Physical Chemistry B* 107(27):6497-6499.
76. Fujiwara K, Watarai H, Itoh H, Nakahama E, & Ogawa N (2006) Measurement of antibody binding to protein immobilized on gold nanoparticles by localized surface plasmon spectroscopy. *Analytical and Bioanalytical Chemistry* 386(3):639-644.
77. Haes AJ & Van Duyne RP (2002) A nanoscale optical blosensor: Sensitivity and selectivity of an approach based on the localized surface plasmon resonance spectroscopy of triangular silver nanoparticles. *Journal of the American Chemical Society* 124(35):10596-10604.
78. Melendez J*, et al.* (1996) A commercial solution for surface plasmon sensing. *Sensors and Actuators B-Chemical* 35(1-3):212-216.
79. Wang X, Zhan S, Huang Z, & Hong X (2013) Review: Advances and Applications of Surface Plasmon Resonance Biosensing Instrumentation. *Instrumentation Science & Technology* 41(6):574-607.
80. Font MP*, et al.* (2004) Repression of transcription at the human T-cell receptor V beta 2.2 segment is mediated by a MAX/MAD/mSin3 complex acting as a scaffold for HDAC activity. *Biochemical and Biophysical Research Communications* 325(3):1021-1029.
81. Bellon S*, et al.* (2009) Hyphenation of Surface Plasmon Resonance Imaging to Matrix-Assisted Laser Desorption Ionization Mass Spectrometry by On-Chip Mass Spectrometry and Tandem Mass Spectrometry Analysis. *Analytical Chemistry* 81(18):7695-7702.
82. Diltemiz SE, Denizli A, Ersoz A, & Say R (2008) Molecularly imprinted ligand-exchange recognition assay of DNA by SPR system using guanosine and guanine recognition sites of DNA. *Sensors and Actuators B-Chemical* 133(2):484-488.
83. Szunerits S, Knorr N, Calemczuk R, & Livache T (2004) Approach to writing and simultaneous reading of micropatterns: Combining surface plasmon resonance imaging with scanning electrochemical microscopy (SECM). *Langmuir* 20(21):9236-9241.
84. Malic L, Veres T, & Tabrizian M (2009) Biochip functionalization using electrowetting-on-dielectric digital microfluidics for surface plasmon resonance imaging detection of DNA hybridization. *Biosensors & Bioelectronics* 24(7):2218-2224.
85. Malic L, Veres T, & Tabrizian M (2009) Two-dimensional droplet-based surface plasmon resonance imaging using electrowetting-on-dielectric microfluidics. *Lab on a Chip* 9(3):473-475.
86. Lee HJ, Goodrich TT, & Corn RM (2001) SPR imaging measurements of 1-D and 2-D DNA microarrays created from microfluidic channels on gold thin films. *Analytical Chemistry* 73(22):5525-5531.

87. Fiche JB, Fuchs J, Buhot A, Calemczuk R, & Livache T (2008) Point mutation detection by surface plasmon resonance imaging coupled with a temperature scan method in a model system. *Analytical Chemistry* 80(4):1049-1057.
88. Huang L, Wang WJ, & Murphy MC (1999) Peltier-effect module for highly localized temperature manipulations. *Review of Scientific Instruments* 70(11):4398-4403.
89. Samanta D & Sarkar A (2011) Immobilization of bio-macromolecules on self-assembled monolayers: methods and sensor applications. *Chemical Society Reviews* 40(5):2567-2592.
90. Conde J*, et al.* (2014) Revisiting 30 years of biofunctionalization and surface chemistry of inorganic nanoparticles for nanomedicine. *Frontiers in chemistry* 2:48-48.
91. Scarano S, Scuffi C, Mascini M, & Minunni M (2010) Surface plasmon resonance imaging (SPRi)-based sensing: A new approach in signal sampling and management. *Biosensors & Bioelectronics* 26(4):1380-1385.
92. Hunt HK & Armani AM (2010) Label-free biological and chemical sensors. *Nanoscale* 2(9):1544-1559.
93. Harder P, Grunze M, Dahint R, Whitesides GM, & Laibinis PE (1998) Molecular conformation in oligo(ethylene glycol)-terminated self-assembled monolayers on gold and silver surfaces determines their ability to resist protein adsorption. *Journal of Physical Chemistry B* 102(2):426-436.
94. Nuzzo RG & Allara DL (1983) Adsorption of Bifunctional Organic Disulfides on Gold Surfaces. *Journal of the American Chemical Society* 105(13):4481-4483.
95. Graham MBD (2006) Self-Assembled Monolayers: Advantages of Pure Alkanethiols. *Material Matters* 1.2(3).
96. Agonafer DD, Chainani E, Oruc ME, Lee KS, & A. SM (2012) Study of Insulating Properties of Alkanethiol Self-Assembled Monolayers Formed Under Prolonged Incubation Using Electrochemical Impedance Spectroscopy. *Journal of Nanotechnology in Engineering and Medicine* 3(031006-1).
97. Love JC, Estroff LA, Kriebel JK, Nuzzo RG, & Whitesides GM (2005) Self-assembled monolayers of thiolates on metals as a form of nanotechnology. *Chemical Reviews* 105(4):1103-1169.
98. Mittlerneher S*, et al.* (1995) Spectroscopic and Surface-Analytical Characterization of Self-Assembled Layers on Au. *Biosensors & Bioelectronics* 10(9-10):903-916.
99. Szleifer I (1997) Polymers and proteins: Interactions at interfaces. *Current Opinion in Solid State & Materials Science* 2(3):337-344.
100. Currie EPK, Norde W, & Stuart MAC (2003) Tethered polymer chains: surface chemistry and their impact on colloidal and surface properties. *Advances in Colloid and Interface Science* 100:205-265.
101. Park J-W, Kim H, & Han M (2010) Polymeric self-assembled monolayers derived from surface-active copolymers: a modular approach to functionalized surfaces. *Chemical Society Reviews* 39(8):2935-2947.
102. Gao XH*, et al.* (2005) In vivo molecular and cellular imaging with quantum dots. *Current Opinion in Biotechnology* 16(1):63-72.
103. Kalia J & Raines RT (2010) Advances in Bioconjugation. *Current Organic Chemistry* 14(2):138-147.

104. Schroeder H*, et al.* (2009) User Configurable Microfluidic Device for Multiplexed Immunoassays Based on DNA-Directed Assembly. *Analytical Chemistry* 81(3):1275-1279.
105. Ahuja T, Mir IA, Kumar D, & Rajesh (2007) Biomolecular immobilization on conducting polymers for biosensing applications. *Biomaterials* 28(5):791-805.
106. Jung Y, Jeong JY, & Chung BH (2008) Recent advances in immobilization methods of antibodies on solid supports. *Analyst* 133(6):697-701.
107. Hosta-Rigau L, Zhang Y, Teo BM, Postma A, & Staedler B (2013) Cholesterol - a biological compound as a building block in bionanotechnology. *Nanoscale* 5(1):89-109.
108. Nilsson J, Stahl S, Lundeberg J, Uhlen M, & Nygren PA (1997) Affinity fusion strategies for detection, purification, and immobilization of recombinant proteins. *Protein Expression and Purification* 11(1):1-16.
109. Cronan JE (1990) Biotination of Proteins Invivo - a Posttranslational Modification to Label, Purify, and Study Proteins. *Journal of Biological Chemistry* 265(18):10327-10333.
110. Trilling AK, Beekwilder J, & Zuilhof H (2013) Antibody orientation on biosensor surfaces: a minireview. *Analyst* 138(6):1619-1627.
111. Ohno M, Karagiannis P, & Taniguchi Y (2014) Protein Expression Analyses at the Single Cell Level. *Molecules* 19(9):13932-13947.
112. Liu C, Cui D, & Li H (2010) A hard-soft microfluidic-based biosensor flow cell for SPR imaging application. *Biosensors & Bioelectronics* 26(1):255-261.
113. Noh J, Kim HC, & Chung TD (2011) Biosensors in Microfluidic Chips. *Microfluidics: Technologies and Applications,* Topics in Current Chemistry), Vol 304, pp 117-152.
114. Whitesides GM (2006) The origins and the future of microfluidics. *Nature* 442(7101):368-373.
115. Hsu W-T*, et al.* (2011) Integration of fiber optic-particle plasmon resonance biosensor with microfluidic chip. *Analytica Chimica Acta* 697(1-2):75-82.
116. Sheehan PE & Whitman LJ (2005) Detection limits for nanoscale biosensors. *Nano Letters* 5(4):803-807.
117. Myszka DG (1997) Kinetic analysis of macromolecular interactions using surface plasmon resonance biosensors. *Current Opinion in Biotechnology* 8(1):50-57.
118. Travers A & Buckle M (2000) *DNA-Protein Interactions - A Practical Approach* (Oxford, UK).
119. Wu HY, Shyy S, Wang JC, & Liu LF (1988) Transcription Generates Positively and Negatively Supercoiled Domains in the Template. *Cell* 53(3):433-440.
120. Vogel U & Jensen KF (1994) The Rna Chain Elongation Rate in Escherichia-Coli Depends on the Growth-Rate. *Journal of Bacteriology* 176(10):2807-2813.
121. Nelson DL & Cox MM (2006) *Principles of Biochemistry* IV Ed.
122. Sydow JF & Cramer P (2009) RNA polymerase fidelity and transcriptional proofreading. *Current Opinion in Structural Biology* 19(6):732-739.
123. Erie DA, Hajiseyedjavadi O, Young MC, & Vonhippel PH (1993) Multiple Rna-Polymerase Conformations and Grea - Control of the Fidelity of Transcription. *Science* 262(5135):867-873.
124. Ninio J (1991) Connections between Translation, Transcription and Replication Error-Rates. *Biochimie* 73(12):1517-1523.

125. Pribnow D (1975) Nucleotide-Sequence of an Rna-Polymerase Binding-Site at an Early T7 Promoter. *Proceedings of the National Academy of Sciences of the United States of America* 72(3):784-788.
126. Browning DF & Busby SJW (2004) The regulation of bacterial transcription initiation. *Nature Reviews Microbiology* 2(1):57-65.
127. Zacharias M, Goringer HU, & Wagner R (1989) Influence of the Gcgc Discriminator Motif Introduced into the Ribosomal-Rna P2 and Tac Promoter on Growth-Rate Control and Stringent Sensitivity. *Embo Journal* 8(11):3357-3363.
128. Gowers DM, Wilson GG, & Halford SE (2005) Measurement of the contributions of 1D and 3D pathways to the translocation of a protein along DNA. *Proceedings of the National Academy of Sciences of the United States of America* 102(44):15883-15888.
129. Gorman J & Greene EC (2008) Visualizing one-dimensional diffusion of proteins along DNA. *Nature Structural & Molecular Biology* 15(8):768-774.
130. DeHaseth PL, Zupancic ML, & Record MT (1998) RNA polymerase-promoter interactions: the comings and goings of RNA polymerase. *Journal of Bacteriology* 180(12):3019-3025.
131. Buckle M, Buc H, & Travers AA (1992) DNA Deformation in Nucleoprotein Complexes between Rna-Polymerase, Camp Receptor Protein and the Lac Uv5 Promoter Probed by Singlet Oxygen. *Embo Journal* 11(7):2619-2625.
132. Buckle M, Geiselmann J, Kolb A, & Buc H (1991) Protein-DNA Cross-Linking at the Lac Promoter. *Nucleic Acids Research* 19(4):833-840.
133. Buckle M, Pemberton IK, Jacquet MA, & Buc H (1999) The kinetics of sigma subunit directed promoter recognition by E-coli RNA polymerase. *Journal of Molecular Biology* 285(3):955-964.
134. Kubori T & Shimamoto N (1996) A branched pathway in the early stage of transcription by Escherichia coli RNA polymerase. *Journal of Molecular Biology* 256(3):449-457.
135. Hsu LLM, Vo NV, Kane CM, & Chamberlin MJ (2003) In vitro studies of transcript initiation by Escherichia coli RNA polymerase. 1. RNA chain initiation, abortive initiation, and promoter escape at three bacteriophage promoters. *Biochemistry* 42(13):3777-3786.
136. McClure WR (1985) Mechanism and Control of Transcription Initiation in Prokaryotes. *Annual Review of Biochemistry* 54:171-204.
137. Craig ML*, et al.* (1998) DNA footprints of the two kinetically significant intermediates in formation of an RNA polymerase-promoter open complex: Evidence that interactions with start site and downstream DNA induce sequential conformational changes in polymerase and DNA. *Journal of Molecular Biology* 283(4):741-756.
138. Shimamoto N, Kamigochi T, & Utiyama H (1986) Release of the Sigma-Subunit of Escherichia-Coli DNA-Dependent Rna-Polymerase Depends Mainly on Time Elapsed after the Start of Initiation, Not on Length of Product Rna. *Journal of Biological Chemistry* 261(25):1859-1865.
139. Krummel B & Chamberlin MJ (1989) Rna Chain Initiation by Escherichia-Coli Rna-Polymerase - Structural Transitions of the Enzyme in Early Ternary Complexes. *Biochemistry* 28(19):7829-7842.
140. Mukhopadhyay J*, et al.* (2001) Translocation of sigma(70) with RNA polymerase during transcription: Fluorescence resonance energy transfer assay for movement relative to DNA. *Cell* 106(4):453-463.

141. Mekler V*, et al.* (2002) Structural organization of bacterial RNA polymerase holoenzyme and the RNA polymerase-promoter open complex. *Cell* 108(5):599-614.
142. Brodolin K, Zenkin N, Mustaev A, Mamaeva D, & Heumann H (2004) The sigma(70) subunit of RNA polymerase induces lacUV5 promoter-proximal pausing of transcription. *Nature Structural & Molecular Biology* 11(6):551-557.
143. Nickels BE, Mukhopadhyay J, Garrity SJ, Ebright RH, & Hochschild A (2004) The sigma(70) subunit of RNA polymerase mediates a promoter-proximal pause at the lac promoter. *Nature Structural & Molecular Biology* 11(6):544-550.
144. Roberts JW, Shankar S, & Filter JJ (2008) RNA Polymerase Elongation Factors. *Annual Review of Microbiology,* Annual Review of Microbiology), Vol 62, pp 211-233.
145. Epshtein V, Toulme F, Rahmouni AR, Borukhov S, & Nudler E (2003) Transcription through the roadblocks: the role of RNA polymerase cooperation. *Embo Journal* 22(18):4719-4727.
146. Toulme F*, et al.* (2000) GreA and GreB proteins revive backtracked RNA polymerase in vivo by promoting transcript trimming. *Embo Journal* 19(24):6853-6859.
147. Toulme F, Mosrin-Huaman C, Artsimovitch I, & Rahmouni AR (2005) Transcriptional pausing in vivo: A nascent RNA hairpin restricts lateral movements of RNA polymerase in both forward and reverse directions. *Journal of Molecular Biology* 351(1):39-51.
148. Yarnell WS & Roberts JW (1999) Mechanism of intrinsic transcription termination and antitermination. *Science* 284(5414):611-615.
149. Schwartz A, Rahmouni AR, & Boudvillain M (2003) The functional anatomy of an intrinsic transcription terminator. *Embo Journal* 22(13):3385-3394.
150. Schwartz A, Walmacq C, Rahmouni AR, & Boudvillain M (2007) Noncanonical interactions in the management of RNA structural blocks by the transcription termination Rho helicase. *Biochemistry* 46(33):9366-9379.
151. Ciampi MS (2006) Rho-dependent terminators and transcription termination. *Microbiology-Sgm* 152:2515-2528.
152. Geiselmann J, Yager TD, Gill SC, Calmettes P, & Vonhippel PH (1992) Physical-Properties of the Escherichia-Coli Transcription Termination Factor Rho .1. Association States and Geometry of the Rho Hexamer. *Biochemistry* 31(1):111-121.
153. Geiselmann J, Yager TD, & Vonhippel PH (1992) Functional Interactions of Ligand Cofactors with Escherichia-Coli Transcription Termination Factor-Rho .2. Binding of Rna. *Protein Science* 1(7):861-873.
154. Buc H & Strick T (2009) *RNA Polymerases as Molecular Motors* (RSC Publishing) p 331.
155. Kolb A, Busby S, Buc H, Garges S, & Adhya S (1993) Transcriptional Regulation by Camp and Its Receptor Protein. *Annual Review of Biochemistry* 62:749-795.
156. Lewis M (2005) The lac repressor. *Comptes Rendus Biologies* 328(6):521-548.
157. Murakami KS, Masuda S, Campbell EA, Muzzin O, & Darst SA (2002) Structural basis of transcription initiation: An RNA polymerase holoenzyme-DNA complex. *Science* 296(5571):1285-1290.
158. Mooney RA, Darst SA, & Landick R (2005) Sigma and RNA polymerase: An on-again, off-again relationship? *Molecular Cell* 20(3):335-345.

159. Yura T & Nakahigashi K (1999) Regulation of the heat-shock response. *Current Opinion in Microbiology* 2(2):153-158.
160. Jurado P, Fernandez LA, & de Lorenzo V (2003) Sigma 54 levels and physiological control of the Pseudomonas putida Pu promoter. *Journal of Bacteriology* 185(11):3379-3383.
161. Feklistov A, Sharon BD, Darst SA, & Gross CA (2014) Bacterial Sigma Factors: A Historical, Structural, and Genomic Perspective. *Annual Review of Microbiology, Vol 68,* Annual Review of Microbiology), Vol 68, pp 357-376.
162. Borukhov S & Nudler E (2003) RNA polymerase holoenzyme: structure, function and biological implications. *Current Opinion in Microbiology* 6(2):93-100.
163. Geszvain K & Landick R (2005) The structure of bacterial RNA polymerase. *Bacterial Chromosome*:283-+.
164. Buc H & McClure WR (1985) Kinetics of Open Complex-Formation between Escherichia-Coli Rna-Polymerase and the Lac Uv5 Promoter - Evidence for a Sequential Mechanism Involving 3 Steps. *Biochemistry* 24(11):2712-2723.
165. Buckle M & Buc H (1989) Fine Mapping of DNA Single-Stranded Regions Using Base-Specific Chemical Probes - Study of an Open Complex Formed between Rna-Polymerase and the Lac Uv5 Promoter. *Biochemistry* 28(10):4388-4396.
166. Buckle M & Buc H (1994) On the Mechanism of Promoter Recognition by E. coli RNA Polymerase. *Transcription: Mechanisms and Regulation*, ed Conaway RCJ (Raven Press, New York).
167. Spassky A, Kirkegaard K, & Buc H (1985) Changes in the DNA-Structure of the Lac Uv5 Promoter during Formation of an Open Complex with Escherichia-Coli Rna-Polymerase. *Biochemistry* 24(11):2723-2731.
168. Studier FW & Moffatt BA (1986) Use of Bacteriophage-T7 Rna-Polymerase to Direct Selective High-Level Expression of Cloned Genes. *Journal of Molecular Biology* 189(1):113-130.
169. Place C, Oddos J, Buc H, McAllister WT, & Buckle M (1999) Studies of contacts between T7 RNA polymerase and its promoter reveal features in common with multisubunit RNA polymerases. *Biochemistry* 38(16):4948-4957.
170. Ikeda RA & Richardson CC (1986) Interactions of the Rna-Polymerase of Bacteriophage-T7 with Its Promoter during Binding and Initiation of Transcription. *Proceedings of the National Academy of Sciences of the United States of America* 83(11):3614-3618.
171. Jia YP & Patel SS (1997) Kinetic mechanism of transcription initiation by bacteriophage T7 RNA polymerase. *Biochemistry* 36(14):4223-4232.
172. Milligan JF, Groebe DR, Witherell GW, & Uhlenbeck OC (1987) Oligoribonucleotide Synthesis Using T7 Rna-Polymerase and Synthetic DNA Templates. *Nucleic Acids Research* 15(21):8783-8798.
173. Golomb M & Chamberl.M (1974) Characterization of T7-Specific Ribonucleic-Acid Polymerase .4. Resolution of Major Invitro Transcripts by Gel-Electrophoresis. *Journal of Biological Chemistry* 249(9):2858-2863.
174. McClure WR (1980) Rate-Limiting Steps in Rna Chain Initiation. *Proceedings of the National Academy of Sciences of the United States of America-Biological Sciences* 77(10):5634-5638.
175. Ganguly A, Rajdev P, & Chatterji D (2009) Sequence Specific Interaction between Promoter DNA and Escherichia coli RNA Polymerase: Comparative Thermodynamic Analysis with One Immobilized Partner. *Journal of Physical Chemistry B* 113(46):15399-15408.

176. Delplanque A*, et al.* (2014) UV/ozone surface treatment increases hydrophilicity and enhances functionality of SU-8 photoresist polymer. *Applied Surface Science* 314:280-285.
177. Cao C*, et al.* (2011) Surface modification of photoresist SU-8 for low autofluorescence and bioanalytical applications. *15th International Conference on Miniaturized Systems for Chemistry and Life Science,*.
178. Abgrall P, Conedera V, Camon H, Gue A-M, & Nguyen N-T (2007) SU-8 as a structural material for labs-on-chips and microelectromechanical systems. *Electrophoresis* 28(24):4539-4551.
179. del Campo A & Greiner C (2007) SU-8: a photoresist for high-aspect-ratio and 3D submicron lithography. *Journal of Micromechanics and Microengineering* 17(6):R81-R95.
180. Delezoide C, Lautru J, Zyss J, Ledoux-Rak I, & Chi Thanh N (2012) Vertically coupled polymer microresonators for optofluidic label-free biosensors. *Integrated Optics: Devices, Materials, and Technologies Xvi* 8264.
181. Nordstrom M, Marie R, Calleja M, & Boisen A (2004) Rendering SU-8 hydrophilic to facilitate use in micro channel fabrication. *Journal of Micromechanics and Microengineering* 14(12):1614-1617.
182. Sikanen T*, et al.* (2007) Performance of SU-8 microchips as separation devices and comparison with glass microchips. *Analytical Chemistry* 79(16):6255-6263.
183. Tao SL, Popat KC, Norman JJ, & Desai TA (2008) Surface modification of SU-8 for enhanced biofunctionality and nonfouling properties. *Langmuir* 24(6):2631-2636.
184. Blagoi G, Keller S, Johansson A, Boisen A, & Dufva M (2008) Functionalization of SU-8 photoresist surfaces with IgG proteins. *Applied Surface Science* 255(5):2896-2902.
185. Deepu A, Sai VVR, & Mukherji S (2009) Simple surface modification techniques for immobilization of biomolecules on SU-8. *Journal of Materials Science-Materials in Medicine* 20:25-28.
186. Joshi M, Kale N, Lal R, Rao VR, & Mukherji S (2007) A novel dry method for surface modification of SU-8 for immobilization of biomolecules in Bio-MEMS. *Biosensors & Bioelectronics* 22(11):2429-2435.
187. Marie R*, et al.* (2006) Immobilisation of DNA to polymerised SU-8 photoresist. *Biosensors & Bioelectronics* 21(7):1327-1332.
188. Jokinen V, Suvanto P, & Franssila S (2012) Oxygen and nitrogen plasma hydrophilization and hydrophobic recovery of polymers. *Biomicrofluidics* 6(1).
189. Ji Y, Yuan K, & Chung JN (2006) Numerical simulation of wall roughness on gaseous flow and heat transfer in a microchannel. *International Journal of Heat and Mass Transfer* 49(7-8):1329-1339.
190. Winzeler HB & Belfort G (1993) Enhanced Performance for Pressure-Driven Membrane Processes - the Argument for Fluid Instabilities. *Journal of Membrane Science* 80(1-3):35-47.
191. Chang JS, Eom SC, Sung GY, & Shin JH (2009) On-chip, planar integration of Er doped silicon-rich silicon nitride microdisk with SU-8 waveguide with sub-micron gap control. *Optics Express* 17(25):22918-22924.
192. Mathieson I & Bradley RH (1996) Improved adhesion to polymers by UV/ozone surface oxidation. *International Journal of Adhesion and Adhesives* 16(1):29-31.

193. Nie HY, Walzak MJ, Berno B, & McIntyre NS (1999) Atomic force microscopy study of polypropylene surfaces treated by UV and ozone exposure: modification of morphology and adhesion force. *Applied Surface Science* 144-45:627-632.
194. Haack LP*, et al.* (2000) Chemistry of surface modification with UV/ozone for improved intercoat adhesion in multilayered coating systems. *Surface and Interface Analysis* 29(12):829-836.
195. Keller S, Blagoi G, Lillemose M, Haefliger D, & Boisen A (2008) Processing of thin SU-8 films. *Journal of Micromechanics and Microengineering* 18(12).
196. Zhang Z, Zhao P, Xiao G, Watts BR, & Xu C (2011) Sealing SU-8 microfluidic channels using PDMS. *Biomicrofluidics* 5(4).
197. Chang C-J, Yang C-S, Lan L-H, Wang P-C, & Tseng F-G (2010) Fabrication of a SU-8-based polymer-enclosed channel with a penetrating UV/ozone-modified interior surface for electrokinetic separation of proteins. *Journal of Micromechanics and Microengineering* 20(11).
198. Henke L, Nagy N, & Krull UJ (2002) An AFM determination of the effects on surface roughness caused by cleaning of fused silica and glass substrates in the process of optical biosensor preparation. *Biosensors & Bioelectronics* 17(6-7):547-555.
199. Wang Y*, et al.* (2007) Surface graft polymerization of SU-8 for bio-MEMS applications. *Journal of Micromechanics and Microengineering* 17(7):1371-1380.
200. Chen AK, Cheng Z, Behlke MA, & Tsourkas A (2008) Assessing the sensitivity of commercially available fluorophores to the intracellular environment. *Analytical Chemistry* 80(19):7437-7444.
201. Mrksich M & Whitesides GM (1997) Using self-assembled monolayers that present oligo(ethylene glycol) groups to control the interactions of proteins with surfaces. *Poly(Ethylene Glycol): Chemistry and Biological Applications,* Acs Symposium Series), Vol 680, pp 361-373.
202. Backmann N*, et al.* (2005) A label-free immunosensor array using single-chain antibody fragments. *Proceedings of the National Academy of Sciences of the United States of America* 102(41):14587-14592.
203. Evans MR & Read CA (1992) 32p, 33p and 35s - Selecting a Label for Nucleic-Acid Analysis. *Nature* 358(6386):520-521.
204. Paiva D, Brezesinski G, Pereira MdC, & Rocha S (2013) Langmuir Monolayers of Monocationic Lipid Mixed with Cholesterol or Fluorocholesterol: DNA Adsorption Studies. *Langmuir* 29(6):1920-1925.
205. Matsuoka K, Takagi K, & Honda C (2013) Micelle formation of sodium hyodeoxycholate. *Chemistry and Physics of Lipids* 172:6-13.
206. Meyer EE, Rosenberg KJ, & Israelachvili J (2006) Recent progress in understanding hydrophobic interactions. *Proceedings of the National Academy of Sciences of the United States of America* 103(43):15739-15746.
207. Erkan Y, Czolkos I, Jesorka A, Wilhelmsson LM, & Orwar O (2007) Direct immobilization of cholesteryl-TEG-modified oligonucleotides onto hydrophobic SU-8 surfaces. *Langmuir* 23(10):5259-5263.
208. Erkan Y*, et al.* (2008) Controlled release of Chol-TEG-DNA from nano- and micropatterned SU-8 surfaces by a spreading lipid film. *Nano Letters* 8(1):227-231.
209. Nes WD (2011) Biosynthesis of Cholesterol and Other Sterols. *Chemical Reviews* 111(10):6423-6451.

210. Wang J, Li Z, Yoon R-H, & Eriksson JC (2012) Surface forces in thin liquid films of n-alcohols and of water-ethanol mixtures confined between hydrophobic surfaces. *Journal of Colloid and Interface Science* 379:114-120.
211. Ederth T (2000) Substrate and solution effects on the long-range "hydrophobic" interactions between hydrophobized gold surfaces. *Journal of Physical Chemistry B* 104(41):9704-9712.
212. Blanco RM, Terreros P, Munoz N, & Serra E (2007) Ethanol improves lipase immobilization on a hydrophobic support. *Journal of Molecular Catalysis B-Enzymatic* 47(1-2):13-20.
213. Hu W*, et al.* (2014) Polydopamine-Functionalization of Graphene Oxide to Enable Dual Signal Amplification for Sensitive Surface Plasmon Resonance Imaging Detection of Biomarker. *Analytical Chemistry* 86(9):4488-4493.
214. Katsamba PS*, et al.* (2006) Kinetic analysis of a high-affinity antibody/antigen interaction performed by multiple Biacore users. *Analytical Biochemistry* 352(2):208-221.
215. Zammatteo N*, et al.* (2000) Comparison between different strategies of covalent attachment of DNA to glass surfaces to build DNA microarrays. *Analytical Biochemistry* 280(1):143-150.
216. Steel AB, Levicky RL, Herne TM, & Tarlov MJ (2000) Immobilization of nucleic acids at solid surfaces: Effect of oligonucleotide length on layer assembly. *Biophysical Journal* 79(2):975-981.
217. Paunov VN, Xu C, Taylor P, Ersoz M, & Fletcher PDI (2005) Properties and applications of novel DNA-based surfactants. *Nanoscale Materials Science in Biology and Medicine,* Materials Research Society Symposium Proceedings), Vol 845, pp 137-142.
218. Cristofolini L, Berzina T, Erokhina S, Konovalov O, & Erokhin V (2007) Structural study of the DNA dipalmitoylphosphatidylcholine complex at the air-water interface. *Biomacromolecules* 8(7):2270-2275.
219. Saha K, Agasti SS, Kim C, Li X, & Rotello VM (2012) Gold Nanoparticles in Chemical and Biological Sensing. *Chemical Reviews* 112(5):2739-2779.
220. Janshoff A, Galla HJ, & Steinem C (2000) Piezoelectric mass-sensing devices as biosensors - An alternative to optical biosensors? *Angewandte Chemie-International Edition* 39(22):4004-4032.
221. Baldrich E, Laczka O, Javier Del Campo F, & Xavier Munoz F (2008) Gold immuno-functionalisation via self-assembled monolayers: Study of critical parameters and comparative performance for protein and bacteria detection. *Journal of Immunological Methods* 336(2):203-212.
222. Chaki NK & Vijayamohanan K (2002) Self-assembled monolayers as a tunable platform for biosensor applications. *Biosensors & Bioelectronics* 17(1-2):1-12.
223. Orth RN, Clark TG, & Craighead HG (2003) Avidin-biotin micropatterning methods for biosensor applications. *Biomedical Microdevices* 5(1):29-34.
224. Herne TM & Tarlov MJ (1997) Characterization of DNA probes immobilized on gold surfaces. *Journal of the American Chemical Society* 119(38):8916-8920.
225. Shcherbakova DM & Verkhusha VV (2013) Near-infrared fluorescent proteins for multicolor in vivo imaging. *NATURE METHODS* 10(8):751-+.
226. Smale ST & Kadonaga JT (2003) The RNA polymerase II core promoter. *Annual Review of Biochemistry* 72:449-479.
227. Kadonaga JT (1998) Eukaryotic transcription: An interlaced network of transcription factors and chromatin-modifying machines. *Cell* 92(3):307-313.

228. Sims RJ, 3rd, Belotserkovskaya R, & Reinberg D (2004) Elongation by RNA polymerase II: the short and long of it. *Genes & development* 18(20):2437-2468.
229. Durniak KJ, Bailey S, & Steitz TA (2008) The structure of a transcribing T7 RNA polymerase in transition from initiation to elongation. *Science* 322(5901):553-557.
230. Zhou Y & Martin CT (2006) Observed instability of T7 RNA polymerase elongation complexes can be dominated by collision-induced "bumping". *Journal of Biological Chemistry* 281(34):24441-24448.
231. Karlsson R, Katsamba PS, Nordin H, Pol E, & Myszka DG (2006) Analyzing a kinetic titration series using affinity biosensors. *Analytical Biochemistry* 349(1):136-147.
232. Frenzel D & Willbold D (2014) Kinetic Titration Series with Biolayer Interferometry. *PLoS One* 9(9).
233. Daube SS & Bar-Ziv RH (2013) Protein nanomachines assembly modes: cell-free expression and biochip perspectives. *Wiley Interdisciplinary Reviews-Nanomedicine and Nanobiotechnology* 5(6):613-628.
234. Bracha D, Karzbrun E, Daube SS, & Bar-Ziv RH (2014) Emergent Properties of Dense DNA Phases toward Artificial Biosystems on a Surface. *Accounts of Chemical Research* 47(6):1912-1921.
235. Takahashi S, Hisanaga K, Yoshida A, & Okahata Y (2012) Real-time monitoring of a stepwise transcription reaction on a quartz-crystal microbalance. *Analytical Biochemistry* 421(2):732-741.

APPENDIX

1. Sequences of DNA

1.1. Sequences of 50, 500 and 1000 bp DNA used for surface functionalization studies *(Chapter III, Sections 2, 3, 4)*

Name	Modification	Exact length (bp)	Sequence (5' → 3')
50bp DNA	OH/NH_2/SH/biot/ chol	50	TCCATCAGTCACTCGCCGGATCCATCTTGAGACTCTGTC ACACGTAGTCG
500bp DNA	OH/NH_2/SH/biot	495	TCCGGCGTAGAGGATCGAGATCTCGCGATTCATTAATGC AGCTGGCACGACAGGTTTCCCGACTGGAAAGCGGGCAG TGAGCGCAACGCAATTAATGTGAGTTAGCTCACTCATT AGGCACCCCAGGCTTTACACTTTATGCTTCCGGCTCGTA TAATGTGTGGAATTGTGAGCGGATAACAATTTCACACA GGAAACAGCTATGACCATGATTACGGATTCACTGGAAG GAGATATACCATGGCACATATGAGCGGCCGCGTCGACTC GAGCGAGCTCCCGGGGGGGGTTCTCATCATCATCATCAT CATTAATAAAAGGGCGAATTCCAGCACACTGGCGGCCG TTACTAGTGGATCCGGCTGCTAACAAAGCCCGAAAGGA AGCTGAGTTGGCTGCTGCCACCGCTGAGCAATAACTAGC ATAACCCCTTGGGGCCTCTAAACGGGTCTTGAGGGGTTT TTTGCTGAAAGGAGGAACTATATCCGGATATCC
1 kbp DNA	OH/NH_2/SH/biot	1037	TCCGGCGTAGAGGATCGAGATCTCGATCCCGCGAAATTA ATACGACTCACTATAGGGAGACCACAACGGTTTCCCTCT AGAAATAATTTTGTTTAACTTTAAGAAGGAGATATACC ATGGCACATATGGGAGAGGATAGCGAGCTGATCTCCGA GAACATGCACACGAAACTGTACATGGAGGGCACCGTGA ACGGCCACCACTTCAAGTGCACATCCGAGGGCGAAGGCA AGCCCTACGAGGGCACCCAGACCTGTAAGATCAAGGTG GTCGAGGGCGGCCCTCTCCCCTTCGCCTTCGACATCCTG GCTACCAGCTTCATGTACGGCAGCAAAACCTTTATCAAC CACACCCAGGGCATCCCCGACTTCTTTAAGCAGTCCTTC CCTGAGGGCTTCACATGGGAGAGGATCACCACATACGA AGACGGGGGCGTGCTGACCGCTACCCAGGACACCAGCCT CCAGAACGGCTGCCTCATCTACAACGTCAAGATCAACGG GGTGAACTTCCCATCCAACGGCCCTGTGATGCAGAAGAA AACACTCGGCTGGGAGGCCAACACCGAGATGCTGTACCC CGCTGACAGCGGTCTGAGAGGCCATAATCAGATGGCCCT GAAGCTCGTGGGCGGGGGCTACCTGCACTGCTCCCTCAA GACCACATACAGATCCAAGAAACCCGCTAAGAACCTCAA GATGCCCGGCTTCTACTTCGTGGACCGTAAACTGGAAAG AATCAAGGAGGCCGACAAAGAGACCTACGTCGAGCAGC ACGAGATGGCTGTGGCCAGGTACTGCGACCTGCCCTCGA GCGAGCTCCCGGGGGGGGTTCTCATCATCATCATCATCA TTAATAAAAGGGCGAATTCCAGCACACTGGCGGCCGTT ACTAGTGGATCCGGCTGCTAACAAAGCCCGAAAGGAAG CTGAGTTGGCTGCTGCCACCGCTGAGCAATAACTAGCAT AACCCCTTGGGGCCTCTAAACGGGTCTTGAGGGGTTTTT TGCTGAAAGGAGGAACTATATCCGGATATCC

1.2. Vector map and linker sequence of plasmid pIVEX 2.3d.

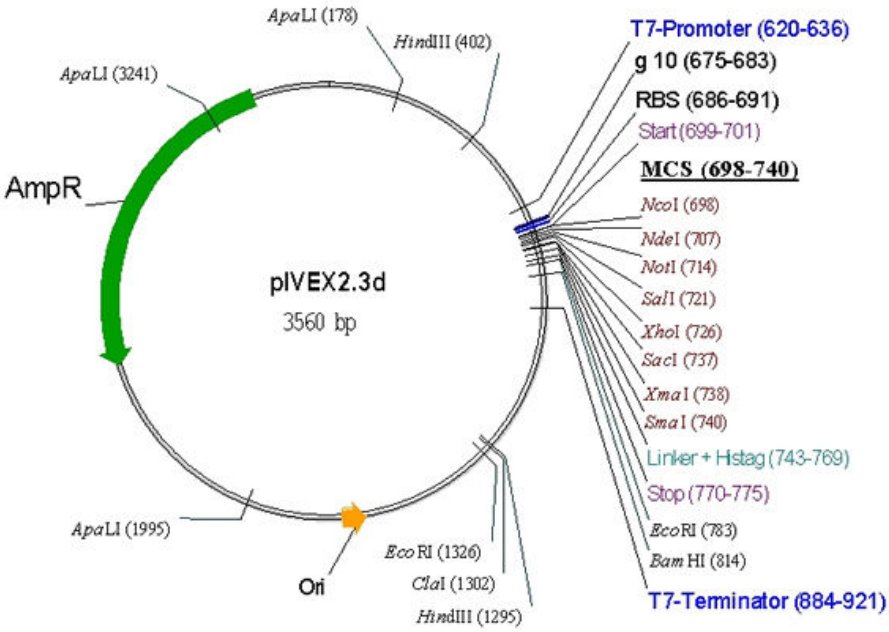


```
                                T7-Promoter
601    GATCTCGATC CCGCGAAATT AATACGACTC ACTATAGGGA GACCACAACG
       CTAGAGCTAG GGCGCTTTAA TTATGCTGAG TGATATCCCT CTGGTGTTGC

                                     g10 ε       RBS          NcoI
651    GTTTCCCTCT AGAAATAATT TTGTTTAACT TTAAGAAGGA GATATACCAT
       CAAAGGGAGA TCTTTATTAA AACAAATTGA AATTCTTCCT CTATATGGTA
                                                          Me

                                                  XmaI
           NdeI     NotI     SalI  XhoI     SacI SmaI    Linker
701    GGCACATATG AGCGGCCGCG TCGACTCGAG CGAGCTCCCG GGGGGGGTTC
       CCGTGTATAC TCGCCGGCGC AGCTGAGCTC GCTCGAGGGC CCCCCCCAAG
       tAlaHisMet SerGlyArgV alAspSerSe rGlu          GlyGlySe

        Histag                                      EcoRI
751    TCATCATCAT CATCATCATT AATAAAAGGG CGAATTCCAG CACACTGGCG
       AGTAGTAGTA GTAGTAGTAA TTATTTTCCC GCTTAAGGTC GTGTGACCGC
       rHisHisHis HisHisHis* *****
```

1.3. Sequences used to RNA transcription studies (Chapter IV). Parts of sequences labeled with colours stand respectively for: blue – forward primer, green – T7 promoter, grey – *lac*UV$_5$ promoter, light blue – NiR-FP gene, purple – RNAP terminator, yellow – reverse primer.

Name of oligomer	**Sequence (5' → 3')**
371 *(with T7 RNAP promoter)*	TCCGGCGTAGAGGATCGAGATCTCGATCCCGCGAAATTAATACGACTCACTATAGGGA GACCACAACGGTTTCCCTCTAGAAATAATTTTGTTTAACTTTAAGAAGGAGATATACC ATGGCACATATGAGCGGCCGCGTCGACTCGAGCGAGCTCCCGGGGGGGGTTCTCATCAT CATCATCATCATTAATAAAAGGGCGAATTCCAGCACACTGGCGGCCGTTACTAGTGGA TCCGGCTGCTAACAAAGCCCGAAAGGAAGCTGAGTTGGCTGCTGCCACCGCTGAGCAAT AACTAGCATAACCCCTTGGGGCCTCTAAACGGGTCTTGAGGGGTTTTTTGCTGAAAGG

	AGGAACTATATCCGGATATCC
1kb *(with T7 RNAP promoter)*	TCCGGCGTAGAGGATCGAGATCTCGATCCCGCGAAATTAATACGACTCACTATAGGGA GACCACAACGGTTTCCCTCTAGAAATAATTTTGTTTAACTTTAAGAAGGAGATATACC ATGGCACATATGGGAGAGGATAGCGAGCTGATCTCCGAGAACATGCACACGAAACTGT ACATGGAGGGCACCGTGAACGGCCACCACTTCAAGTGCACATCCGAGGGCGAAGGCAA GCCCTACGAGGGCACCCAGACCTGTAAGATCAAGGTGGTCGAGGGCGGCCCTCTCCCCT TCGCCTTCGACATCCTGGCTACCAGCTTCATGTACGGCAGCAAAACCTTTATCAACCAC ACCCAGGGCATCCCCGACTTCTTTAAGCAGTCCTTCCCTGAGGGCTTCACATGGGAGAG GATCACCACATACGAAGACGGGGGCGTGCTGACCGCTACCCAGGACACCAGCCTCCAGA ACGGCTGCCTCATCTACAACGTCAAGATCAACGGGGTGAACTTCCCATCCAACGGCCCT GTGATGCAGAAGAAAACACTCGGCTGGGAGGCCAACACCGAGATGCTGTACCCCGCTG ACAGCGGTCTGAGAGGCCATAATCAGATGGCCCTGAAGCTCGTGGGCGGGGGCTACCTG CACTGCTCCCTCAAGACCACATACAGATCCAAGAAACCCGCTAAGAACCTCAAGATGCC CGGCTTCTACTTCGTGGACCGTAAACTGGAAAGAATCAAGGAGGCCGACAAAGAGACC TACGTCGAGCAGCACGAGATGGCTGTGGCCAGGTACTGCGACCTGCCCTCGAGCGAGCT CCCGGGGGGGGTTCTCATCATCATCATCATCATTAATAAAAGGGCGAATTCCAGCACAC TGGCGGCCGTTACTAGTGGATCCGGCTGCTAACAAAGCCCGAAAGGAAGCTGAGTTGG CTGCTGCCACCGCTGAGCAATAACTAGCATAACCCCTTGGGGCCTCTAAACGGGTCTTG AGGGGTTTTTTGCTGAAAGGAGGAACTATATCCGGATATCC
0.5kb *(with E. coli RNAP promoter)*	TCCGGCGTAGAGGATCGAGATCTCGCGATTCATTAATGCAGCTGGCACGACAGGTTTCC CGACTGGAAAGCGGGCAGTGAGCGCAACGCAATTAATGTGAGTTAGCTCACTCATTAG GCACCCCAGGCTTTACACTTTATGCTTCCGGCTCGTATAATGTGTGGAATTGTGAGCGG ATAACAATTTCACACAGGAAACAGCTATGACCATGATTACGGATTCACTGGAAGGAGA TATACCATGGCACATATGAGCGGCCGCGTCGACTCGAGCGAGCTCCCGGGGGGGGTTCT CATCATCATCATCATCATTAATAAAAGGGCGAATTCCAGCACACTGGCGGCCGTTACTA GTGGATCCGGCTGCTAACAAAGCCCGAAAGGAAGCTGAGTTGGCTGCTGCCACCGCTGA GCAATAACTAGCATAACCCCTTGGGGCCTCTAAACGGGTCTTGAGGGGTTTTTTGCTGA AAGGAGGAACTATATCCGGATATCC
1kb *(with E. coli RNAP promoter)*	TCCGGCGTAGAGGATCGAGATCTCGCGATTCATTAATGCAGCTGGCACGACAGGTTTCC CGACTGGAAAGCGGGCAGTGAGCGCAACGCAATTAATGTGAGTTAGCTCACTCATTAG GCACCCCAGGCTTTACACTTTATGCTTCCGGCTCGTATAATGTGTGGAATTGTGAGCGG ATAACAATTTCACACAGGAAACAGCTATGACCATGATTACGGATTCACTGGAAGGAGA TATACCATGGCACATATGGGAGAGGATAGCGAGCTGATCTCCGAGAACATGCACACGA AACTGTACATGGAGGGCACCGTGAACGGCCACCACTTCAAGTGCACATCCGAGGGCGAA GGCAAGCCCTACGAGGGCACCCAGACCTGTAAGATCAAGGTGGTCGAGGGCGGCCCTCT CCCCTTCGCCTTCGACATCCTGGCTACCAGCTTCATGTACGGCAGCAAAACCTTTATCA ACCACACCCAGGGCATCCCCGACTTCTTTAAGCAGTCCTTCCCTGAGGGCTTCACATGG GAGAGGATCACCACATACGAAGACGGGGGCGTGCTGACCGCTACCCAGGACACCAGCCT CCAGAACGGCTGCCTCATCTACAACGTCAAGATCAACGGGGTGAACTTCCCATCCAACG GCCCTGTGATGCAGAAGAAAACACTCGGCTGGGAGGCCAACACCGAGATGCTGTACCCC GCTGACAGCGGTCTGAGAGGCCATAATCAGATGGCCCTGAAGCTCGTGGGCGGGGGCT ACCTGCACTGCTCCCTCAAGACCACATACAGATCCAAGAAACCCGCTAAGAACCTCAAG ATGCCCGGCTTCTACTTCGTGGACCGTAAACTGGAAAGAATCAAGGAGGCCGACAAAG AGACCTACGTCGAGCAGCACGAGATGGCTGTGGCCAGGTACTGCGACCTGCCCTCGAGC GAGCTCCCGGGGGGGGTTCTCATCATCATCATCATCATTAATAAAAGGGCGAATTCCA GCACACTGGCGGCCGTTACTAGTGGATCCGGCTGCTAACAAAGCCCGAAAGGAAGCTG AATTGGCTGCTGCCACCGCTGAACAATAACTAGCATAACCCCTTGGGGCCTCTAAACGG GTCTTGAGGGGTTTTTTGCTGAAAGGAGGAACTATATCCGGATATCC

2. Articles published in peer-review journals during realization of the PhD project

(1) *UV/Ozone Surface Treatment Increases Hydrophilicity and Enhances Functionality of SU-8 Photoresist Polymer*, A. Delplanque et al., Applied Surface Science, 314 (2014) 280-285

(2) DNA base pair resolution measurements using resonance energy transfer efficiency in lanthanide doped nanoparticles, A. Delplanque et al., PLoS ONE 10(3): e0117277.

Applied Surface Science 314 (2014) 280–285

Contents lists available at ScienceDirect

Applied Surface Science

journal homepage: www.elsevier.com/locate/apsusc

UV/ozone surface treatment increases hydrophilicity and enhances functionality of SU-8 photoresist polymer

Aleksandra Delplanque[a], Etienne Henry[a], Joseph Lautru[b], Hervé Leh[a], Malcolm Buckle[a], Claude Nogues[a,*]

[a] Laboratory of Applied Biology and Pharmacology, ENS de Cachan, CNRS; 61 Avenue du President Wilson, 94230 Cachan, France
[b] The Alembert Institute, ENS de Cachan; 61 Avenue du President Wilson, 94230 Cachan, France

ARTICLE INFO

Article history:
Received 21 January 2014
Received in revised form 8 May 2014
Accepted 9 June 2014
Available online 7 July 2014

Keywords:
SU-8 polymer
UV/ozone
Surface (bio) functionalization
Monolayer

ABSTRACT

SU-8 photoresist polymer is widely used in the fabrication of microdevices. However, for biological applications, the problem of efficiently modifying SU-8 surfaces without perturbing roughness has not been successfully resolved. We present UV/ozone (UVO) surface pre-treatment as an effective method to increase the hydrophilicity of SU-8 films without affecting surface roughness, thus improving specific covalent binding of bio-molecules. We demonstrate that 30 s UVO treatment suffices to create carboxyl groups at the surface that can then be used for high density binding of molecules via amide bond formation. We further demonstrate that a two-step surface modification where the surface is first protected with an ethylene glycol monolayer leads to an increase in binding specificity. Finally, to illustrate the controlled binding and accessibility of immobilized molecules, we show three cycles of reversible interactions between anti-tamra antibody and tamra-cadaverine immobilized on the surface of SU-8.

© 2014 Elsevier B.V. All rights reserved.

1. Introduction

SU-8 is a negative photosensitive polymer with a low Young's modulus and excellent chemical and thermal stability, widely used in the manufacture of extremely robust microstructures [1,2]. The optical properties of SU-8, including transparency above 360 nm, coupled with its relatively low refractive index, make it an ideal material for optical waveguides and the development of label-free biosensors [3,4].

However, the surface of SU-8 is highly hydrophobic, thus incompatible with many applications in biotechnology [5–7]. Surface modifications of SU-8 to enhance its wettability and to allow controlled immobilization of (bio)molecules of interest have been developed [8–11]. Modifications essentially addressed the means of activating SU-8 surfaces using wet or dry pre-treatment methods. Wet pre-treatment methods use a cross-linker that reacts with hydroxyl and/or carboxyl groups generated by acid and/or alkali treatment [7–9]. Dry pre-treatment methods use oxygen or ammonia plasma [12] or pyrolytic dissociation of ammonia [10]. In both cases surface roughness increases significantly; this is detrimental for liquid distribution in a static fluid microdevice and results in an unsteady secondary flow in a flowing microchannel [13,14]. In addition, surface roughness induces optical loss in waveguides due to scattering on sidewalls [15] and promotes non-specific adsorption of (bio)molecules to the surface [16].

In this paper we present UV/ozone (UVO) pre-treatment as a straightforward method to activate SU-8 surfaces [17–19] and control chemisorption of molecules [3,4]. Because UVO leads to a milder surface oxidation than argon or oxygen plasma treatment, the SU-8 surface roughness is not affected by UVO exposition. Using water contact angle measurements (wCA), FT-IR spectroscopy and AFM, we characterized treated SU-8 films and, taking advantage of the fluorescence properties of tamra-cadaverine, we optimized experimental conditions to favor specific chemisorption of biomolecules on the UVO activated SU-8 surface.

To reinforce the specificity of biomolecule adsorption on the UVO activated SU-8 surface we compared one-step direct adsorption of biomolecules with a two-step adsorption process in which biomolecules were immobilized following the deposition of an anti-fouling layer composed of oligomers of ethylene glycol [20–22].

Finally, to illustrate biosensing applications, we followed the decrease of the fluorescence intensity upon association of anti-tamra with immobilized tamra-cadaverine. We demonstrate not only that the surface modification allows controlled immobilization of biomolecules but also does not impact on their functional integrity.

* Corresponding author. Tel.: +33 01 47 40 76 87.
E-mail address: claude.nogues@lbpa.ens-cachan.fr (C. Nogues).

http://dx.doi.org/10.1016/j.apsusc.2014.06.053
0169-4332/© 2014 Elsevier B.V. All rights reserved.

2. Materials and methods

2.1. Substrates and chemical reagents

Experiments were performed with double distilled water; all buffers were filtered before use with a low protein binding non-pyrogenic 0.8/0.2 μm filter. Silicon wafers used as a substrate were purchased from ACM-PVD (France). SU-8 2002 was purchased from Micro-Chem (USA). N-[3-Dimethylaminopropyl]-N′-ethylcarbodiimide hydrochloride (EDC) and N-Hydroxysuccinimide (NHS) were purchased from Sigma–Aldrich. Carboxy-amine *n*-ethylene glycol reagents ($CA(EG)_8$ and $CA(EG)_{24}$) were purchased from Thermo Scientific. Tetramethylrhodamine (tamra) cadaverine and anti-tetramethylrhodamine rabbit IgG fraction (anti-tamra) were purchased from Invitrogen – Molecular Probes.

2.2. Fabrication of the SU-8 photoresist film

2-inch silicon wafers were cleaned for 10 min in the UVO-Cleaner (model 42-220, Jelight, USA). Microscope glass slides were cleaned with ethanol and acetone followed by cleaning in the UVO-Cleaner for 10 min. 2–3 μm thick SU-8 films were obtained, following the method developed by Camille Delezoïde [3,4,23]. It consists in spin coating of SU-8 2002 at 500 rpm for 7 s with an acceleration of 100 rpm/s; followed by 3000 rpm for 30 s with an acceleration of 300 rpm/s using Spin-Coater RC8, Suss MicroTec. The films were softbaked on a hotplate for 1 min at 65 °C, followed by 2 min at 95 °C for a silicon wafer and at 65 °C for 6 min for a glass slide. Samples were flood-exposed in UV light for 15 s, using the UV-Aligner MJB4, Suss MicroTec. Post-exposure baking was performed on a hotplate for 1 min at 65 °C, followed by 3 min at 95 °C for a silicon wafer and 6 min at 95 °C for a glass slide. Samples were then hardbaked under three different conditions: at 90 °C for 5 h, at 120 °C for 3 h or at 180 °C for 2 h. The thickness of the films was controlled using Dektak 150 Surface Profiler, Veeco. Prepared surfaces were stored under nitrogen or used directly in the following experiments.

2.3. UV/ozone (UVO) treatment

Prepared surfaces were exposed to the UVO using the UVO-Cleaner (low pressure mercury vapor grid lamp: 28,000 μW/cm^2 at 254 nm; model 42-220, Jelight, USA). Exposure of the samples to UVO lasted from 15 s till 20 min.

2.4. Fourier transform infrared spectroscopy (FTIR)

The surfaces before and after 30 s and 5 min of UVO treatment were analyzed in FT-IR spectrometer with resolution of 8.00 cm^{-1}, 1000 scans (apparatus Nexus – Thermo Electron Corporation, USA). A silicon wafer was used as a background. All measurements were carried out in adsorption mode.

2.5. Atomic force microscopy (AFM)

Surface topography and roughness before and after 5 min of UVO treatment were measured using microcantilever tips OMCL-AC240TS-R3 (Olympus, Japan) in Veeco nanoscope V. Measurements were performed in tapping mode with a scan rate of 1 Hz and scan sizes of 1 and 5 μm. Images were taken at minimum three randomly selected areas. The software option 'Section' was used to calculate a root mean surface roughness (spectral RMS amplitude).

2.6. Water contact angle measurements (wCA)

wCA were measured on SU-8 films before and after UVO treatment. Measurements were carried out with Digidrop MCAT Analyzer (GBX, France). All measurements were taken at room temperature. 0.5 μl water droplets were dispensed from a needle and the wCA was calculated on captured images, 500 ms after placing a drop on the surface. Each given wCA was the average value of five consecutive contact angle measurements.

2.7. Binding of tamra-cadaverine

The surfaces before and after 15 and 30 s, 1, 2, 5 and 15 min of UVO treatment were immersed in a diluted solution of EDC/NHS (ratio 1:1, EDC: 0.4 M N-[3-Dimethylaminopropyl]-N′-ethylcarbodiimide hydrochloride; NHS: 0.1 M N-Hydroxysuccinimide) [24] for 30–60 min. After rinsing with double distilled water, samples were incubated 1 h either directly with 10 μM tamra-cadaverine in 10 mM NaOAc buffer pH 5.2 or with 0.1 mM $CA(EG)_8$ or $CA(EG)_{24}$ diluted in water. For pegylated SU-8 surfaces, samples were again immersed in EDC/NHS for 1 h and then rinsed with a buffer or sonicated twice for 2 min. Dried surfaces were analyzed in Typhoon scanner with an emission filter of 580 nm. The density of tamra-cadaverine on the SU-8 surface was deduced from a calibration curve: using a Typhoon imager, the fluorescence intensity of 1 μl of an increasing concentration of tamra-cadaverine solution was measured to obtain a linear calibration curve. The concentration range used for the calibration curve was chosen according to the contrast obtained after scanning all samples with a Typhoon scanner so the calibration curves and the number of moles per unit area for each sample was within the same intensity range.

2.8. Tamra-cadaverine/anti-tamra interactions

Pretreated SU-8 thin films were used to spot 10 μM tamra-cadaverine in 10 mM NaOAc buffer pH 5.2 with 1% v/v glycerol. Spots with the dimension of around 300 μm were deposited using a Vikalex Spotter (Vikalex Technologies, France). 10 μg/ml of anti-tamra diluted in PBS buffer was incubated on the tamra-cadaverine functionalized surface for 1 h after which the surface was rinsed with 10 mM glycine–HCl pH 2.0 to remove antibodies retained on the surface. All reactions were performed under liquid on the protected SU-8 surface; microfluidic flowcells were prepared on the glass slides using Sticky Slides VI$^{0.4}$ (ibidi, Germany). Three cycles were carried out for the reaction between immobilized tamra-cadaverine molecules and anti-tamra immobilized on the surface in a microfluidic flowcell, followed by surface regeneration with a glycine solution. Fluorescence images were recorded using an inverted epifluorescence microscope (Leica MicroSystems) equipped with a 4× objective and fluorescence filters suitable for tamra (excitation bandpass 510–560 nm, emission bandpass 590–680 nm). Average fluorescence intensity was calculated using ImageJ Software (NIH) after subtracting a background for each spot.

3. Results and discussion

3.1. Characterization of SU-8 surface after UV/ozone (UVO) treatment

In order to access a range of cross-linking densities on the SU-8 surface [25–27], we studied three hardbaking conditions following UVO exposure: 90 °C for 5 h, 120 °C for 3 h and 180 °C for 2 h. The degree of SU-8 reticulation, and thus the amount of reactive epoxy groups present on the surface, is largely conditioned by the hardbaking step [25,26,28]. The impact of UVO exposure time on

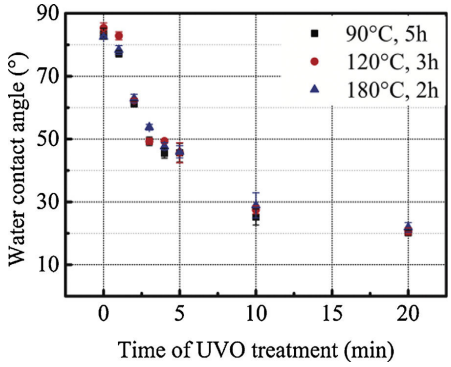

Fig. 1. Variation of the wCA with increasing UVO exposure time of SU-8 thin film prepared with three different hardbaking conditions. Each data point corresponds to the average of five wCA measurements.

SU-8 surfaces prepared under these three different conditions was followed using wCA, AFM and FT-IR spectroscopy.

wCA allowed characterization of the evolution of the SU-8 surface energy for each UVO exposure time. As shown in Fig. 1, starting from a wCA of 83.5 ± 1.5, independently of the hardbaking conditions and in agreement with published data [7,9,28], the wCA decreased below 30° after 10 min of UVO exposure and reached a plateau around 22° after 20 min of UVO treatment.

The increase of surface energy of the SU-8 surface after UVO treatment might be explained by the creation of polar groups at the SU-8 surface upon oxidation [28]. Using a surface profiler we demonstrated that the thickness of the SU-8 layer was not affected after 20 min of UVO exposure (data not shown). In addition, it has been demonstrated that the optical properties of an SU-8 waveguide were not altered by such UVO treatment [3,4].

wCA measurements were extremely reproducible and no significant difference between the left and the right wCA (±0.3°) could be measured, indicating that the UVO treatment did not affect the SU-8 surface roughness.

To confirm this last point, both peak-to-valley and root-mean-square (RMS) roughness were measured by AFM on the three SU-8 samples before and after UVO treatment. Fig. 2 shows AFM images and the corresponding height profiles with the RMS roughness analysis of SU-8 thin film hardbaked at 120 °C for 3 h before and after 5 min of UVO treatment. The SU-8 surface before UVO is homogenous, with a peak-to-valley roughness of 1.7 nm and a RMS roughness of 0.121 nm. After 5 min under UVO, the surface remains homogenous with a peak-to-valley roughness of 1.9 nm and a RMS roughness of 0.144 nm. In addition, post-exposure hardbaking conditions had no significant influence on the SU-8 surface roughness before and after UVO treatment time (Fig. 2c).

We analyzed SU-8 thin layers prepared using FT-IR spectroscopy (Fig. 3). The most relevant signals for the SU-8 photoresist are: 862 and 913 cm^{-1} corresponding to the epoxy ring [29]; between 1030 and 1295 cm^{-1} for C–O and C–O–C vibrations; between 1502 and 1604 cm^{-1} corresponding to phenyl groups and at around 1700 cm^{-1} a wide peak corresponding to the C=O of a carbonyl group [10,33–34].

While the intensity of peaks corresponding to the long molecular chains of SU-8 polymer was not affected by UVO treatment, significant variations were observed for peaks corresponding to epoxy groups and to carboxyl groups [28]. As the UVO treatment time increased, the intensity of the signal from the epoxy groups decreased concomitantly with an increase in peak intensity corresponding to carboxyl groups.

Most of the epoxy groups within the thin SU-8 layer cross-linked during the post-exposure baking step [27,28], we thus deduced that the small peak intensities of the epoxy groups corresponded to epoxy groups present on the surface of the SU-8 film. In addition, the increase in carboxyl group peak intensity after 5 min of UVO treatment was larger than the decrease in the intensity of the epoxy groups peaks, indicating that oxidation of SU-8 was reaching the bulk of the SU-8 layer after relatively long UVO exposure time (5 min). Therefore, activation of the SU-8 surface with 30 s UVO exposure time should allow efficient (bio)molecule immobilization.

Of particular interest was that, although there was the presence of carboxyl groups and lower peak intensities corresponding

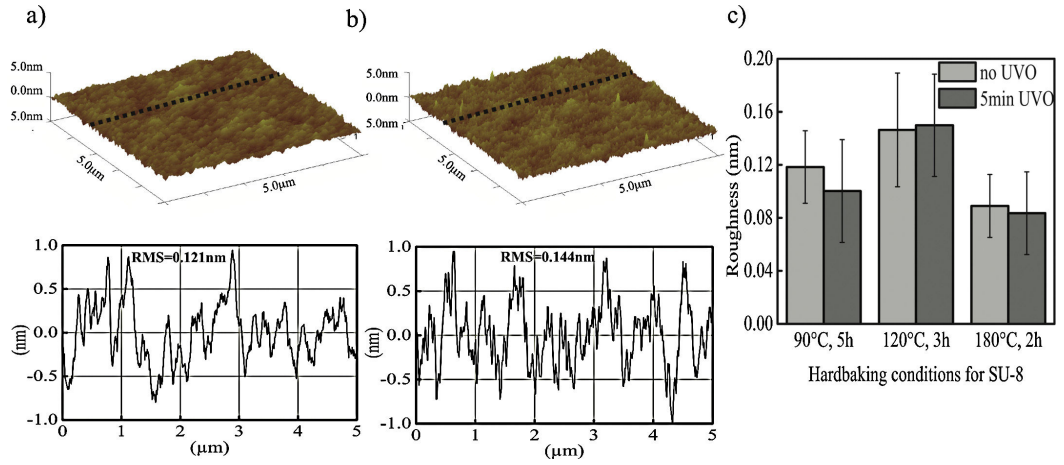

Fig. 2. AFM topography images and height profiles of SU-8 surfaces hardbaked at 120 °C for 3 h: a) before UVO treatment and b) after 5 min of UVO treatment. Dotted lines indicate where the height profiles were taken. c) Comparison of the root-mean-square (RMS) roughness for SU-8 films hardbaked with different conditions. Standard deviations were calculated based on three randomly selected areas; four height profiles per area were taken.

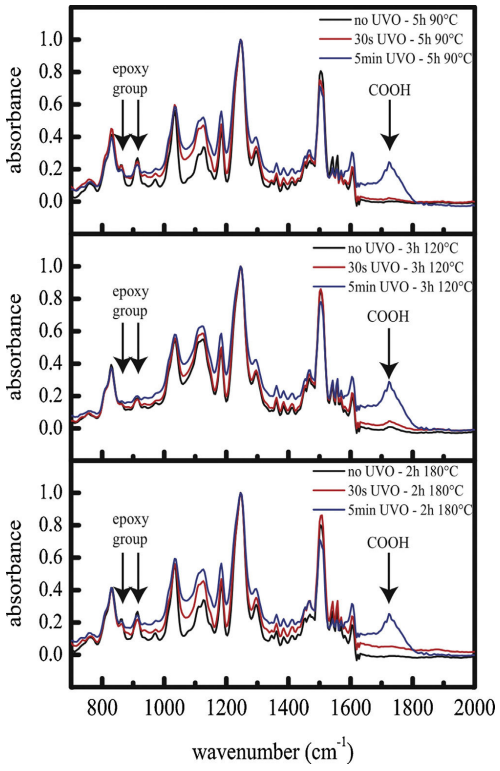

Fig. 3. FT-IR spectra of SU-8 film prepared with three hardbaking conditions indicated in the legend before and after 30 s and 5 min of UVO treatment. Peaks of epoxy (862 and 913 cm^{-1}) and carboxyl groups (wide peak around 1700 cm^{-1}) are indicated with arrows. All spectra were normalized to the peak at 1246 cm^{-1}.

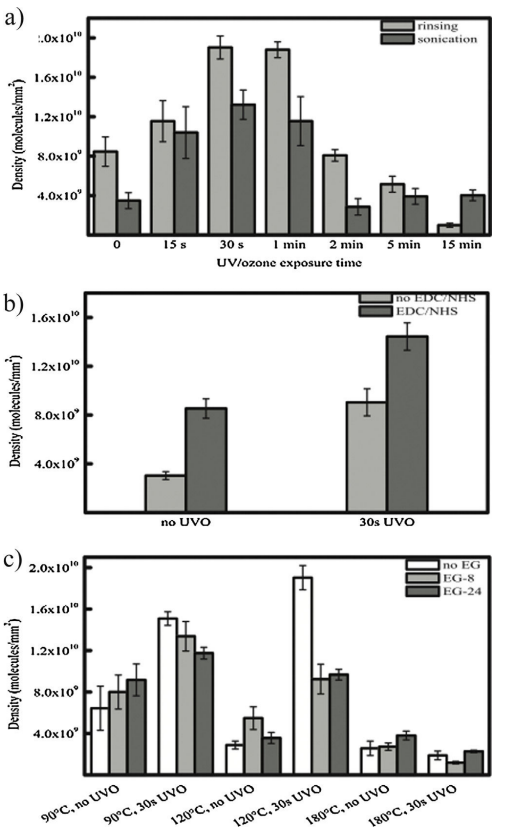

Fig. 4. Density of tamra-cadaverine molecules per mm^2 immobilized on the SU-8 surfaces, a) depending on UVO exposure time and rinsing method; SU-8 thin film hardbaked at 120 °C for 3 h, rinsed twice with 10 mM NaOAc buffer pH 5.2 or sonicated twice for 2 min; b) dependance on the EDC/NHS pre-incubation step c) depending on the surface pegylation method; SU-8 hardbaked in three different conditions and with or without activation by 30-s UVO treatment. Standard deviations were calculated based on six independent measurements.

to epoxy groups on the SU-8 film hardbaked at 120 °C for 3 h before UVO treatment, yet no carboxyl groups were detected on the SU-8 film prepared under the other two hardbaking conditions. The presence of carboxylic groups on the SU-8 surface could be due to oxidation of epoxy groups at the surface and/or to the presence of some residual solvent from the thin SU-8 film [25]. This observation is, in both hypotheses, coupled with a lower peak intensity of the epoxy group on the surface of SU-8 hardbaked at 120 °C for 3 h than with the other hard baking conditions.

FT-IR revealed that changes in the oxidation state of the SU-8 layer occurred both at the surface and in the bulk of the SU-8 film for long UVO exposure time (up to 5 min). While the amount of reactive epoxy groups on the SU-8 surface is defined by the degree of reticulation of the polymer upon the post exposure hardbaking, the surface density of carboxyl groups can be potentially controlled by short UVO exposure time (30 s). Consequently, the exposure time of SU-8 microstructure to UVO should allow modulation of the surface density of subsequent (bio)molecules following chemisorption.

3.2. Covalent binding of tamra-cadaverine to the surface

We used chemisorption of tamra-cadaverine to activated SU-8 surfaces through specific reactions with carboxyl groups via an EDC/NHS-mediated reaction to form amide bonds at the interface and provide a useful model to quantify the amount of material retained on the surface by measuring the intensity of tamra fluorescence when excited at 580 nm.

Following SU-8 substrate preparation [3,4], surfaces were exposed to UVO for times ranging from 0 to 15 min and sequentially incubated with a solution of EDC/NHS for 60 min, thoroughly rinsed with distilled water and incubated with 10 μM solution of tamra-cadaverine for 60 min (see Section 2.7). Samples were then dipped in 10 ml of buffer (10 mM NaOAc, pH 5.2) and either agitated for 2 × 20 min or sonicated twice for 2 min in the same buffer. The influence of UVO treatment time on the density of immobilized tamra-cadaverine molecules on the SU-8 sample hardbaked at 120 °C for 3 h is shown in Fig. 4a. For the SU-8 not exposed to UVO treatment, the density of surface retained tamra-cadaverine was not negligible. In addition, the surface molecular density after sonication was significantly lower than for samples rinsed thoroughly and agitated in a large volume of buffer, indicating that remaining molecules were covalently attached to the SU-8 surface. It follows that the presence of residual reactive epoxy and

carboxyl groups at the interface, highlighted by FT-IR (Fig. 3), was in itself sufficient to allow some specific binding. Second, the molecular density on the surface increased for UVO treatment lasting less than 1 min and decreased significantly with longer exposure. In all cases, sonication of samples, removing most non-covalently bound molecules strengthens the observation that the exposure of SU-8 surfaces between 30 s and 1 min of UVO treatment created the highest density of reactive carboxyl groups at the interface. Longer UVO exposure time most likely oxidizes SU-8 surfaces forming unreactive chemical groups, leading to lower densities of bound molecules. To conclude, the highest density of immobilized molecules (1.9×10^{10} molecules/mm^2) was obtained after 30 s or 1 min of UVO exposure.

To demonstrate the specific adsorption of tamra-cadaverine on the UVO activated surface, we characterized the molecular density on the SU-8 surface avoiding the EDC/NHS pre-incubation step (Fig. 4b). The density of tamra-cadaverine increased significantly when EDC/NHS was applied on SU-8 thin layer both with and without UVO surface treatment, confirming the specific adsorption of tamra-cadaverine on the SU-8 surface. The tamra-cadaverine density on the surface without UVO was three times higher after pre-incubation with EDC/NHS than without EDC/NHS pre-treatment, confirming the presence of COOH groups on the surface hardbaked at 120 °C for 3 h and the low level of non-specific interactions (corresponding to 1/3 of the specifically bound tamra-cadaverine). After 30 s UVO treatment the level of non-specific binding of tamra-cadaverine increased three fold (when no EDC/NHS was applied to the surface) relative to the SU-8 surface without UVO treatment. Finally the surface density was 1.4×10^{10} molecules/mm^2 while the non-specific interaction was 9.0×10^9 molecules/mm^2 when both UVO and EDC/NHS were applied to the SU-8 surface prior to the tamra-cadaverine deposition. It is important to note that the amount of non-specific interactions of tamra-cadaverine with the SU-8 surface after UVO treatment and with EDC/NHS pretreatment is expected to be significantly lower than the non-specific interactions when no EDC/NHS is employed. Indeed EDC/NHS pretreatment activates the COOH groups so the specific interaction (formation of an amide bond) is largely favored over the non-specific interactions, as demonstrated on the sample with no UVO treatment.

Although rinsing by sonication was shown to efficiently remove non-covalently bound molecules, it may pose a problem for biological applications through denaturation of bio molecules. Thus, to decrease non specific interactions of tamra-cadaverine and subsequent anti-tamra adsorption with the SU-8 surface, we studied the effect of pre-functionalization with carboxyl-amine *n*-ethylene glycol ($CA(EG)_8$ and $CA(EG)_{24}$) [20–22].

The influence of the EG chain-length and short UVO treatment on the density of tamra-cadaverine for each SU-8 hardbaking condition is presented in Fig. 4c. We confirmed that short UVO treatment significantly increased tamra-cadaverine density on the bare surface for the three-hardbaking conditions (Fig. 4c, no EG). Furthermore, we clearly observed that hardbaking conditions influenced molecular density. Thus, in agreement with data presented above and for samples with no UVO treatment and no EG, the tamra-cadaverine surface density was the highest after hardbaking at 120 °C for 3 h. Although pre-immobilization of $CA(EG)_8$ or $CA(EG)_{24}$ did not significantly influence tamra-cadaverine surface density for SU-8 film hardbaked at 90 °C for 5 h and 180 °C for 2 h, we observed a lower tamra-cadaverine surface density for samples pre-functionalized with $CA(EG)_8$ or $CA(EG)_{24}$ and hardbaked at 120 °C for 3 h. When compared to the tamra-cadaverine surface density after sonication (Fig. 4a), we noticed that the amplitude of the drop in molecular density was similar, indicating that pre-treatment of the surface with $CA(EG)_8$ or $CA(EG)_{24}$ produced an efficient anti-fouling layer. Tamra-cadaverine surface density was lower following immobilization on pre-functionalized SU-8 surfaces than on a bare SU-8 film treated with sonication (9.5×10^9 compared to 1.3×10^{10} molecules/mm^2 respectively) indicating that the final amount of reactive carboxyl groups was lower. The EG chain-length had no influence on the tamra-cadaverine surface density.

The SU-8 surface hardbaked at 120 °C for 3 h then activated by 30 s UVO treatment was adopted as a standard protocol for preparing SU-8 surfaces because it resulted in homogeneous samples with fewer disparities in the density of immobilized molecules (Fig. 4c).

To demonstrate the relevance of the surface modification method for bio-sensing applications, we analyzed fluorescence quenching following the interaction of anti-tamra with immobilized tamra-cadaverine.

Fluorescent microscope images at different times following injection of anti-tamra across the pre-treated SU-8 surface containing spots of immobilized tamra-cadaverine are shown in Fig. 5a. The relatively small variations in fluorescence intensity observed during the three cycles of interaction/regeneration may

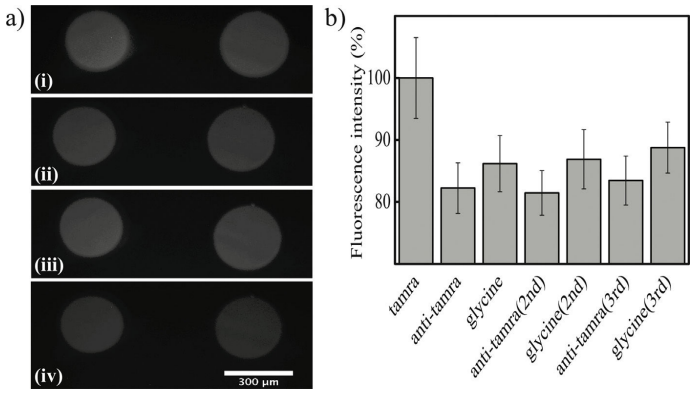

Fig. 5. a) Fluorescent microscope images of tamra-cadaverine and anti-tamra interaction cycle. (i) Image of spots of immobilized 10 µM tamra-cadaverine, (ii) image taken after injection of 10 µg/ml anti-tamra and rinsing with PBS buffer, (iii) image taken after regeneration of the surface with a solution of 10 mM glycine–HCl pH 2.0 [31] and (iv) image taken after an additional injection of anti-tamra and rinsing with PBS buffer. b) Changes in fluorescence intensity during three reaction cycles.

be explained by the low quenching efficiency after complex formation. Indeed, as characterized in the literature, quenching efficiency is not expected to exceed ~57% of the initial intensity of the free tamra fluorophore diluted in a buffer solution [30]. In addition, since the average distance between tamra-cadaverine immobilized on the SU-8 surface was approximately 7 nm (deduced from Fig. 4c), not all immobilized tamra-cadaverine molecules can be involved in a complex with anti-tamra because of possible steric hindrance. Therefore, we quantified the intensity of fluorescence on each tamra-cadaverine spot and in each step of the association/regeneration cycle described in Fig. 5a. Fig. 5b summarizes the variation of fluorescence intensity (after correction for the background intensity signal) during three cycles of injection and regeneration. Considering the initial fluorescence intensity of the immobilized tamra-cadaverine spots to be 100%, we observed a drop in the intensity of fluorescence to approximately 82% after anti-tamra/tamra-cadaverine complex formation on the SU-8 surface. The fluorescence signal was recovered up to 86% after regeneration with 10 mM glycine–HCl, pH 2.0 solution. The loss of the signal from the immobilized tamra-cadaverine after regeneration might be due to desorption of tamra-cadaverine non-covalently bound to the surface but initially involved in complex formation and from undissociated complex that remains irreversibly on the surface. A second injection of anti-tamra again decreased the detected fluorescent signal to 81% and a second regeneration of the surface allowed total recovery of the signal intensity. A third cycle of association/regeneration showed similar variation of the fluorescence intensity demonstrating the specificity of the interaction on the pre-treated SU-8 surface.

4. Conclusions

We showed that UVO surface treatment is very promising compared to conventional wet or dry surface activation techniques known to significantly increase roughness [10]. We demonstrated that short exposure to UVO selectively oxidized SU-8 surfaces and increased hydrophilicity without damaging either thickness or surface roughness. Optimal conditions of hardbaking were established as being 120 °C for 3 h. Such UVO activated SU-8 surfaces were then used to covalent immobilization of tamra-cadaverine with high density. The binding process was specific and bound molecules were accessible for further antigen–antibody reactions. This specific and reversible reaction between molecules interacting with immobilized tamra-cadaverine molecules confirms that the SU-8 UVO activation method can be directly applied to the controlled immobilization of a range of (bio)molecules on SU-8 surfaces.

Acknowledgment

We would like to thank Camille Delezoide for insightful discussions which led to the development of the SU-8 UVO activation method described in the present paper; the characterization of Materials Platform of The Institute d'Alembert for the use of the FT-IR instrument. This work has been supported by the DIM Nano'K Région Ile de France, the MIRODE project (ANR-11-BSV5-0017), the Laboratoire d'Excellence Nanosaclay and Palm for the project BOAB.

References

[1] A. del Campo, C. Greiner, SU-8: a photoresist for high-aspect-ratio and 3D submicron lithography, J. Micromech. Microeng. 17 (2007) R81–R95.
[2] P. Abgrall, V. Conedera, H. Camon, A.M. Gue, N.T. Nguyen, SU-8 as a structural material for labs-on-chips and microelectromechanical systems, Electrophoresis 28 (2007) 4539–4551.
[3] C. Delezoide, J. Lautru, J. Zyss, I. Ledoux-Rak, C.T. Nguyen, Vertically coupled polymer microresonators for optofluidic label-free biosensors, in: J.E. Broquin, G.N. Conti (Eds.), Integrated Optics: Devices, Materials, and Technologies, Xvi, 2012.
[4] C. Delezoide, M. Salsac, J. Lautru, H. Leh, C. Nogues, J. Zyss, M. Buckle, I. Ledoux-Rak, C.T. Nguyen, Vertically coupled polymer microracetrack resonators for label-free biochemical sensors, IEEE Photon. Technol. Lett. 24 (2012) 270–272.
[5] M. Nordstrom, R. Marie, M. Calleja, A. Boisen, Rendering SU-8 hydrophilic to facilitate use in micro channel fabrication, J. Micromech. Microeng. 14 (2004) 1614–1617.
[6] T. Sikanen, L. Heikkila, S. Tuornikoski, R.A. Ketola, R. Kostiainen, S. Franssila, T. Kotiaho, Performance of SU-8 microchips as separation devices and comparison with glass microchips, Anal. Chem. 79 (2007) 6255–6263.
[7] S.L. Tao, K.C. Popat, J.J. Norman, T.A. Desai, Surface modification of SU-8 for enhanced biofunctionality and nonfouling properties, Langmuir 24 (2008) 2631–2636.
[8] G. Blagoi, S. Keller, A. Johansson, A. Boisen, M. Dufva, Functionalization of SU-8 photoresist surfaces with IgG proteins, Appl. Surf. Sci. 255 (2008) 2896–2902.
[9] A. Deepu, V.V.R. Sai, S. Mukherji, Simple surface modification techniques for immobilization of biomolecules on SU-8, J. Mater. Sci. Mater. Med. 20 (2009) 25–28.
[10] M. Joshi, N. Kale, R. Lal, V.R. Rao, S. Mukherji, A novel dry method for surface modification of SU-8 for immobilization of biomolecules in Bio-MEMS, Biosens. Bioelectron. 22 (2007) 2429–2435.
[11] R. Marie, S. Schmid, A. Johansson, L.E. Ejsing, M. Nordstrom, D. Hafliger, C.B.V. Christensen, A. Boisen, M. Dufva, Immobilisation of DNA to polymerised SU-8 photoresist, Biosens. Bioelectron. 21 (2006) 1327–1332.
[12] V. Jokinen, P. Suvanto, S. Franssila, Oxygen and nitrogen plasma hydrophilization and hydrophobic recovery of polymers, Biomicrofluidics 6 (2012) 16501–16510.
[13] Y. Ji, K. Yuan, J.N. Chung, Numerical simulation of wall roughness on gaseous flow and heat transfer in a microchannel, Int. J. Heat Mass Transf. 49 (2006) 1329–1339.
[14] H.B. Winzeler, G. Belfort, Enhanced performance for pressure-driven membrane processes – the argument for fluid instabilites, J. Membr. Sci. 80 (1993) 35–47.
[15] J.S. Chang, S.C. Eom, G.Y. Sung, J.H. Shin, On-chip, planar integration of Er doped silicon-rich silicon nitride microdisk with SU-8 waveguide with sub-micron gap control, Opt. Express 17 (2009) 22918–22924.
[16] C. Cao, S.W. Birtwell, J. Hogberg, A. Wolff, H. Morgan, D.D. Bang, Surface modification of photoresist SU-8 for low autofluorescence and bioanalytical applications, in: 15th International Conference on Miniaturized Systems for Chemistry and Life Science, Seattle, Washington, USA, 2011.
[17] L.P. Haack, A.M. Straccia, J.W. Holubka, A. Bhurke, M. Xie, L.T. Drzal, Chemistry of surface modification with UV/ozone for improved intercoat adhesion in multilayered coating systems, Surf. Interface Anal. 29 (2000) 829–836.
[18] H.Y. Nie, M.J. Walzak, B. Berno, N.S. Mclntyre, Atomic force microscopy study of polypropylene surfaces treated by UV and ozone exposure: modification of morphology and adhesion force, Appl. Surf. Sci. 144–145 (1999) 627–632.
[19] M.L. Sham, J. Li, P.C. Ma, J.K. Kim, Cleaning and functionalization of polymer surfaces and nanoscale carbon fillers by UV/Ozone treatment: a review (vol 43, pg 1537, 2009), J. Compos. Mater. 43 (2009) 3328.
[20] M. Mrksich, G.M. Whitesides, Using self-assembled monolayers that present oligo(ethylene glycol) groups to control the interactions of proteins with surfaces, in: J.M. Harris, S. Zalipsky (Eds.), Poly(Ethylene Glycol): Chemistry and Biological Applications, 1997, pp. 361–373.
[21] C. Nogues, H. Leh, C.G. Langendorf, R.H.P. Law, A.M. Buckle, M. Buckle, Characterisation of peptide microarrays for studying antibody-antigen binding using surface plasmon resonance imagery, Plos One 5 (2010) e12152–e12158.
[22] C. Nogues, H. Leh, J. Lautru, O. Delelis, M. Buckle, Efficient antifouling surface for quantitative surface plasmon resonance based biosensor analysis, Plos One 7 (2012) e44287–e44297.
[23] Y. Sanogo, A.F. Obaton, C. Delezoide, J. Lautru, M. Lievre, J. Dubard, I. Ledoux-Rak, C.T. Nguyen, Phase sensitive-optical low coherence interferometer: a new protocol to evaluate the performance of optical micro-resonators, J. Lightwave Technol. 31 (2013) 111–117.
[24] M.E. Fischer, Amine coupling through EDC/NHS: a practical approach, in: N.J. Mol, M.J.E. Fischer (Eds.), Surface Plasmon Resonance, Humana Press, 2010, pp. 55–73.
[25] S. Keller, G. Blagoi, M. Lillemose, D. Haefliger, A. Boisen, Processing of thin SU-8 films, J. Micromech. Microeng. 18 (2008) 125020–125030.
[26] Z.Y. Zhang, P. Zhao, G.Z. Xiao, B.R. Watts, C.Q. Xu, Sealing SU-8 microfluidic channels using PDMS, Biomicrofluidics 5 (2011) 046503–046508.
[27] C http://www.microchem.com
[28] C.J. Chang, C.S. Yang, L.H. Lan, P.C. Wang, F.G. Tseng, Fabrication of a SU-8-based polymer-enclosed channel with a penetrating UV/ozone-modified interior surface for electrokinetic separation of proteins, J. Micromech. Microeng. 20 (2010) 115031–115042.
[29] Y.L. Wang, J.H. Pai, H.H. Lai, C.E. Sims, M. Bachman, G.P. Li, N.L. Allbritton, Surface graft polymerization of SU-8 for bio-MEMS applications, J. Micromech. Microeng. 17 (2007) 1371–1380.
[30] A.K. Chen, Z.L. Cheng, M.A. Behlke, A. Tsourkas, Assessing the sensitivity of commercially available fluorophores to the intracellular environment, Anal. Chem. 80 (2008) 7437–7444.
[31] N. Backmann, C. Zahnd, F. Huber, A. Bietsch, A. Pluckthun, H.P. Lang, H.J. Guntherodt, M. Hegner, C. Gerber, A label-free immunosensor array using single-chain antibody fragments, Proc. Natl. Acad. Sci. U.S.A. 102 (2005) 14587–14592.

université PARIS-SACLAY | ÉCOLE DOCTORALE Structure et dynamique des systèmes vivants (SDSV)

Titre: Systemes artificiales pour l'expression des genes *in vitro*

Mots clés: *biocapteur, fonctionnalisation de surfaces, puce ADN, expression des genes, ARN polymerase, ARN*

Résumé: La transcription par l'ARN polymérase ADN dépendante (ARNP) est un processus biochimique central de l'expression des gènes dont les mécanismes ne sont pas entièrement caractérisés. Notamment la dynamique de la reconnaissance du promoteur puis l'évasion et l'élongation dans le contexte cellulaire où la densité et les concentrations moléculaires ainsi que l'influence de la proximité des molécules voisines sont des facteurs importants. L'objectif de cette thèse est de développer une méthode robuste qui permette de suivre *in vitro* et en temps réel les différentes étapes de la transcription dans des conditions rigoureusement contrôlées.

Une étape majeure de ce travail à consister à optimiser une chimie de surface permettant l'immobilisation d'ADN de différentes tailles et de contrôler leur densité et orientation sur la surface du capteur (couche mince de polymère et d'or). La dynamique des interactions entre les molécules d'ADN ainsi immobilisés et les ARNP en solution (T7 bacteriophages et holoenzyme d'*E. coli*) ont été suivi par imagerie de la résonance des plasmons de surface (SPRi). Les ARN transcrits sur la biopuce ont été recueillies et semi-quantifiés. Les développements futurs seraient de profiter des données fournies ici sur la synthèse d'ARN et concevoir biocapteurs permettant de suivre en temps réel la production de protéines *in vitro*.

Title: Artificial systems for *in vitro* gene expression

Keywords : *surface based biosensor, surface functionalization, DNA microarray, gene expression, RNA polymerase, RNA*

Abstract : Transcription with DNA-dependent RNA polymerase (RNAP) is a central biochemical process in gene expression and is still not fully characterized, especially with respect to the dynamics of promoter recognition, escape and elongation in a cell like context where molecular density, concentrations and nearest neighbour effects are prevalent.

The goal of this thesis was to develop a robust method that would allow real time monitoring of RNAP reaction *in vitro* under rigorously controlled conditions. A major axis was to develop a surface-based biosensor that would allow the characterization of the main steps of the transcription reaction.

Sensor surfaces (polymer coated glass and 50-nm thin layer gold) were biofunctionalized and characterized in order to immobilize DNA in a controlled manner. Interactions between DNA molecules immobilized on a sensor surface and free RNAPs (monomeric bacteriophage T7 and holoenzyme of *E. coli*) delivered to the surface were examined using surface plasmon resonance imaging (SPRi) to obtain kinetics data. RNA transcripts produced in the biochip were collected and semi quantified.

Potential future developments would take advantage of the data provided here on RNA synthesis to design biosensors that could track real time *in vitro* protein production